DEPARTAMENTO DE FÍSICA TEÓRICA
& INSTITUTO DE FÍSICA TEÓRICA

UNIVERSIDAD AUTÓNOMA DE MADRID

Dynamical SUSY Breaking in String Theory

Memoria de Tesis Doctoral presentada ante la Facultad de Ciencias,
Sección de Ciencias Físicas, de la Universidad Autónoma de Madrid,
por **Fouad Ghassan Saad,**

Trabajo dirigido por el Doctor **D. Ángel M. Uranga Urteaga**
Científico Titular del Instituto de Física Teórica IFT.
Universidad Autónoma de Madrid y
Consejo Superior de Investigaciones Científicas.

Madrid, Abril de 2007

Contents

Chapter 1

Introducción

Los principios del siglo veinte dieron lugar a una revolución en la física con la teoría de la relatividad especial y general y el descubrimiento de la mecnica cuántica. Mientras que la relatividad general trata de interacciones gravitacionales, la mecnica cuántica explica las interacciones atómicas. La necesidad de reconciliar la mecnica cuántica con la relatividad especial dio lugar al desarrollo de la teoría cuántica de campos por Feynman, Schwinger Tomonaga y muchos otros y culminó con la formulación del Modelo Estándar por Salam, Weinberg y Glashow.

El Modelo Estándar es una teoría cuántica de campos renormalizable, y que describe todas las fuerzas fundamentales excepto la gravedad. Además, ha sido confirmada por todos los experimentos hasta ahora. No obstante, quedan muchos problemas abiertos, algunos son:

- Resultados experimentales restringen la masa del Higgs al orden de 100 GeV. Para tener esta masa, la 'bare mass' en el Lagrangiano tiene que estar ajustada muy precisamente para cancelar la divergencias radiativas, que van como el cuadrado de la escala de nueva física. Esto es el problema de 'fine-tuning'.

- Aunque el parámetro θ del instanton se puede ajustar, cambiando la fase de la matriz de masa para los fermiones, no hay ninguna razón para que estos dos parámetros se cancelan. Pero todos los experimentos han puesto el valor de θ cerca de cero. Esto es el 'strong-CP problem'.

- No hay ninguna razon aparente para explicar los termios de masas y de mixing que vienen de los Yukawas. La diagonalisación de los Yukawas da masas con

diferencias de cinco ordenes de magnitud, algo que no parece muy natural.

Finalmente, aunque el Modelo Estándar es una teoría cuántica de campos consistente, está vista cómo una teoría efectiva de otra teoría que incluye interacciones gravitacionales. Todos los intentos para extender el Modelo Estándar para que incluye gravitación, añadiendo una partícula de espin dos, han fracasado porque las teorías generadas no eran renormalizables. El hecho que el acoplo gravitacional tiene dimension de masa -2 significa la teoría de gravitación no es renormalizable y tiene que aparecer nueva física a la escala de Planck. Entonces hace falta encontrar lo que va a completar el Modelo Estándar en el ultravioleta. Otra indicación de la existencia de nueva física viene de las oscilaciones de neutrinos. El mecanismo 'see-saw' predice la existencia de neutrinos 'right' al orden de la escala de gran unificación, sugiriendo la existencia de nueva física a escalas más altas. Aparte de estas cuestiones, uno se puede también preguntar de donde vienen los 19 parámetros (sin incluir los neutrinos), las tres familias, el grupo gauge $SU(3) \times SU(2) \times U(1)$ y porque sólo vemos cuatro dimensiones.

Una extensión interesante del Modelo Estándar es supersimetría. Aparte de las simetrías gauge, esta también tiene una simetría entre bosones y fermiones. Los fermiones y bosones se juntan en representaciones de esta simetría llamados supermultipletes. La extensión supersimétrica del Modelo Estándar (MSSM) tiene multipletes chirales y vectoriales, donde cada boson gauge viene con su par fermionico (gaugino) y cada quark viene con su par bosonico (squark). Esta teoría es interesante porque resuelve el problema de 'fine-tuning'. El hecho que los términos del superpotencial no se renormalizan, hace que la masa del Higgs diverge logarithmicamente con la escala de nueva física. También, la extensión supersimétrica del Modelo Estándar unifica los acoplos gauge a una escala de 10^16 GeV. Además, el neutralino es un buen candidato para materia obscura.

En los últimos veinte años, la Teoría de Cuerdas se ha ilustrado cómo el mejor candidato para unificar interacciones gauge y gravitacionales. El hecho de describir las partículas no cómo puntos sino cómo cuerdas, da lugar a una partícula de espin dos que es justamente el graviton. Esta teoría entonces unifica las interacciones gauge y gravitacionales a nivel cuántico. Además, las interacciones de las cuerdas son finitas orden por orden en teoría de perturbaciones. La Teoría de Cuerdas es muy potente porque permite la creación de fermiones chirales en cuatro dimensiónes y puede dar

lugar a teorías en el infrarrojo cerca al MSSM. Además, esta Teoría a mejorado nuestro entendimiento de la física de agujeros negros y de la estructura fundamental del espacio-tiempo. Finalmente, la Teoría de Cuerdas relaciona de manera profunda muchos campos de matemática y física y ha dado lugar a muchos avances en estos dos campos.

Aunque se cree que la Teoría de Cuerdas es una extensión ultravioleta del Modelo Estándar, muchos problemas quedan a resolver. El hecho que la teoría de Cuerdas tiene que vivir en 10 dimensiónes (11 para M-theory), uno supone que las seis dimensiónes transversas a las cuatro que observemos, son compactas. La forma de este espacio transverso da lugar a la física que observemos en cuatro dimensiónes. Entonces uno de los retos es de reproducir la física que observemos en cuatro dimensiónes. De hecho, aunque es posible de reproducir modelos cerca al MSSM, estos tienen en general demasiadas partículas sin masa (moduli). Entonces encontrar un mecanismo para estabilizar estas direcciones planas es todavía una pregunta abierta. También, si uno logra obtener el MSSM a bajas energías, un mecanismo para romper supersimetría es necesario para obtener el Modelo Estándar. Finalmente, otros problemas a resolver son el tamaño de la constante cosmologica obtenida en la mayoría de los modelos no supersimétricos y el gran numero de vacíos consistentes obtenidos en la Teoría de Cuerdas. En este trabajo nos concentraremos sobre el problema de encontrar teorías cerca al MSSM y acoplarles a sectores que rompen supersimetría.

Un aspecto elegante de la Teoría de Cuerdas que será crucial para nuestro trabajo es la existencia de D–branas. Las D–branas son objetos extendidos tal que las cuerdas abiertas se acaban en su superficie. Su belleza está en el hecho que todos los campos gauge están localizados en su volumen y interaccionan con el espacio entero a través de la gravitación. Entonces ofrecen muchas posibilidades porque uno puedes especular que en la teoría Tipo IIB, el Modelo Estándar vive en una D3–brana y interacciona con el espacio diez-dimensiónal a través de la fuerza gravitacional.

Ahora, la teoría que vive dentro de una D3–brana es $\mathcal{N} = 4$ Super Yang-Mills, entonces uno tiene que romper SUSY a $\mathcal{N} = 1$ si desea obtener teorías gauge cerca de la realidad. De hecho, sólo $\mathcal{N} = 1$ tiene chiralidad. Las D–branas puestas en singularidades son muy interesantes en este respeto porque pueden dar lugar a teoría gauge cerca al MSSM. También son muy útiles en la construcción de modelos porque

uno puede deducir los grupos gauge, el contenido de materia y la renormalización de los acoplos de la teoría efectiva todo a partir de la geometría local. La compactificación global será relevante sólo si uno quiere determinar el valor exacto de los Yukawas, que son función del 'string coupling', o si uno quiere encontrar la teoría completa hasta el ultravioleta.

En este trabajo nos vamos a enfocar en el estudio de branas en singularidades toricas (ver apendice B). Estas singularidades, que incluyen las singularidades orbifold, corresponden a fibras T^3 que van a cero a ciertos puntos. Las singularidades toricas Calabi-Yau, están totalmente caracterizadas por un diagrama 2-dimensiónal, el diagrama torico. En general, para obtener la teoría gauge de D3–branas en una singularidad torica, uno empieza con una singularidad oribifold y hace un higgsing para llegar a la singularidad querida (ver [8, 9] y [10] para una aplicación). La singularidad que queda está determinada viendo el espacio moduli, porque este espacio parametriza el espacio transverso donde se mueven las D3–branas. Aunque este método es sistemático, es muy largo y se vuelve impractico para geometrías muy singulares. En [14, 15, 18], los autores muestran una correspondencia directa entre las teorías gauge de D3–branas en singularidades toricas, y los diagramas 'dimer', que son 'tilings' dos-dimensiónal del toro T^2. Esta correspondencia ha sida demostrada de manera más explicita en [16] donde muestran que el diagrama 'dimer' esta relacionado a una superficie de Riemann en la Tipo IIA 'mirror'. En nuestro trabajo, utilizamos estos resultados para desarrollar un método sistemático y sencillo para determinar la teoría gauge para singularidades toricas arbitrarias.

Ahora, dado un teoría gauge que vive dentro de D3—branas, queda el problema de romper SUSY. Las branas fraccionarias, que corresponden a D5–branas enrolladas en ciclos que van a cero, ofrecen posibilidades interesantes. En la teoría gauge las branas fraccionarias corresponden a asignaciones para los rangos de los grupos gauge que cancelan anomalías. En [20], Klebanov y Strassler muestran que la introducción de branas fraccionarias en la singularidad conifold rompe invariancia conforme y da lugar a una teoría gauge que confina en el infrarrojo. Las branas fraccionarias pueden entonces dar lugar a dinámica interesante en el infrarrojo. En nuestro trabajo extendemos estos resultados y encontramos que branas fraccionarias en algunas singularidades pueden dar lugar a una ruptura dinámica de supersimetría en el infrarrojo. La supersimetría esta rota a bajas energías por efectos no-perturbativos que vienen de instantones o condensación de gauginos. Pero cuando uno incluye los

acoplos a cuerdas cerradas, los modelos dan lugar a un compartamiento 'runaway' donde el mínimo supersimétrico está en el infinito.

En [25], los autores muestran que $\mathcal{N} = 1$ SQCD con sabores masivos genera un vacío metastable donde SUSY está roto a bajas energías. Uranga y Franco [24] construyen un modelo de cuerdas donde usan estos resultados. Poniendo D7–branas con branas fraccionarias en una singularidad dP_1, muestran que el modelo genera un vacío metastable donde SUSY está roto a bajas energías. En nuestro trabajo, extendemos estos resultados a singularidades toricas arbitrarias mostrando cómo uno puede determinar la existencia de un vacío metastable de manera sencilla y sistemática.

En [26], los autores lograron obtener una teoría muy cerca al MSSM poniendo D3–branas en una singularidad oribifold $\mathbb{C}^3/\mathbb{Z}_3$ y añadiendo D7–branas para sabores. Pero hace falta romper SUSY para recuperar el Modelo Estándar. Cómo hemos dicho antes, supersimetría tiene muchas ventajas cómo la unificación de los acoplos gauge y el hecho que soluciona el problema de 'fine-tuning' en el Modelo Estándar. Ahora, el hecho que SUSY no se ha observado, una pregunta natural es cómo esta simetría esta rota a bajas energías. Cualquier mecanismo que rompe SUSY lo tiene que hacer a bajas energías porque la escala de ruptura de SUSY define el 'fine-tuning' de la masa del Higgs. Los términos que rompen SUSY tienen entonces que ser dimensiónal para que SUSY se restaure a energías altas. Ahora, aún si uno tiene un sector que rompe SUSY, acoplarlo al MSSM no es trivial porque se puede mostrar que cualquier acoplo renormalizable a tree-level da lugar a masas de squarks mas bajas, en contradicción con datos experimentales [27]. Entonces si SUSY está rota es a través de términos soft en el Lagrangiano *Efectivo*. Estos términos soft tienen que ser universales respeto a los sabores i.e no romper la simetría de sabor $U(3)$. Aúnque esta simetría está rota por acoplos de Yukawa, términos soft que rompen la simetría de sabor a grande escala dan grandes contribuciones a los 'flavor-changing neutral currents', algo prohibido por datos experimentales. Un modelo consistente con estas restricciones es el de 'gauge-mediated SUSY breaking'. En este modelo, el sector que rompe SUSY tiene supermultipletes que cogen masas diferentes para sus componentes (los 'messengers'). Aunque estos 'messengers' no tienen acoplos a tree-level al MSSM, están cargados bajos sus grupos gauge y dan masas no supersimétricas a los campos en el MSSM a uno o dos loops. El hecho que no sean cargados bajo el grupo de flavor, no generan 'flavor-changing neutral currents'.

En [28] los autores muestran cómo introducir este mecanismo dentro de la teoría de cuerdas. Poniendo dos D–branas separadas por una distancia menor que la escala de la cuerda, muestran que si una da lugar a ruptura de supersimetría en el infrarrojo, se acopla a la otra a través de 'gauge mediation'. Empezando por mostrar cómo uno puede separar una singularidad en dos, usamos las ideas previas poniendo branas en una singularidad dP_1 para generar un vacío metastable que rompe SUSY, y ponemos branas en una singularidad $\mathbb{C}^3/\mathbb{Z}_3$ adyacente para generar un modelo similar al MSSM. Para separaciones menores que la escala de la cuerda, la brana que rompe SUSY se acoplará a la brana que tiene el MSSM a través de 'gauge mediation'. Entonces, usando D–branas, hemos conseguido generar un modelo cerca al MSSM y rompa supersimetría en el infrarrojo a través de 'gauge mediation', todo en el contexto de la Teoría de Cuerdas.

En capitulo 3 empezamos por un resumen de los resultados de Klebanov-Strassler. En [20], Klebanov y Strassler muestran que poner branas fraccionarias en una singularidad conifold rompe invariancia conforme y da lugar a una teoría gauge que confina en el infrarrojo. De hecho la teoría gauge pasa por una cascada de dualidades de Seiberg mientras fluye al infrarrojo. Después ponen una D3–brana que actúa como un probe para mostrar que el espacio de moduli se ha modificado por efectos no-perturbativos, y corresponde a una deformación (hacer crecer S^3) de la singularidad conifold. Entonces hay una relación intrínseca entre la dinámica en el infrarrojo de la teoría gauge y las propiedades de la singularidad torica. Esta relación ha sido generalizada a muchas singularidades toricas en [13], donde los autores muestran que branas fraccionarias que corresponden a deformaciones dan lugar a teorías gauge que pasan por cascadas de dualidades y confinan en el infrarrojo. Resumimos sus resultados en sección 3.2.2. No obstante, hay branas fraccionarias que no corresponden a deformaciones de las singularidades toricas. En sección 3.3 mostramos que estos branas fraccionarias genéricas dan lugar a ruptura dinámica de supersimetría en el infrarrojo (DSB). En la teoría gauge, estas branas corresponden en general a grupos gauge con rangos diferentes. Cuando la teoría corre en el infrarrojo algunos grupos dan lugar a un superpotencial no-perturbativo Affleck, Dine, Seiberg [22]. Pero cuando la dinámica de las cuerdas cerradas esta incluida, que hace que los términos Fayet-Iliopoulos se vuelven dinámicos, esto da lugar a un comportamiento 'runaway' donde hay un mínimo supersimétrico en el infinito.

En capitulo 4, empezamos resumiendo los resultados de [14, 15, 18], donde muestran que las teorías gauge de D3–branas en singularidades toricas están totalmente representadas por los diagramas 'dimer'. Estos son recubrimientos 'bi-partite' de T^2, donde las caras corresponden a grupos gauge, los lados corresponden a bifundamentales y los nodos corresponden a términos en el superpotencial. El hecho que el dimer sea 'bi-partite' permite darle una orientación. En [16], los autores muestran una correspondencia directa entre diagramas dimer y el 'mirror' en la tipo IIA. La simetría 'mirror' mapea D3–branas en la tipo IIB a D6–branas en la tipo IIB, y los autores han mostrado que estas D6–branas se intersecan en una superficie de Riemann que corresponde a un ensanchamiento del diagrama web. En nuestro trabajo, usamos esta correspondencia para implementar la resolución parcial (hacer crecer un S^2) de la singularidad torica. Esta correspondencia da un mapa directa entre la resolución en el diagrama web y el efecto en los diagramas dimer. La resolución parcial corresponde en la teoría gauge a un higgsing de la teoría encendiendo términos Fayet-Illipoulos, y en nuestro trabajo mostramos cómo uno puede determinar la asignación de vevs directamente del diagrama web y del diagrama dimer. Esto nos permite encontrar de manera sencilla la teoría gauge de D3–branes en singularidades arbitrarias.

En capitulo 5, empezamos con un resumen de los resultados de Intriligator, Seiberg, Shih [25], donde presentan un modelo muy sencillo para generar un vacío metastable que rompe supersimetría. Usando $\mathcal{N} = 1$ SQCD y añadiendo sabores con masas muchas mas pequeñas que la escala dinámica de la teoría genera un vacío metastable, separado de un vacío supersimétrico por una gran barrera. También muestran que este mínimo sobrevive suficiente tiempo. Estos resultados han sido generados a partir de Teoría de Cuerdas en [24], donde muestran que añadir D7–branas a branas fraccionarias DSB localizadas en una singularidad dP_1 genera un vacío metastable que rompe supersimetría. Este mínimo esta separado del mínimo 'runaway' por una gran barrera lo que hace que sobrevive a largo plazo. Usando estos resultados, mostramos como se puede determinar la presencia de un vacío metastable para singularidades toricas arbitrarias.

En capitulo 6, mostramos que poner D3, D7 y branas fraccionarias en singularidades toricas y hacer un higgsing de una manera apropiada da lugar a dos series de branas, con un sector que corresponde al donde se rompe SUSY, y el que corresponde a una teoría cerca al MSSM. Cuando la separación es menor que la escala de la cuerda,

la ruptura de SUSY se hace en el sector visible a través de 'gauge-mediation'. Los 'messengers' corresponden a las cuerdas massivas que se extienden entre las dos series de branas. También hacemos una computación explicita para determinar los 'messengers'.

El apéndice A es un review de resultados útiles de supersimetría. Apéndice B es un review de geometría torica y es crucial para una buena comprensión de este trabajo.

Chapter 2

Introduction

The beginning of the 20th century saw a revolution take place in physics with the advent of special and general relativity and the discovery of quantum mechanics. Whereas general relativity explained gravitational interactions, quantum mechanics was concerned with atomic interactions. The need to reconcile quantum mechanics and special relativity later led to the development of quantum field theory by Feynman, Schwinger, Tomonaga and numerous others, which culminated in the 1970's with the formulation of the Standard Model by Salam, Weinberg and Glashow.

The Standard Model is a renormalizable field theory which describes all the fundamental forces of nature except for gravity, and has withstood all experimental tests to date. However, numerous issues remain to be resolved, some of which are:

- Experimental bounds place the mass of the Higgs at the order of 100 GeV. To achieve such a physical mass the bare mass has to be adjusted very precisely to cancel the radiative corrections, which go as the square of the scale of new physics. This is the principal fine-tuning problem.
- Although the instanton θ parameter can be shifted by giving a phase to the mass matrix for fermions, there is no reason why these should be related, yet all experimental tests place the physical value of θ very close to zero for a real mass matrix. This is the strong-CP problem.
- There is no apparent explanation for the pattern of masses and mixings stemming from the Yukawa couplings. Indeed, diagonalisation of Yukawas leads to mass terms spanning five orders of magnitude, which seems quite unnatural.

Most importantly, although the Standard Model is a consistent quantum field theory it is viewed as a low-energy effective theory of another theory which would include gravitational interactions. All attempts to extend the Standard Model to include gravity by adding a spin-two particle have failed since the theories generated are non-renormalizable and break unitarity at loop levels. Indeed, since the gravitational coupling has mass dimension -2, the theory of gravity is non-renormalizable and new physics should appear at the Planck scale. Thus a complete ultraviolet completion of the Standard Model is still needed. Another indication of the existence of new physics comes from neutrino oscillations. The see-saw mechanism predicts a right handed neutrino at the order of the GUT scale thus hinting at the existence of new physics. Besides theses issues one can also wonder why there are 19 free parameters (not including neutrino parameters), three families, gauge group $SU(3) \times SU(2) \times U(1)$ and why we only see four dimensions.

An interesting extension of the Standard Model can be found in supersymmetry. Besides gauge symmetries these theories also contain a symmetry between bosons and fermions. The fermions and bosons thus come in representations of this symmetry called supermultiplets. The supersymmetric extension of the Standard Model (MSSM) contains chiral and vector supermulitplets, where each gauge boson comes with its fermionic pair (gaugino) and each quark comes with its bosonic pair (squark). This theory is interesting since it solves the fine-tuning problem for the higgs field. Indeed, since the terms in the superpotential are not renormalized, the higgs mass runs logarithmically with the scale of new physics. Also, the supersymmetric extension of the Standard Model has been shown to unify the gauge couplings at a scale of 10^{16}. The neutralino is also a very likely candidate for dark matter.

In the last twenty years, String Theory has proved to be the most viable candidate to unify gravitational and gauge interactions. Indeed, treating particles as strings instead of points leads to the emergence of a spin-two particle shown to be the graviton. It thus provides a unification at the quantum level between gauge and gravitational interactions. Moreover, string interactions are finite order by order in perturbation theory. String Theory is also extremely versatile since it can generate chiral fermions in four dimensions and can lead to effective theories in the infrared close to the MSSM. Moreover, it can give us new insight into the nature of black hole physics and space-time itself. Finally String Theory provides a very rich interplay between mathematics and physics and has led to numerous advances in both fields.

Although it is believed that String Theory is a possible ultraviolet completion of the Standard Model numerous issues have yet to be resolved. Since consistency requires that String Theory live in 10 dimensions (11 for M-theory), one assumes that the six-dimensional space transverse to the observed four-dimensional space-time is compact. The shape of the transverse space leads to the observed physics in four dimensions. One of the challenges is therefore to actually reproduce the observed physics in four dimensions. Although it is possible to obtain string models close to the MSSM in structure, these tend to have way too many flat directions (moduli). Indeed, generic string compactifications tend to lead to moduli related to e.g. the geometry of the internal manifold. These moduli are problematic since they lead to free parameters in the theory. Hence there must be mechanisms to stabilize the moduli and give them masses. These masses should be large enough to avoid the cosmological moduli problem (overclosing of the universe due to too much energy density accummulated on moduli fields). This remains an open question. Also, even if one were to obtain the MSSM at low energies, a mechanism to break supersymmetry is needed to obtain the Standard Model. Finally, other issues which need to be resolved are the largeness of the cosmological constant obtained in most non-supersymmetric models as well as the degeneracy of consistent vacua which arise in String Theory. In this work we will only focus on the issue of generating MSSM-like theories in the infrared and coupling them to a SUSY breaking sector.

A particularly elegant aspect of String Theory which will be crucial in our work is the existence of Dp–branes. These are extended $p+1$–dimensional objects such that open strings end on them. Their elegance lies in the fact that all gauge fields are localized on their worldvolume and they interact with the bulk only through gravitational interactions. Thus, they offer very rich structures since one can speculate that in Type IIB String Theory, the Standard Model lives on a D3–brane with the gravitational interactions lying in the bulk ten–dimensional space.

Now since the gauge theory living on a D3–brane is $\mathcal{N} = 4$ Super Yang-Mills, it must be broken to $\mathcal{N} = 1$ if one is to obtain a realistic gauge theory. Indeed, only $\mathcal{N} = 1$ SUSY can incorporate chirality. D–branes located at singularities are particularly interesting in that respect since they can generate chiral theories close to the MSSM. Also, they are very useful in model building since one is able to determine the gauge

groups, matter content and coupling constant renormalization of the effective theory all from the local geometry. The global compactification will be relevant amongst other things, if one wants to determine the exact values of Yukawa couplings, which are a function of the string coupling, or find the ultraviolet completion of the effective theory, or determine the Kahler potential. It will also be relevant for cosmology.

In this work we will focus in particular on branes at toric singularities (see appendix B). These singularities, which include abelian orbifold singularities, correspond to T^3 fibers, with 1-cycles vanishing at specific points and the whole fiber vanishing at the singularity. For toric Calabi-Yau geometries, they are completely described by a 2-dimensional graph, the toric diagram. In general, to obtain the gauge theory for D3–branes at a given toric singularity, one starts with the gauge theory on an orbifold singularity and higgses it in the appropriate way (see [8, 9] and [10] for an example). The residual singularity is determined by looking at the moduli space of the gauge theory since it parametrizes the space in which the D3-branes move i.e the transverse space. Although this method is systematic, it is long and becomes intractable for very singular geometries. In [14, 15, 18] the authors show a direct correspondence between gauge theories on D3–branes at toric singularities and dimer diagrams, two-dimensional tilings of the torus. This correspondence is made more explicit in [16] where they show how the dimer diagram is related to a Riemann surface in the Type IIA mirror. In our work, we use these results to develop a systematic and simple method to determine the gauge theory for arbitrary toric Calabi-Yau singularities.

Now given a gauge theory living on D3–branes, the issue of SUSY breaking still remains. Fractional branes, which correspond to D5-branes wrapped on vanishing cycles, offer interesting possibilities in that respect. In the gauge theory fractional branes correspond to anomaly free rank assignments for the gauge groups. In [20] Klebanov and Strassler show that placing fractional branes on a conifold singularity breaks conformal invariance and leads to a confining gauge theory in the infrared. Thus fractional branes on toric singularities can lead to interesting low energy dynamics. In our work, we extend these results and find that placing fractional branes on some toric singularities generates dynamical supersymmetry breaking in the infrared. Supersymmetry is broken at low energies by non-perturbative effects arising from instantons or gaugino condensation. However, when one takes into account coupling to closed string modes, the models exhibit a runaway behavior to a super-

symmetric minimum.

In [25], the authors show that $N = 1$ SQCD with massive flavors generates a metastable SUSY breaking minimum at low energies. Uranga and Franco [24] embed these results into String Theory by showing that fractional branes coupled to D7-branes at a dP_1 singularity also generate metastable SUSY breaking vacua at low energies. We extend their results to arbitrary toric singularities by showing how one can determine the existence of metastable vacua in a simple and systematic manner.

In [26], the authors were able to obtain a gauge theory very similar to the MSSM by placing D3-branes at a $\mathbb{C}^3/\mathbb{Z}_3$ orbifold singularity and adding flavor D7-branes. One would however like to break SUSY so as to recover the Standard Model. As stated before, supersymmetry has numerous advantages such as solving the fine-tuning problem and unifying gauge coupling constants. However since supersymmetry is not observed, a natural question which arises is how this symmetry is broken at low energies. Indeed any mechanism which breaks supersymmetry must do so spontaneously, and the scale at which supersymmetry is broken dictates the fine-tuning of the higgs mass. This leads to soft terms[1] in the low energy effective action. Now even if one has a sector to break SUSY, coupling it to the MSSM is not trivial since it can be shown that any renormalisable tree-level couplings to the matter sector would lead to masses for the squarks lower than their fermionic partners, and this is not observed experimentally [27]. So if SUSY is broken it is through soft-terms in the *Effective* Lagrangian. And these soft-terms have to be flavor universal i.e. not violate the $U(3)$ flavor symmetry. Although this symmetry is broken by Yukawa couplings, flavor violating soft-terms occurring at a large scale could give large contributions to flavor changing neutral currents forbidden by experimental observation. A scenario consistent with these conditions is that of gauge-mediated supersymmetry breaking. In this model, the SUSY breaking sector contains supermultiplets which get non-degenerate masses for their component fields (messengers). Although these messengers have no tree-level couplings to the MSSM visible sector, they are charged with respect to its gauge groups, thus giving fields in the MSSM non-SUSY masses at one or two-loops. Since they are not charged with respect to the flavor group, they do not generate flavor changing neutral currents.

[1] terms whose coupling parameters have positive dimension of mass

In [28], the authors show how to embed this mechanism into String Theory. By placing two D–branes separated by a distance smaller than the string scale, they show that if one D-brane generates SUSY breaking in the infrared, the other D–brane will couple to it via gauge mediation. By first showing how it is possible to split a singularity into two separated ones, we apply the above idea by placing fractional and D7 branes on a dP_1 singularity to generate a metastable SUSY breaking vacua, and place D3-branes and D7-branes on an adjacent $\mathbb{C}^3/\mathbb{Z}_3$ singularity to generate an MSSM-like theory. For separation lengths smaller than the string scale, the SUSY breaking brane will couple via gauge mediation to the MSSM sector. Thus, using D–branes we have been able to generate an MSSM-like model which exhibits SUSY breaking in the infrared via gauge mediation, all within the context of String Theory [5].

In Chapter 3 we start by reviewing the Klebanov-Strassler solution. In [20], Klebanov and Strassler show that placing fractional branes on a conifold singularity breaks conformal invariance and leads to a confining gauge theory in the infrared. Indeed, the gauge theory goes through a cascade of Seiberg dualities as it flows to the infrared. They then place a D3–brane probe and show that the moduli space has been modified due to non-perturbative effects, and corresponds to a deformation (blow-up of an S^3) of the conifold singularity. There is thus an intricate relation between the infrared dynamics of the gauge theory and the properties of the toric singularity. This relation was generalized to numerous toric singularities in [13], where the authors showed that fractional branes corresponding to deformations lead to duality cascades and confining gauge theories in the infrared. We review their results in Section 3.2.2. There are however fractional branes which do not correspond to deformations of the toric singularity. In Section 3.3 we show that these fractional branes generically lead to dynamical supersymmetry breaking (DSB) in the infrared. These fractional branes correspond in general to theories with gauge groups of different ranks. As the theory runs in the infrared, some nodes develop a non-perturbative Affleck, Dine, Seiberg superpotential [22]. The combination of this term with the original superpotential term breaks supersymmetry. However, when the dynamics of closed string moduli is included, rendering the Fayet-Iliopoulos terms dynamical, a runaway behavior is observed and supersymmetry is restored at infinity.

In chapter 4, we start by reviewing the results of [14, 15, 18] where they show that the gauge theories of D3–branes at toric singularities are completely determined by

the so-called dimer diagrams. These are bi-partite tilings of T^2, where faces correspond to gauge groups, edges correspond to bifundamentals, and nodes correspond to superpotential terms. The bi-partite nature of the graph (i.e nodes can be colored black or white with each black node only connected to white nodes and vice-versa) confers an orientation to the graph. In [16] the authors show a direct correspondence between these dimer diagrams and the IIA mirror configuration. Mirror symmetry maps D3–branes in type IIB to D6–branes in type IIA, and the authors showed that these D6–branes intersect on a Riemann surface which corresponds to a thickening of the web diagram. We use this correspondence to implement partial resolution (blow-up of an S^2) of a toric singularity. Indeed, this correspondence gives us a direct map between the resolution in the web diagram and the effect on the dimer diagram. Partial resolution corresponds on the gauge theory side to a higgsing of the theory by turning on Fayet-Ilipoulos terms, and we show how the assignation of vevs can be directly determined from the web and dimer diagrams. This permits us to determine in a simple manner the gauge theory of D3–branes at arbitrary toric singularities.

In chapter 5, we start by reviewing the work of Intriligator, Seiberg, Shih, [25], where they present a very simple model to generate metastable supersymmetry breaking vacua. Taking $\mathcal{N} = 1$ SQCD and adding flavors with masses much smaller than the dynamical scale of the theory generates a local metastable vacua, separated from a supersymmetric vacua by a large potential barrier. This minimum is shown to be parametrically long-lived. These results are embedded into String Theory in [24], where the authors show that adding D7–branes to a DSB fractional brane located at a dP_1 singularity generates a metastable supersymmetry breaking vacua. This minimum is separated from the runaway direction of the DSB fractional brane by a large potential barrier, rendering it parametrically long-lived. Using these results, we then show how one can determine the presence of metastable vacua for arbitrary toric singularities.

In chapter 6, we show that placing D3, D7 and fractional branes at toric singularities, and higgsing in the appropriate manner can lead to two separated sets of branes, with one sector containing the supersymmetry breaking sector and the other containing an MSSM-like sector. We give an explicit realization of this, with a hidden sector corresponding to the dP_1 singularity and breaking supersymmetry at a local metastable minimum, and the visible sector corresponding to the $\mathbb{C}^3/\mathbb{Z}_3$ and

generating an MSSM-like theory. When the separation between the sets of branes is smaller than the string scale, supersymmetry breaking takes place in the visible sector via gauge mediation. The messengers correspond to massive strings stretching between both sets of branes. We also provide an explicit computation of this messenger sector.

Appendix A is a review of useful results in supersymmetry. Appendix B is a review of toric geometry and is crucial for a proper understanding of this work.

In this thesis we will not summarize our work in [2] since it is not really relevant for the discussion. Also, we have not commented on the relation between the AdS/CFT correspondence and fractional branes. The interested reader can consult our work in [3].

Chapter 3

Fractional Branes and IR dynamics

3.1 Introduction

D3–branes located at toric singularities generically lead to conformal $\mathcal{N} = 1$ SUSY theories in their worldvolume. Klebanov, Strassler showed that placing fractional branes (e.g D5–branes wrapped on vanishing 2–cycles) on a conifold singularity breaks conformal invariance and leads to a confining gauge theory in the infrared. Indeed, the gauge theory living on the worldvolume of these fractional branes has a renormalization group (RG) flow that takes the form of a duality cascade[1]. The ultraviolet (UV) behavior of cascading theories is markedly different from that of ordinary field theories. Instead of having a UV fixed point, they have an infinite tower of dual theories with a steadily increasing number of colors and matter fields towards the UV.

In section 3.2.1 we review the Klebanov-Strassler solution [20]. In section 3.2.2 we review the work of [13] where they extend the results of Klebanov, Strassler to arbitrary singularities. In the last section we show that whereas fractional branes related to deformation (i.e blow-up of an S^3) of the toric singularity lead to confining gauge theories in the infrared, the generic fractional brane leads to dynamical supersymmetry breaking in the infrared.

[1] In a duality cascade, Seiberg duality is used to change to a dual description every time any of the gauge groups becomes strongly coupled.

3.2 Fractional Branes and Cascading Gauge Theories

3.2.1 The Klebanov-Strassler solution

The metric of the conifold can be written as

$$ds^2 = dr^2 + r^2 ds^2_{T^{11}} \tag{3.1}$$

This is a cone over T^{11}, where T^{11} has topology $S^2 \times S^3$ and both these cycles vanish at the singular point $r = 0$, as seen in Figure 3.1. Now, the singular point

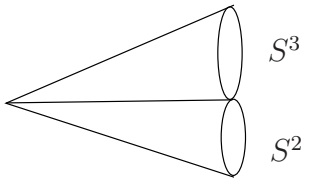

Figure 3.1: Illustration of the conifold as a cone over T^{11}.

can be smoothed out by either giving a finite size to S^2, this is called *resolution*, or by giving a finite size to S^3, this is called *deformation* (see appendix B on toric geometry). This is illustrated in the web diagram shown in Figure 3.2.

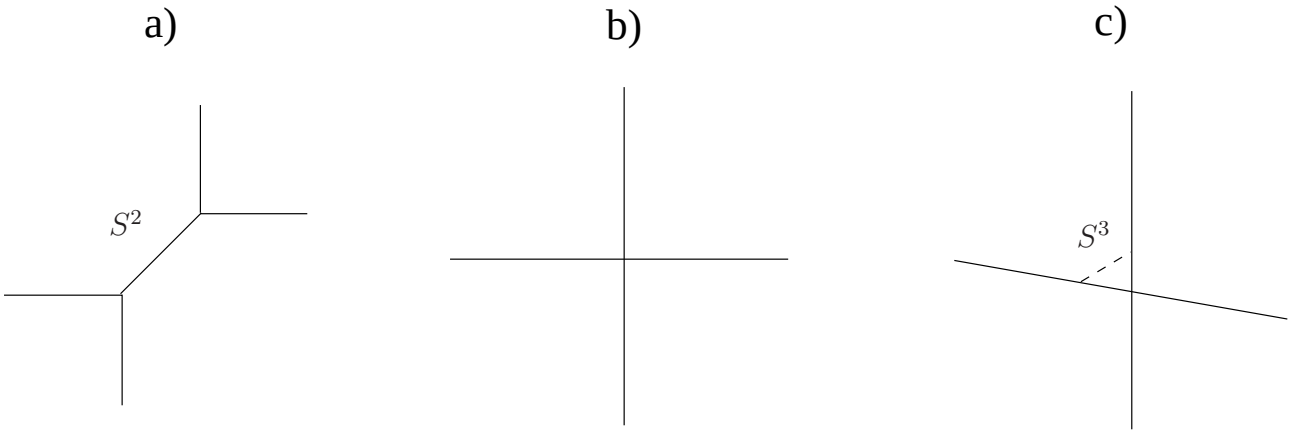

Figure 3.2: Web diagram of a) Resolved conifold b) Conifold c) Deformed conifold

The conifold can also be described by the following equation in complex variables

$$xy = zw \quad x, y, z, w \in \mathbb{C} \tag{3.2}$$

If we place N D3-branes and M fractional[2] D3-branes on the conifold, we obtain the gauge theory $SU(N+M) \times SU(N)$ shown in the quiver of Figure 3.3 with superpotential

$$W = \lambda_1 \mathrm{tr}\ (X_{12}Y_{21}Y_{12}X_{21} - X_{12}X_{21}Y_{12}Y_{21}) \tag{3.3}$$

The quiver represents an $\mathcal{N} = 1$ SUSY gauge theory where nodes represent gauge

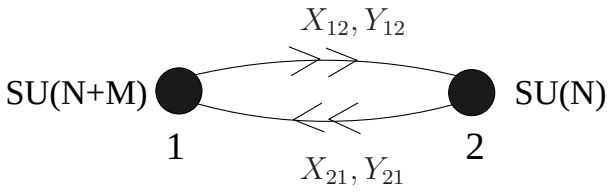

Figure 3.3: Quiver of the conifold.

groups (with the associated vector mutiplets) and arrows represent bifundamental chiral multiplets (e.g X_{12} transforms in the fundamental, anti-fundamental of gauge groups 1 and 2 respectively). For $N = 1$ and $M = 0$, the F-term equations are automatically satisfied. The D-terms become

$$|X_{12}| + |Y_{12}| - |X_{21}| - |Y_{21}| = 0 \tag{3.4}$$

The solution to this equation, modulo gauge invariance is parametrized by gauge invariant monomials (see appendix A on supersymmetry). These monomials are $x = X_{12}X_{21}$, $y = Y_{12}Y_{21}$, $z = X_{12}Y_{21}$ and $w = Y_{12}X_{21}$. However these are not independent. The moduli space is therefore $xy = zw$ and we recover the equation for the conifold (3.2). This is consistent since the moduli space of the gauge theory living in the worldvolume of D3–branes parametrises the transverse space to these branes. In our case this transverse space is the conifold. The gauge theory thus encodes the geometry in which the D3–branes move. The above analysis easily extends to the non-abelian case as shown in [20]. Now in the case M=0, the gauge theory is conformal. For the case where $M \neq 0$, we get the following β-functions

$$\frac{d}{d\log(\Lambda/\mu)}\frac{8\pi^2}{g_1^2} \sim 3(N+M) - 2N(1-\gamma)\ , \tag{3.5}$$

$$\frac{d}{d\log(\Lambda/\mu)}\frac{8\pi^2}{g_2^2} \sim 3N - 2(N+M)(1-\gamma)\ , \tag{3.6}$$

which leads to

$$\frac{8\pi^2}{g_1^2} - \frac{8\pi^2}{g_2^2} \sim M\ln(\Lambda/\mu)[3 + 2(1-\gamma)]\ , \tag{3.7}$$

[2]Fractional branes consist of D–5 branes wrapped around collapsed 2–cycles at the singularity of the conifold.

where γ is the anomalous dimension and Λ is the scale of the theory. The essential observation is that $1/g_1^2$ and $1/g_2^2$ flow in opposite directions and, according to (3.5), there is a scale where the $SU(N+M)$ coupling g_1 diverges. To continue past this infinite coupling, we perform a $\mathcal{N}=1$ Seiberg duality transformation on this gauge group factor (see appendix A on supersymmetry). The $SU(N+M)$ gauge factor has $2N$ flavors in the fundamental representation. Under a Seiberg duality transformation, this becomes an $SU(2N-[N+M])=SU(N-M)$ gauge group with $2N$ flavors. We also get the fields $\tilde{X}_{12}$, $\tilde{X}_{21}$, $\tilde{Y}_{12}$, $\tilde{Y}_{21}$, dual to X_{21}, X_{12}, Y_{21}, Y_{12} respectively. As well as the mesons $M_1=X_{21}X_{12}$, $M_2=X_{21}Y_{12}$, $M_3=Y_{21}X_{12}$, $M_4=Y_{21}Y_{12}$. $\tilde{X}_{12}$ and $\tilde{Y}_{12}$ are in the fundamental of $SU(N)$ and $\tilde{X}_{21}$, $\tilde{Y}_{21}$ in the antifundamental. The mesons are in the adjoint-plus-singlet of $SU(N)$. The superpotential after the transformation is

$$W=\lambda_1 \mathrm{tr}\ (M_1M_4-M_2M_3)+\frac{1}{\mu}\mathrm{tr}\ (M_1\tilde{X}_{21}\tilde{X}_{12}+M_2\tilde{Y}_{21}\tilde{X}_{12}+M_3\tilde{X}_{21}\tilde{Y}_{12}+M_4\tilde{Y}_{21}\tilde{Y}_{12}) \tag{3.8}$$

where μ is the matching scale for the duality transformation. The M's are massive so we integrate them out[3], thus obtaining a superpotential

$$W=\lambda_2 \mathrm{tr}\ (\tilde{X}_{12}\tilde{X}_{21}\tilde{Y}_{12}\tilde{Y}_{21}-\tilde{X}_{12}\tilde{Y}_{21}\tilde{Y}_{12}\tilde{X}_{21}) \tag{3.9}$$

We thus obtain an $SU(N)\times SU(N-M)$ theory which resembles closely the theory we started with. The new scales Λ_2 and $\tilde{\Lambda}_2$ are related to the old ones via the relation

$$\lambda_2 \propto \frac{1}{\mu^2\lambda_1} \tag{3.10}$$

and

$$\Lambda_1^{3(N+M)-2N}\tilde{\Lambda}_2^{3(N-M)-2N} \propto \mu^{2N} \propto \lambda_1^M \tilde{\Lambda}_1^{3N-2(N+M)}\lambda_2^{-M}\Lambda_2^{3N-2(N-M)} \tag{3.11}$$

Remarkably this theory has the same form as the previous one with $N \to N-M$. The next step is that the $SU(N)$ gauge group now becomes strongly coupled, and under a Seiberg duality transformation the full gauge group becomes $SU(N-M)\times SU(N-2M)$, and so forth. However, the duality transformation is valid in the window $3N_c > N_f > \frac{3}{2}N_c$ where N_c is the number of colors (i.e the rank of the strongly coupled gauge group) and N_f is the number of flavors (i.e twice the rank of the weakly coupled gauge group, the fact that it is weakly coupled one assumes that it acts like additional flavors with negligible dynamics). The RG flow thus proceeds

[3] i.e we replace them by their equations of motion $\frac{\partial W}{\partial M_i}=0$

step by step until the gauge group has the form $SU(M+p) \times SU(p)$ for $0 < p \leq M$. At this point the moduli space is drastically modified and a more careful analysis has to be performed.

If there are no D3–branes left ($p = 0$), we are left with pure $\mathcal{N} = 1$ Yang–Mills in the infrared, a theory which breaks its $\mathbb{Z}_{2M}$ R–symmetry to $\mathbb{Z}_2$, and has M isolated vacua, domain walls and confinement [20]. However, we have no access to the moduli space and therefore to the supergravity dual, which is singular in the infrared. We can probe the geometry by adding a D3-brane ($p = 1$).

For $p = 1$ (the results apply for any p), the gauge group is $SU(M+1) \times SU(1)$, in short simply $SU(M+1)$. This corresponds to the configuration of M fractional branes and one D3–brane which acts as a probe. In this gauge theory, we have the chiral superfields X_{12}, Y_{12} in the $\mathbf{M+1}$ representation and X_{21}, Y_{21} in the $\overline{\mathbf{M+1}}$ representation. The superpotential is

$$W = \lambda \text{ tr } (X_{12}Y_{21}Y_{12}X_{21} - X_{12}X_{21}Y_{12}Y_{21}) \tag{3.12}$$

Since $N_f < N_c$, the theory confines in the IR and we can write the superpotential in terms of the gauge invariant mesons $M_1 = X_{21}X_{12}$, $M_2 = X_{21}Y_{12}$, $M_3 = Y_{21}X_{12}$, $M_4 = Y_{21}Y_{12}$. The theory develops a non-perturbative Affleck, Dine, Seiberg term [22] (see appendix A) and the superpotential becomes

$$W = \lambda(M_1M_4 - M_2M_3) + (M-1)\left[\frac{2\Lambda^{3M+1}}{(M_1M_4 - M_2M_3)}\right]^{\frac{1}{M-1}} \tag{3.13}$$

The F–term equations for a SUSY vacuum give us the solutions

$$(M_1M_4 - M_2M_3)^M = \frac{2\Lambda^{3M+1}}{\lambda^{M-1}} \tag{3.14}$$

This equation has M independent branches, in each of which $(M_1M_4 - M_2M_3)$ is an M^{th} root of $2\Lambda^{3M+1}/\lambda^{M-1}$. One should mention that the $U(1)_R$ global symmetry is anomalous, there is however a residual $\mathbb{Z}_{2M}$ R–symmetry. This discrete non-anomalous R–symmetry rotates $(M_1M_4 - M_2M_3)$ by a phase $e^{2\pi i/M}$ and thus M branches transform into one another under the symmetry. Thus, the $\mathbb{Z}_{2M}$ is spontaneously broken down to $\mathbb{Z}_2$. On each of these branches the classical condition on the M_i's (see equation 3.2) has been modified to

$$(M_1M_4 - M_2M_3) = \left(\frac{2\Lambda^{3M+1}}{\lambda^{M-1}}\right)^{1/M} \tag{3.15}$$

This is the equation for a *deformed* conifold. Indeed, in terms of the variables in equation 3.2 the deformed conifold obeys the relation

$$xy - zw = \epsilon^2 \tag{3.16}$$

which is exactly the same as the one above. Klebanov and Strassler have thus shown how fractional branes can lead to a theory which flows in the IR to $SU(M)$ and exhibits many of the qualitative properties of pure $SU(M)$ Yang–Mills, such as domain walls, confinement, magnetic screening and other related phenomena. Also, the infrared dynamics is closely related to the geometry since the non-perturbative effects encode the *deformation* of the singularity (i.e blow-up of an S^3).

3.2.2 Extension to other singularities

As we saw in the previous section, the infrared dynamics of the gauge theory of D3–branes at a conifold singularity is closely related to the geometry. Indeed, non-perturbative effects in the infrared cause a deformation of the singularity. Thus, one can wonder if any toric singularities which admit deformation will exhibit similar infrared dynamics. This is what was done in [13] and we summarize their results in this section.

del Pezzo surfaces

del Pezzo surfaces are as affine cones over B_k, where B_k is $\mathbf{P^2}$ blown up at k points. dP_0 is $\mathbb{C}^3/\mathbb{Z}_3$ and whereas dP_1, dP_2, dP_3 are toric, $dP_4, \ldots, dP_8$ are not. Non-generic blow-ups which lead to toric geometries have been constructed for the latter and these are the so-called Pseudo del Pezzos (see [45, 19, 48, 47, 46, 49] for more details on the geometry and the construction of the corresponding quiver diagrams).

The cone over dP_0 does not admit any fractional branes and therefore cannot be taken away from the conformal regime. The quiver diagram for the cone over dP_1 is presented in Figure 3.4. The corresponding superpotential is (a trace is implied)

$$W = \epsilon_{\alpha\beta} X_{34}^{\alpha} X_{41}^{\beta} X_{13} - \epsilon_{\alpha\beta} X_{34}^{\alpha} X_{42} X_{23}^{\beta} + \epsilon_{\alpha\beta} X^{12} X_{34}^{3} X_{41}^{\alpha} X_{23}^{\beta} \tag{3.17}$$

The web diagram is shown in the figure below, where one clearly sees that it does not admit any complex deformation since there are no sub-webs in equilibrium.

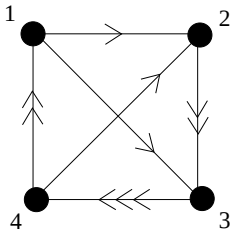

Figure 3.4: Quiver diagram for D3-branes at the cone over dP_1.

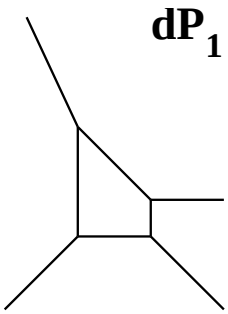

Figure 3.5: Web diagram for the cone over dP_1

This theory admits one kind of fractional brane, given by the rank vector $(0, 3, 1, 2)$. The number and rank of the fractional branes is determined as follows. Given a quiver diagram one can assign arbitrary rank to each node consistent with cancellation of anomalies[4]. Now, cancellation of anomalies imposes that at each node, the number of chiral multiplets in the fundamental representation (number of flavors) is equal to the number of chiral multiplets in the anti–fundamental representation. Thus, in this case, defining N_i as the rank of node i (see Figure 3.4). We obtain the system of equations

$$\begin{aligned} N_3 + N_2 &= 2N_4 \\ N_1 + N_4 &= 2N_3 \\ N_1 + 2N_2 &= 3N_4 \\ 2N_1 + N_2 &= 3N_3 \end{aligned}$$

This gives two independent equations

$$\begin{aligned} N_3 + N_2 &= 2N_4 \\ N_1 + N_4 &= 2N_3 \end{aligned}$$

[4]This corresponds to D–branes wrapped on collapsed cycles at the singularity, consistent with cancellation of RR tadpoles

Since we have two equations with four variables, we obtain two independent solutions

$$N_1 = N_2 = N_3 = N_4 \quad \text{and} \quad N_1 = 0\ ,\ N_2 = 3\ ,\ N_3 = 1\ ,\ N_4 = 2 \tag{3.18}$$

The first is a D3–brane, the second is a fractional brane. The addition of these fractional branes leads to an RG cascade . The superpotential (3.17) preserves an $SU(2) \times U(1)$ global symmetry. The R-charges turn out to be irrational numbers. This is the simplest example of a singularity whose gauge theory has irrational R-charges. Thus, it is very interesting to understand the associated cascades in detail.

The resulting RG flow is logarithmic and periodic. For an appropriate choice of initial couplings, the sequence of dualized nodes in a period is 2, 4, 3, 1, after which $N \to N - 4M$ and M. The quivers for several steps in the cascade are shown in Figure 3.6.

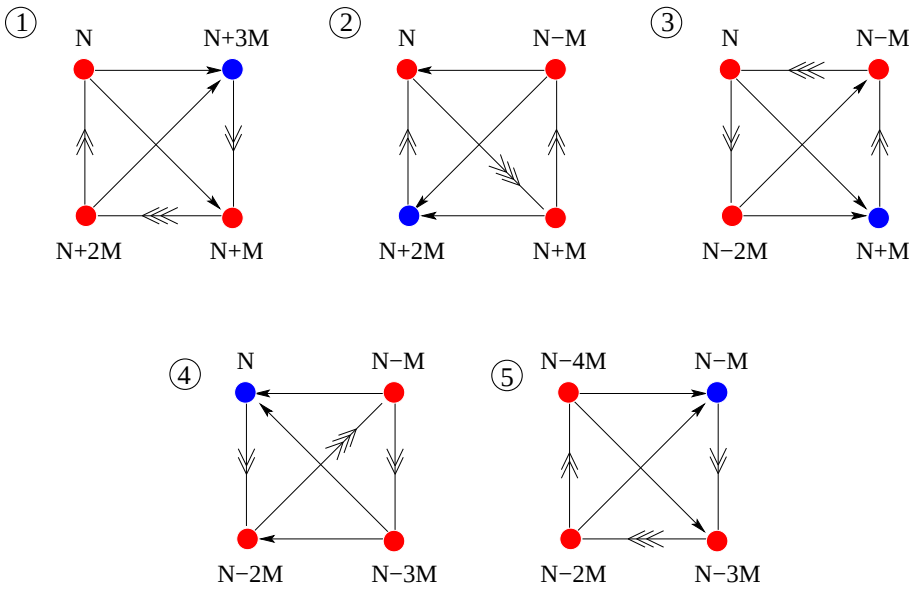

Figure 3.6: Quivers in a duality cycle in the duality cascade of dP_1. We have indicated in dark grey the dualized node at each step.

The β–functions at each step are shown in the table below,

	N_1	N_2	N_3	N_4	β_1/M	β_2/M	β_3/M	β_4/M
1	N	$N+3M$	$N+M$	$N+2M$	$-10+\sqrt{13}$	$\mathbf{10-\sqrt{13}}$	$22-7\sqrt{13}$	$-22+7\sqrt{13}$
2	N	$N-M$	$N+M$	$N+2M$	$22-7\sqrt{13}$	$-10+\sqrt{13}$	$-22+7\sqrt{13}$	$\mathbf{10-\sqrt{13}}$
3	N	$N-M$	$N+M$	$N-2M$	$-22+7\sqrt{13}$	$22-7\sqrt{13}$	$\mathbf{10-\sqrt{13}}$	$-10+\sqrt{13}$
4	N	$N-M$	$N-3M$	$N-2M$	$\mathbf{10-\sqrt{13}}$	$-22+7\sqrt{13}$	$-10+\sqrt{13}$	$22-7\sqrt{13}$
5	N	$N-4M$	$N-3M$	$N-2M$	$-10+\sqrt{13}$	$\mathbf{10-\sqrt{13}}$	$22-7\sqrt{13}$	$-22+7\sqrt{13}$

(3.19)

where we have indicated the beta functions of the dualized nodes with a bold font.

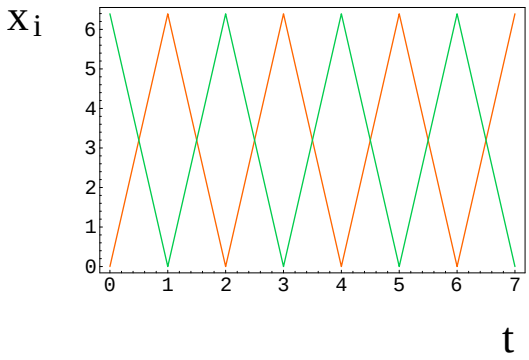

Figure 3.7: Evolution of the inverse squared couplings $x_i = 8\pi^2/g_i^2$ as a function of $t = \log \mu$ for the dP_1 cascade under consideration. UV couplings have been chosen respecting the quiver symmetries and such that the sequence given by Figure 3.6 and table 3.19 is followed. x_1 and x_2 start at the top left, x_3 and x_4 start at the bottom left.

As already mentioned, the geometry does not admit a complex deformation, hence the naked singularity at the infrared is not removed by this mechanism. We will deal with this case in the next section.

The first non-trivial example of complex deformation is provided by the cone over dP_2. The web diagram is shown in Figure 3.8a, and the corresponding quiver diagram is shown in Figure 3.9.

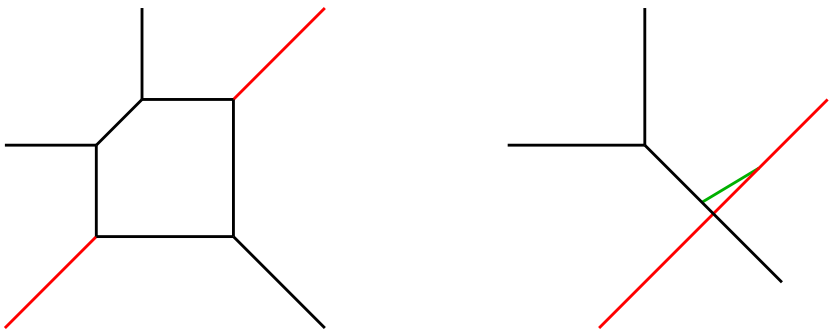

Figure 3.8: The web diagram for the complex cone over dP_2 and its complex deformation.

The superpotential for this theory is given by

$$\begin{aligned} W &= X_{34}X_{45}X_{53} - (X_{53}Y_{31}X_{15} + X_{34}X_{42}Y_{23}) \\ &+ (Y_{23}X_{31}X_{15}X_{52} + X_{42}X_{23}Y_{31}X_{14}) - X_{23}X_{31}X_{14}X_{45}X_{52} \end{aligned} \tag{3.20}$$

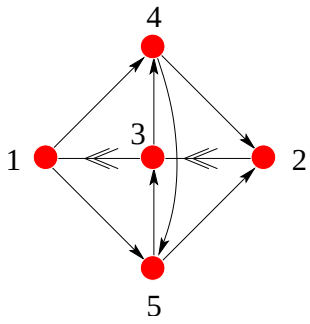

Figure 3.9: Quiver diagram for D3-branes at the cone over dP_2.

The two independent fractional branes can be taken to correspond to the rank vectors $(1,1,0,0,0)$ and $(0,1,0,1,-1)$.

The cascade ending in the deformation shown in Figure 3.8b corresponds to the first type of fractional brane. We thus proceed to study it, taking initial ranks of the form

$$\vec{N} = N(1,1,1,1,1) + M(1,1,0,0,0) \tag{3.21}$$

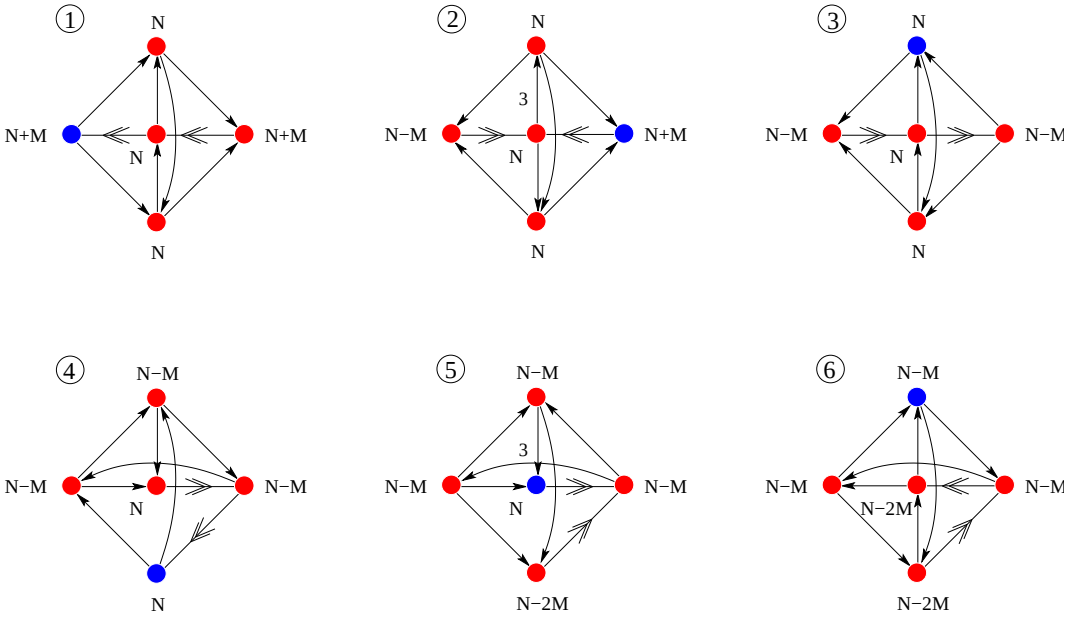

Figure 3.10: Some quivers in a duality cycle in the duality cascade of dP_2. We have indicated in black the dualized node at each step.

The sequence of gauge group ranks and beta functions for the gauge couplings is given by the table below

	N_1	N_2	N_3	N_4	N_5	β_1/M	β_2/M	β_3/M	β_4/M	β_5/M
1	$N+M$	$N+M$	N	N	N	**3**	3	$\frac{3}{4}(-9+\sqrt{33})$	$\frac{3}{8}(1-\sqrt{33})$	$\frac{3}{8}(1-\sqrt{33})$
2	$N-M$	$N+M$	N	N	N	-3	**3**	0	0	0
3	$N-M$	$N-M$	N	N	N	-3	-3	$\frac{3}{4}(9-\sqrt{33})$	$\frac{\mathbf{3}}{\mathbf{8}}(\mathbf{-1+\sqrt{33}})$	$\frac{3}{8}(-1+\sqrt{33})$
4	$N-M$	$N-M$	N	$N-M$	N	$\frac{3}{8}(1-\sqrt{33})$	$\frac{3}{4}(-9+\sqrt{33})$	3	$\frac{3}{8}(1-\sqrt{33})$	**3**
5	$N-M$	$N-M$	N	$N-M$	$N-2M$	0	0	**3**	0	-3
6	$N-M$	$N-M$	$N-2M$	$N-M$	$N-2M$	$\frac{3}{8}(-1+\sqrt{33})$	$\frac{3}{4}(9-\sqrt{33})$	-3	$\frac{\mathbf{3}}{\mathbf{8}}(\mathbf{-1+\sqrt{33}})$	-3

(3.22)

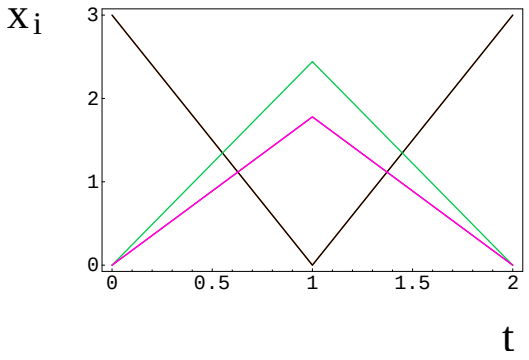

Figure 3.11: Evolution of the inverse squared couplings $x_i = 8\pi^2/g_i^2$ as a function of $t = \log \mu$ for some steps in the dP_2 cascade under consideration. UV couplings have been chosen respecting the quiver symmetries and such that the sequence given by Figure 3.10 and equation 3.22 is followed. From the middle, x_1 and x_2 are in black, x_3 is at the top, and x_4 and x_5 are in the middle.

Figure 3.11 shows a typical evolution of gauge couplings in this case. For simplicity, Figure 3.10 and the above table only show six steps in the duality cascade. At the end of this pattern of dualization, one obtains a quiver similar to the original one, up to a reduction of the number of D3-branes and a rotation of the diagram. Hence continuation of this pattern eventually leads to a full duality cycle, and thus a periodic cascade.

Let us now explore the behavior of the theory for a small number of regular D3-branes, which corresponds to the infrared of the RG cascade. For that, we consider M D3-branes probing the theory at the IR end of the cascade. Recall that since fractional branes are D5–branes wrapped on collapsed two-cycles, they are not free to move in the transverse geometry. One thus needs to add D3–branes to probe this space. Now let us consider the gauge theory described by the rank vector

$$\vec{N} = M(1,1,1,1,1) + M(1,1,0,0,0) \tag{3.23}$$

In this situation the nodes 1 and 2 have $N_f = N_c$ and develop a quantum deformed moduli space (see appendix A). The meson fields for nodes 1 and 2 are

$$\mathcal{M} = \begin{bmatrix} M_{34} & M_{35} \\ \tilde{M}_{34} & \tilde{M}_{35} \end{bmatrix} = \begin{bmatrix} X_{31}X_{14} & X_{31}X_{15} \\ Y_{31}X_{14} & Y_{31}X_{15} \end{bmatrix} \quad ; \quad \mathcal{N} = \begin{bmatrix} N_{43} & N_{53} \\ \tilde{N}_{43} & \tilde{N}_{53} \end{bmatrix} = \begin{bmatrix} X_{42}X_{23} & X_{52}X_{23} \\ X_{42}Y_{23} & X_{52}Y_{23} \end{bmatrix}$$

The quantum modified superpotential becomes

$$\begin{aligned} W &= X_{34}X_{45}X_{53} - (X_{53}Y_{31}X_{15} + X_{34}X_{42}Y_{23}) \\ &+ (Y_{23}X_{31}X_{15}X_{52} + X_{42}X_{23}Y_{31}X_{14}) - X_{23}X_{31}X_{14}X_{45}X_{52} \\ &+ X_1\left(\det\mathcal{M} - \mathcal{B}\tilde{\mathcal{B}} - \Lambda^{4M}\right) + X_2\left(\det\mathcal{N} - \mathcal{C}\tilde{\mathcal{C}} - \Lambda^{4M}\right) \end{aligned} \tag{3.24}$$

Along the mesonic branch we have

$$\begin{gathered} X_1 = \Lambda^{4-4M} \quad ; \quad \mathcal{B} = \tilde{\mathcal{B}} = 0 \quad ; \quad X_2 = -\Lambda^{4-4M} \quad ; \quad \mathcal{C} = \tilde{\mathcal{C}} = 0 \\ \det\mathcal{M} = \Lambda^{4M} \quad ; \quad \det\mathcal{N} = \Lambda^{4M} \end{gathered} \tag{3.25}$$

The expectation values for the mesons higgs the gauge group to a single diagonal combination of the nodes 3, 4 and 5. Restricting to the Abelian case, the superpotential becomes

$$\begin{aligned} W &= X_{34}X_{45}X_{53} - N_{53}M_{34}X_{45} - X_{53}\tilde{M}_{35} - X_{34}\tilde{N}_{43} \\ &+ \tilde{N}_{53}M_{35} + N_{43}\tilde{M}_{34} + M_{34}\tilde{M}_{35} - \tilde{M}_{34}M_{35} - N_{43}\tilde{N}_{53} + \tilde{N}_{43}N_{53} \end{aligned} \tag{3.26}$$

where M_{ij}, N_{ij} are the fluctuations around the minimum (see [13] for details). Integrating out the massive fields, we replace them by their equations of motion, this gives

$$M_{34} = X_{53} \quad , \quad M_{35} = N_{43} \quad , \quad X_{34} = N_{53} \tag{3.27}$$

Plugging this into (3.26) gives

$$W = X_{34}X_{45}X_{53} - X_{34}X_{53}X_{45} \tag{3.28}$$

Renaming $X_{34} = X$, $X_{45} = Y$ and $X_{53} = Z$, we obtain the $\mathcal{N} = 4$ field content and superpotential

$$W = X[Y, Z] \tag{3.29}$$

which in any event vanishes in the Abelian case, but is crucial in non-Abelian situations. Hence, the moduli space of the D3-brane probes is given by the complex deformation of the cone over dP_2 to a smooth space, as expected from the geometrical analysis.

The suspended pinch point

To illustrate that the ideas of cascades and infrared deformations are very general, we would like to consider a further example, based on the suspended pinch point (SPP) singularity. This geometry is given by the equation $xy = zw^2$ in complex variables. Its web diagram is shown in Figure 3.12a, while its deformation is shown in Figure 3.12b.

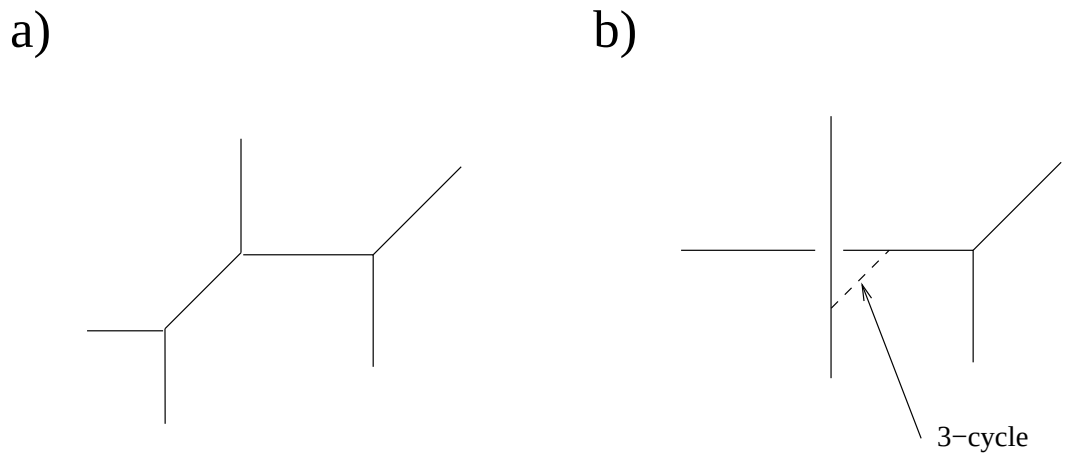

Figure 3.12: Web diagram for the SPP and its deformation to a smooth geometry.

The quiver diagram was determined in [8, 11] and is shown in figure 3.13a, and the superpotential is

$$W = X_{21}X_{12}X_{23}X_{32} - X_{32}X_{23}X_{31}X_{13} + X_{13}X_{31}X_{11} - X_{12}X_{21}X_{11} \tag{3.30}$$

The theory is non-chiral so the ranks of the gauge groups are independent, so there are two independent fractional branes, which can be taken to be $(0, 1, 0)$ and $(0, 0, 1)$. The theory has a very nice and simple duality cascade, which as we show ends in the deformed geometry shown in Figure 3.12b. Similarly to what happens in the flows considered for dP_1 and dP_2, this cascade shares a very special feature with the conifold cascade: it is periodic and involves a single quiver. Considering the starting point given by the ranks

$$\vec{N} = N(1, 1, 1) + M(0, 1, 0) \tag{3.31}$$

By following the pattern of dualizing the most strongly coupled node at each step, one is led to a cascade that repeats the following sequence of dualizations $(2, 1, 3, 2, 1, 3)$. The quiver theories at each step of this sequence are shown in figure 3.14. The node in dark grey indicates the one that gets dualized at each step.

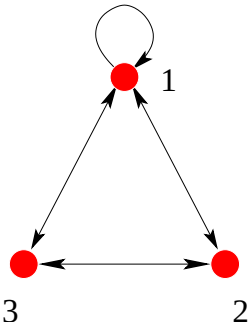

Figure 3.13: Quiver diagram for SPP.

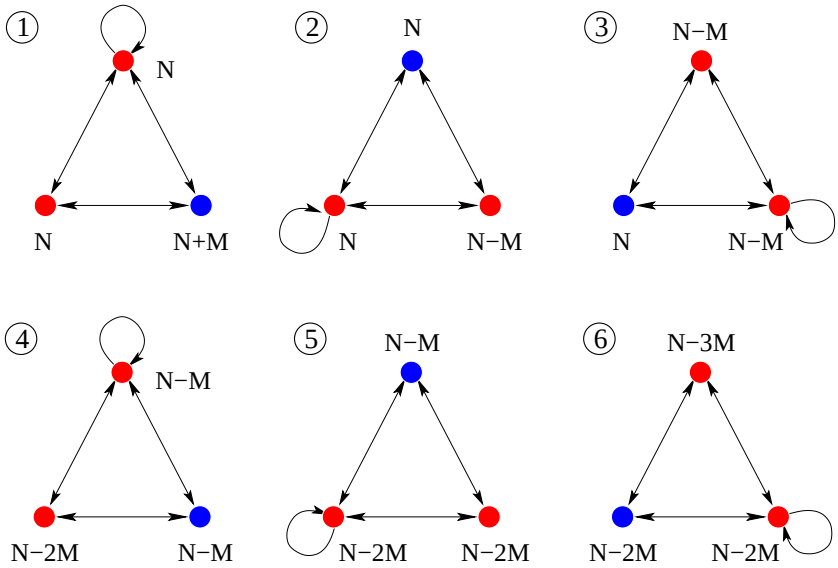

Figure 3.14: Sequence of quivers in one period of the SPP cascade. We have indicated in dark grey the dualized node at each step.

In more detail, the ranks of the gauge groups and the β–functions for this series of dualizations are

	N_1	N_2	N_3	β_1/M	β_2/M	β_3/M
1	N	$N+M$	N	$-3/2$	**3**	$-3/2$
2	N	$N-M$	N	**3/2**	-3	$3/2$
3	$N-M$	$N-M$	N	$-3/2$	$-3/2$	**3**
4	$N-M$	$N-M$	$N-2M$	$3/2$	**3/2**	-3
5	$N-M$	$N-2M$	$N-2M$	**3**	$-3/2$	$-3/2$
6	$N-3M$	$N-2M$	$N-2M$	-3	$3/2$	**3/2**
7	$N-3M$	$N-2M$	$N-3M$	$-3/2$	**3**	$-3/2$

(3.32)

After six dualizations (step **7** in the previous table), the quiver comes back to itself, with $N \to N-3M$ and M constant.

It is important that at every step in the cascade the most strongly coupled node is never the one with the adjoint chiral field. This allows the cascade to proceed via standard Seiberg dualizations. In the previous table, bold font has been used for the β–function of the dualized node at each step. It still remains to show that it is possible to choose initial couplings such that the proposed dualities take place along the RG flow. In fact, it is possible to do so, as shown in Figure 3.15 for a particular choice of UV couplings. Moreover, the pattern is completely generic.

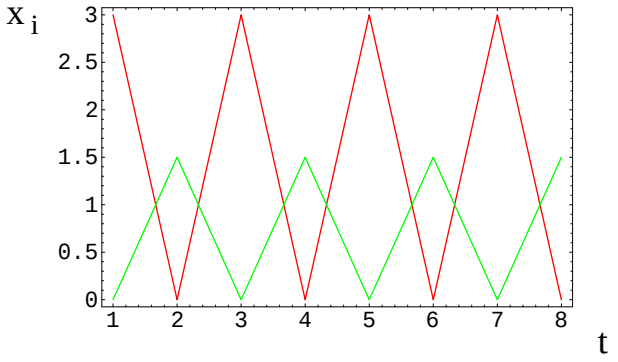

Figure 3.15: Evolution of the inverse squared couplings $x_i = 8\pi^2/g_i^2$ as a function of $t = \log\mu$ for the SPP cascade. Dark grey lines indicate x_2 and light grey lines indicate x_1 and x_3.

As usual, the cascade proceeds until the effective number of D3-branes is comparable to M. At this point, the gauge theory strong dynamics take over and induce a geometric transition. Indeed, the SPP singularity admits a complex deformation, shown in figure 3.12b.

In order to study the infrared end of the cascade, one studies the gauge theory describing M D3-branes probing it. This corresponds to the quiver theory with rank vector

$$\vec{N} = M(1,1,1) + M(0,1,0) \tag{3.33}$$

In this case, one only need consider mesons and baryons for node 2. The mesons are given by

$$\mathcal{M} = \begin{bmatrix} M_{13} & M_{11} \\ M_{33} & M_{31} \end{bmatrix} = \begin{bmatrix} X_{12}X_{23} & X_{12}X_{21} \\ X_{32}X_{23} & X_{32}X_{21} \end{bmatrix} \tag{3.34}$$

Since node 2 has $N_f = N_c$, it develops a quantum deformed moduli space, the superpotential becomes

$$\begin{aligned} W = & - M_{33}X_{31}X_{13} + X_{13}X_{31}X_{11} - M_{11}X_{11} + M_{33}M_{11} \\ & + X\left(\det \mathcal{M} - \mathcal{B}\tilde{\mathcal{B}} - \Lambda^{4M}\right) \end{aligned} \tag{3.35}$$

Choosing the mesonic branch gives

$$\det \mathcal{M} = \Lambda^{4M} \quad ; \quad \mathcal{B} = \tilde{\mathcal{B}} = 0 \quad ; \quad X = \Lambda^{4-4M} \tag{3.36}$$

Restricting to the Abelian case, the superpotential reads

$$W = -M_{33}X_{31}X_{13} + X_{13}X_{31}X_{11} - M_{11}X_{11} + M_{33}M_{11} \tag{3.37}$$

Since M_{11} is massive, we integrate it out using its equation of motion, which reads $X_{11} = M_{33}$, so

$$W = -M_{33}X_{31}X_{13} + X_{13}X_{31}M_{33} \tag{3.38}$$

The gauge group is $SU(M)$ (due to the breaking by meson vevs $M \propto \mathbf{1}$). All three fields transform in the adjoint representation (a singlet in the Abelian case). The above theory clearly describes the field content and superpotential of $\mathcal{N} = 4$ SYM, i.e. the theory describing the smooth geometry left over after the deformation.

In addition, there remain some additional light fields, namely M_{11}, M_{13}, M_{31}, M_{33}, subject to the constraint

$$M_{13}M_{31} - M_{33}M_{11} = \Lambda^4 \tag{3.39}$$

The dynamics is that of probe D3-branes in the geometry corresponding to the deformation of the SPP to flat space. This matches nicely the geometric expectation,

from the web diagrams in Figure 3.12, from which one sees that the result of the deformation is a smooth geometry.

The relation between the field theory and the more geometrical description of the deformation can be done also using the toric geometry language. Now, as explained in appendix A, the solution to the D-term equations, modulo gauge transformations is given by the gauge invariant monomials. These are

$$x = X_{13}X_{32}X_{21}, \quad y = X_{31}X_{12}X_{23}, \quad z = X_{11}, \quad w = X_{13}X_{31} \tag{3.40}$$

Writing this in terms of mesons gives

$$x = X_{13}M_{31}\ ,\ y = X_{31}M_{13}\ ,\ z = X_{11}\ ,\ w = M_{11} \tag{3.41}$$

Now, we also have to solve the F-term equations for the superpotential (3.35) and this gives $X_{13}X_{31} = M_{11}$ and $X_{11} = M_{33}$ (where we have not taken the $X\,(\det \mathcal{M} - \mathcal{B}\tilde{\mathcal{B}} - \Lambda^{4M})$ term into account). So we get the monomials

$$x = X_{13}M_{31}\ ,\ y = X_{31}M_{13}\ ,\ z = X_{11} = M_{33}\ ,\ w = X_{13}X_{31} = M_{11} \tag{3.42}$$

Since $M_{31}M_{13} = M_{33}M_{11}$ (see eq 3.34) it is easy to see that the monomials satisfy $xy - zw^2 = 0$ at the classical level, namely

$$X_{13}X_{31}(M_{31}M_{13} - M_{33}M_{11}) = 0 \tag{3.43}$$

However, the quantum deformation of the moduli space of the field theory imposes $M_{31}M_{13} - M_{33}M_{11} = \Lambda^4$, and thus leads to

$$X_{13}X_{31}(M_{31}M_{13} - M_{33}M_{11}) = \epsilon X_{13}X_{31} \tag{3.44}$$

which in terms of the monomials can be written as $xy - zw^2 = \epsilon w$. This is the equation for the geometric deformation in Figure 3.12b. Thus the description provided has a direct link with the geometric description of the deformation. There is a subtle point which needs clarifying. At first sight there might seem to be a contradiction since from eq 3.38 we obtained $\mathcal{N} = 4$ SYM and a moduli space which is just flat space. Whereas in the above analysis we found that the moduli space was the SPP or deformed SPP (when the quantum deformation in the infrared is taken into account). The crucial point is that to obtain eq 3.38, we had to impose the vevs in eq 3.36 and thus went to a specific point in moduli space. At this point, the space is flat. Whereas in the above analysis we did not assign any vevs, so the moduli space is that of the full geometry.

A similar analysis was also carried out for numerous other geometries in [13].

3.3 Fractional Branes and Dynamical Supersymmetry Breaking

In the two previous sections we saw that fractional branes placed at toric singularities which admit deformation (blow-up of an S^3) generically lead to confining gauge theories in the infrared. Henceforth we shall refer to these as 'deformation fractional branes.

There is another class of fractional branes which generically lead to $\mathcal{N} = 2$ gauge theories in the infrared. The simplest examples are provided by fractional branes whose quiver (i.e. the quiver in the absence of any other type of fractional branes or probe D3-branes) corresponds to a closed loop of arrows passing through all nodes, with the corresponding gauge invariant polynomial not appearing in the superpotential. The vev for this operator is F-flat, and parametrizes a one-dimensional moduli space, along which the dynamics has an accidental $N = 2$ supersymmetry (8 supercharges) and in the simplest case is described by an $N = 2$ SYM theory. Geometrically, these fractional branes appear for non-isolated singularities, which have (complex) curves of singularities passing through the origin. The fractional branes wrap the 2-cycles collapsed at the singularity, which exist at any point in the curve. For toric geometries, the singularity on the curve is always of $\mathbb{C}^2/\mathbb{Z}_N$ type. The curves of singularities are associated to the existence of points on the boundary of the toric polygon, or equivalently to parallel semi-infinite legs in the dual web diagram.

As we saw in the previous section, there are toric singularities such as the cone over dP_1, which do not admit deformation. It therefore remains an open question to determine the gauge theory in the infrared for such singularities. As we will show in the following, these theories generically lead to Dynamical Supersymmetry Breaking (DSB). The prototypical field theory for such fractional branes corresponds to a set of nodes of generically different ranks, with bi-fundamental matter. The non-perturbative dynamics typically contains a contribution from a node generating a non-perturbative Affleck, Dine, Seiberg (ADS) superpotential (see appendix on supersymmetry). In cases with classical flat directions, they are lifted in a runaway fashion by this superpotential. In cases without flat directions, DSB arises from an incompatibility between the ADS superpotential and the classical potential forcing all vevs to vanish (one recovers runaway behavior when Fayet-Illiopoulos (FI) terms are considered dynamical, or equivalently when one eliminates the $U(1)$ factors and

allows for dibaryonic operators).

An important point is that the generic fractional brane case falls in this class. More concretely, generically the combination of an $N = 2$ fractional brane with a deformation fractional brane is a DSB combination. Also, in general the combination of two deformation fractional branes, for different and incompatible deformations, is also a DSB fractional brane. Examples will make this clearer.

3.3.1 The dP_1 case

The dP_1 theory provides the simplest example of a duality cascade with fractional branes, where the infrared behavior is not described by confinement/complex deformation (or by $N = 2$ like dynamics). Namely, from the web diagram in Figure 3.16, there is no possibility of splitting a subweb in equilibrium, hence there are no complex deformations of this geometry.

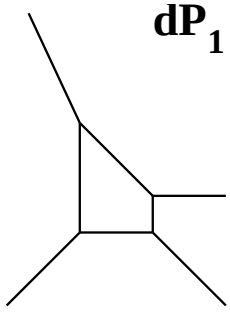

Figure 3.16: Web diagram for the cone over dP_1

In this section the dP_1 gauge theory is studied in detail, thus providing a proposal for the IR behavior.

Quiver theory and UV cascade

Consider the cone over dP_1 geometry. The quiver field theory on D3-branes at this singularity has been constructed in [19].

Out of the different Seiberg dual theories corresponding to this geometry, we focus on the phase with quiver diagram shown in Figure 3.17 and superpotential

$$W = \epsilon_{\alpha\beta} X^{\alpha}_{23} X^{\beta}_{34} X_{42} + \epsilon_{\alpha\beta} X^{\alpha}_{34} X^{\beta}_{41} X_{13} - \epsilon_{\alpha\beta} X_{12} X^{\alpha}_{23} X^{3}_{34} X^{\beta}_{41} \tag{3.45}$$

where α, β take values in $1, 2$ and label a doublet representation of $SU(2)$. Also, subindices indicate the bifundamental representation under the corresponding nodes. The web diagram is shown in Figure 3.16.

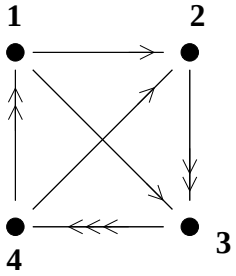

Figure 3.17: Quiver diagram for the dP_1 theory

There is only one kind of fractional brane, corresponding to the rank vector $(0, 3, 1, 2)$. Starting with ranks $(N, N + 3M, N + M, N + 2M)$, this fractional brane triggers a duality cascade. Along the cascade, the effective number of D3-branes decreases, while the number of fractional branes remains constant. Hence, for a suitable UV choice of the number of D3-branes N, the infrared limit of the cascade is expected to be described by the theory in Figure 3.18, in which the smallest rank node has reached zero rank and disappeared from the quiver.

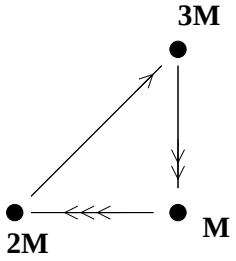

Figure 3.18: The theory at the end of the duality cascade triggered by M fractional branes. Here labels indicate ranks for the node gauge factors.

Notice that this gauge theory does not correspond to the quiver of a deformation brane. For instance, it does not correspond to a set of decoupled $SU(M)$ SYM theories without matter. The quiver in Figure 3.18 should be contrasted with what happens for example in the well studied example of the conifold, where there are no bifundamental fields unless D3-branes are included. Hence, we expect a behavior which is qualitatively different from that of the conifold [20]. Indeed, this is also supported by the geometric side, since the web diagram in Figure 3.16 does not admit a recombination of external legs into a subweb in equilibrium. Namely, the

cone over dP_1 does not admit a complex deformation or extremal transition in which 2- and 4-cycles disappear and 3-cycles grow (as in Figure 3.2 for the conifold).

It is an interesting question to find the field theory dynamics which dominates the infrared limit of this cascade, and its corresponding gravity dual. In the coming sections a simple field theory analysis is carried out to show that the answer is dynamical supersymmetry breaking.

Dynamical supersymmetry breaking in dP_1

-Field theory analysis

The dynamics of the infrared limit of the cascade is controlled by the quiver theory of Figure 3.18. It corresponds to considering M fractional D-branes, without any D3-branes, $N = 0$. It leads to a theory with gauge group $SU(3M)_2 \times SU(M)_3 \times SU(2M)_4$, with fields X_{42}, $X_{23} = X^1_{23}$, $Y_{23} = X^2_{23}$, $X_{34} = X^1_{34}$, $Y_{34} = X^2_{34}$, $Z_{34} = X^3_{34}$ (where we have simplified notation with respect to that of equation 3.45), and superpotential

$$W = X_{42}X_{23}Y_{34} - X_{42}Y_{23}X_{34} \tag{3.46}$$

There are several ways to support the idea of the onset of dynamical supersymmetry breaking in this theory, by using several standard criteria (see [23] for a very complete introduction to DSB). One of the simplest ways is as follows: Consider a theory without classical flat directions, and such that the classical D and F-term constraints force all vevs of the theory to vanish. In such a situation, if one of the gauge factors of the theory has $N_f < N_c$, then the non-perturbative Affleck-Dine-Seiberg superpotential (see appendix A) for its mesons diverges at the origin, and pushes the corresponding vevs towards infinity. The theory breaks supersymmetry due to the impossibility to satisfy all F and D-term constraints, coming from classical and quantum contributions. The combination of the classical and the non-perturbative superpotential lead to a scalar potential with a minimum at non-zero energy. A detailed application to the dP_1 case follows.

Furthermore, based on the physical interpretation of fractional branes, it is easy to realize that the above theory does not have flat directions (since they would correspond to removal of the branes out of the singularity, which is not possible for fractional branes). This can also be directly recovered from the field theory analysis, by looking for D and F-flat directions. However, a crucial issue in getting

the correct result is the following. The string theory construction leads to a gauge group $U(3M) \times U(M) \times U(2M)$. The three $U(1)$ factors in this gauge group have $B \wedge F$ couplings to 2-forms which are localized at the singularity (these arise from reduction of the RR 6- and 4-form on the 4- and the two 2-cycles on the cone over dP_1). These couplings of the form $\int d^4x (A_\mu - \partial_\mu c^{(0)})^2$ with $c^{(0)}$ a scalar [12] (which are crucial in the Green-Schwarz cancellation of mixed anomalies [50]) make the $U(1)$'s massive, so that they are not present at low energies. On the other hand, the D-term constraints with respect to these $U(1)$'s remain, and have to be taken into account in order to derive the correct moduli space. This is implicit in the statement (implied by supersymmetry) that the NSNS partners of the above RR fields couple to the D-branes as Fayet-Illiopoulos terms. The coupling has the form $\int d^4x \phi \int d^2\theta d^2\bar{\theta} V$ with ϕ a scalar and V a vector supermultiplet, the FI term thus becomes a vev [12].

We thus parametrize D-flat directions by operators invariant under the $SU(3M) \times SU(M) \times SU(2M)$ gauge symmetry [5]. There are 6 such operators,

$$\begin{aligned} &X_{42}X_{23}X_{34}, \quad X_{42}X_{23}Y_{34}, \quad X_{42}X_{23}Z_{34}, \\ &X_{42}Y_{23}X_{34}, \quad X_{42}Y_{23}Y_{34}, \quad X_{42}Y_{23}Z_{34}. \end{aligned} \tag{3.47}$$

In order to impose F-flatness, we use e.g. the equations of motion

$$\frac{\partial W}{\partial Y_{34}} = X_{42}X_{23} = 0 \quad , \quad \frac{\partial W}{\partial X_{34}} = X_{42}Y_{23} = 0 \tag{3.48}$$

so that all operators are forced to vanish, and the origin is the only supersymmetric point. The classical superpotential thus lifts all flat directions.

It is now easy to argue that this theory breaks supersymmetry. Consider the regime where the $SU(3M)$ gauge factor dominates the dynamics. Since $SU(3M)$ has $2M$ flavors, we have $N_f < N_c$ for this theory, and it generates a non-perturbative Affleck-Dine-Seiberg superpotential which pushes the vevs for the $SU(3M)$ mesons $X_{42}X_{23}$ and $X_{42}Y_{23}$ away from zero. Combining this with the classical superpotential, we conclude that supersymmetry is broken. A more detailed analysis is presented below, in a slightly different limit.

An independent argument for DSB in this theory follows from the following alternative criterion. In a theory with no classical flat directions and with some

[5] Recall that looking for the possible vevs for the gauge invariant operators of a theory is equivalent to solving the D–term equations (see appendix A)

spontaneously broken global symmetry, supersymmetry breaking occurs (see e.g. [23]). The argument is that the complex scalar in the Goldstone supermultiplet would parametrize a non-compact flat direction, which would reach the semiclassical regime, in contradiction with the absence of classical flat directions. With supersymmetry breaking, the Goldstone boson still parametrizes a compact flat direction, but the non-compact direction associated to its partner is lifted[6]. In the present case, the theory originally has a global $SU(2)$ symmetry, under which the $SU(3M)$ mesons $X_{42}X_{23}$ and $X_{42}Y_{23}$ transform in the spin-1/2 representation. The global $SU(2)$ is thus spontaneously broken by the meson vevs triggered by the ADS superpotential. Hence the criterion for DSB is satisfied.

The physical realization of the gauge field theory in terms of fractional D-branes makes also clear that there should exist a non-supersymmetric minimum at finite distance in field space, since the scalar potential grows both for large and small vevs.

Some qualitative features of the remaining theory at the minimum can be suggested. By taking the most symmetric choice of $SU(3M)$ meson vevs $\mathcal{M} = \mathbf{1}$, the gauge symmetry $SU(2M) \times SU(M)$ is broken to just $SU(M)$. In addition, the superpotential makes the mesons massive together with the X_{34} and Y_{34} fields. Hence at the minimum we have an $SU(M)$ theory with some adjoint matter (coming e.g. from the Z_{34} fields). A more detailed description of the minimum is also possible in other regimes, e.g. when the $SU(2M)$ dynamics dominates (see below).

-Analysis in a different regime

The physics of the model can be analyzed also in other regimes, e.g. when the $SU(2M)$ dynamics dominates, this is due to the fact that if DSB occurs, it occurs in all regimes [23]. Consider the above $SU(3M)_2 \times SU(M)_3 \times SU(2M)_4$, with weakly gauged $SU(3M) \times SU(M)$, and dynamics dominated by the $SU(2M)$ factor. We can analyze the resulting dynamics by replacing it by its Seiberg dual. The gauge group of the resulting theory is $SU(3M)_2 \times SU(M)_3 \times SU(M)_4$. The fields include

[6]More precisely, the initial theory obeys two conditions, no flat directions and a spontaneously broken symmetry. Now, since the theory has a spontaneously broken symmetry, the goldstone theorem implies that there is a massless scalar, thus parametrizing a flat direction which is usually compact. Now since supersymmetry is not broken, this massless scalar is accompanied by another one to form the complex scalar in the chiral multiplet. This scalar also parametrizes flat directions but these are usually not compact. Thus, for this scalar, if one takes vevs giving very high masses, one should obtain the classical theory since the massive particles have little effect in the loops. Thus we obtain a contradiction since in this limit the theory has flat directions, whereas the classical theory does not. Thus supersymmetry is broken.

the original $SU(2M)$ singlets X_{23}, Y_{23}, dual quarks X_{24}, X_{43}, Y_{43}, Z_{43} and mesons $M_{32}(= X_{34}X_{42})$, $N_{32}(= Y_{34}X_{42})$, $P_{32}(= Z_{34}X_{42})$. The superpotential is

$$W = N_{32}X_{23} - M_{32}Y_{23} + X_{24}\left(X_{43}M_{32} + Y_{43}N_{32} + Z_{43}P_{32}\right) \tag{3.49}$$

The first two terms give masses to the corresponding fields. Integrating them out, we are left with a theory $SU(3M)_2 \times SU(M)_3 \times SU(M)_4$, and fields X_{24}, X_{43}, Y_{43}, Z_{43}, P_{32} as shown in Figure 3.19. The superpotential is $W = X_{24}Z_{43}P_{32}$. The

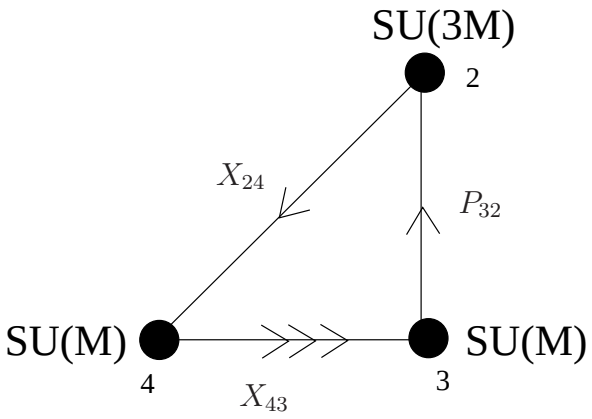

Figure 3.19: Quiver of dP_1 after $SU(2M)$ has been dualized.

$SU(2M)$ dynamics thus preserves supersymmetry. However, dynamical supersymmetry breaking is recovered when we consider the $SU(3M)$ dynamics. Taking $M = 1$ for simplicity,we see that $SU(3)$ has $N_f < N_c$ so the theory confines and generates an ADS term. The superpotential thus becomes

$$W = M_{34}Z_{43} + 2\left(\frac{\Lambda^8}{M_{34}}\right)^{1/2} \tag{3.50}$$

where $M_{34} = P_{32}X_{24}$ is the meson. Now, looking for the minimum, the F-term equations are

$$\begin{aligned} \frac{\partial W}{\partial Z_{43}} &= 0 \Rightarrow M_{34} = 0 \\ \frac{\partial W}{\partial M_{34}} &= 0 \Rightarrow Z_{43} + \Lambda^4 M_{34}^{\frac{-3}{2}} = 0 \end{aligned} \tag{3.51}$$

So the minimum occurs for $M_{34} \to 0$ and $Z_{43} = -\Lambda^4 M_{34}^{-3/2} \to \infty$. On the other hand, Z_{43} also appears in the additional $U(1)$ D-term potential, of the form $V_D = |Z_{43}|^4$, which grows for large Z_{43} vevs for fixed FI parameter, becoming a 'barrier' that prevents Z_{43} from running away. The combination of these two contributions

establishes the existence of the non-supersymmetric minimum for fixed FI terms, but a more quantitative analysis is unreliable since there is seemingly no tunable parameter which allows to make the minimum lie in the semiclassical large vev region. In the next section the effect of including the dynamics of FI terms in the analysis is discussed.

-Dynamical FI terms

In this section an important fact that was not incorporated in the above determination of the non-trivial minimum is discussed. Namely, closed string fields at the singularity are dynamical, and couple as FI terms. Taking that into account, the relevant part of the D-term potential should be written as $V_D = (|Z_{43}|^2 - \xi)^2$. This shows that one can afford to take large vevs for Z_{43} (hence making the F-terms arbitrarily small) by simply allowing for a large FI ξ (keeping the D-terms vanishing). Namely the system relaxes to minimization of its potential by dynamically allowing the closed string modes to blow up the singularity.

Hence, we conclude that the full inclusion of localized closed string fields leads to runaway behavior in those directions. One should keep in mind that this situation will hold in subsequent examples, hence the corresponding discussion will be skipped and the emphasis will simply be placed on the different gauge theory dynamics, namely the open string sector.

Additional D-brane probes

In this section we comment on the interesting question of what happens in the presence of many fractional branes and a single or a few regular D3-brane probes. The classical moduli space of this theory is the moduli space of the additional D3-brane probe(s) (while the fractional ones remain stuck at the singular point).

Consider the theory with ranks $(1, 3M+1, M+1, 2M+1)$. The gauge group is $U(1) \times U(3M+1) \times U(M+1) \times U(2M+1)$. The theory has a moduli space which corresponds to the position of the regular D3-brane in the cone over dP_1.

Once non-perturbative dynamics is taken into account, it is clear that the theory with the additional D3-brane probe does not have a vacuum and in particular there is a runaway behavior for the vevs. Starting with the gauge theory given by Figure 3.17, with superpotential

$$W = X_{23}Y_{34}X_{42} - Y_{23}X_{34}X_{42} + X_{34}Y_{41}X_{13} - Y_{34}X_{41}X_{13}$$

$$- \quad X_{12}X_{23}Z_{34}Y_{41} + X_{12}Y_{23}Z_{34}X_{41} \tag{3.52}$$

Considering the regime where the $U(3M+1)$ dynamics dominates, the $U(3M+1)$ gauge group has $2M+2$ flavors, so it develops an ADS superpotential for the mesons (since $N_f < N_c$). The superpotential thus becomes

$$\begin{aligned} W &= M_{43}Y_{34} - N_{43}X_{34} + X_{34}Y_{41}X_{13} - Y_{34}X_{41}X_{13} - M_{13}Z_{34}Y_{41} \\ &+ N_{13}Z_{34}X_{41} + \Big(\frac{\Lambda}{det\mathcal{M}}\Big)^{\frac{1}{M-1}} \end{aligned} \tag{3.53}$$

where

$$M_{13} = X_{12}X_{23},\ N_{13} = X_{12}Y_{23},\ M_{43} = X_{42}X_{23},\ N_{43} = X_{42}Y_{23} \tag{3.54}$$

and

$$\mathcal{M} = \begin{pmatrix} M_{13} & N_{13} \\ M_{43} & N_{43} \end{pmatrix} \tag{3.55}$$

Now, X_{34}, N_{43}, Y_{34}, M_{43} become massive, replacing them by their equations of motion we get

$$N_{43} = Y_{41}X_{13} \quad , \quad M_{43} = X_{41}X_{13} \tag{3.56}$$

and

$$W = N_{13}Z_{34}X_{41} - M_{13}Z_{34}Y_{41} + \Big(\frac{\Lambda}{det\begin{pmatrix} M_{13} & N_{13} \\ X_{41}X_{13} & Y_{41}X_{13} \end{pmatrix}}\Big)^{\frac{1}{M-1}} \tag{3.57}$$

and the resulting gauge theory is given by the quiver diagram below

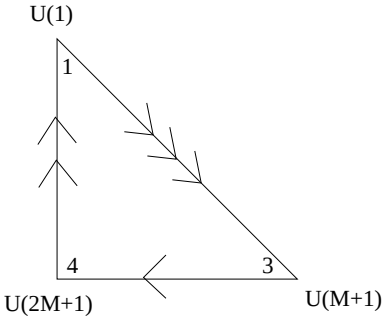

Figure 3.20: Quiver diagram after $U(3M+1)$ has confined.

The gauge invariant operators (i.e vevs from the D–term equations) are $X_{13}Z_{34}X_{41}$, $X_{13}Z_{34}Y_{41}$, $M_{13}Z_{34}X_{41}$, $M_{13}Z_{34}Y_{41}$, $N_{13}Z_{34}X_{41}$, $N_{13}Z_{34}Y_{41}$. The moduli space is determined using the F–term equations

$$\frac{\partial W}{\partial Z_{34}} = 0 \quad \Rightarrow \quad X_{41}N_{13} = Y_{41}M_{13} \tag{3.58}$$

and

$$\frac{\partial W}{\partial M^a_{13}} = 0 \ , \ \frac{\partial W}{\partial N^a_{13}} = 0 \quad \Rightarrow \quad \frac{\partial W}{\partial M^a_{13}} M^a_{13} + \frac{\partial W}{\partial N^a_{13}} N^a_{13} = 0 \tag{3.59}$$

So

$$N_{13}Z_{34}X_{41} - M_{13}Z_{34}Y_{41} - \frac{1}{M-1}\Big(\frac{\Lambda^{1/M}}{det\begin{pmatrix} M_{13} & N_{13} \\ X_{41}X_{13} & Y_{41}X_{13} \end{pmatrix}}\Big)^{\frac{M}{M-1}} det\begin{pmatrix} M_{13} & N_{13} \\ X_{41}X_{13} & Y_{41}X_{13} \end{pmatrix} = 0$$

$$\Rightarrow \quad N_{13}Z_{34}X_{41} - M_{13}Z_{34}Y_{41} - \frac{1}{M-1}\Big(\frac{\Lambda}{det\begin{pmatrix} M_{13} & N_{13} \\ X_{41}X_{13} & Y_{41}X_{13} \end{pmatrix}}\Big)^{\frac{1}{M-1}} = 0 \tag{3.60}$$

Using equation 3.58, one obtains

$$\frac{1}{M-1}\Big(\frac{\Lambda}{det\begin{pmatrix} M_{13} & N_{13} \\ X_{41}X_{13} & Y_{41}X_{13} \end{pmatrix}}\Big)^{\frac{1}{M-1}} = 0 \tag{3.61}$$

Thus showing that the vevs are pushed to infinity, exhibiting a runaway behavior. Physically, the D3-brane is repelled from the origin.

Finally, one should mention the possibility of combining different types of fractional branes to reach new physical situations and to illustrate that in general such combinations do not lead to a simple superposition of the behaviors associated to the individual branes. Consider for instance combining a fractional brane $(0, 3, 1, 2)$ with a fractional brane $(3, 0, 2, 1)$. Although each of them independently leads to DSB as described above, their combination adds up to the rank vector $(3, 3, 3, 3)$ that corresponds to a set of D3-branes, which clearly preserves supersymmetry.

3.3.2 The SPP example

In this section we consider fractional branes in the suspended pinch point (SPP) singularity, where a new effect takes place. In this theory, there exists two independent kinds of fractional branes which independently do not break supersymmetry. One kind leads to a duality cascade, confinement and complex deformation as shown in section 3.2.2, while the other belongs to an $N = 2$ subsector. However, as we will discuss, combinations of the two fractional branes may be incompatible and lead

to runaway behavior (in this case even before considering localized closed string modes/baryonic directions).

Consider the theory on D3-branes at an SPP singularity, defined by $xy = zw^2$. The theory has a quiver shown in Figure 3.21

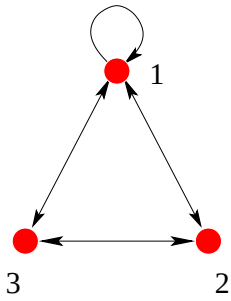

Figure 3.21: The quiver for the SPP theory

The superpotential is

$$W = X_{21}X_{12}X_{23}X_{32} - X_{32}X_{23}X_{31}X_{13} + X_{13}X_{31}X_{11} - X_{12}X_{21}X_{11} \tag{3.62}$$

There are two independent fractional branes, and a basis for them is provided by the rank vectors $(1,0,0)$ and $(0,1,0)$. The physics of each independent fractional brane is well-known. The $(0,1,0)$ triggers the complex deformation shown in Figure 3.22. The $(1,0,0)$ corresponds to a fractional brane of an $N = 2$ subsector. Notice that this kind of fractional brane has a modulus, parametrized by the adjoint chiral multiplet, that corresponds to sliding the fractional brane along the curve of A_1 singularities of the geometry, parametrized by z in $xy = zw^2$. This can be seen in the web diagram by the S^2 between two parallel exterior lines (in Figure 3.22b take the S^3 to zero). Since the size of the S^2 does not change along these two lines, it costs no energy to move it in this direction, thus leading to a singularity parametrized by a line[7].

It is natural to consider what happens when both kinds of fractional branes are simultaneously present. In the following, we consider the generic case where the

[7]For a complex manifold defined by an algebraic equation in complex variables e.g $xy = zw^2$, an easy way to find the singular points is

$$\begin{array}{rcl} f & \equiv & xy - zw^2 \\ \dfrac{\partial f}{\partial x} & = & 0 \Rightarrow y = 0 \quad ; \quad \dfrac{\partial f}{\partial y} = 0 \Rightarrow x = 0 \quad ; \quad \dfrac{\partial f}{\partial z} = 0 \Rightarrow w = 0 \quad ; \quad \dfrac{\partial f}{\partial w} = 0 \Rightarrow zw = 0 \end{array}$$

So the singular points are at $x = y = w = 0$ and z arbitrary

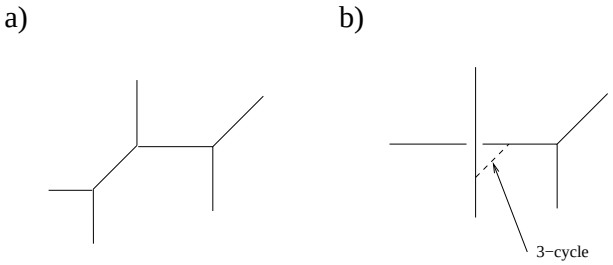

Figure 3.22: Complex deformation for the SPP theory

numbers of fractional branes are different. Geometrically, there is an incompatibility between the branes, since the $(0,1,0)$ triggers a complex deformation that smoothes out the space, and hence also removes the curve of A_1 singularities, i.e. the collapsed 2-cycle at the latter gets a finite size. In that situation, the $(1,0,0)$ branes which are wrapped over the 2-cycle get an additional tension, and break supersymmetry. Supersymmetry would in principle be restored if the brane $(1,0,0)$ escapes to infinity along the curve of singularities as the complex deformation takes place. Figure 3.23 gives a pictorial depiction of this situation. It would be interesting to understand whether this picture goes beyond being a nice intuitive representation and we can associate to it a more quantitative geometric meaning.

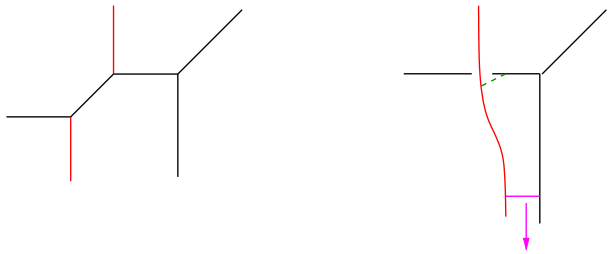

Figure 3.23: Web picture of the incompatibility of complex deformation and $N = 2$ fractional brane. The dashed segment represents the 3-cycle in the complex deformation, while the continuous segment represents the 2-cycle associated to the $N = 2$ brane. The picture suggests a physical interpretation of the runaway behavior of ADS superpotentials in this case: The complex deformation increases the tension of the $N = 2$ fractional brane, unless it escapes to infinity.

One may therefore expect a runaway behavior in this system. In order to verify this in detail, take M branes of type $(1,0,0)$ and P branes of type $(0,1,0)$. The quiver for such a theory is shown in Figure 3.24 and the superpotential is $W = X_{12}X_{21}X_{11}$. Consider the case $P \gg M$, the dynamics is hence dominated by the $SU(P)$ theory which has M flavors and generates an ADS superpotential for the meson $\phi = X_{12}X_{21}$,

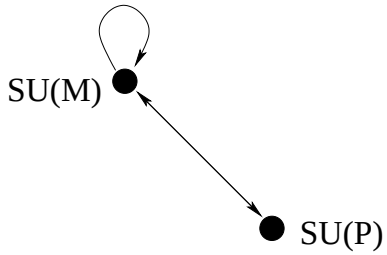

Figure 3.24: Quiver for SPP with M branes of type $(1,0,0)$ and P branes of type $(0,1,0)$

which is in the adjoint of $SU(M)$. The superpotential is

$$W = X_{11}\phi + (P-M)\left(\frac{\Lambda^{3P-M}}{\det\phi}\right)^{\frac{1}{P-M}} \tag{3.63}$$

It is clear that there is no supersymmetric vacuum in this case, since F-term constraints cannot be satisfied.

It is also easy to realize that there is a runaway direction for large ϕ. In order to make it explicit, let us restrict to the simplest case of one fractional brane of type $(1,0,0)$ and P of type $(0,1,0)$. Then the gauge theory is just $SU(P)$ with one flavor, and the complete superpotential is

$$W = \phi X_{11} + (P-1)\left(\frac{\Lambda^{3P-1}}{\phi}\right)^{\frac{1}{P-1}} \tag{3.64}$$

Notice that in this case the determinant in the ADS part is very simple, since ϕ is just a complex number. The F-terms are

$$\frac{\partial W}{\partial X_{11}} = \phi \quad , \quad \frac{\partial W}{\partial \phi} = X_{11} + \Lambda^{\frac{3P-1}{P-1}}\phi^{-\frac{P}{P-1}} \tag{3.65}$$

Clearly there is no supersymmetric vacuum. Looking for minima of the F-term scalar potential

$$V = \phi\phi^* + (X_{11} - \Lambda^{\frac{3P-1}{P-1}}\phi^{-\frac{P}{P-1}})(X_{11}^* + (\Lambda^*)^{\frac{3P-1}{P-1}}(\phi^*)^{-\frac{P}{P-1}}) \tag{3.66}$$

and upon extremization we obtain

$$\begin{aligned} \frac{\partial V}{\partial X_{11}} &= 0 \rightarrow X_{11}^* + (\Lambda^*)^{\frac{3P-1}{P-1}}(\phi^*)^{-\frac{P}{P-1}} = 0 \\ \frac{\partial V}{\partial \phi} &= 0 \rightarrow \phi^* + \Lambda^{\frac{3P-1}{P-1}}(\frac{P}{P-1})\phi^{-\frac{2P-1}{P-1}}(X_{11}^* + (\Lambda^*)^{\frac{3P-1}{P-1}}(\phi^*)^{-\frac{P}{P-1}}) = 0 \end{aligned} \tag{3.67}$$

Substituting the first equation into the second gives $\phi^* = 0$, and the first gives $X_{11} \rightarrow \infty$. This means that there is a runaway to a minimum at infinity in X_{11},

namely the $N = 2$ fractional brane runs to infinity. This agrees with the above physical interpretation that the fractional brane $(1, 0, 0)$ is thus pushed to infinity along this curve of singularities.

This is the first example of a situation where fractional branes which by themselves lead to $N = 1$ supersymmetric RG flows, do not have a supersymmetric vacuum when combined. The analysis of this section was applied to numerous other geometries such as dP_2, dP_3 and $Y^{p,q}$ (see [54, 59] for a description of these quiver gauge theories and their supergravity duals) and it was shown that the generic fractional brane exhibits DSB in the infrared [3].

3.4 Conclusion

Since fractional branes generically break conformal invariance, they can lead to interesting dynamics in the infrared. Indeed, we have observed an intricate relation between the gauge theory on fractional branes and the toric singularities in which they lie. Fractional branes corresponding to deformation of the singularities lead to confining gauge theories in the infrared. Whereas fractional branes corresponding to non-isolated singularities lead to $\mathcal{N} = 2$ theories in the infrared. The fractional brane which corresponds to neither of these two cases generically leads to dynamical supersymmetry breaking in the infrared. However, when one takes into account coupling to closed string modes, the potential has a runaway behavior and supersymmetry is recovered at infinity. These results could thus lead to interesting model building tools, since fractional branes offer very rich dynamics. However, one still needs to find a proper way of implementing a supersymmetry breaking mechanism using D–branes at singularities. This is achieved in Chapter 5.

In this work we have not dealt with the AdS/CFT correspondence. Indeed, deformation and $\mathcal{N} = 2$ fractional branes have interesting supergravity duals and offer interesting checks of AdS/CFT (see [53, 29, 54, 55, 56, 57, 58, 59] for examples of supergravity solutions and their dual quiver gauge theories). The supergravity dual of DSB fractional branes remains an open question with some hints being provided in our work [3]. We also want to mention that other authors independently reached conclusions similar to ours [51, 52].

Chapter 4

Gauge theories at resolved singularities using dimers

4.1 Introduction

As we saw in the previous chapter, the gauge theories for D3-branes placed at toric singularities are described by a quiver and superpotential. An equivalent and more elegant description was provided in [14, 15] in terms of dimer diagrams. The relation between the gauge theories for D3-branes at toric singularities and dimer diagrams was made more explicit in [16]. They showed that D3–branes placed at toric singularities in Type IIB are mirror to D6-branes intersecting on a Riemann surface in Type IIA. This Riemann surface is just a fattening of the web diagram of the toric singularity. In this chapter we use these results to develop a method of determining the gauge theories which survive in two daughter singularities after the mother singularity has been resolved (i.e blow-up of an S^2), on the gauge theory side this arises from higgsing by turning on certain Fayet-Iliopoulos terms. These results enable us to determine the gauge theories for D3-branes at arbitrary singularities in a simple and systematic fashion.

4.2 Review of dimer diagrams

In this section we review some background material on dimer diagrams and their relevance to quiver gauge theories.

4.2.1 Quiver gauge theories and dimer diagrams

As discussed in the previous chapter, D3-branes placed at a toric singularities break supersymmetry to $\mathcal{N} = 1$. These theories are completely determined by a quiver diagram and superpotential. An example is shown in Figure 4.1, where nodes represent gauge groups (with the associated vector multiplet), and arrows represent bifundamental chiral multiplets (the base of the arrow transforms in the fundamental and the tip in the anti-fundamental).

Recently it has been shown that all the gauge theory information, including the gauge group, the matter content and the superpotential, can be encoded in a so-called brane tiling or dimer graph [14, 15]. This is a tiling of $\mathbf{T^2}$ defined by a bipartite graph, namely one whose nodes can be colored black and white, with no edges connecting nodes of the same color. The dictionary associates faces in the dimer diagram to gauge factors in the field theory, edges with bifundamental fields (fields in the adjoint in the case that the same face is at both sides of the edge), and nodes with superpotential terms. The bipartite character of the diagram is important in that it defines an orientation for edges (e.g. from black to white nodes), which determines the chirality of the bifundamental fields. Also, the color of a node determines the sign of the corresponding superpotential term.

The explicit mapping between this bipartite graph and the gauge theory, is illustrated in one example in Figure 4.1. In the quiver, there are four nodes each corresponding to a gauge group. These nodes correspond to faces in the dimer diagram. Terms in the superpotential correspond to nodes in the dimer diagram and the sign of the superpotential term is associated to the color of the node (e.g positive sign for a black node and negative for a white node). Also, one can give an orientation to each node (e.g clockwise for a white node and anti-clockwise for a black node). In the quiver, the arrow going from node 1 to 2 represents a chiral multiplet transforming in the fundamental and anti-fundamental of gauge groups 1 and 2 respectively. It corresponds in the dimer diagram, to a line between faces 1 and 2 with orientation given by that of the nodes.

Finally, note that in the dimer a bi-valent node corresponds to a mass term and integrating it out corresponds in the dimer to shrinking both edges of this node to zero size, as shown in Figure 4.2.

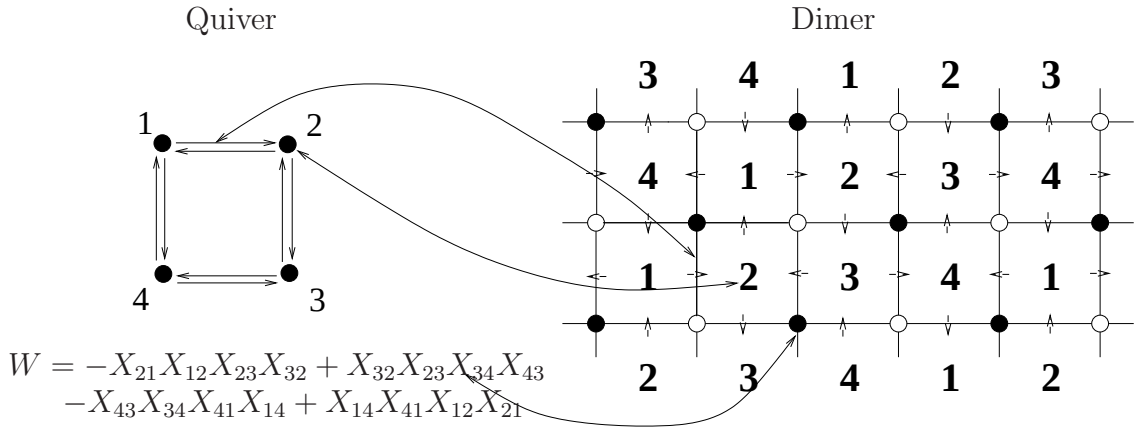

Figure 4.1: Quiver and dimer for D3–branes at a $\mathbf{Z_2}$ orbifold of the conifold. Faces in the dimer correspond to gauge groups, edges correspond to bi-fundamentals and each vertex corresponds to a superpotential term. Edges have an orientation determined by the coloring of the adjacent nodes.

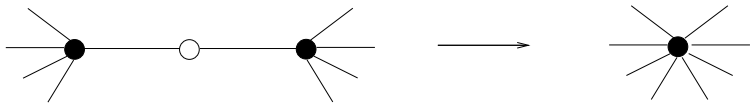

Figure 4.2: Integrating out massive terms corresponds to shrinking the edges to zero size.

4.2.2 Dimer diagrams and the mirror Riemann surface

There are two interesting ways to relate physically the dimer diagram with the gauge theory. As described in [15] the diagram can be considered to specify a configuration of NS5- and D5-branes. The NS5-branes extend in the 0123 directions and wrap a holomorphic curve in the 4567 directions. The D5-branes span the 012346 directions and are bounded by the NS branes in the 46 directions. These directions are compact and parametrize a torus. The NS branes thus generate a tiling of this $\mathbf{T^2}$, represented by a bipartite graph of the kind described above, hence the name brane tiling.

A second useful and more explicit viewpoint on the correspondence between the gauge theory on D3-branes at toric singularities and dimer diagrams was provided in [16] by using mirror symmetry, as we now describe. The mirror geometry to a toric singularity $\mathcal{M}$ is specified by a double fibration over the complex plane W given by

$$W = P(z,w) \tag{4.1}$$

$$W = uv \tag{4.2}$$

with $w, z \in \mathbf{C}^*$ and $u, v \in \mathbf{C}$. Here $P(z, w)$ is the Newton polynomial[1] of the toric diagram of $\mathcal{M}$. The surface $W = P(z, w)$ describes a genus g Riemann surface[2] Σ_W with punctures[3], fibered over W. The genus g equals the number of internal points of the toric diagram. The fiber over $W = 0$, denoted simply Σ, will be important for our purposes. It corresponds to a smooth Riemann surface which can be thought of as a thickening of the web diagram dual to the toric diagram, see Figure 4.3.

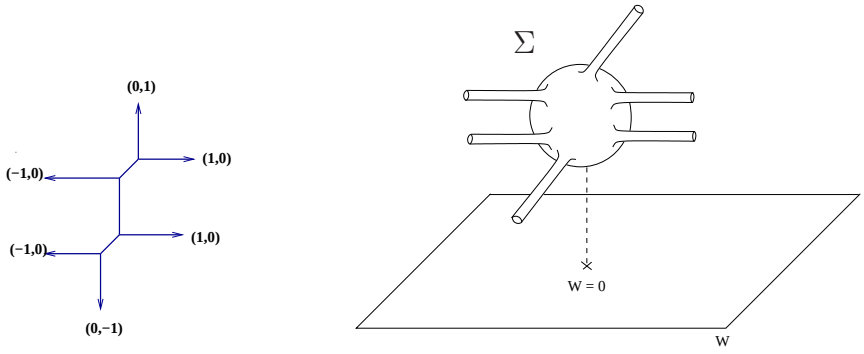

Figure 4.3: a) An example of a web diagram (for the theory in Figure 4.1); b) the corresponding Riemann surface Σ in the mirror geometry.

At critical points $W = W^*$, a cycle in Σ_W degenerates and pinches off. Also, at $W = 0$ the S^1 in $W = uv$ degenerates. One can use these degenerations to construct non-trivial 3-cycles in the mirror geometry as follows. Consider the segment in the W-plane which joins $W = 0$ with one of the critical points $W = W^*$, and fiber over it the $\mathbf{S^1}$ in $W = uv$ times the 1-cycle in Σ_W degenerating at $W = W^*$, see Figure 4.4. The result is a 3-cycle with an $\mathbf{S^3}$ topology. The number of critical points $W = W^*$, and hence the number of such 3-cycles, is given by twice the area of the toric diagram.

Now the D3–branes on the toric singularity in type IIB are mirror in type IIA to D6–branes wrapping the different 3-cycles. These 3-cycles intersect over $W = 0$. The D6–branes thus wrap 1-cycles over the Riemann surface Σ. Chiral bifundamental fields arise from open strings stretching at the intersections of such cycles. Moreover, disks in Σ bounded by pieces of different 1-cycles lead to superpotential terms generated by world-sheet instantons.

[1]The Newton polynomial is a polynomial characterising the toric geometry. It will not be relevant for this work.

[2]A Riemann surface is a 1-dimensional compact, orientable, complex manifold.

[3]A puncture corresponds in the removal of a point.

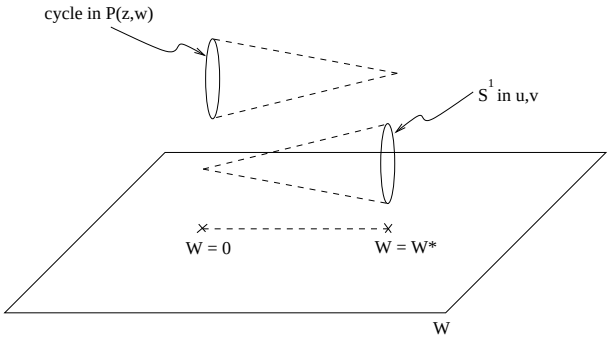

Figure 4.4: There is a 1-cycle in $P(z,w)$ which goes to zero at $W = W^*$. There is also an S^1 in $W = uv$ which goes to zero at $W = 0$. By fibering these two 1-cycles over the segment between $W = 0$ and $W = W^*$, one gets a non-trivial 3-cycle.

The structure of the 3-cycles is thus determined by the 1-cycles in the fiber Σ over $W = 0$. This structure admits a natural projection to a $\mathbf{T^2}$ which is precisely the dimer diagram of the gauge theory.

This last process is perhaps better understood (and of more practical use) by recovering the Riemann surface Σ from the dimer diagram of the gauge theory, as follows. Given a dimer diagram, one can define zig-zag paths as paths composed of edges, and which turn maximally to the right at e.g. black nodes and maximally to the left at white nodes. They can be conveniently shown as oriented lines that cross once at each edge and turn at each vertex, as shown in Figure 4.5. Notice that

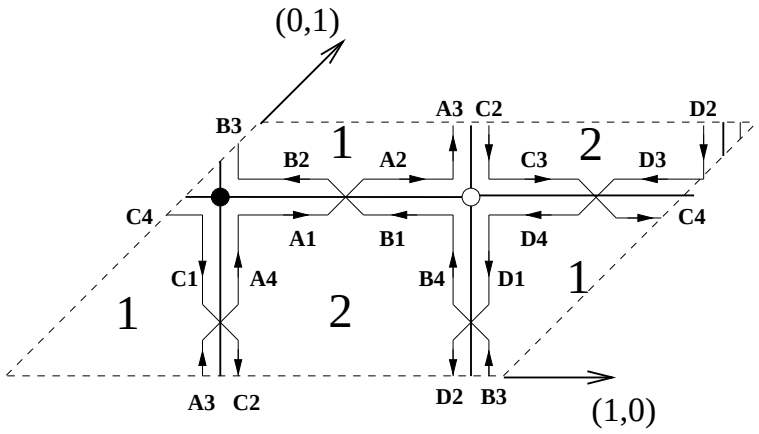

Figure 4.5: Dimer of the conifold with the corresponding zig-zag paths.

at each edge two zig-zag paths must have opposite orientations. For dimer models describing toric gauge theories, these zig-zag paths never intersect themselves and form closed loops wrapping (p, q) cycles on the $\mathbf{T^2}$. This is shown for the conifold in Figure 4.5 where the zig-zag paths A, B, C and D have charges (0,1), (-1,1), (1,-1), (0,-1) respectively.

As shown in [16], the zig-zag paths of the dimer diagram associated to D3-branes at a singularity lead to a tiling of the Riemann surface Σ in the mirror geometry. Specifically, each zig-zag path encloses a face of the tiling of Σ which includes a puncture, and the (p, q) charge of the associated leg in the web diagram is the (p, q) homology charge of the zig-zag path in the $\mathbf{T^2}$. The touching of two of these faces in the tiling of Σ corresponds to the coincidence of the corresponding zig-zag paths along an edge of the dimer diagram. An example will make this clearer. In the case of the conifold, one obtains the Riemann surface in the following manner:

- Draw the zig-zag paths in the dimer diagram.
- Number each zig-zag path such that its number is incremented by one at each crossing or turn as shown in Figure 4.5.
- Now each zig-zag path corresponds to a face in the Riemann surface with the same number of edges e.g zig-zag path A in Figure 4.5 has two edges so face A in Figure 4.6a has two edges.
- The adjacency relations follow from those in the dimer e.g since zig-zag path A_1A_2 crosses the same edge as B_1B_2, in the Riemann surface edges A_1A_2 and B_1B_2 are adjacent.

Following this procedure, one can systematically draw the Riemann surface corresponding to any dimer diagram. One also observes that in the dimer, zig-zag path A has homology class (0,1) and in the Riemann surface the corresponding face A wraps a puncture which corresponds to leg A in the web diagram (shown in Figure4.6b). This leg has the same (p,q) charge (0,1). This a very elegant and simple way to retrieve the moduli space of the gauge theory. One starts by placing D3-branes at a toric singularity, the gauge theory is encoded by a dimer diagram, one then draws zig-zag paths in the dimer diagram and calculates their homology class. Each zig-zag path then corresponds to an external leg of the web diagram with the (p,q) charge equal to the homology class. In this manner, we obtain the web diagram[4] in

[4]Recall that web and toric diagrams are defined modulo $SL(2, \mathbb{Z})$.

Figure 4.6b from the homology cycles of the zig-zag paths in Figure 4.5. The moduli space of the gauge theory is thus encoded in a very deep manner within the dimer diagram.

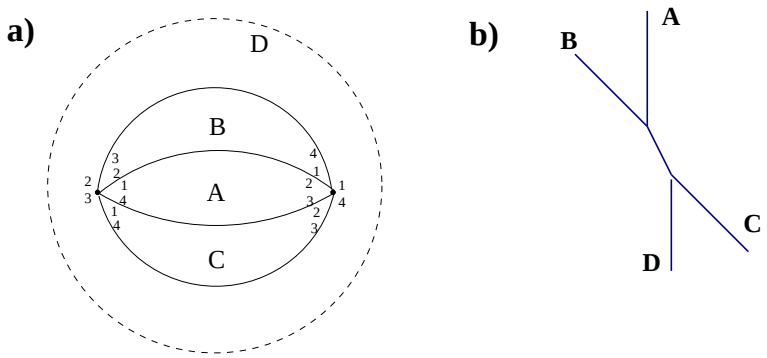

Figure 4.6: a) Tiling of the Riemann surface (which is topologically a sphere) for the case of D3-branes at a conifold singularity. b) The web diagram, providing a skeleton of the Riemann surface, with asymptotic legs corresponding to punctures (and hence to faces of the tiling of Σ, and zig-zag paths of the original dimer diagram).

The dimer diagram moreover encodes the 1-cycles in the mirror Riemann surface, associated to the different gauge factors in the gauge theory. Consider a gauge factor associated to a face in the dimer diagram. One can consider the ordered sequence of zig-zag path pieces that appear on the interior side of the edges enclosing this face. By following these pieces in the tiling of Σ one obtains a non-trivial 1-cycle in Σ which corresponds precisely to that used to define the 3-cycle wrapped by the mirror D6-branes carrying that gauge factor. For example, in the case of the conifold, face 2 of the dimer diagram in Figure 4.5 is circled by $A_1B_1B_4D_2D_3C_3C_2A_4$. By following this path in the Riemann surface, one obtains the 1-cycle wrapped by the D6-brane corresponding to gauge group 2 (see Figure 4.7). Using this map, it is possible to verify all dimer diagram rules (edges are bi-fundamentals, nodes are superpotential terms) mentioned at the beginning. An amusing feature is that these non-trivial 1-cycles in Σ are given by zig-zag paths of the tiling of Σ. The non-trivial 1-cycles in the mirror Riemann surface for the case of the conifold are shown in Figure 4.7.

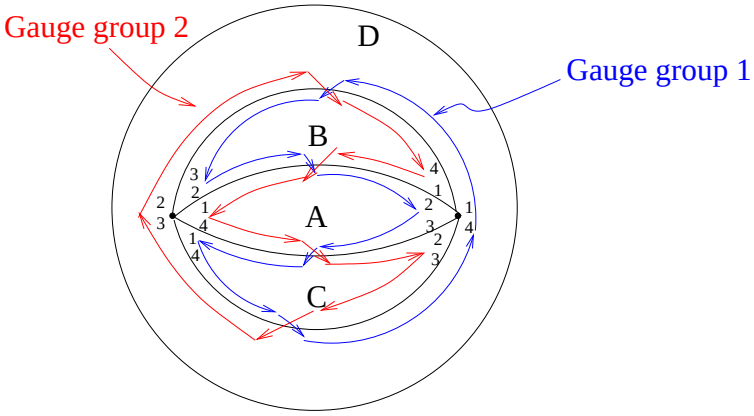

Figure 4.7: Tiling of the Riemann surface for the case of D3-branes at a conifold singularity, with the 1-cycles corresponding to the two gauge factors (shown as zig-zag paths of the tiling of Σ).

4.2.3 Perfect matchings

A last concept we would like to discuss is that of perfect matchings for a dimer diagram. A perfect matching is a subset of edges of the dimer diagram, such that every vertex of the graph is the endpoint of exactly one such edge. In Figure 4.8 we show the four perfect matchings for the conifold. For future convenience, we consider the edges in each perfect matching to carry an orientation, e.g. from black to white nodes.

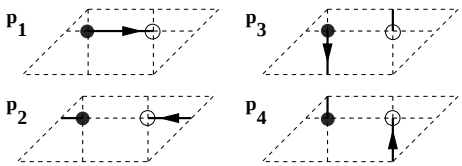

Figure 4.8: Perfect matchings for the dimer of the conifold.

There is a one to one correspondence between the perfect matchings for a dimer diagram and the linear sigma model fields that arise in the construction of the moduli space of the quiver gauge theory [15, 17]. This implies that each perfect matching has an associated location in the toric diagram of the corresponding singularity. This can be obtained as follows. Fix a given perfect matching as reference matching,

denoted p_0. Then for any perfect matching p_i we can consider the path $p_i - p_0$, obtained by superimposing the edges of p_i and those of p_0, with flipped orientation for the latter. With the convention that repeated edges with opposite orientation annihilate, we obtain a (possibly trivial, or even empty) path in the dimer diagram, carrying a (possibly trivial) $\mathbf{T^2}$ homology charge (n_i, m_i). Then the location of the matching p_i in the toric diagram is given by $(-m_i, n_i)$. Clearly the choice of reference matching simply amounts to a choice of origin in the toric diagram.

To illustrate this, in Figure 4.9a we have shown the paths $p_{1i} = p_i - p_1$ in the dimer diagram for the conifold. The location of the perfect matchings in the toric diagram, given by $(-m, n)$ where (n, m) is the homology cycle of the paths p_{1i}, is shown in Figure 4.9b [5]

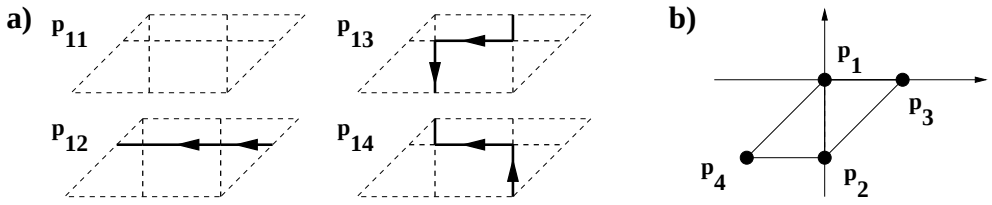

Figure 4.9: The paths $p_{1i} = p_i - p_1$ for the dimer of the conifold are associated to specific locations $(-m, n)$ in the toric diagram, where (n, m) are the homology charges of $p_i - p_1$.

Although not emphasized in the literature, there is a beautiful interpretation of pairs of perfect matchings. From a construction similar to the above, to any pair of perfect matchings p_i, p_j one can associate a path (which we call 'difference path') $p_{ij} = p_j - p_i$ in the dimer diagram, with $\mathbf{T^2}$ homology charge $(\Delta n, \Delta m)$. In the toric diagram this is associated to the segment joining the location of p_i to that of p_j, which as a vector is given by the slope difference $(\Delta h_x, \Delta h_y) = (-\Delta m, \Delta n)$. Now clearly, the homology charge $(\Delta n, \Delta m)$ is precisely the (p, q) charge of the segment in the web diagram dual to that segment in the toric diagram. This suggests a natural interpretation of $p_j - p_i$ in the mirror Riemann surface. Indeed, by lifting the dimer path $p_j - p_i$ to the mirror Riemann surface (using the tiling of the latter) one obtains a non-trivial 1-cycle which winds around the tube corresponding to the thickening of the leg in the web diagram. This is illustrated in Figure 4.10 for the case of the conifold.

Clearly, the dimer paths associated to adjacent external matchings (i.e. matchings

[5] Recall that the toric diagram is defined modulo an $SL(2, \mathbb{Z})$ transformation.

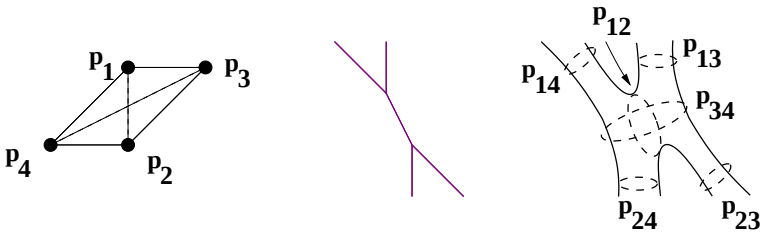

Figure 4.10: The perfect matchings for the dimer of the conifold are associated to specific locations in the toric diagram, as determined by the slopes. The paths $p_{ij} = p_i - p_j$ correspond to 1-cycles in the mirror Riemann surface wrapped around the tubes dual to the segment joining p_i and p_j in the toric diagram.

which are at adjacent locations on the boundary of the toric diagram) carry the same charges as zig-zag paths (although in general may not coincide edge by edge with them). This thus shows the equivalence of the two ways we have described to obtain the toric diagram associated to a dimer diagram, namely construction of the web diagram by using charges of zig-zag paths, and construction of the toric diagram using perfect matchings.

4.3 Partial resolution

As shown in the appendix on toric geometry, any toric singularity can be made less singular either through resolution or deformation. Whereas resolution consists in the blow-up of a 2-cycle, deformation consists in the blow-up of a 3-cycle. Also, whereas the resolution of a toric singularity remains a toric singularity, the same is not necessarily true of deformation. Now, in [8] it was shown that minimal partial resolution [6], which consists in the removal of only one triangle from the toric diagram (or separating only two external edges in the web diagram), corresponds to higgsing the gauge theory via the addition of a Fayet-Iliopoulos term. Since the moduli space of the gauge theory living on D3-branes parametrises the transverse space, one only need analyse the moduli space of the higgsed theory to determine the residual geometry in which the D3-branes move. Thus, up to now, the process followed to determine the gauge theory on an arbitrary toric geometry was to start with the gauge theory on an orbifold singularity (more singular than the desired geometry),

[6]Partial resolution is equivalent to resolution but the residual geometries can remain singular

and higgs the gauge theory until one obtains the desired moduli space (see [8] and [10] for examples). This process was long since it only permitted minimal partial resolutions at each step (not general resolutions). It also was not systematic since it was not clear what fields needed to acquire vevs to generate the desired resolved geometry. Moreover, the process of higgsing a theory using dimers is not simple since, as pointed out and explained in [18], arbitrary addition/removal of edges in a dimer diagram can lead to inconsistent theories.

We saw in the previous section the intricate relation between dimer diagrams encoding the gauge theory of D3–branes at a toric singularity and the web and toric diagrams characterising the singularity. Indeed, we saw that the zig-zag paths of the dimer each correspond to a leg in the web diagram. Since resolution of a singularity is easily expressed in terms of separation of legs in a web diagram, one can use this intuition to devise a method to determine the gauge theory in the residual geometry. In this section we consider an arbitrary partial resolution of a toric singularity, typically splitting it into several. We consider the original set of D3-branes to split accordingly into subsets located at the daughter singular points. Hence one expects that the original gauge theory splits (via a Higgs mechanism) into several gauge sectors, decoupled at the level of massless modes, and correspondingly that the original dimer diagram splits into several sub-dimers associated to the subsets of D3-branes at the daughter singularities. We provide a simple construction of the splitting of dimer diagrams that corresponds to a given partial resolution. In addition, we provide a simple recipe for the bifundamental vevs that trigger the corresponding Higgsing in the gauge theory.

As a prototypical example we consider partial resolutions splitting a singularity into two. Other cases, like minimal partial resolutions, can be recovered as a particular case as mentioned above. Splitting into more than two daughter singularities can be easily obtained by iteration of our procedure.

4.3.1 An example in detail

Let us start with a simple example of the splitting via partial resolution of a singularity into two singularities, using concepts and techniques from dimers.

Consider the singularity whose toric diagram and web diagram are shown in Figure 4.11. We refer to it as the double conifold. The dimer diagram shown in Figure 4.12 represents the gauge theory on D3-branes at this double conifold singularity.

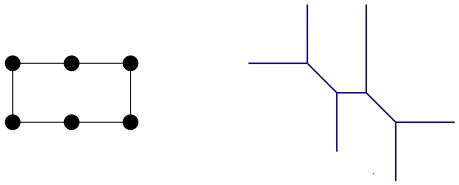

Figure 4.11: The toric diagram and web diagram of the double conifold singularity $xy = s^2w^2$. For clarity, we show the web diagram for a slightly resolved geometry.

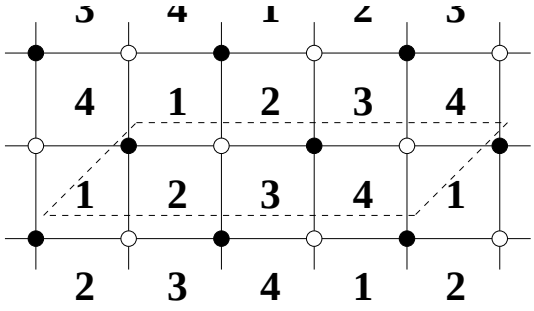

Figure 4.12: Dimer diagram corresponding to the double conifold singularity in Figure 4.11. The dashed line corresponds to the unit cell of the periodic tiling.

The above singularity admits partial resolutions to geometries with two separated singularities. One such partial resolution is illustrated in Figure 4.13a, and corresponds to a large blow-up of an $\mathbf{S^2}$, smoothing the initial geometry to two isolated conifold singularities. A different splitting, into two $\mathbb{C}^2/\mathbb{Z}_2 \times \mathbb{C}$ singularities, is shown in Figure 4.13b.

The partial resolution corresponds to turning on Fayet-Iliopoulos terms in the D3-brane gauge theory. These FI terms force some of the bi-fundamental scalars to acquire a vev, breaking the gauge symmetry. For the case of a partial resolution splitting a singularity, the left over field theory must correspond to two gauge sectors, corresponding to the gauge theories on stacks of D3-branes at the two singularities. These two sectors are decoupled at the level of massless states. Namely, the only states charged under both sectors are massive, with mass controlled by the bifundamental vevs, and hence by the size of the 2-sphere responsible for the splitting. This agrees with the picture of open strings stretching between the two stacks of D3-branes. In Section 4.3.3 we will be more explicit about the precise set of vevs corresponding to splitting singularities.

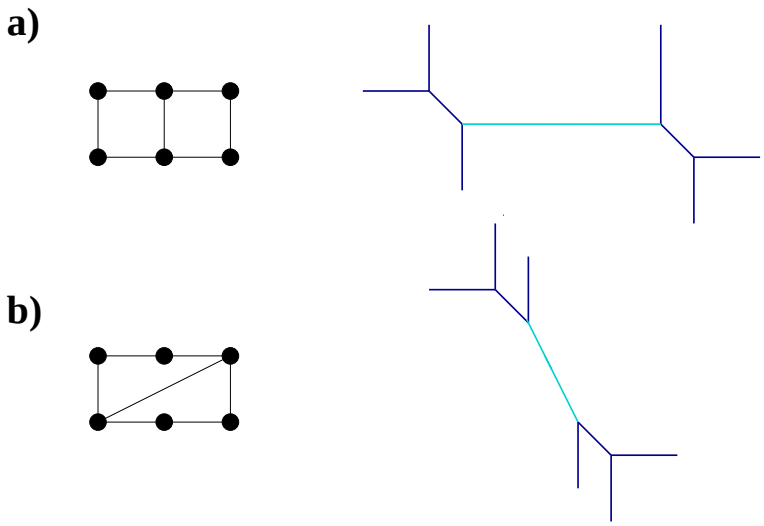

Figure 4.13: Partial resolution of the double conifold singularity in figure 4.11, splitting the initial singularity into (a) two isolated conifold singularities; (b) two $\mathbb{C}^2/\mathbb{Z}_2 \times\mathbb{C}$ singularities. The distance between the daughter singularities is controlled by the size of the $\mathbf{S^2}$ corresponding to the grey segment in the associated web diagram. For clarity the web diagrams of the left-over singularities are shown for slightly resolved geometries.

In this section, our aim is to provide a simple recipe that implements the effect of the resolution on the gauge field theory. This will be expressed in terms of a simple operation that, starting from the dimer of the initial singularity, leads to two sub-dimers corresponding to the gauge theories in the two daughter singularities.

The geometrical effect of partial resolutions is most manifest in the web diagram. Let us for concreteness consider the partial resolution of the double conifold to two conifolds, Figure 4.13a. As described in Section 4.2.2 the web diagram is encoded in the dimer diagram via its structure of zig-zag paths [18, 16]. The zig-zag paths corresponding to the dimer in Figure 4.12 are shown in Figure 4.14. The corresponding asymptotic legs in the web diagram, and the tiling of the mirror Riemann surface Σ, are shown in Figure 4.15.

In this language, it is easy to realize that the partial resolution corresponds to factorizing the Riemann surface Σ by an elongated tube, as in Figure 4.16a. The structure of the two left over singularities can be determined by analyzing the local structure of the two daughter Riemann surfaces. Due to the factorization along the infinite tube, each daughter Riemann surface has a new puncture, denoted G,

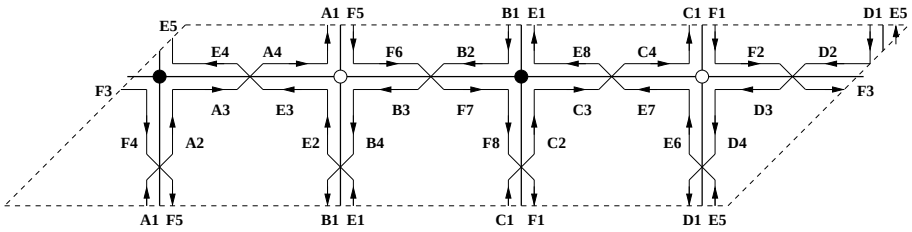

Figure 4.14: Zig-zag paths for the dimer diagram of the double conifold.

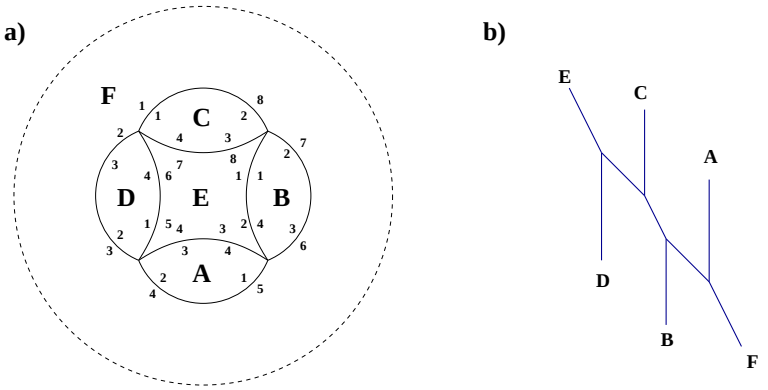

Figure 4.15: a) The adjacency relations among zig-zag paths encode a tiling of the mirror Riemann surface Σ, which in this case corresponds to a 2-sphere with six punctures, realized in the picture as the complex plane (with the point at infinity). b) Zig-zag paths in Figure 4.14 correspond to external legs in the web diagram of the singularity.

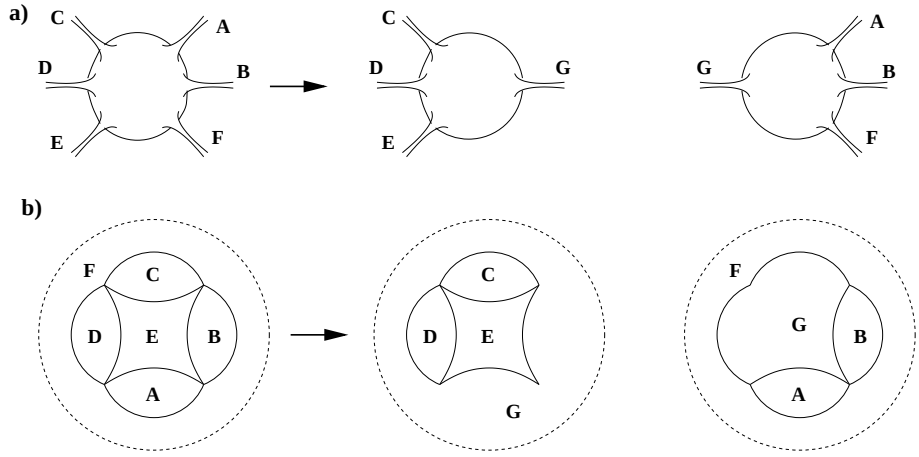

Figure 4.16: (a) Schematic representation of the factorization of the mirror Riemann surface Σ. (b) Decomposition of the tiling of Σ upon factorization. The two new sets of zig-zag paths, and their adjacency relations, can be used to construct the two dimers corresponding to D3-branes at the two singularities after splitting of the geometry.

which must correspond to a new zig-zag path in the corresponding daughter dimer diagram. In particular, the decomposition of the tiling of Σ upon this factorization, shown in Figure 4.16b, leads to two sets of zig-zag paths, namely C, D, E, G and A, B, F, G, respectively, with specific adjacency relations. This information can be used to construct two dimer diagrams, which encode the gauge theories on D3-branes at the two singular points in the geometry after partial resolution.

In Figure 4.17 we show the two sets of zig-zag paths. For convenience, the inherited paths are drawn in the locations corresponding to the original dimer. The information from the zig-zag paths allows to construct the dimer diagram corresponding to D3-branes at each of the left-over singularities after partial resolution. The dimer diagrams are also shown in the picture.

It is easy to convince oneself that the two theories are isomorphic (as expected from the symmetric factorization of the Riemann surface, or of the web diagram). Hence, it is enough to focus in one of them, say that shown in Figure 4.18a. Since this theory has a bi-valent node, one should integrate out the corresponding massive matter, with the result shown in Figure 4.18b. This can be redrawn as in Figure 4.18c, and one recognizes the dimer diagram for the conifold singularity, as expected (see Figure 4.5) . Hence the above technique of zig-zag paths provides a simple tool to determine the effect of a splitting by partial resolution on the dimer diagram

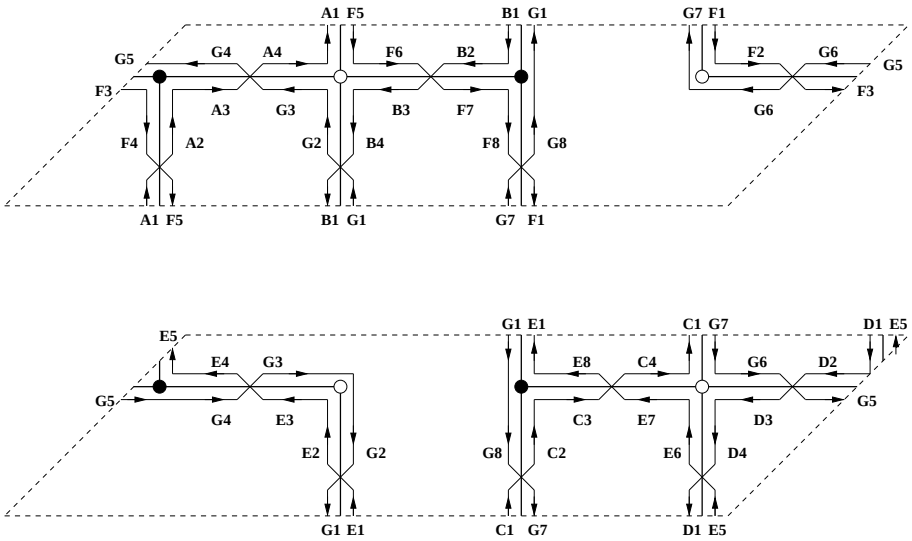

Figure 4.17: Zig-zag paths corresponding to the two daughter theories, in the splitting of the double conifold singularity to two conifold singularities, with the corresponding dimers shown as thick lines.

of the D3-brane gauge theory, as a specific splitting of the initial dimer into two sub-dimers. Moreover, in Section 4.3.3 we will show that the operation in the dimer diagram encodes in a simple manner the set of bi-fundamental vevs that corresponds in the gauge field theory to the partial resolution of the singularity.

The whole procedure can be summed up in a simple operation in the dimer diagram, without the need to go through the Riemann surface.

- Draw the zig-zag paths in the original dimer
- Determine the homology of each zig-zag path
- Each zig-zag path corresponds to an external leg of the web diagram, with the (p,q) charge of the leg equal to the homology cycle of the zig-zag path
- Perform the desired partial resolution in the web diagram e.g separating C,D,E from A,B,F
- To determine the dimer for the residual singularity e.g C,D,E , remove all other zig-zag paths from the original dimer (e.g remove zig-zag paths A,B,F).
- Complete with one (or more) zig-zag paths until all edges have two zig-zag paths going through them (G in this case).

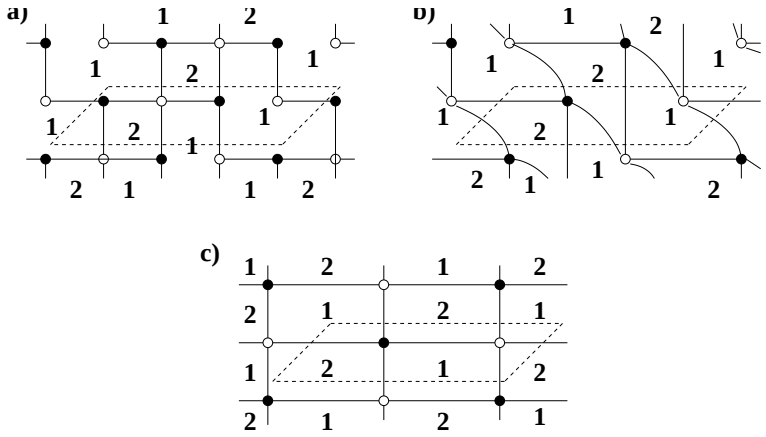

Figure 4.18: (a) Dimer diagram corresponding to the first picture in Figure 4.17. Figure (b) shows the dimer of the theory after integrating out massive modes. An equivalent diagram is shown in Figure (c), where one recognizes the dimer diagram of the conifold theory.

- Remove all edges which have no zig-zag paths going through them to obtain the dimer for the residual singularity.

One notices that the next to last point is not crucial. One does not need to draw any new zig-zag paths (e.g G), all that is needed in that case is to remove all edges not crossed by at least one zig-zag path. In the remaining examples we will obtain our results by using this simple method.

4.3.2 Further examples and comments

Double conifold to two $\mathbb{C}^2/\mathbb{Z}_2$ singularities

The technique we have described in the above example is fully general, and can be applied to any partial resolution. To provide an additional example, consider for instance the splitting of the above singularity into two $\mathbb{C}^2/\mathbb{Z}_2$ singularities, Figure 4.13b. Starting with the zig-zag paths in Figure 4.14, the partial resolution corresponds to a factorization of the mirror Riemann surface splitting the set of paths into two subsets, namely A, C, F, and B, D, E. Each set, along with a new path H from the new puncture in the daughter Riemann surface, allow to read off the dimer diagrams (and hence the quiver gauge theories) for D3-branes in the two left-over

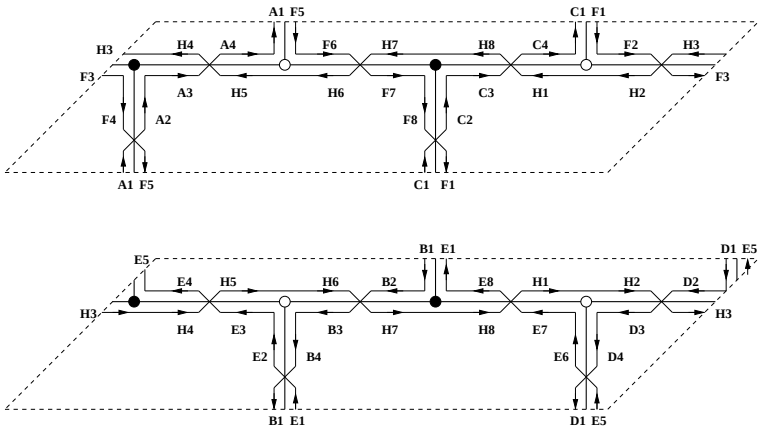

Figure 4.19: Zig-zag paths corresponding to the two daughter theories, in the splitting of the double conifold singularity to two $\mathbb{C}^2/\mathbb{Z}_2$ singularities, with the corresponding dimers shown as thick lines.

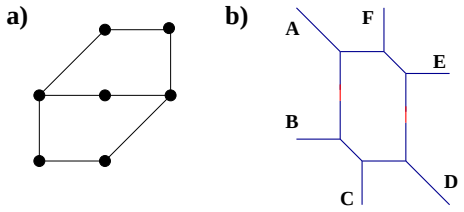

Figure 4.20: The toric diagram and web diagram of the complex cone over dP_3, in a splitting to two SPP singularities. For clarity, the web diagrams of the left-over SPP singularities are shown for slightly resolved geometries. For future convenience, we have labeled external legs.

singularities. This is shown in Figure 4.19, where one indeed recognizes the dimer diagrams of two $\mathbb{C}^2/\mathbb{Z}_2$ theories.

From dP_3 to two SPP's

Before concluding this section, we present a further example, where the factorization lowers the genus of the mirror Riemann surfaces. Namely, the factorization implies elongating several segments in the web diagram. Consider for instance the splitting of the complex cone over dP_3 to two suspended pinch point (SPP) singularities, shown in Figure 4.20.

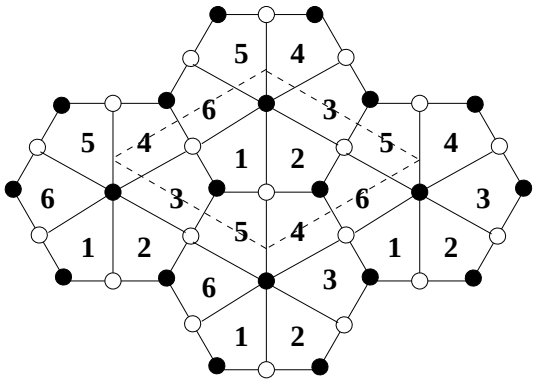

Figure 4.21: The dimer diagram for the gauge theory of D3-branes on the complex cone over dP_3.

The dimer diagram for (a toric phase of) the gauge theory on D3-branes at the cone over dP_3 is shown in Figure 4.21. The unit cell of the corresponding dimer diagram is shown in Figure 4.22, where we also show the zig-zag paths. The partial resolution in Figure 4.20 has the effect of splitting this dimer diagram into the two dimer diagrams in Figure 4.23. After integrating out massive fields, they can be shown to correspond to the gauge theories of D3-branes at SPP singularities, in agreement with the underlying geometric picture. Although this example follows from exactly the same rules as previous ones, we encounter the new feature that the splitting of the dimer involves two new zig-zag paths (denoted G and H) rather than one. This simply reflects the fact that the factorization of the Riemann surface involves two elongated tubes, hence two new punctures for each daughter Riemann surface.

Minimal partial resolution

To conclude this section, we would like to mention that this technique can be applied to asymmetric splittings, where the two daughter geometries are not the same. One particular extremal case is a minimal partial resolution (removing only one triangle from the toric diagram). Hence, only one singularity is left over after the partial resolution (namely the second singularity turns out to be a smooth patch). Let us describe this more explicitly.

In terms of the web diagram, this simply corresponds to elongating a tube that separates two external legs from the rest of the web. Using the zig-zag paths, it is

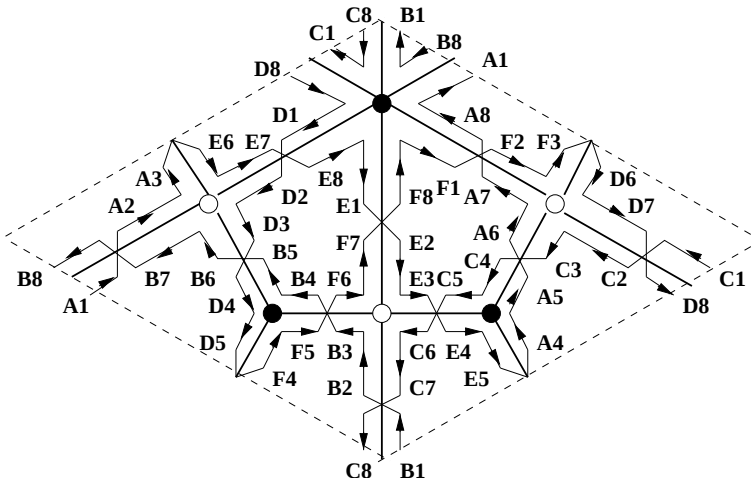

Figure 4.22: The figure shows the unit cell of the dimer diagram for the gauge theory of D3-branes on the complex cone over dP_3, and the set of zig-zag paths.

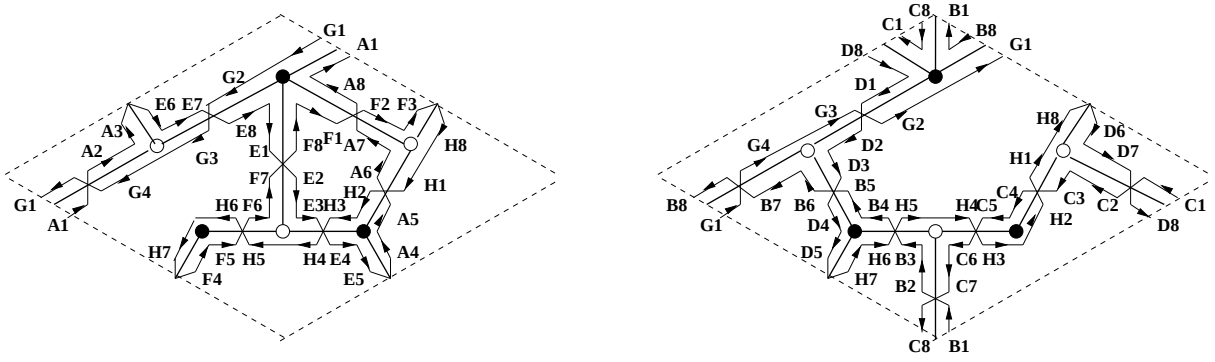

Figure 4.23: The two dimers obtained upon the splitting by small resolution shown in Figure 4.20. They can be shown to be equivalent to two copies of the SPP dimer diagram.

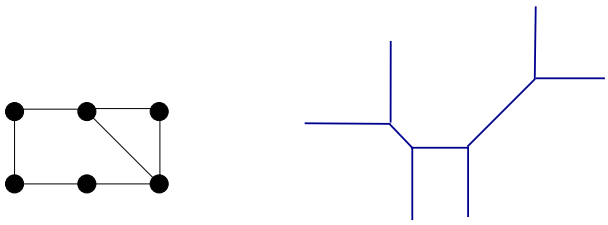

Figure 4.24: Toric and web diagram for the resolution of the double conifold to an SPP singularity.

easy to show that the left-over singularity corresponds to a dimer diagram obtained from the initial one by the removal of some edges. These edges are precisely those over which the two zig-zag paths associated to the removed legs overlap[7].

To provide one particular example, we describe the partial resolution of the double conifold to an SPP singularity via the removal of one triangle in the corresponding toric diagram (see Figure 4.24). Concretely, consider separating the legs A and F in Figure 4.15b from the rest of the web diagram, by stretching the intermediate segment. Since the corresponding zig-zag paths overlap over the lower left edge of the dimer diagram in Figure 4.14, this is the edge to be removed. In field theoretic terms this means that the corresponding bifundamental gets a vev, and the two faces (gauge groups) sharing the edge join (gauge factors break to the diagonal combination). The resulting dimer diagram is that of the SPP theory, as can be checked by computing the gauge theory data. We hope these examples suffice to illustrate the general validity of the above prescription.

4.3.3 Field theory interpretation

As discussed in [8], partial resolutions of singularities correspond to turning on Fayet-Iliopoulos terms i nthe gauge theory of D3-branes sitting at them. These FI terms force some of the bifundamental scalars to acquire vevs, preserving supersymmetry but partially breaking gauge symmetry, in precise agreement with the quiver gauge

[7]This description explains as in [18] the possibility of the appearance of inconsistent dimer diagrams by arbitrary addition/removal of edges. For instance, consider a minimal partial resolution involving two zig-zag paths overlapping over more than one edge. The removal on only one of these edges does not correspond to a consistent separation of zig-zag paths and leads to an inconsistent diagram.

theory on D3-branes at the final left-over singularity.

In this section we show that the operation of splitting a dimer, as described in the previous section, encodes in a very precise fashion the field theory data corresponding to the Higgs mechanism and gauge symmetry breaking. Moreover we show that dimer techniques can be efficiently used to show the F- and D-flatness of such vevs.

For simplicity, we center on a gauge theory with all gauge factors having equal rank N. Discussion of other situations (fractional branes) is postponed until Section 4.3.5. We also consider that after the splitting, N_1 D3-branes remain at the first singularity and N_2 remain at the second.

In order to describe the bifundamental vevs in the field theory, we notice that in the dimer splitting there are three different kinds of bi-fundamental fields, according to the behavior of the corresponding edge: a) those appearing in the two daughter dimers; b) those not appearing in the first sub-dimer, but present in the second; c) those not appearing in the second, but present in the first. This suggests the following ansatz for their vevs, which we denote V_0, V_1, V_2, respectively:

$$V_0 = \begin{pmatrix} 0 & 0 \\ 0 & 0 \end{pmatrix} \quad ; \quad V_1 = \begin{pmatrix} v\,\mathbf{1}_{N_1} & 0 \\ 0 & 0 \end{pmatrix} \quad ; \quad V_2 = \begin{pmatrix} 0 & 0 \\ 0 & v\,\mathbf{1}_{N_2} \end{pmatrix} \tag{4.3}$$

where bi-fundamental fields are regarded as $N \times N$ matrices, and the entries are blocks of dimension appropriate to the partition $N = N_1 + N_2$. Here we take v to be adimensional, and we consider that a dimensionful constant enters into the vev of each bi-fundamental, exponentiated to the appropriate power to match its conformal dimension. This factor does not change the discussion of flatness, hence we ignore it in what follows.

The interpretation of this ansatz is very clear. The N_1, N_2 entries in the diagonal determine the pattern of gauge symmetry breaking triggered by that bifundamental for the set of N_1, N_2 D3-branes in the first and second dimer respectively. An edge absent in a sub-dimer implies a local recombination of the corresponding set of D3-branes across the associated bifundamental. Namely, there is a non-vanishing vev in the corresponding set of entries (e.g an edge absent in sub-dimer 1 gets vevs V_1). Similarly, for edges present in a sub-dimer there is no vev in the corresponding entries of the associated bi-fundamentals.

The proof that the above assignment of vevs satisfies the flatness conditions in the field theory is provided in appendix 4.5. However it is useful to work out an explicit example, so consider for instance the splitting of the double conifold to two conifold singularities. Using the information in Figure 4.12 for the initial dimer, and Figure

4.17 for the sub-dimers, we obtain the following set of vevs

$$\begin{aligned} \Phi_{12} &= V_2 \quad , \quad \Phi_{23} = V_2 \quad , \quad \Phi_{34} = V_0 \quad , \quad \Phi_{41} = V_0 \\ \Phi_{21} &= V_0 \quad , \quad \Phi_{32} = V_0 \quad , \quad \Phi_{43} = V_1 \quad , \quad \Phi_{14} = V_1 \end{aligned} \tag{4.4}$$

where we have introduced the notation Φ_{ij} for a bi-fundamental $(\square_i, \overline{\square}_j)$, and take Φ_{12} to correspond to the vertical edge in the left part of the depicted unit cell (i.e Figure 4.12 has clockwise orientation for white nodes and anti-clockwise for black nodes).

It is now straightforward to analyze the flatness conditions on the set of vevs for this example. Concerning the F-term conditions, all nodes are 4-valent, hence the superpotential is a sum of quartic terms. Moreover, any such term contains at least two fields without vev. Hence, the F-terms conditions are automatically satisfied. Concerning the non-abelian D-term conditions, we write the generators of $SU(N)$ as

$$T = \begin{pmatrix} T_{11} & T_{12} \\ T_{21} & T_{22} \end{pmatrix} \tag{4.5}$$

and obtain that the D-term contributions for the $SU(N)_i$ factors are

$$\begin{aligned} SU(N)_1 \qquad & \operatorname{tr}(\Phi_{12}^\dagger T \Phi_{12}) + \operatorname{tr}(\Phi_{14}^\dagger T \Phi_{14}) = |v|^2 (\operatorname{tr} T_{11} + \operatorname{tr} T_{22}) = 0 \\ SU(N)_2 \qquad & -\operatorname{tr}(\Phi_{12}^\dagger T \Phi_{12}) + \operatorname{tr}(\Phi_{23}^\dagger T \Phi_{23}) = |v|^2 (\operatorname{tr} T_{22} - \operatorname{tr} T_{22}) = 0 \\ SU(N)_3 \qquad & -\operatorname{tr}(\Phi_{23}^\dagger T \Phi_{23}) - \operatorname{tr}(\Phi_{43}^\dagger T \Phi_{43}) = -|v|^2 (\operatorname{tr} T_{11} + \operatorname{tr} T_{22}) = 0 \\ SU(N)_4 \qquad & \operatorname{tr}(\Phi_{43}^\dagger T \Phi_{43}) - \operatorname{tr}(\Phi_{14}^\dagger T \Phi_{14}) = |v|^2 (\operatorname{tr} T_{11} - \operatorname{tr} T_{11}) = 0 \end{aligned} \tag{4.6}$$

where we have used tracelessness of $SU(N)$ generators. Finally, concerning the abelian D-term conditions, the above vevs lead to non-zero contributions which are suitably canceled by the non-zero FI terms. This effective absence of $U(1)$ D-term constraints can be equivalently regarded as the statement that there are $B \wedge F$ couplings (related to the FI terms by supersymmetry) which render the $U(1)$'s massive, so that they are not present at low energies and hence no D-term constraints have to be imposed.

The description in this section generalizes in a straightforward fashion to the splitting of a dimer into more than two sub-dimers.

4.3.4 Effect on perfect matchings

It is interesting to consider the effect of partial resolution on perfect matchings. This can be easily analyzed at the level of the dimer diagrams, as we do in what follows in

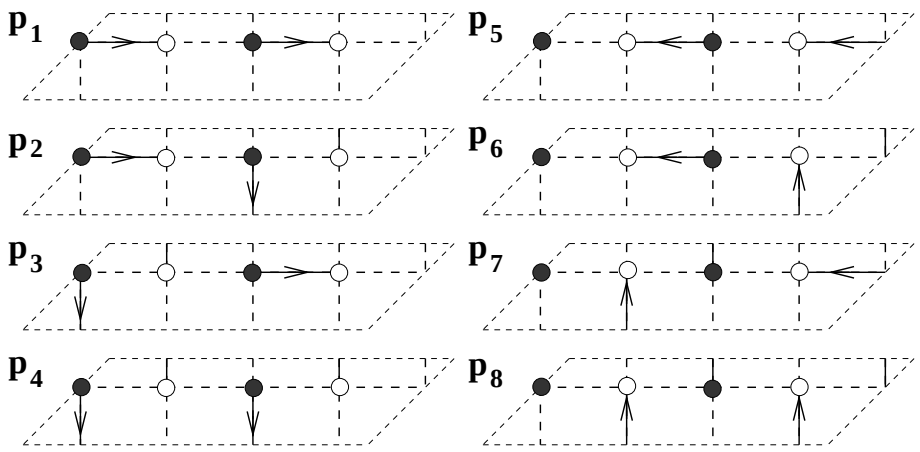

Figure 4.25: The eight perfect matchings for the dimer diagram of the double conifold.

a particular example. Consider the double conifold, whose dimer diagram is shown in Figure 4.12. The eight perfect matchings for this diagram are shown in Figure 4.25. The location of these matchings in the toric diagram, obtained as described in Section 4.2.3, using p_1 as reference matching, are shown in Figure 4.26a [8].

Consider the partial resolution of the double conifold to two conifolds, studied in Section 4.3.1, whose two resulting sub-dimers are shown in Figure 4.17. The splitting of the dimer into sub-dimers implies that the perfect matchings of the original dimer fall into different classes:

- The perfect matchings p_4, p_5 descend to perfect matchings of the first sub-dimer.
- The perfect matchings p_1, p_8 descend to perfect matchings of the second sub-dimer.
- The perfect matchings p_2, p_7 correspond to perfect matchings of both the first and second sub-dimer.
- The perfect matchings p_3, p_6 do not correspond to perfect matchings of either sub-dimer.

This correspondence becomes nicely meaningful when one considers the location of the different perfect matchings in the toric diagram. The partial resolution splits

[8]Recall that toric diagrams are defined modulo $SL(2,\mathbb{Z})$.

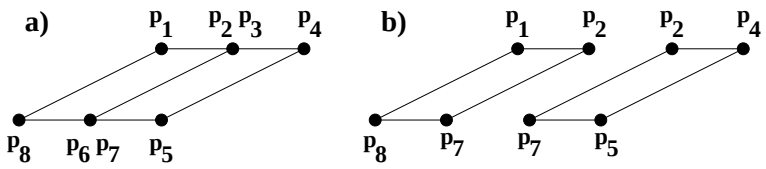

Figure 4.26: In a partial resolution, the original perfect matchings descending to perfect matchings of one or the other subdimer end up located at one or the other toric subdiagram, as shown here for the resolution of the double conifold to two conifolds.

the toric diagram into two pieces, separated by a common internal segment. Perfect matchings of the original dimer which descend to perfect matchings of a given sub-dimer are located at points on the piece of the toric diagram describing the corresponding daughter singularity. Perfect matchings descending to matchings of both singularities are located along the common segment in the toric diagram. This is described for the double conifold in Figure 4.26.

It is possible to show that this pattern is completely general, and that for a general partial resolution perfect matchings fall into one of these four classes. Namely, we label the edges of the dimer diagram with labels 1, 2 and 3, according to whether it is present in sub-dimer one, or in sub-dimer 2, or in both. Perfect matchings involving edges of type 1 and 3 end up in the interior of toric sub-diagram 1; perfect matchings involving edges of type 2 and 3 end up in the interior of toric sub-diagram 2; perfect matchings only involving edges of type 3 appear on both toric sub-diagrams, along their common boundary; perfect matchings with edges of type 1 and 2 (and possibly 3) disappear.

One can also obtain the effect of the partial resolution on the perfect matchings from the viewpoint of the Riemann surface. For that, one can use the relation described in Section 4.2.3 between pairs of perfect matchings and 1-cycles on the mirror Riemann surface. The first observation is that a partial resolution corresponds in the toric diagram to the introduction of a segment joining two external non-adjacent perfect matchings p, p'. This is just dual to separating the web diagram by elongating the leg dual to that segment. Notice that cases where there are multiple matchings at the corresponding points in the toric diagram simply correspond to cases where there are several parallel legs in the web diagram, and correspondingly several possibilities to perform the partial resolution. For instance, in our above example, the partial resolution corresponds to choosing the perfect matchings p_2 and p_7.

To such a pair of perfect matchings one can associate a path $p' - p$ (e.g $p_2 - p_7$) in the dimer diagram and a 1-cycle in the mirror Riemann surface. In fact, this 1-cycle wraps around the tube which becomes infinitely elongated in the partial resolution process. In terms of the dimer diagram, it means that the path in the dimer diagram becomes the new zig-zag path (denoted G in our example in Section 4.3.1) introduced to construct the new sub-dimers.

Given that this 1-cycle separates the Riemann surfaces in two pieces, which are naturally associated to the two daughter singularities, it is possible to interpret the four classes of perfect matchings in terms of their behavior on the Riemann surface Σ. Consider one of the external perfect matchings e.g. p_7. For any other matching p_i one can consider the 1-cycles associated to $p_i - p_7$ obtained using the tiling of Σ. If the whole of such 1-cycle lies on one component of Σ, the matching p_i will correspond to a perfect matching of the corresponding sub-dimer, and to a point in the corresponding toric sub-diagram. If all pieces of the 1-cycle are included in the 1-cycle $p' - p$ (e.g $p_2 - p_7$) , then p_i will correspond to a perfect matching of both sub-dimers, and will appear in both toric diagrams (concretely, along the common boundary). Finally if the 1-cycle contains pieces lying in both components of Σ, the corresponding perfect matching disappears in the process of partial resolution (e.g p_3, p_6).

These properties are easily explicitly checked in our above example, and can be generalized to any partial resolution.

4.3.5 Partial resolutions with fractional branes

In this section we would like to study partial resolutions for singularities in the presence of fractional branes[9], and their description using dimers. For concreteness we center on a particular example, although our conclusions are of general validity.

Let us consider the splitting of the double conifold to two conifold singularities. The dimer diagram for the double conifold, with the most general set of fractional branes, is shown in Figure 4.27a. Since the field theory is non-chiral, there are no restrictions on the gauge factor ranks, and hence there are three kinds of fractional branes.

When the singularity is split into two conifolds, the latter may contain fractional

[9]Recall that fractional branes correspond in the gauge theory to rank assignments for the gauge groups consistent with anomaly cancellation

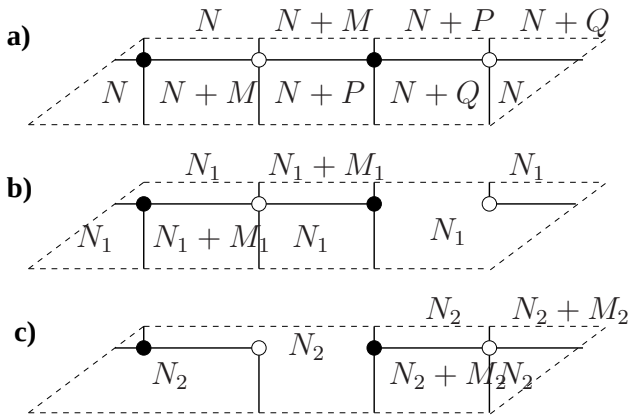

Figure 4.27: a) The dimer for the double conifold with the most general set of fractional branes. b,c) The sub-dimers for the daughter conifold singularities, with their fractional branes.

branes as well. The most general possibility is shown in Figure 4.27b, c. Since each conifold allows for one kind of fractional brane, there are two possible fractional branes in the final system.

It is thus a natural question to ask what happens with the third kind of fractional brane. The answer, that we can recover from different viewpoints, is that it obstructs the partial resolution. A pictorial way to derive this result is to compare the original dimer and the daughter sub-dimers in Figures 4.27a and b,c, respectively. In order to have a proper splitting, the number of branes in a given face of the original dimer must agree with the sum of the numbers of branes in the corresponding location in the sub-dimers. In our particular case, this implies

$$N = N_1 + N_2 \quad , \quad M = M_1 \quad , \quad P = 0 \quad , \quad Q = M_2 \tag{4.7}$$

Hence we see that the splitting necessarily forces the fractional brane changing the rank of the gauge group 3 to be absent, in the sense that only in the absence of such a brane the splitting is possible. More precisely, what obstructs the splitting is the fractional brane which controls the difference between the ranks of the gauge factors 1 and 3.

In what follows we present several interpretations for this fact. From the viewpoint of the field theory of the initial singularity, it means that the theory with different ranks for the factors 1 and 3 does not have the corresponding flat direction. This can be argued in general, but is suffices to discuss one particular example, for instance $M = Q = 0$, $P \neq 0$. It is simple to show that the D-term conditions for gauge

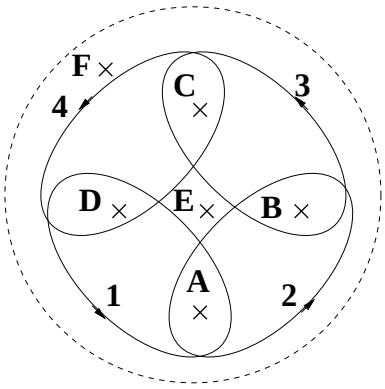

Figure 4.28: The 1-cycles in Σ corresponding to the D-branes controlling the rank of the different gauge factors in the double conifold gauge theory.

factor 3 cannot be satisfied. Indeed, the natural ansatz is similar to (4.4), with the only difference that for non-square matrices, the entries in the $M \times P$ additional submatrix are taken to be zero. In computing the D-term, as in (4.6), for the gauge factor 3, one notices that the non-zero vevs do not suffice to complete the full $SU(M+P)$ trace, and hence the D-term does not vanish.

An interpretation of the obstruction in terms of the mirror geometry, with a very explicit version of the above picture can be derived. In order to do that, consider the 1-cycles on the mirror Riemann surface Σ which correspond to the different fractional branes, in our case, to the different faces in the dimer. These are sketched in Figure 4.28.

The structure of these 1-cycles, and in particular their winding around the punctures of Σ, leads to a natural explanation of the obstruction. Consider introducing only fractional branes changing the rank of the gauge factor 3. In the mirror this corresponds to introducing D-branes along the cycle that surrounds the punctures B, C. These punctures end up in different daughter Riemann surfaces in the splitting (see figure 4.16) hence in trying to perform the partial resolution, the D-brane stretches along the elongated tube, hence increases its tension and breaks supersymmetry. Moreover, it is not possible to express this 1-cycle in terms of a combination of brane cycles not stretching along the tube, hence no process restoring supersymmetry can take place. The same argument goes through if one considers only fractional branes of type 1, since they surround the punctures A, D. Notice that there is no problem if one considers instead fractional branes of type 2 or of type 4, since they

do not correspond to cycles stretching along the tube.

Finally, consider introducing the same number of fractional branes of type 1 and 3. This case leads to equal rank for gauge factors 1 and 3, and hence we expect no obstruction. Indeed, although the branes correspond to cycles stretching along the tube, it is possible to deform them topologically to a sum of cycles of type 2 and 4, which do not stretch.

As mentioned above, this picture generalizes to more involved situations. The general lesson is that sets of fractional branes associated to cycles stretching along the tubes which elongate in the factorization of the Riemann surface lead to obstructions of the partial resolution.

4.4 Conclusion

In this chapter we have seen how all the gauge theory information of D3–branes at toric singularities can be encoded in a dimer diagram. We have also seen how this diagram encodes the moduli space of the theory via the structure of zig-zag paths. Indeed each zig-zag path corresponds to an external leg of the web diagram of the toric singularity where the D3–branes lie. Since in the web diagram, resolution corresponds to separating external legs by blowing up an S^2, we have used the correspondence between legs and zig-zag paths to devise a simple and intuitive way to implement this on the dimer. In the gauge theory this corresponds to higgsing the theory by giving vevs to the appropriate fields. We have also shown how the dimer encodes the right assignation of vevs necessary to implement this resolution. This methodology thus permits us to derive the gauge theory of D3-branes at an arbitrary singularity by starting with the gauge theory of a more singular orbifold geometry and resolving it in the appropriate manner (see Figure B.21). It also permits us to start with a given singularity and resolve it, so that we are left with two left-over singularities separated by the blown up S^2. In [4], we also show how one can implement complex deformation of a toric singularity (i.e blow-up of an S^3) in the dimer diagram language.

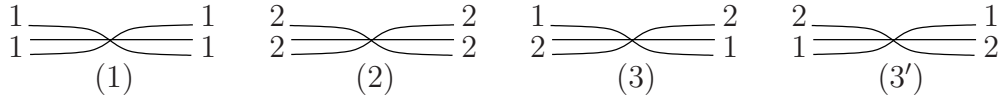

Figure 4.29: The four possible types of edges, classified according to the zig-zag paths meeting at the edge.

4.5 Appendix: Proof of flatness

The flatness conditions can be checked in the general case, by a slight generalization of the analysis in the example in Section 4.3.3. We recall that in this section we are considering original dimer diagrams not containing bi-valent nodes (hence they have been integrated out if originally present).

F-flatness conditions: As described in Section 4.3.4, in partial resolutions each sub-dimer contains at least one perfect matching of the original dimer diagram. This implies that every sub-dimer contains all the nodes of the original dimer diagram. From this follows that in any sub-dimer, for any node there are at least two edges ending on it in every sub-dimer. At the level of the gauge theory, this implies that for each superpotential term of the original theory there are a sufficient number of bi-fundamentals with zero vevs to automatically satisfy the F-term conditions. Hence the assignment of vevs dictated by the dimer rules is F-flat.

Non-abelian D-flatness conditions: As described in Section 4.3, we divide the set of zig-zag paths into two disjoint sets, where each set admits a dual interpretation as the set of external legs in the web diagram that we take to infinity. Let us denote collectively the elements belonging to the first set as 1 and those belonging to the other set as 2.

Consider a given face in the dimer diagram, and orient its edges by running through them e.g. counterclockwise. Each edge can then be classified into 4 types depending on which kind of zig-zag paths intersect over it. We will denote the four kinds as type 1, 2, 3 and 3′, see figure 4.29, where 3 and 3′ are distinguished by the orientation [10].

In this fashion, we assign to each face a (periodic) string of symbols given by the kind of edges we encounter when traversing the face counterclockwise. A typical

[10]The similar notation for edges and zig-zag paths is introduced to (hopefully) improve the readability. In the rest of this section we mostly deal with edges, so this should not cause too much confusion.

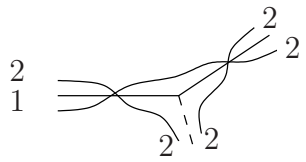

Figure 4.30: Inconsistent gluing of edges (3′2). Note that the only constraints come from the joining of the interior zig-zag paths. The exterior ones can be arbitrary as they do not need to be joined (in the absence of bi-valent nodes) since they "run off" along some extra edge, denoted by the dashed line in the drawing.

string will then look like:

$$\ldots 3'1323'3\ldots$$

where we have written just the period. It is easy to realize that any valid string should satisfy a few rules which we can read from the dimer diagram. Namely there are some sequences of symbols that are not allowed, for example 3′2. To see this, focus on the zig-zag paths "interior" to the edge. The given sequence would tell us that a type 1 zig-zag path exits the 3′ vertex from the right, and then joins a type 2 zig-zag path in the next edge, see Figure 4.30. This is obviously not allowed. The other disallowed sequences are 13′, 23, 31, 33, 3′3′, 12 and 21.

We can then associate to the most general face in a dimer a sequence of symbols not containing these forbidden words. It is easy to convince oneself that in any such string, at least one of the following substitutions applies and gives rise to another consistent sequence with two symbols removed in the period ("·" denotes the empty word):

$$\begin{array}{lllllllll} 11 & \longrightarrow \cdot & ; & 22 \longrightarrow \cdot & ; & 33' \longrightarrow \cdot & ; & 3'3 \longrightarrow \cdot & \\ 132 & \longrightarrow 3 & ; & 23'1 \longrightarrow 3' & & & & & \end{array} \tag{4.8}$$

As an example, applying the rules one would get the following sequence of strings:

$$3'133'1132 \longrightarrow 3'11132 \longrightarrow 3'132 \longrightarrow 3'3 \longrightarrow \cdot$$

Since we can always apply one of these rules, and all of them reduce the length of the string by two, we have found that it is always possible to reduce an arbitrary string to nothing [11]. The interesting fact about these operations is that on the field theory side they do not change the value of the D-term. Essentially, the first four

[11] The sequences always have even length, consistently with anomaly cancellation.

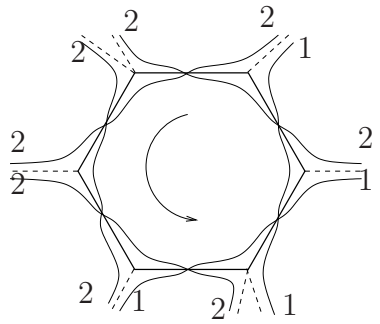

Figure 4.31: A possible face in a dimer, where we have indicated the relevant classification for the zig-zag paths. External edges are denoted by the dashed lines, and the arrow indicates the traversal direction used in the text when enumerating the edges.

rules in (4.8) preserve the D-term value because the disappeared edges correspond to a fundamental and an antifundamental with the same vev, hence with canceling contributions to the D-term[12]. For the last two rules, the disappeared edges have vevs whose contributions add up to the trace of an $SU(N)$ generator, which is zero. One can in this way easily translate between the language used in equation 4.6 and this language of sequences. What this means is that the value of the D-term for all possible faces in a dimer is given by the D-term of the empty sequence, which is equal to zero.

As an example, let us study the configuration depicted in Figure 4.31. The periodic string we associate with the face is given by $\ldots 223'132 \ldots$. Applying the rules we have described a possible reduction to nothing would be

$$223'132 \longrightarrow 23'32 \longrightarrow 22 \longrightarrow \cdot$$

This proves that the D-term for the relevant gauge group vanishes.

[12]This is due to the fact that edges 1, 2 ,3 and 3' in Figure 4.29 have vevs V_2, V_1, V_0 and V_0 (eq 4.3) respectively

Chapter 5

SUSY Breaking Metastable Vacua with Branes at Singularities

5.1 Introduction

In Chapter 3 we saw how placing fractional branes, D5–branes wrapped around vanishing cycles, can lead to gauge theories exhibiting dynamical supersymmetry breaking (DSB) in the infrared. However, when including closed string modes, the scalar potential exhibits runaway behavior and supersymmetry is restored at infinity. In [25], Intriligator, Seiberg and Shih (ISS) showed, with an extremely simple model, how one can obtain metastable vacua breaking supersymmetry. The authors showed that the addition of massive flavors to $SU(N)$ SQCD, with masses much smaller than the dynamical scale of the gauge sector, leads to the appearance of local metastable supersymmetry breaking minima. These minima are separated from a supersymmetric vacua by a large potential barrier and can be made parametrically long-lived.

In [24], the authors expand on these ideas and show how they can be incorporated into String Theory. Starting with fractional branes on the complex cone over dP_1, which we saw in Chapter 3 leads to DSB in the infrared, the authors add massive flavors with cubic couplings to the bifundamentals. The analysis of the low-energy limit of the theory shows the appearance of a local metastable supersymmetry breaking minimum, separated from the runaway at infinity by a large potential barrier. This strongly suggests that most DSB fractional branes should exhibit metastable SUSY breaking minima after the addition of massive flavors.

In Section 5.2 we fist start by reviewing the ISS solution [25] and in Section 5.3 we review the dP_1 case [24]. Whereas both papers show that the minima are metastable by calculating the 1-loop effective potential via the Coleman-Weinberg formula [30], we derive the same results by placing ourselves at a minimum (the most symmetric one) and calculating the 1-loop contributions to all massless perturbations around this minimum. The advantage of such a methodology is that we can obtain closed expressions for the mass corrections which will help us in determining the existence of metastability for arbitrary DSB fractional branes more easily. In Section 5.4 we apply this methodology to the complex cone over dP_2, and generalize the result to arbitrary DSB fractional branes in Section 5.5. Indeed, we show that given a specific addition of flavors, the analysis of metastability only involves looking at the original superpotential. The determination of metastability is thus greatly simplified. In Section 5.6, we apply this criteria to other examples.

5.2 Review of ISS

5.2.1 ISS

Let us start by briefly reviewing the ISS construction [25] [1]. One starts with $\mathcal{N} = 1$ $SU(N_c)$ theory with N_f flavors, and adds small masses to them via a superpotential of the form

$$W_{\text{electric}} = m\text{Tr}\,\phi\tilde{\phi} \tag{5.1}$$

where ϕ and $\tilde{\phi}$ are the quarks of the theory. We also choose the number of colors and flavors such that we are in the free magnetic phase (see appendix on supersymmetry)

$$N_c + 1 \leq N_f < \frac{3}{2}N_c \tag{5.2}$$

This condition guarantees that the Seiberg dual is infrared free. The Seiberg dual is an $SU(n = N_f - N_c)$ theory with N_f flavors of dual quarks q and $\tilde{q}$ and the meson M. The dual superpotential is given by rewriting (5.1) in terms of the mesons and adding the usual coupling between the meson and the dual quarks

$$W_{\text{magnetic}} = h(\text{Tr}\,\tilde{q}Mq - \mu^2\text{Tr}\,M) \tag{5.3}$$

[1] Apart from the original article, another good reference for these and other models of dynamical supersymmetry breaking are the lecture notes [35].

where h and μ can be expressed in terms of the parameters m and Λ, and some (unknown) information about the dual Kähler metric[2]. It was also argued in [25] that it is possible to study the supersymmetry breaking minimum in the origin of (dual) field space without taking into account the gauge dynamics (their main effect in this discussion consists of restoring supersymmetry dynamically far in field space). In the following we will assume that this is always the case, and we will forget completely about the gauge dynamics of the dual.

Once we forget about gauge dynamics, studying the vacua of the dual theory becomes a matter of solving the F-term equations coming from the superpotential (5.3). The mesonic F-term equation is particularly interesting, it reads

$$-\overline{F}_{M_{ij}} = h\tilde{q}^i \cdot q^j - h\mu^2\delta^{ij} = 0 \tag{5.4}$$

where i and j are flavor indices and the dot denotes color contraction. This cannot be solved in general, since the identity matrix δ^{ij} has rank N_f while $\tilde{q}^i \cdot q^j$ has rank $n = N_f - N_c$, which means that this theory spontaneously breaks supersymmetry at tree level. This mechanism for F-term supersymmetry breaking is called the *rank condition*.

Once one minimizes the tree-level potential one finds that some flat bosonic directions remain, but it turns out that the one-loop potential lifts all of the non-Goldstone directions, which are usually called pseudo-moduli. The way we will study this lifting is the following:

- First we choose an ansatz for the one-loop vacuum, we will expand around this vacuum. The ansatz we will choose in general sets

$$q = \tilde{q}^{\mathrm{T}} = \begin{pmatrix} \mu \\ 0 \end{pmatrix} \tag{5.5}$$

  with the rest of the fields set to 0. This is the one-loop vacuum in the ISS model, and also in the other cases we have studied.

- Then we expand the theory linearly around this vacuum, and identify the pseudo-moduli.

[2]The exact expressions can be found in eq. 5.7 in [25], but we will not need them for our analysis. We just assume that all masses in the electric description are small enough for the analysis of the metastable vacuum to be reliable.

- As a final step we compute two point functions for the pseudo-moduli via conventional Feynman diagrams, as explained in more detail in appendix 5.8.1 and illustrated below for a few cases.

This is different from the usual approach, which builds the one loop effective potential over all pseudo-moduli space via the Coleman-Weinberg formula [30]

$$V = \frac{1}{64\pi^2}\mathrm{Tr}\left(\mathcal{M}_B^4 \log\frac{\mathcal{M}_B^2}{\Lambda^2} - \mathcal{M}_F^4 \log\frac{\mathcal{M}_F^2}{\Lambda^2}\right) \tag{5.6}$$

This has the advantage that it gives the location of the minimum explicitly, but has the disadvantage that since it requires diagonalizing the mass matrix it does not admit a closed expression for complicated theories, such as the ones we will be interested in studying. As long as we choose the correct ansatz the results we will get for the masses will be equal, but we will be able to provide closed expressions. If we get positive masses (given by the two point functions) at one loop for all pseudo-moduli, and negligible tadpoles[3], then the putative vacuum is indeed stable.

Let us illustrate the method for the ISS case we are studying. We parametrize the expansion around the ansatz as

$$q = \begin{pmatrix} \mu + \frac{1}{\sqrt{2}}(\xi_+ + \xi_-) \\ \frac{1}{\sqrt{2}}(\rho_+ + \rho_-) \end{pmatrix}, \qquad \tilde{q}^{\mathrm{T}} = \begin{pmatrix} \mu + \frac{1}{\sqrt{2}}(\xi_+ - \xi_-) \\ \frac{1}{\sqrt{2}}(\rho_+ - \rho_-) \end{pmatrix}, \qquad M = \begin{pmatrix} Y & Z \\ \tilde{Z}^{\mathrm{T}} & \Phi \end{pmatrix} \tag{5.7}$$

where we have taken linear combinations of the fields in such a way that the bosonic mass matrix is diagonal. This will also be convenient in Section 5.2.2, where we discuss the Goldstone bosons in greater detail. The superpotential for this theory is given by

$$W = h(\mathrm{Tr}\, qM\tilde{q} - \mu^2 \mathrm{Tr}\, M) \tag{5.8}$$

In order to perform the calculation, we will expand the superpotential in terms of the fluctuations around the ansatz. The exercise is straightforward, we get

$$\begin{aligned} W &= \sqrt{2}\mu\xi_+ Y + \frac{1}{\sqrt{2}}\mu Z\rho_+ + \frac{1}{\sqrt{2}}\mu Z\rho_- + \frac{1}{\sqrt{2}}\mu\rho_+\tilde{Z} - \frac{1}{\sqrt{2}}\mu\rho_-\tilde{Z} \\ &\quad + \frac{1}{2}\rho_+^2\Phi - \frac{1}{2}\rho_-^2\Phi - \mu^2\Phi + \dots \end{aligned} \tag{5.9}$$

where we have not displayed terms of order three or higher in the fluctuations, unless they contain Φ, since they are irrelevant for the one loop computation we

[3]Since supersymmetry is spontaneously broken the effective potential will get renormalized, and thus the position of the vacuum might shift slightly because of a one-loop effect.

will perform. Note also that we have set $h = 1$ and we have removed the trace (the matricial structure is easy to restore later on, here we just set $N_f = 2$ for simplicity). The bosonic massless fluctuations are given by $\mathrm{Re}\,\rho_+$, $\mathrm{Im}\,\rho_-$, Φ and ξ_-. The first two together with $\mathrm{Im}\,\xi_-$ are Goldstone bosons, as explained in Section 5.2.2. The pseudo-moduli we are interested in are given by Φ and $\mathrm{Re}\,\xi_-$. Let us focus on Φ (the case of $\mathrm{Re}\,\xi_-$ admits a similar discussion). In this case the relevant terms in the superpotential simplify further, and just the following superpotential contributes

$$\begin{aligned} W &= \mu Z \frac{1}{\sqrt{2}}(\rho_+ + \rho_-) + \mu \tilde{Z} \frac{1}{\sqrt{2}}(\rho_+ - \rho_-) \\ &\quad + \frac{1}{2}\rho_+^2 \Phi - \frac{1}{2}\rho_-^2 \Phi - \mu^2 \Phi + \dots \end{aligned} \tag{5.10}$$

which we recognize, up to a field redefinition, as the symmetric model of appendix 5.8.2. We can thus read the result directly, it is given by

$$\delta m_\Phi^2 = \frac{|h|^4 \mu^2}{8\pi^2}(\log 4 - 1) \tag{5.11}$$

This matches the value given in [25], which was found using the Coleman-Weinberg potential.

5.2.2 Goldstone bosons

One aspect of the method that merits some explanation concerns the Goldstone bosons. When one does the 1-loop computation using just the interactions described above, the two point function does not vanish. The simplest way to understand this is that there is a 1-loop tadpole, and thus there is another contribution to the one loop amplitude given by

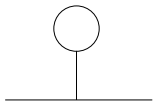

(5.12)

Once one adds the contribution arising from this diagram the two point function vanishes, signaling the existence of a massless particle in the spectrum, as expected. This tadpole does not affect the computation of the one loop pseudo-moduli masses, as it is straightforward to check.

We can also understand the same result from a different point of view, which might be useful in some cases. Let us work in the effective field formalism, so we are only interested in 1PI diagrams and thus (5.12) does not enter into our calculations. It

is possible to prove the Goldstone theorem in this formalism, as we will do below. The proof can be found in slightly more detail, together with other proofs, in [1].

Let us denote by V the effective potential we find up to one loop. The statement that the action is invariant under a given symmetry implies for the potential that

$$\frac{\delta V}{\delta \phi_i}\Delta\phi_i = 0 \tag{5.13}$$

where we denote by $\Delta\phi_i$ the variation of the field ϕ_i under the symmetry, which will in general be a function of all the fields in the theory. Let us take the derivative of this equation with respect to some other field ϕ_k

$$\frac{\delta^2 V}{\delta\phi_i\delta\phi_k}\Delta\phi_i + \frac{\delta V}{\delta\phi_i}\cdot\frac{\delta\Delta\phi_i}{\delta\phi_k} = 0 \tag{5.14}$$

In the absence of tadpoles the second term vanishes when evaluating around the classical minimum, and the first one becomes a statement about the mass matrix. In particular, under the action of each spontaneously broken generator of the symmetry, the value of $\Delta\phi_i$ gives a nonvanishing eigenvector of the mass matrix with zero eigenvalue. In this way we can easily identify the Goldstone bosons of the theory. As an example, let us study the ISS model described above for the case with two flavors. We will keep using the parametrization of the fields given by equation 5.7.

Of the original symmetries of the problem, there are three that are broken around the tree-level minimum, which we have taken to be

$$\langle q\rangle = \langle \tilde{q}^{\mathrm{T}}\rangle = \begin{pmatrix} \mu \\ 0 \end{pmatrix}, \qquad \langle M\rangle = \begin{pmatrix} 0 & 0 \\ 0 & 0 \end{pmatrix} \tag{5.15}$$

In particular, the symmetry group of the potential is given by $SU(2)\times U(1)$, and it gets broken down to a $U(1)'$ which can be understood as a combination of the original $U(1)$ and the t_z generator of $SU(2)$. We can then find the Goldstone bosons by studying equation 5.14 for the three broken generators, which we can take to be the three generators of $SU(2)$. Let us do the case of t_z in detail. We have that for the action of t_z the only nonvanishing vev is

$$\langle \Delta \mathrm{Im}\,\xi_-\rangle = \langle \mathrm{Re}\,\xi_+\rangle + 2\mu = 2\mu \tag{5.16}$$

where we are assuming μ to be real, so only the imaginary part of ξ_- changes. This tells us that $\mathrm{Im}\,\xi_-$ is the desired Goldstone field. Repeating the exercise for t_x and t_y one finds the corresponding Goldstone fields $\mathrm{Im}\,\rho_-$ and $\mathrm{Re}\,\rho_+$.

This was fine at tree level. Now let us try to compute the effective potential at one loop for the ISS model. It turns out that we find two somewhat puzzling results. First, the tree level Goldstone fields acquire a mass (their two point function is finite but nonvanishing). The second result is a finite tadpole for the real part of ξ_+.

The calculation of the tadpole at one loop is straightforward, and we will only present here the result. We have a tadpole amplitude only for $\mathrm{Re}\,\xi_+$, and it is given by

$$i\mathcal{M} = \frac{-i|h|^4\mu^3}{(4\pi)^2}(2\log 2) \tag{5.17}$$

The result for the Goldstone two point function is also simple to calculate, we get

$$i\mathcal{M} = \frac{-i|h|^4\mu^2}{(4\pi)^2}(\log 2) \tag{5.18}$$

We also know the variations of the relevant fields under the symmetry generator (which we will be taking to be t_z, a very similar discussion applies to the other generators). They are given by

$$\Delta\mathrm{Re}\,\xi_+ = -\mathrm{Im}\,\xi_- \tag{5.19}$$

$$\Delta\mathrm{Im}\,\xi_- = \mathrm{Re}\,\xi_+ + 2\mu \tag{5.20}$$

When we plug these ingredients in formula 5.14 remembering to truncate everything to one loop, so just the tree level vevs of $\Delta\phi_i$ are needed, one obtains that there is no contradiction between the equation giving the Goldstone theorem and the results we found

$$\left\langle \frac{\delta^2 V}{\delta\phi_i\delta\phi_k}\Delta\phi_i + \frac{\delta V}{\delta\phi_i}\cdot\frac{\delta\Delta\phi_i}{\delta\phi_k}\right\rangle = m^2_{\mathrm{Im}\,\xi_-}\cdot 2\mu + (\mathrm{Re}\,\xi_+\text{tadpole})\cdot(-1) = 0 \tag{5.21}$$

A very similar discussion applies to t_x and t_y.

5.3 dP_1 case

Let us study a slightly more complicated theory, which is also more representative of the difficulties one faces when analysing a general quiver coming from a brane at a toric singularity. We will be studying the gauge theory arising from a fractional brane located at the singularity of the complex cone over dP_1 with massive flavors, and in particular the lifting of the flat directions at one loop. This was already studied in detail in [24] using the Coleman-Weinberg potential, here we analyse it

again using the Feynman diagram technique in order to further familiarise ourselves with the method.

Let us repeat here for completeness the basic steps in order to obtain the magnetic description of the metastable vacuum. We start with an electric theory given by the quiver shown in Figure 5.1. The superpotential in the electric theory is given by

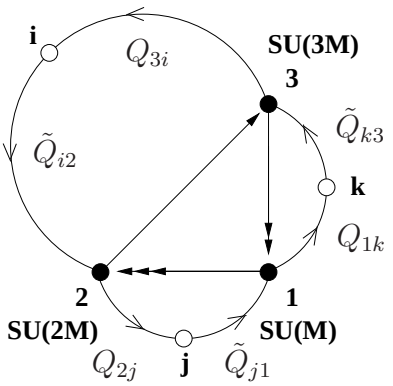

Figure 5.1: Extended quiver diagram for a dP_1 theory with flavors, from [24]. Black and white nodes denote gauge and flavor groups respectively.

$$\begin{aligned} W &= \lambda(X_{23}X_{31}Y_{12} - X_{23}Y_{31}X_{12}) \\ &+ \lambda'(Q_{3i}\tilde{Q}_{i2}X_{23} + Q_{2j}\tilde{Q}_{j1}X_{12} + Q_{1k}\tilde{Q}_{k3}X_{31}) \\ &+ m_3 Q_{3i}\tilde{Q}_{k3}\delta_{ik} + m_2 Q_{2j}\tilde{Q}_{i2}\delta_{ji} + m_1 Q_{1k}\tilde{Q}_{j1}\delta_{kj} \end{aligned} \tag{5.22}$$

where the subindices denote the groups under which the field is charged. The first line comes from the theory of the fractional brane, the second line from couplings between the flavor branes and the fractional brane, and the last line from couplings between the flavor branes themselves. Since node 3 has the highest rank we assume that it confines first, and we also assume that it is in the free magnetic phase, for which we require

$$M + 1 \leq N_{f,1} < \frac{5}{2}M \tag{5.23}$$

where we have denoted by $N_{f,1}$ the rank of the flavor group. As an aside, let us note that in the dP_1 theory there is a massless field that decouples even at the superpotential level, usually called Z. This massless field does not get stabilized by our perturbative considerations, so we leave it as an open problem for the dP_1 case[4].

[4]This moduli is not problematic since it does not run towards a SUSY restoring vacua i.e giving large vevs to this moduli will not restore supersymmetry.

We proceed to do the Seiberg duality on node 3, for which we introduce the dual mesons

$$\begin{array}{rclcrcl} M_{21} &=& \frac{1}{\Lambda} X_{23} X_{31} & ; & N_{k1} &=& \frac{1}{\Lambda} \tilde{Q}_{k3} X_{31} \\ M'_{21} &=& \frac{1}{\Lambda} X_{23} Y_{31} & ; & N'_{k1} &=& \frac{1}{\Lambda} \tilde{Q}_{k3} Y_{31} \\ N_{2i} &=& \frac{1}{\Lambda} X_{23} Q_{3i} & ; & \Phi_{ki} &=& \frac{1}{\Lambda} \tilde{Q}_{k3} Q_{3i} \end{array} \tag{5.24}$$

and we also replace the electric quarks Q_{3i}, $\tilde{Q}_{k3}$, X_{23}, X_{31}, Y_{31} by their magnetic duals $\tilde{Q}_{i3}$, Q_{3k}, X_{32}, X_{13}, Y_{13}. The magnetic superpotential is given by rewriting the confined fields in terms of the mesons and adding the coupling between the mesons and the dual quarks, we get

$$\begin{aligned} W &= h\,(\, M_{21} X_{13} X_{32} + M'_{21} Y_{13} X_{32} + N_{2i} \tilde{Q}_{i3} X_{32} \\ &+ N_{k1} X_{13} Q_{3k} + N'_{k1} Y_{13} Q_{3k} + \Phi_{ki} \tilde{Q}_{i3} Q_{3k}\,) \\ &+ h\mu_0\,(\, M_{21} Y_{12} - M'_{21} X_{12}\,) + \mu'\, Q_{1k} N_{k1} + \mu'\, N_{2i} \tilde{Q}_{i2} \\ &- h\mu^2 \mathrm{Tr}\,\Phi + \lambda'\, Q_{2j} \tilde{Q}_{j1} X_{12} + m_2 Q_{2i} \tilde{Q}_{i2} + m_1 Q_{1i} \tilde{Q}_{i1} \end{aligned} \tag{5.25}$$

This is the theory we want to study. It is possible to integrate out some massive fields without affecting the low energy dynamics, simplifying the expressions somewhat, but we will not do so since it does not simplify the analysis of the lifting of the pseudo-moduli.

The next step to take, as before, is realizing that this theory breaks supersymmetry via the rank condition in the same way as ISS did above, in fact we can identify $\tilde{Q}_{i3}$, Q_{3k} and Φ_{ki} in this case with q, $\tilde{q}$ and M in the ISS case discussed above. This motivates the following linear expansion

$$\begin{array}{ccccc} \Phi = \begin{pmatrix} \phi_{00} & \phi_{01} \\ \phi_{10} & \phi_{11} \end{pmatrix} & ; & \tilde{Q}_{i3} = \begin{pmatrix} \mu e^{\theta} + Q_{3,1} \\ \tilde{Q}_{3,2} \end{pmatrix} & ; & Q_{3i}^{\mathrm{T}} = \begin{pmatrix} \mu e^{-\theta} + Q_{3,1} \\ Q_{3,2} \end{pmatrix} \\ \tilde{Q}_{k1} = \begin{pmatrix} \tilde{Q}_{1,1} \\ y \end{pmatrix} & ; & Q_{2j} = \begin{pmatrix} Q_{2,11} & x \\ Q_{2,21} & x' \end{pmatrix} & ; & M_{21} = \begin{pmatrix} M_{21,1} \\ M_{21,2} \end{pmatrix} \\ Y_{13} = (Y_{13}) & ; & X_{12}^{\mathrm{T}} = \begin{pmatrix} X_{12,1} \\ X_{12,2} \end{pmatrix} & ; & X_{32}^{\mathrm{T}} = \begin{pmatrix} X_{32,1} \\ X_{32,2} \end{pmatrix} \\ Y_{12}^{\mathrm{T}} = \begin{pmatrix} Y_{12,1} \\ Y_{12,2} \end{pmatrix} & ; & N'_{k1} = \begin{pmatrix} N'_{k1,1} \\ z \end{pmatrix} & ; & M'_{21} = \frac{\lambda'}{h\mu_0} \begin{pmatrix} M'_{21,1} \\ M'_{21,2} \end{pmatrix} \\ & & X_{13} = (X_{13}) & & \end{array} \tag{5.26}$$

Note that we have chosen to introduce the nonlinear expansion in θ in order to reproduce the results found in the literature in their exact form. Also note that we have not been explicit about the ranks of the different matrices, this is for clarity

of the exposition. They can be easily worked out (or for this case, looked up in [24]), we will restrict ourselves to the two flavor case where the matricial structure is trivial. As a last remark, we are not being explicit about the definitions of the different couplings in terms of the electric theory. This is because, as in the ISS case, there is always some uncertainty associated with the Kähler potential, and also because the contribution is always positive definite, no matter the exact values of the coefficients in the superpotential.

Having done the parametrization of the fluctuations around the ansatz, the next step consists in expanding the superpotential and identifying the massless fields. We get the following quadratic contributions to the superpotential

$$\begin{aligned} W_{\text{mass}} &= 2h\mu\phi_{00}\tilde{Q}_{3,1} + h\mu\phi_{01}\tilde{Q}_{3,2} + h\mu\phi_{10}Q_{3,2} \\ &+ h\mu_0 M_{21,1}Y_{12,1} + h\mu_0 M_{21,2}Y_{12,2} + -\lambda' M'_{21,1} - \lambda' M'_{21,2}X_{12,2} \\ &+ h\mu N'_{k1,1}Y_{13} - h_1\mu\tilde{Q}_{1,1}X_{13} - h_2\mu Q_{2,11}X_{32,1} - h_2\mu Q_{2,21}X_{32,2} \end{aligned} \quad (5.27)$$

In this way we identify the fields massless at tree level. They are given by x, x', y, z, ϕ_{11}, θ, $Q_{3,2}$ and $\tilde{Q}_{3,2}$. Three of these are Goldstone bosons as described in the previous section, they are given (for real μ) by $\text{Im}\,\theta$, $\text{Re}\,(\tilde{Q}_{3,2} + Q_{3,2})$ and $\text{Im}\,(\tilde{Q}_{3,2} - Q_{3,2})$. We will see that the other fields get masses at 1-loop.

As a first step towards finding the 1-loop correction, notice that the supersymmetry breaking mechanism is extremely similar to the one in the ISS model before, in particular it comes only from the following coupling in the superpotential

$$W_{\text{rank}} = hQ_{3,2}\tilde{Q}_{3,2}\phi_{11} - h\mu^2\phi_{11} + \dots \quad (5.28)$$

This gives a non-supersymmetric spectrum for $Q_{3,2}$ and $\tilde{Q}_{3,2}$. Let us compute now the correction to the mass of x, for example. For the one loop computation we just need the terms cubic in the pseudo-modulus, the supersymmetry breaking sector, and any cuadratic terms containing the fields appearing in the previous two sectors. From the complete expansion one finds the following supersymmetry breaking sector

$$W_{\text{symm.}} = h\phi_{11}Q_{3,2}\tilde{Q}_{3,2} + h\mu\phi_{01}\tilde{Q}_{3,2} + h\mu\phi_{10}Q_{3,2} - h\mu^2\phi_{11} \quad (5.29)$$

The cubic term in the pseudo-modulus x is given by

$$W_{\text{cubic}} = -h_2 x\tilde{Q}_{3,2}X_{32,1} \quad (5.30)$$

and we must also consider any mass coupling between $X_{32,1}$ and other fields, this comes from

$$W_{\text{mass coupling}} = -h_2\mu Q_{2,11}X_{32,1} \quad (5.31)$$

Assembling the three previous equations, we find that the superpotential we need to study is in fact the model we called *asymmetric* in appendix 5.8.2, so we can write the answer immediately

$$\delta m_x^2 = \frac{1}{16\pi^2}|h|^4\mu^2\mathcal{C}\left(\frac{|h_2|^2}{|h|^2}\right) \tag{5.32}$$

Proceeding in a similar way we can obtain the results for ϕ_{11}, x', y and z

$$\begin{aligned}
\delta m_{\phi_{11}}^2 &= \frac{1}{8\pi^2}|h|^4\mu^2(\log 4 - 1) \\
\delta m_{x'}^2 &= \frac{1}{16\pi^2}|h|^4\mu^2\mathcal{C}\left(\frac{|h_2|^2}{|h|^2}\right), \\
\delta m_y^2 &= \frac{1}{16\pi^2}|h|^4\mu^2\mathcal{C}\left(\frac{|h_1|^2}{|h|^2}\right) \\
\delta m_z^2 &= \frac{1}{16\pi^2}|h|^4\mu^2(\log 4 - 1)
\end{aligned} \tag{5.33}$$

There is just one pseudo-modulus left, $\mathrm{Re}\,\theta$, which is qualitatively different to the others. From examining the superpotential, and applying a reasoning similar to the one above, one concludes that it is necessary to study a superpotential of the following form

$$W = h(X\phi_1\phi_2 + \mu e^{\theta}\phi_1\phi_3 + \mu e^{-\theta}\phi_2\phi_4 - \mu^2 X) \tag{5.34}$$

We see that we are dealing with a non-renormalizable, in the power counting sense, term for θ. We have to take into account this term when doing the 1-loop computation, as it enters via a vertex with two bosons and two fermions. We proceed to calculate the relevant Feynman diagrams, and we obtain that the imaginary part of θ remains massless (matching the fact that it is a Goldstone boson), while the real part obtains a correction given by

$$\delta m_{\mathrm{Re}\,\theta}^2 = \frac{1}{4\pi^2}|h|^4\mu^4(\log 4 - 1) \tag{5.35}$$

5.4 dP_2 case

In [24] the authors showed that placing a DSB fractional brane on a dP_1 singularity and coupling it with an appropriate choice of D7-branes generates a parametrically long-lived metastable vacuum. To see if it is possible to generalize this result to arbitrary singularities, let us first start by analysing the case of the complex cone over dP_2 using the formalism developed in the previous section. The quiver diagram for dP_2 is given in Figure 5.2 below. The superpotential is

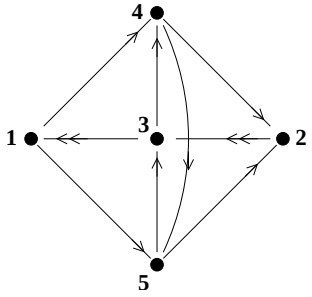

Figure 5.2: Quiver diagram for the dP_2 theory.

$$\begin{aligned} W &= X_{34}X_{45}X_{53} - X_{53}Y_{31}X_{15} - X_{34}X_{42}Y_{23} + Y_{23}X_{31}X_{15}X_{52} \\ &+ X_{42}X_{23}Y_{31}X_{14} - X_{23}X_{31}X_{14}X_{45}X_{52} \end{aligned} \tag{5.36}$$

The IR theory on M fractional branes is given by the quiver gauge theory with ranks $M(1,0,1,0,2)$ shown in Figure 5.3 below.

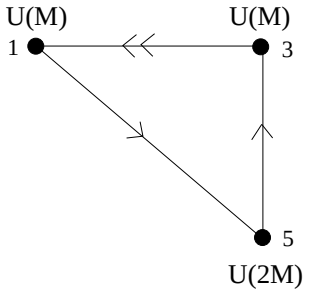

Figure 5.3: Quiver diagram for the dP_2 theory with M fractional branes.

The superpotential is given by

$$W = -\lambda X_{53}Y_{31}X_{15} \tag{5.37}$$

Now, as was shown in [24], for each bifundamental field 33 one can construct a D7-brane with a superpotential coupling 33-37-73. So adding D7-branes, we obtain the previous configuration but with the addition of flavors, as shown in Figure 5.4.

And there is an extra superpotential term given by

$$W_{flavor} = \lambda'(Q_{1i}\tilde{Q}_{i3}Y_{31} + Q_{3j}\tilde{Q}_{j5}X_{53} + Q_{5k}\tilde{Q}_{k1}X_{15}) \tag{5.38}$$

where $1,2,3$ are the gauge group indices and i,j,k are the flavor indices. We can also add mass terms in a gauge invariant way (see appendix 5.9)

$$W_{mass} = m_1 Q_{1i}\tilde{Q}_{k1} + m_2 Q_{3j}\tilde{Q}_{i3} + m_5 Q_{5k}\tilde{Q}_{j5} \tag{5.39}$$

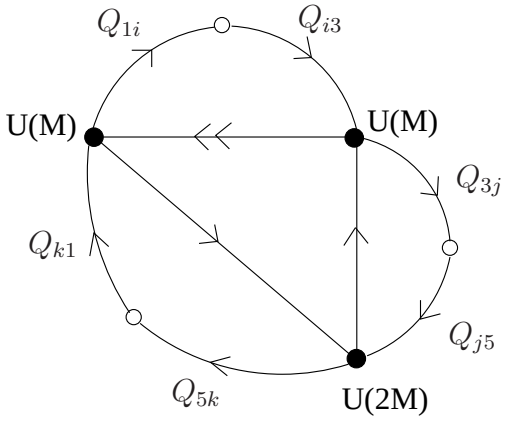

Figure 5.4: Quiver for the dP_2 theory with M fractional branes and flavors.

which mixes the global flavor symmetries. The complete superpotential is thus

$$\begin{aligned} W_{total} &= -\lambda X_{53}Y_{31}X_{15} - \lambda'(Q_{1i}\tilde{Q}_{i3}Y_{31} + Q_{3j}\tilde{Q}_{j5}X_{53} + Q_{5k}\tilde{Q}_{k1}X_{15}) \\ &+ m_1 Q_{1i}\tilde{Q}_{k1} + m_2 Q_{3j}\tilde{Q}_{i3} + m_5 Q_{5k}\tilde{Q}_{j5} \end{aligned} \tag{5.40}$$

Now, we would like to perform Seiberg duality on the $U(2M)$ node in Figure 5.4. We must first make sure that this node is in the free magnetic phase. Taking $N_{f,1}$ to be the rank of the flavor group[5], we want

$$\begin{aligned} N_c + 1 &\leq N_f < \frac{3}{2}N_c \\ 2M + 1 &\leq M + N_{f,1} < 3M \\ M + 1 &\leq N_{f,1} < 2M \end{aligned} \tag{5.41}$$

thus, $N_{f,1} = M+1$ is a possible choice. Now, after a Seiberg Duality the dual gauge factor is $SU(N)$ with $N = N_{f,1} - M$ and dynamical scale Λ. To get the matter content in the dual, we replace the microscopic flavors Q_{5k}, $\tilde{Q}_{j5}$, X_{53}, X_{15} by the dual flavors $\tilde{Q}_{k5}$, Q_{5j}, X_{35}, X_{51} respectively. We also have the mesons related to the fields in the electric theory by

$$\begin{aligned} M_{1k} &= \tfrac{1}{\Lambda}X_{15}Q_{5K} \quad ; \quad \tilde{N}_{j3} = \tfrac{1}{\Lambda}\tilde{Q}_{j5}X_{53} \\ M_{13} &= \tfrac{1}{\Lambda}X_{15}X_{53} \quad ; \quad \tilde{\Phi}_{jk} = \tfrac{1}{\Lambda}\tilde{Q}_{j5}Q_{5k} \end{aligned} \tag{5.42}$$

There is a cubic superpotential coupling the mesons and the dual flavors

$$W_{mes.} = h\,(\,M_{1k}\tilde{Q}_{k5}X_{51} + M_{13}X_{35}X_{51} + \tilde{N}_{j3}X_{35}Q_{5j} + \tilde{\Phi}_{jk}\tilde{Q}_{k5}Q_{5j}\,) \tag{5.43}$$

[5]There is only one residual flavor group since equation 5.39 broke the three flavor groups to the diagonal one.

where $h = \Lambda/\hat{\Lambda}$ with $\hat{\Lambda}$ given by

$$\Lambda_{elect}^{3N_c-N_f}\,\Lambda^{3(N_f-N_c)-N_f} \;=\; \hat{\Lambda}^{N_f} \tag{5.44}$$

where Λ_{elect} is the dynamical scale of the electric theory. Writing the classical superpotential terms of the new fields gives

$$\begin{aligned} W_{clas.} \;&=\; -\,h\,\mu_0\,M_{13}Y_{31} \,+\, \lambda'\,Q_{1i}\tilde{Q}_{i3}Y_{31} \,+\, \mu'\,\tilde{N}_{j3}Q_{3j} \,+\, \mu'\,M_{1k}\tilde{Q}_{k1} \\ &+\; m_1 Q_{1i}\tilde{Q}_{k1} \,+\, m_3 Q_{3j}\tilde{Q}_{i3} \,-\, h\mu^2 \mathrm{Tr}\,\Phi \end{aligned} \tag{5.45}$$

where $\mu_0 = \lambda\Lambda$, $\mu' = \lambda'\Lambda$, and $\mu^2 = -m_5\hat{\Lambda}$. So the complete superpotential in the Seiberg dual is

$$\begin{aligned} W_{dual} \;&=\; -\,h\,\mu_0\,M_{13}Y_{31} \,+\, \lambda'\,Q_{1i}\tilde{Q}_{i3}Y_{31} \,+\, \mu'\,\tilde{N}_{j3}Q_{3j} \,+\, \mu'\,M_{1k}\tilde{Q}_{k1} \\ &+\; m_1 Q_{1i}\tilde{Q}_{k1} \,+\, m_3 Q_{3j}\tilde{Q}_{i3} \,-\, h\mu^2 \mathrm{Tr}\,\Phi \\ &+\; h\,(\,M_{1k}\tilde{Q}_{k5}X_{51} \,+\, M_{13}X_{35}X_{51} \,+\, \tilde{N}_{j3}X_{35}Q_{5j} \,+\, \tilde{\Phi}_{jk}\tilde{Q}_{k5}Q_{5j}\,) \end{aligned} \tag{5.46}$$

This superpotential breaks supersymmetry. So instead of trying to find the moduli which parametrize the vacuum, we can use the formalism established in the previous sections, that is to place ourselves at a minimum (e.g. the most symmetric one) and see if it remains a minimum at 1-loop. The most symmetric minimum arises for the following assignation of vevs

$$\tilde{Q}_{k5} \;=\; \begin{pmatrix} \mu \\ 0 \end{pmatrix} \qquad Q_{5k} \;=\; (\mu; 0) \tag{5.47}$$

with all other vevs set to zero[6] . Parametrizing the perturbations around this minimum, we get

$$\tilde{Q}_{k5} \;=\; \begin{pmatrix} \mu + \delta\tilde{Q}_{5,1} \\ \delta\tilde{Q}_{5,2} \end{pmatrix} \quad ; \quad Q_{5k} \;=\; (\mu + \delta Q_{5,1}\,;\, \delta Q_{5,2}) \quad ; \quad \Phi \;=\; \begin{pmatrix} \delta\Phi_{0,0} & \delta\Phi_{0,1} \\ \delta\Phi_{1,0} & \delta\Phi_{1,1} \end{pmatrix}$$

$$\tilde{Q}_{k1} \;=\; \begin{pmatrix} \delta\tilde{Q}_{1,1} \\ \delta\tilde{Q}_{1,2} \end{pmatrix} \;;\; Q_{1i} \;=\; (\delta Q_{1,1}\,;\, \delta Q_{1,2}) \;;\; \tilde{Q}_{i3} \;=\; \begin{pmatrix} \delta\tilde{Q}_{3,1} \\ \delta\tilde{Q}_{3,2} \end{pmatrix} \;;\; Q_{3j} \;=\; (\delta Q_{3,1}\,;\, \delta Q_{3,2})$$

$$\tilde{N}_{j3} \;=\; \begin{pmatrix} \delta\tilde{N}_{3,1} \\ \delta\tilde{N}_{3,2} \end{pmatrix} \;;\; M_{1k} \;=\; (\delta M_{1,1}\,;\, \delta M_{1,2}) \;;\; M_{13} = \delta M_{13} \;;\; Y_{31} = \delta Y_{31} \;;\; X_{51} = \delta X_{51}$$

$$X_{35} = \delta X_{35} \tag{5.48}$$

[6]Here we take $N_{f,1} = 2$ and $N_c = 1$ for simplicity. This does not affect our conclusions

Inserting this into equation 5.46 gives

$$\begin{aligned} W_{dual} &= -h\,\mu_0\,\delta M_{13}\delta Y_{31} + \lambda'\,\delta Q_{1,1}\delta\tilde{Q}_{3,1}\delta Y_{31} + \lambda'\,\delta Q_{1,2}\delta\tilde{Q}_{3,2}\delta Y_{31} \\ &+ \mu'\,\delta\tilde{N}_{3,1}\delta Q_{3,1} + \mu'\,\delta\tilde{N}_{3,2}\delta Q_{3,2} + \mu'\,\delta M_{1,1}\delta\tilde{Q}_{1,1} + \mu'\,\delta M_{1,2}\delta\tilde{Q}_{1,2} \\ &+ m_1\delta Q_{1,1}\delta\tilde{Q}_{1,1} + m_1\delta Q_{1,2}\delta\tilde{Q}_{1,2} + m_3\delta Q_{3,1}\delta\tilde{Q}_{3,1} + m_3\delta Q_{3,2}\delta\tilde{Q}_{3,2} \\ &- h\mu^2\delta\Phi_{11} + h\,(\,\mu\delta M_{1,1}\delta X_{51} + \delta M_{1,1}\delta\tilde{Q}_{5,1}\delta X_{51} + \delta M_{1,2}\delta\tilde{Q}_{5,2}\delta X_{51} \\ &+ \delta M_{13}\delta X_{35}\delta X_{51} + \mu\delta X_{35}\delta\tilde{N}_{3,1} + \delta X_{35}\delta\tilde{N}_{3,1}\delta Q_{5,1} + \delta X_{35}\delta\tilde{N}_{3,2}\delta Q_{5,2} \\ &+ \mu\delta\tilde{Q}_{5,1}\delta\Phi_{00} + \mu\delta Q_{5,1}\delta\Phi_{00} + \delta Q_{5,1}\delta\tilde{Q}_{5,1}\delta\Phi_{00} + \mu\delta\Phi_{01}\delta\tilde{Q}_{5,2} \\ &+ \delta Q_{5,1}\delta\Phi_{01}\delta\tilde{Q}_{5,2} + \mu\delta\Phi_{10}\delta Q_{5,2} + \delta\tilde{Q}_{5,1}\delta\Phi_{10}\delta Q_{5,2} + \delta\tilde{Q}_{5,2}\delta\Phi_{11}\delta Q_{5,2} \end{aligned} \tag{5.49}$$

Let us put this equation into a friendlier form

$$\begin{aligned} W_{dual} = &- h\,\mu_0\,\phi_1\phi_2 + \lambda'\phi_3\phi_4\phi_2 + \lambda'\phi_5\phi_6\phi_2 \\ &+ \mu'\phi_7\phi_8 + \mu'\phi_9\phi_{10} + \mu'\phi_{11}\phi_{12} \\ &+ \mu'\phi_{13}\phi_{14} + m_1\phi_3\phi_{12} + m_1\phi_5\phi_{14} \\ &+ m_3\phi_8\phi_4 + m_3\phi_{10}\phi_6 - h\mu^2 X \\ &+ h\mu\phi_{11}\phi_{15} + h\phi_{11}\phi_{16}\phi_{15} + h\phi_{13}\phi_{17}\phi_{15} \\ &+ h\phi_1\phi_{18}\phi_{15} + h\mu\phi_{18}\phi_7 + h\phi_{18}\phi_7\phi_{19} \\ &+ h\phi_{18}\phi_9\phi_{20} + h\mu\phi_{16}\phi_{21} + h\mu\phi_{19}\phi_{21} \\ &+ h\phi_{19}\phi_{16}\phi_{21} + h\mu\phi_{22}\phi_{17} + h\phi_{19}\phi_{22}\phi_{17} \\ &+ h\mu\phi_{23}\phi_{20} + h\phi_{16}\phi_{23}\phi_{20} + h\phi_{17}X\phi_{20} \end{aligned} \tag{5.50}$$

where $\phi_1 = \delta M_{13}$, $\phi_2 = \delta Y_{31}$ etc... Analytically solving this superpotential is a daunting task, so we can try to look for a recurring structure. Now, the fields which couple to the SUSY breaking term X are ϕ_{17} and ϕ_{20}. The real and complex parts of these fields get different masses due to SUSY breaking. Therefore any correction at 1-loop to the mass of a field will arise from a coupling to ϕ_{17} or ϕ_{20} (as is the case for the pseudo-moduli in the generalized asymmetric case studied in appendix 5.8.2) [7]. Also, the superpotential above shows that these fields get equal mass terms $\phi_{22}\phi_{17}$

[7]This is due to the following. One can see in 5.50 that the mass terms for ϕ_{17} and ϕ_{20} are decoupled from all other mass terms and the pseudo-moduli only arise in cubic couplings. Now since the scalar potential for the bosonic diagrams is $\left|\frac{\partial W}{\partial \phi}\right|^2$, non-SUSY diagrams will only arise from cubic couplings to ϕ_{17} or ϕ_{20}, all other cubic terms would generate diagrams where the fields running in the loop are supersymmetric.

and $\phi_{23}\phi_{20}$ which are decoupled from the other fields (i.e they don't enter in the mass diagonalization of the other fields). Now, part of the difficulty with the above superpotential comes from having to diagonalize the mass terms. From there we can determine the pseudo-moduli and calculate the correction to their masses. Since the above superpotential contains only quadratic and cubic couplings, diagonalization will give us a superpotential with the general form

$$\begin{aligned} W_{dual} &= h\,X\phi_1\phi_2 \,-\, h\mu^2 X \,+\, h\mu\,\phi_1\,\phi_3 \,+\, h\mu\,\phi_2\,\phi_4 \\ &+ \sum_i c_1^i\,Y\,\phi_1\,\phi_5^i \,+\, \sum_i c_2^i\,Y\,\phi_2\,\phi_5^i \,+\, \sum_i \frac{m_i}{\sqrt{2}}\,h\mu(\phi_5^i)^2 \end{aligned} \tag{5.51}$$

where ϕ_1, ϕ_2 represent ϕ_{17}, ϕ_{20} in the previous equation, and Y is a pseudo-modulus. This is the main structure that would be relevant when trying to calculate the correction to the mass of pseudo-modulus Y, and is just a simple extension of the asymmetric case studied in appendix 5.8.2. Assuming that the masses m_i and constants c_i are real[8], a calculation at 1-loop of the mass of the real part of Y yields the following result[9]

$$\delta m_Y^2 = \frac{h^2\mu^2}{(4\pi)^2}\left\{\sum_i (c_1^i)^2 f(m_i^2) \,+\, \sum_i (c_2^i)^2 f(m_i^2)\right\} \tag{5.52}$$

with

$$f(m_i^2) = \frac{-2}{m_i^2-2}\log 2 \,+\, \frac{m_i^2}{(m_i^2-1)(m_i^2-2)}\log m_i^2 \tag{5.53}$$

a positive definite function. Thus, as long as the coupling constants and masses are real, the correction to the mass of the pseudo-modulus will be positive. The pseudo-moduli of the dP_2 singularity are therefore generically all lifted. The matricial structure of equation 5.46 does not modify these conclusions.

5.5 General case

In the previous section we showed that DSB fractional branes on a dP_2 singularity generically have a metastable vacua since all pseudo-moduli are lifted at 1-loop. In this section we will attempt to make this argument more rigorous and apply it to other singularities. An arbitrary toric singularity with DSB fractional branes

[8]This can be done by an appropriate redefinition of the fields

[9]the imaginary part of Y gets the same mass correction due to holomorphicity

is described by a quiver gauge theory and superpotential. We will show how to add D7–branes in a specific manner so as to generate the appropriate cubic flavor couplings and mass terms. Once this is achieved, the analysis takes place in the Seiberg dual as was done in the previous sections for dP_1 and dP_2. The results of our analysis show that, with the specified configuration of D7–branes, the determination of metastability is greatly simplified and only involves looking at the original superpotential. Thus, although we do not prove that DSB branes on arbitrary singularities generate metastable vacua, we show how one can determine the existence of metastability in a very simple and systematic manner.

We saw that to analyse the infrared dynamics of the gauge theory we take its Seiberg dual. This is usually done by dualizing the gauge group (node) which is in the free magnetic phase. In the following we will always refer to this node as node 2. Now, as we said before, the gauge theory of a fractional DSB brane at a toric singularity is described by a quiver and superpotential. The quiver shown in Figure 5.5 is used as an example and is general enough to show that our conclusions apply to all quiver gauge theories. Now, superpotential terms represent loops running in the quiver e.g $X_{32}X_{21}X_{14}Y_{43}$ in Figure 5.5. From all the superpotential terms, one chooses

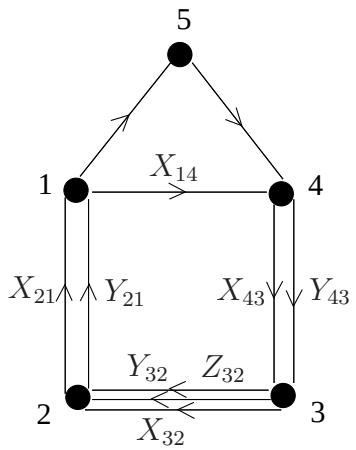

Figure 5.5: Quiver diagram used to illustrate general results. Does not correspond to any geometry in particular.

any term such that it passes through node 2 (the node we wish to dualize). Then one adds flavors to each of the bifundamentals of this term (and only this term), this is always possible [24]. For example, if we choose the term $X_{32}X_{21}X_{14}Y_{43}$ in the superpotential (assuming it exists), then we can add flavors to get Figure 5.6. Now, using the configuration of D7-branes specified in appendix 5.9, one can also add mass terms to each of these flavors in a gauge invariant manner. These arise

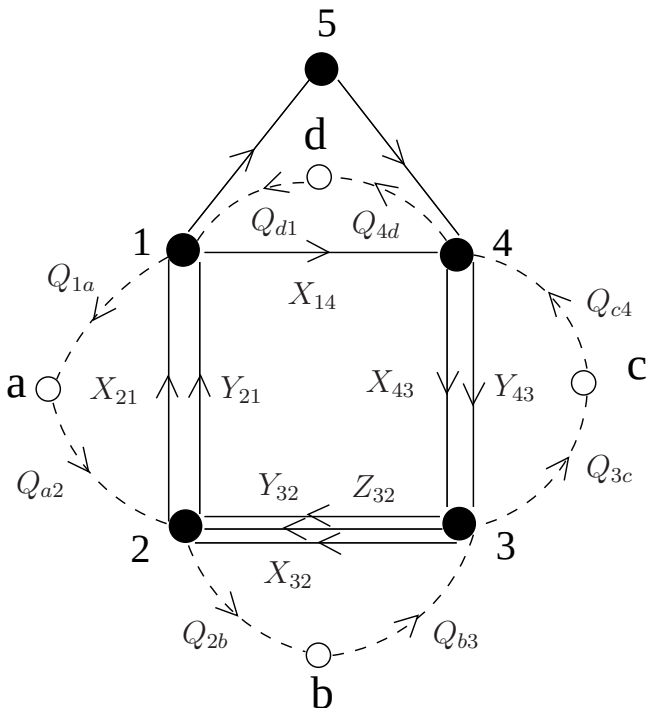

Figure 5.6: Quiver diagram with flavors. White nodes denote flavor groups

from 77-73-37 couplings between D7 and D3–branes. The mass terms can always be introduced in this specific manner and are shown in Figure 5.7, where all but the flavor fields have been removed. So, from the cubic couplings in Figure 5.6 we get the superpotential terms[10]

$$W_{flavor} = \lambda' \left(X_{32} Q_{2b} Q_{b3} + X_{21} Q_{1a} Q_{a2} + X_{14} Q_{4d} Q_{d1} + Y_{43} Q_{3c} Q_{c4} \right) \tag{5.54}$$

we also get the mass terms (see Figure 5.7)

$$W_{mass} = m_2 Q_{a2} Q_{2b} + m_3 Q_{b3} Q_{3c} + m_4 Q_{c4} Q_{4d} + m_1 Q_{d1} Q_{1a} \tag{5.55}$$

where we assume that λ' and m_i are real[11]. These mass terms break the flavor group into a diagonal subgroup.

Summarizing the procedure so far, we start with the gauge theory for a DSB fractional brane, taking the gauge group with highest rank, we pick a superpotential term which passes through this gauge group (recall superpotential terms correspond

[10]Here we assume the same coupling, but the conclusions hold for arbitrary non-zero real couplings

[11]This should be possible by an appropriate redefiniton of the fields

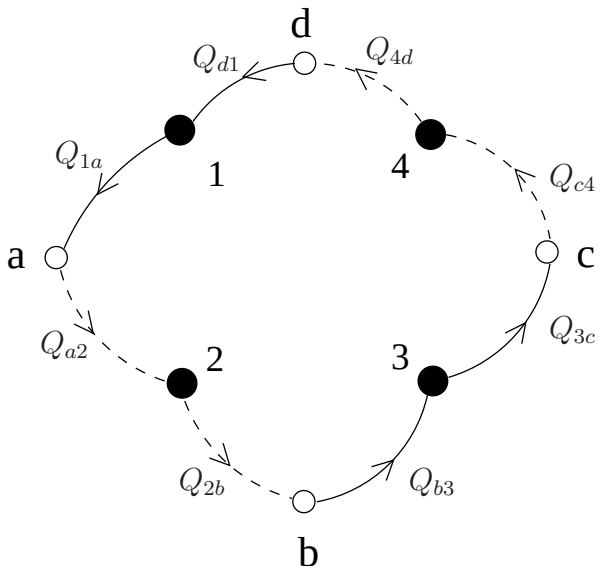

Figure 5.7: Quiver diagram with flavors. Mass terms come in solid pairs and dashed pairs.

to loops in the quiver). We then give cubic couplings to flavors for each bifundamental in this term, and gauge invariant mass terms for all the flavor fields, as illustrated in Figures 5.6 and 5.7 (the fact that this is always possible is shown in appendix 5.9). What we will do in the following is show that in the Seiberg dual of this theory, all fields transforming in at least one the flavor groups (all fields with at least one flavor index), and all fields which get dualized get mass at tree-level or at 1-loop.

Since node 2 is in the free magnetic phase, we take its Seiberg dual. The only relevant fields in this case are the ones connected to node 2, as shown if Figure 5.8. The Seiberg dual gives us Figure 5.9 where the M's are mesons with indices in the gauge groups, R's and S's are mesons with only one index in the flavor group, and X_{ab} is a meson with both indices in the flavor groups. Now, we have to take the dual of the flavor superpotential W_{flavor} and the mass superpotential W_{mass}. We also have to add the superpotential containing the mesons W_{mesons}. The total superpotential (excluding the original one) becomes

$$W_{flavordual} = \lambda' \left(S^1_{3b} Q_{b3} + R^1_{a1} Q_{1a} + X_{14} Q_{4d} Q_{d1} + Y_{43} Q_{3c} Q_{c4} \right) \tag{5.56}$$

$$W_{massdual} = m_2 \underline{X_{ab}} + m_3 Q_{b3} Q_{3c} + m_4 Q_{c4} Q_{4d} + m_1 Q_{d1} Q_{1a} \tag{5.57}$$

$$W_{mesons} = h \left(\underline{X_{ab} \tilde{Q}_{b2} \tilde{Q}_{2a}} \right.$$

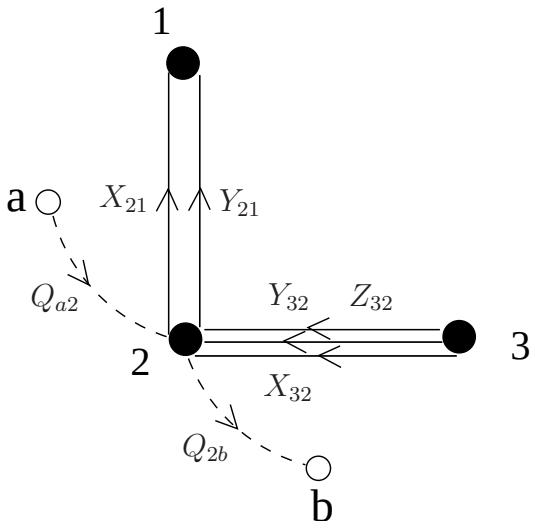

Figure 5.8: Relevant part of quiver before Seiberg duality.

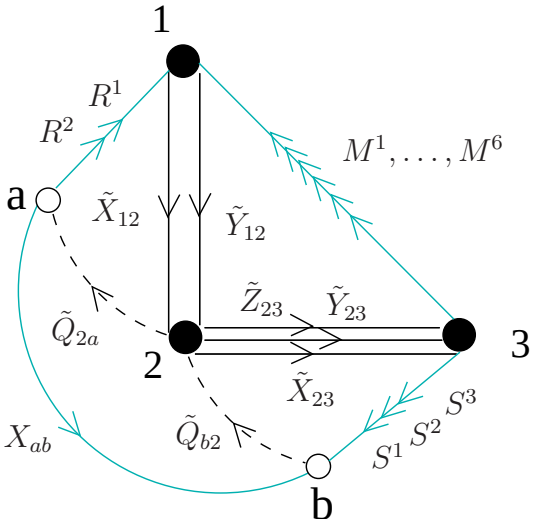

Figure 5.9: Relevant part of the quiver after Seiberg duality on node 2.

$$
\begin{aligned}
&+ \quad R^1_{a1}\tilde{X}_{12}\tilde{Q}_{2a} \,+\, R^2_{a1}\tilde{Y}_{12}\tilde{Q}_{2a} \\
&+ \quad S^1_{3b}\tilde{Q}_{b2}\tilde{X}_{23} \,+\, S^2_{3b}\tilde{Q}_{b2}\tilde{Y}_{23} \,+\, S^3_{3b}\tilde{Q}_{b2}\tilde{Z}_{23} \\
&+ \quad M^1_{31}\tilde{X}_{12}\tilde{X}_{23} \,+\, M^2_{31}\tilde{X}_{12}\tilde{Y}_{23} \,+\, M^3_{31}\tilde{X}_{12}\tilde{Z}_{23} \\
&+ \quad M^4_{31}\tilde{Y}_{12}\tilde{X}_{23} \,+\, M^5_{31}\tilde{Y}_{12}\tilde{Y}_{23} \,+\, M^6_{31}\tilde{Y}_{12}\tilde{Z}_{23}\,)
\end{aligned}
\tag{5.58}
$$

Now, the crucial point is that given the specified configuration, where we give flavors to all bifundamentals of a superpotential term and give masses to all the flavors in a gauge invariant way, we will always end up with a term such as the underlined one ($m_2 X_{ab} + h X_{ab}\tilde{Q}_{b2}\tilde{Q}_{2a}$). This term is precisely the SUSY breaking term studied in the generalized asymmetric case in appendix 5.8.2 (X_{ab}, $\tilde{Q}_{b2}$, $\tilde{Q}_{2a}$ correspond to X, ϕ_1, ϕ_2 respectively). The fields $\tilde{Q}_{b2}$ and $\tilde{Q}_{2a}$ therefore get non-degenerate masses for the real and imaginary parts of their complex scalar and X_{ab} gets mass at 1-loop. Also, as in the generalized asymmetric case, any field which has a cubic coupling to the SUSY breaking fields $\tilde{Q}_{b2}$ or $\tilde{Q}_{2a}$ will get a mass at 1-loop. Now, since W_{mesons} contains all gauge invariant cubic operators passing through node 2, a little thought shows that all dualized fields with no flavor index (e.g $\tilde{X}$, $\tilde{Y}$) and all mesons with one flavor index (e.g R or S) couple to the SUSY breaking fields[12] (Figure 5.9 clarifies this statement). They will thus all get mass at 1-loop. Also, the flavor fields which don't get dualized (e.g Q_{b3}) get mass at tree level from W_{mass}. So the only fields which don't get mass at tree-level or at 1-loop are the mesons with no flavor index, and the bifundamentals which do not get dualized. These don't get masses at 1-loop since they do not couple to the SUSY breaking fields $\tilde{Q}_{b2}$ and $\tilde{Q}_{2a}$. They can however get mass at tree-level from the original superpotential. So, the criteria for a metastable vacua is that the original superpotential give mass to all the bifundamentals after dualization. For example, if we apply this criteria to the dP_2 case studied previously, the original superpotential for the fractional DSB brane is

$$W = -\lambda X_{53} Y_{31} X_{15} \tag{5.59}$$

after dualization, we get

$$W = -\lambda M_{13} Y_{31} \tag{5.60}$$

so this fractional brane, after adding the D7–branes in the appropriate configuration,

[12] This is obvious since the mesons with one flavor are composed of a flavor field with a leg in node 2 and a bifundamental field, whereas a dualized field also has a leg in 2 and so couples to a SUSY breaking term

will generate a metastable vacua will all moduli stabilized[13]. A more rigorous and elaborate proof is provided in the appendix where we take into account the matricial structure, and show that all fields, except for goldstone bosons, get mass at tree-level or at 1-loop.

5.6 Specific examples

5.6.1 dP_3 case

For dP_3, a possible DSB fractional brane is shown in Figure 5.10 below [3].

The superpotential is

$$W = X_{13}X_{35}X_{51} \tag{5.61}$$

Now, node 1 has $N_f < N_c$ so will lead to dynamical supersymmetry breaking in the infrared. Following the procedure of the previous section, we add flavors to the bifundamentals X_{13}, X_{35} and X_{51}. We have to make sure node 1 is in the free magnetic phase

$$\begin{aligned} N_c + 1 &\leq N_f < \frac{3}{2}N_c \\ P + 2 &\leq N_{f,0} + N_{f,1} < \frac{3}{2}(P+1) \\ P + 2 &\leq 1 + N_{f,1} < \frac{3}{2}(P+1) \end{aligned} \tag{5.62}$$

where $N_{f,1}$ is the rank of the flavor group. So we can set $N_{f,1} = P + 1$. Dualizing node 1, the above superpotential becomes

$$W = X_{35}M_{53} \tag{5.63}$$

where M_{53} is the meson $X_{51}X_{13}$. So, following the results of the previous section, we can conclude that this DSB fractional brane generates a metastable vacua with all pseudo-moduli lifted.

[13]There might be free fields, that is fields which appear in the quiver but not in the superpotential. These are flat directions, but are not dangerous since they do not restore SUSY at large vevs, i.e they run orthogonal to the runaway direction. It is assumed they get mass at 2-loops.

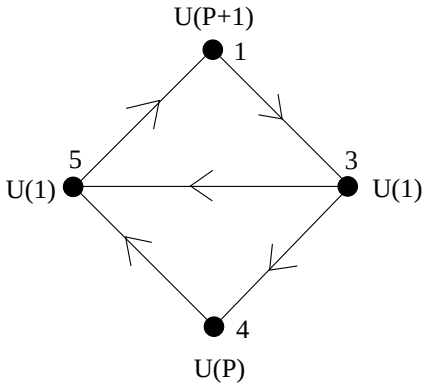

Figure 5.10: Quiver diagram for the dP_3 theory with a DSB fractional branes.

5.6.2 Phase 1 of PdP_4

For phase 1 of PdP_4, a possible DSB fractional brane is shown in Figure 5.11 [3]. The superpotential is

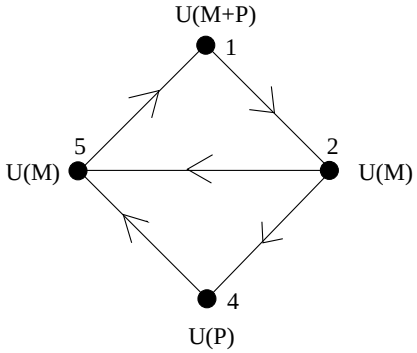

Figure 5.11: Quiver diagram for the dP_4 theory with a DSB fractional branes.

$$W = -X_{25}X_{51}X_{12} \tag{5.64}$$

Now, node 1 has $N_f < N_c$ so will lead to dynamical supersymmetry breaking in the infrared. Following the procedure of the previous section, we add flavors to the bifundamentals X_{12}, X_{25} and X_{51}. We have to make sure node 1 is in the free magnetic phase

$$\begin{aligned} N_c + 1 &\leq N_f < \frac{3}{2}N_c \\ M + P + 1 &\leq M + N_{f,1} < \frac{3}{2}(M+P) \\ P + 2 &\leq M + N_{f,1} < \frac{3}{2}(M+P) \end{aligned} \tag{5.65}$$

where $N_{f,1}$ is the rank of the flavor group. We can set $N_{f,1} = P + 1$. Dualizing node 1, the above superpotential becomes

$$W = X_{25} M_{52} \tag{5.66}$$

where M_{53} is the meson $X_{51} X_{12}$. Again we can conclude that this DSB fractional brane generates a metastable vacua with all pseudo-moduli lifted.

The $Y^{p,q}$ fractional branes have been analysed in [6].

5.7 Conclusion

Using the methodology we developed in Section 5.2, we have devised a simple method of determining whether fractional DSB branes, coupled in the appropriate manner to D7–branes, generate metastable vacua in the infrared. We have also shown how this configuration of D7–branes has a simple description in the mirror Riemann surface. However, we have seen that in the dP_1 case there is a free field which appears in the quiver but not in the superpotential, and although not stated, this is also the case for dP_2 and other geometries. These however do not affect the stability of the SUSY breaking minimum since they run orthogonal to the runaway direction. It is also assumed they will get mass at two-loops. Our results will be helpful in generating metastable supersymmetry breaking sectors coupled to Standard Model like sectors via gauge mediation. In the next chapter, we will show how this can be achieved using D–branes at toric singularities.

5.8 Appendix: Technical details about the calculations via Feynman diagrams

5.8.1 Basic amplitudes

We will be interested in computing two point functions for the pseudo-moduli at one loop, and in section 5.2.2 also tadpole diagrams. There are just a few species of diagrams entering in the calculation, which we will present now for the two point function. The (real) bosonic fields are denoted by ϕ_i and the (Weyl) fermions by ψ_i. The pseudo-modulus we are interested in is denoted by φ.

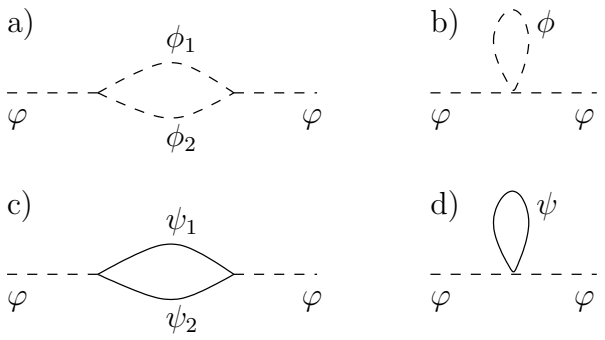

Figure 5.12: Feynman diagrams contributing to the one-loop two point function. The dashed line denotes bosons and the solid one fermions.

Bosonic contributions

These come from two terms in the Lagrangian. First there is a diagram coming from terms of the form (Figure 5.12b)

$$\mathcal{L} = \ldots + \lambda\varphi^2\phi^2 - \frac{1}{2}m^2\phi^2 \tag{5.67}$$

giving an amplitude (we will be using dimensional regularization)

$$i\mathcal{M} = \frac{-2i\lambda}{(4\pi)^2}m^2\left(\frac{1}{\epsilon} - \gamma + 1 + \log 4\pi - \log m^2\right) \tag{5.68}$$

The other contribution comes from the diagram in Figure 5.12a

$$\mathcal{L} = \ldots + \lambda\varphi\phi_1\phi_2 - \frac{1}{2}m_1^2\phi_1^2 - \frac{1}{2}m_2^2\phi_2^2 \tag{5.69}$$

which contributes to the two point function with an amplitude

$$i\mathcal{M} = \frac{i\lambda^2}{(4\pi)^2}\left(\frac{1}{\epsilon} - \gamma + \log 4\pi - \int_0^1 dx \log \Delta\right) \tag{5.70}$$

where here and in the following we denote $\Delta \equiv x m_1^2 + (1-x)m_2^2$.

Fermionic contributions

The relevant vertices here are again of two possible kinds, one of which is non-renormalizable. The cubic interaction comes from terms in the Lagrangian given by the diagram in Figure 5.12c

$$\mathcal{L} = \ldots + \varphi(a\psi_1\psi_2 + a^*\bar{\psi}_1\bar{\psi}_2) + \frac{1}{2}m_1(\psi_1^2 + \bar{\psi}_1^2) + \frac{1}{2}m_2(\psi_2^2 + \bar{\psi}_2^2) \tag{5.71}$$

The contribution from such vertices is given by

$$\begin{aligned} i\mathcal{M} \;=\; & \int_0^1 dx \left\{ \frac{-2im_1m_2}{(4\pi)^2}(a^2 + (a^2)^*)\left(\frac{1}{\epsilon} - \gamma + \log 4\pi - \log\Delta\right)\right. \\ & \left. - \frac{8i|a|^2}{(4\pi)^2}\Delta\left(\frac{1}{\epsilon} - \gamma + \log 4\pi + \frac{1}{2} - \log\Delta\right)\right\} \end{aligned} \tag{5.72}$$

The other fermionic contribution, which one does not need as long as one is dealing with renormalizable interactions only (but we will need in the main text when analyzing the pseudo-modulus θ), is given by terms in the Lagrangian of the form (Figure 5.12d)

$$\mathcal{L} = \ldots + \lambda\varphi^2(\psi^2 + \bar{\psi}^2) + \frac{1}{2}m(\psi^2 + \bar{\psi}^2) \tag{5.73}$$

which contributes to the total amplitude with

$$i\mathcal{M} = \frac{8\lambda m i}{(4\pi)^2}m^2\left(\frac{1}{\epsilon} - \gamma + 1 + \log 4\pi - \log m^2\right) \tag{5.74}$$

5.8.2 Basic superpotentials

The previous amplitudes are the basic ingredients entering the computation, but in general the number of diagrams contributing to the two point amplitudes is quite big, so calculating all the contributions by hand can get quite involved in particular examples. Happily, one finds that complicated models (such as dP_1, studied in the main text) reduce to performing the analysis for only two different superpotentials, which we analyze in this section.

The symmetric case

We want to study in this section a superpotential of the form

$$W = h(X\phi_1\phi_2 + \mu\phi_1\phi_3 + \mu\phi_2\phi_4 - \mu^2 X) \tag{5.75}$$

This model is a close cousin of the basic O'Raifeartaigh model. We are interested in the one loop contribution to the two point function of X, which is massless at tree level.

From the (F-term) bosonic potential one obtains the following terms entering the one loop computation

$$\begin{aligned} V &= \left[|hX\phi_2|^2 + |h|^2\mu(X\phi_2\phi_3^* + X^*\phi_2^*\phi_3) + |h|^2\mu(X\phi_1\phi_4^* + X^*\phi_1^*\phi_4)\right] \\ &\quad + |h|^2\mu^2(\phi_1\phi_2 + \phi_1^*\phi_2^*) + \sum_{i=1}^{4}|h|^2\mu^2|\phi_i|^2 \end{aligned} \tag{5.76}$$

In order to do the computation it is useful to diagonalize the mass matrix by introducing ϕ_+ and ϕ_- such that

$$\phi_1 = \frac{1}{\sqrt{2}}(\phi_+ + i\phi_-) \qquad \phi_2 = \frac{1}{\sqrt{2}}(\phi_+ - i\phi_-) \tag{5.77}$$

and ϕ_a, ϕ_b such that

$$\phi_3^* = \frac{1}{\sqrt{2}}(\phi_a + i\phi_b) \qquad \phi_4^* = \frac{1}{\sqrt{2}}(\phi_a - i\phi_b) \tag{5.78}$$

With these redefinitions the bosonic scalar potential decouples into identical ϕ_+ and ϕ_- sectors, giving two decoupled copies of

$$\begin{aligned} V &= |h|^2|X|^2|\phi_+|^2 + |h|^2\mu^2(|\phi_+|^2 + |\phi_a|^2) \\ &\quad + |h|^2\mu(X\phi_+\phi_a + X^*\phi_+^*\phi_a^*) - \frac{|h|^2\mu^2}{2}\left(\phi_+^2 + (\phi_+^2)^*\right) \end{aligned} \tag{5.79}$$

Calculating the amplitude consists simply of constructing the (very few) two point diagrams from the potential above and plugging the formulas above for each diagram (the fermionic part is even simpler in this case). The final answer is that in this model the one loop correction to the mass squared of X is given by

$$\delta m_X^2 = \frac{|h^4|\mu^2}{8\pi^2}(\log 4 - 1) \tag{5.80}$$

The generalized asymmetric case

The next case is slightly more complicated, but will suffice to analyse completely all the models we encounter. We will be interested in the one loop contribution to the mass of the pseudo-moduli Y in a theory with superpotential

$$W = h(X\phi_1\phi_2 + \mu\phi_1\phi_3 + \mu\phi_2\phi_4 - \mu^2 X) + k(rY\phi_1\phi_5 + \mu\phi_5\phi_7) \tag{5.81}$$

with k and r arbitrary complex numbers. The procedure is straightforward as above, so we will just quote the result. We obtain an amplitude given by

$$i\mathcal{M} = \frac{-i}{(4\pi)^2}|h^2 r\mu|^2 \mathcal{C}\left(\frac{|k|^2}{|h|^2}\right) \tag{5.82}$$

where we have defined $\mathcal{C}(t)$ as

$$\mathcal{C}(t) = \frac{t}{2-t}\left(\log 4 - \frac{t}{t-1}\log t\right) \tag{5.83}$$

Note that this is a positive definite function, meaning that the 1-loop correction to the mass is always positive, and the pseudo-moduli get stabilized for any (nonzero) value of the parameters. Also note that the limit of vanishing t with $|r|^2 t$ fixed (i.e., vanishing masses for ϕ_5 and ϕ_7, but nonvanishing coupling of Y to the supersymmetry breaking sector) gives a nonvanishing contribution to the mass of Y. We will often refer to ϕ_1 and ϕ_2 as the SUSY breaking fields since any cubic coupling to one of them generates a mass at 1-loop.

5.9 Appendix: D7–branes on the Riemann surface

We saw in Chapter 4 that the gauge theory of D3–branes at toric singularities is given by a dimer diagram. This corresponds to a bi-partite tiling of T^2, where faces correspond to gauge groups, edges correspond to bifundamentals, and nodes correspond to superpotential terms. The bi-partite nature of the graph (i.e nodes are black or white, with each white node only connected to black nodes and vice-versa) gives an orientation to the graph, e.g black to white. The dimer diagram of D3–branes on the complex cone over dP_2 is shown in Figure 5.13

As shown in [16], D3–branes on a toric singularity are mirror to D6–branes intersecting on a Riemann surface Σ. This Riemann surface is just a thickening of the

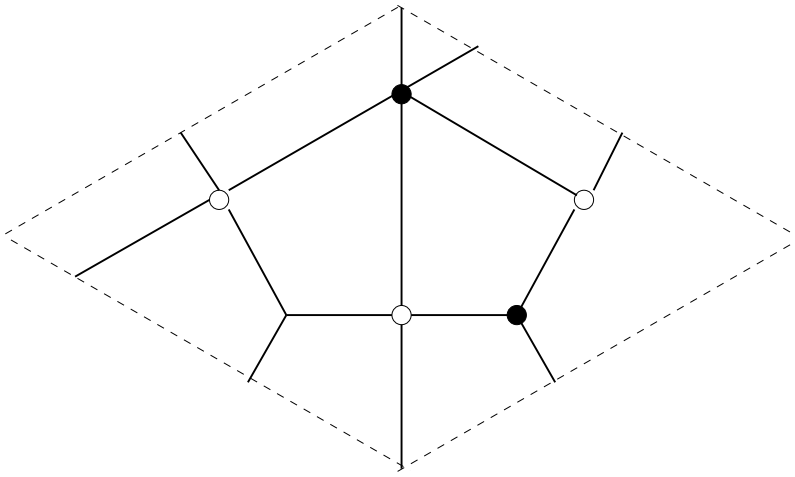

Figure 5.13: Dimer diagram for D3–branes at a dP_2 singularity.

web diagram of the toric singularity, with punctures associated to external legs of the web diagram. Now, D6–branes wrap 1-cycles on this Riemann surface. Each independent 1-cycle wrapped by a D6–brane is associated to a gauge group, bifundamentals arise at the intersections of these 1-cycles, and superpotential terms arise from closed discs bounded by the D6–branes. Also, in [24], the authors showed that D7–branes passing through a toric singularity correspond in the mirror Riemann surface Σ to non-compact 1-cycles which come from infinity at one puncture and go to infinity at another (see Figure 5.14). The Riemann surface mirror to D3 and D7–branes at a dP_2 singularity is shown in Figure 5.15. As we stated in Section

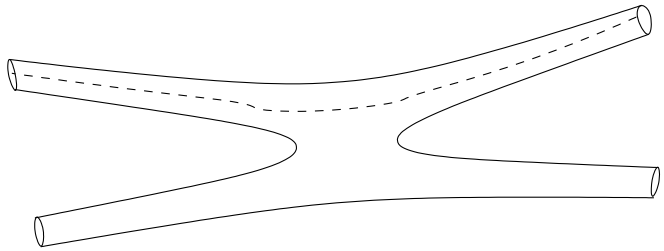

Figure 5.14: Schematic representation of D7–branes on the mirror Riemann surface. In this case the Riemann surface is that of a conifold singularity and the D7–branes represent non-compact 1-cycles extending from one puncture at infinity to another. They are shown as dashed lines.

5.5, given a gauge theory of D3–branes at a toric singularity, we pick a term in the superpotential, this corresponds to a loop in the quiver, and we give this term flavors for each of its bifundamentals and masses for all the flavors (in a gauge invariant way). For example, the quiver with flavors for the dP_2 theory is shown in Figure

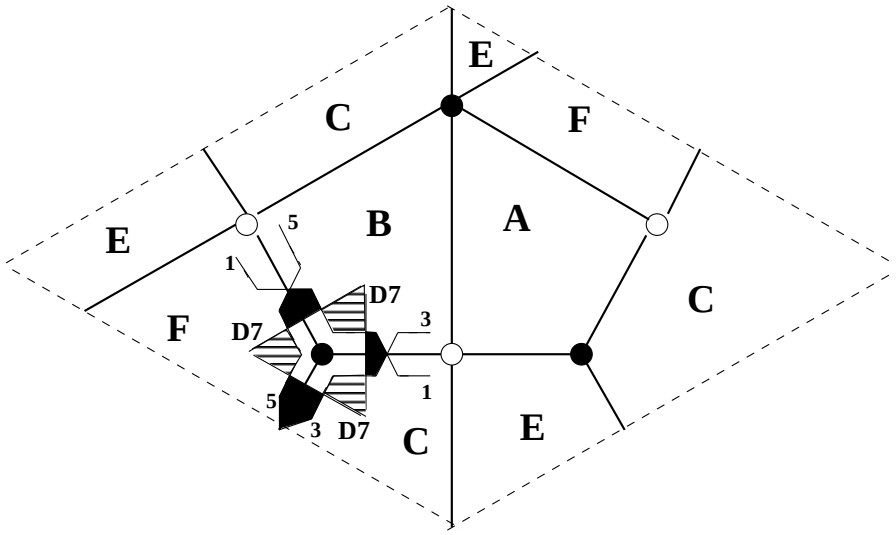

Figure 5.15: Riemann surface mirror to D3 and D7–branes at a dP_2 singularity. The D7–branes extend from one puncture to another. Also, we have shown gauge groups 1, 3, 5 which correspond to zig-zag paths on the Riemann surface.

5.16. It is easy to see that from Figure 5.15, one obtains the flavors in Figure 5.16

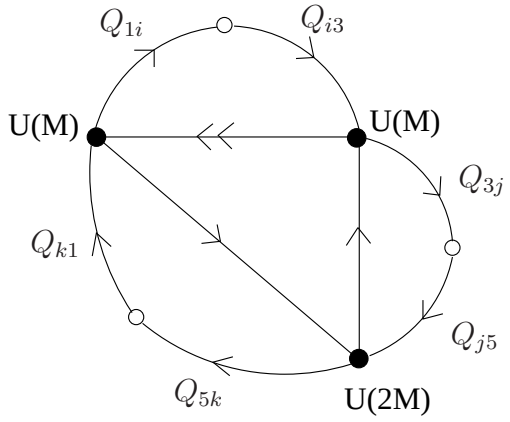

Figure 5.16: Quiver for the dP_2 theory with M fractional branes and flavors.

with superpotential terms

$$W_{flavor} = \lambda'(Q_{1i}\tilde{Q}_{i3}Y_{31} + Q_{3j}\tilde{Q}_{j5}X_{53} + Q_{5k}\tilde{Q}_{k1}X_{15}) \tag{5.84}$$

and mass terms

$$W_{mass} = m_1 Q_{1i}\tilde{Q}_{k1} + m_2 Q_{3j}\tilde{Q}_{i3} + m_5 Q_{5k}\tilde{Q}_{j5} \tag{5.85}$$

Indeed, the procedure is always the same, a superpotential term corresponds to a loop in the quiver, a node in the dimer, and a node in the Riemann surface. If one

places D7–branes in the Riemann surface circling the node, as in Figure 5.15, then one will generate flavors for all the bifundamentals of this superpotential term. This will also generate cubic superpotential terms as in (5.84) and mass terms for all the flavors in a gauge invariant manner as in (5.85). Indeed, the cubic couplings come from disks bounded by one D7 and two D3's (black surface in Figure 5.15) and mass terms come from disks bounded by two D7's and one D3 (striped surface in Figure 5.15). This procedure is completely general and applies to all gauge theories for branes at toric singularities[14].

5.10 Appendix: Detailed proof of Section 5.5

Recall that in Section 5.5, we had as an illustrative example, the gauge theory given by the quiver in Figure 5.17. Since node 2 is the one we wish to dualize, the only

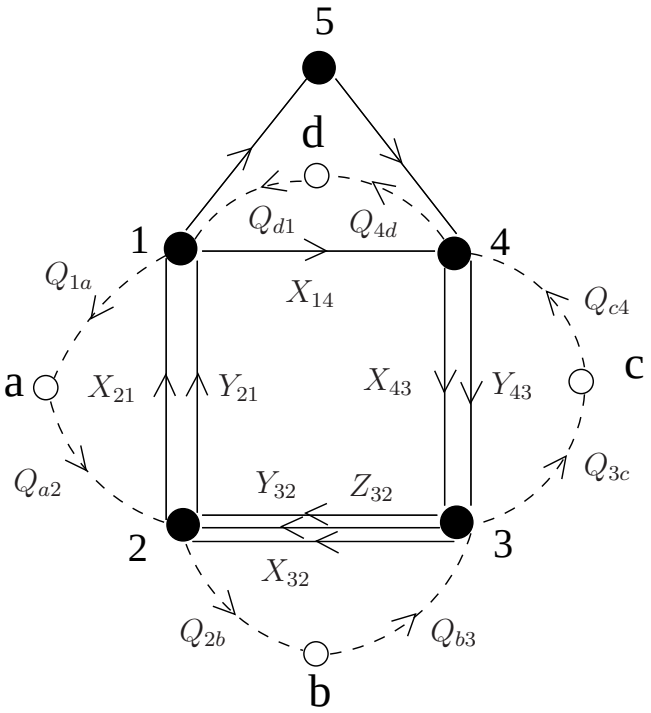

Figure 5.17: Quiver diagram with flavors. White nodes denote flavor groups

relevant part of the diagram is shown in Figure 5.18. And the Seiberg dual gives us Figure 5.19. The above choice of D7–branes, which we showed in appendix 5.9 can

[14]This procedure does not apply if the superpotential passes through the same dualized gauge group twice. However no example of this has been found for any DSB fractional branes.

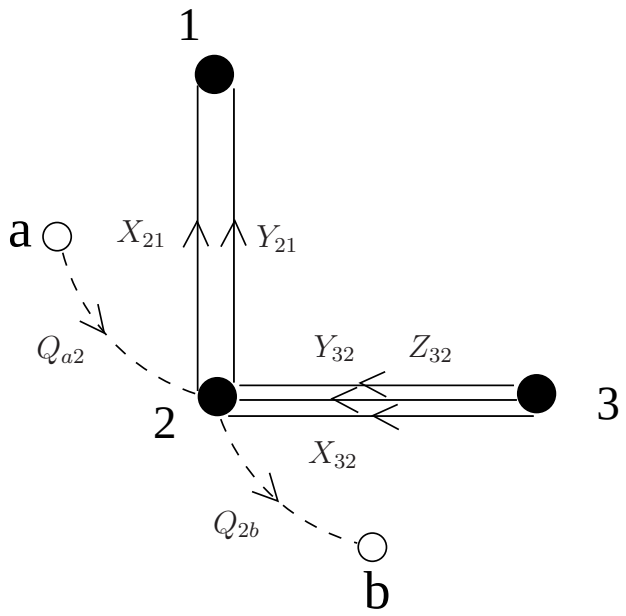

Figure 5.18: Relevant part of quiver before Seiberg duality.

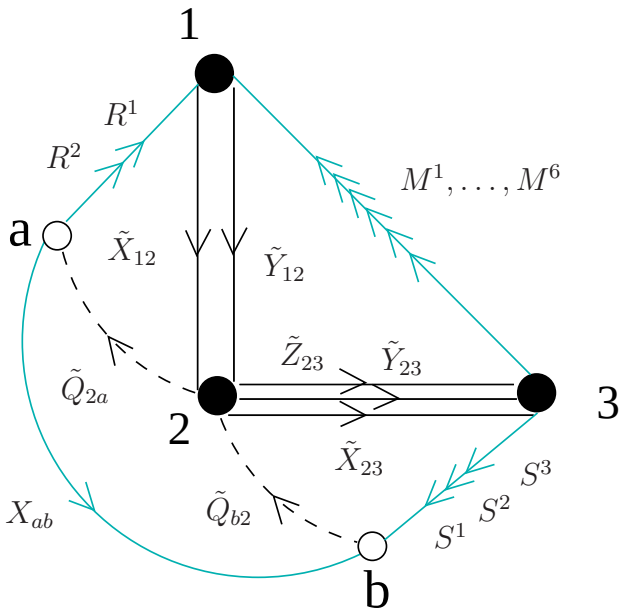

Figure 5.19: Relevant part of the quiver after Seiberg duality on node 2.

be applied to arbitrary toric singularities, gives us the superpotential terms

$$W_{flavor} = \lambda' \left(X_{32} Q_{2b} Q_{b3} + X_{21} Q_{1a} Q_{a2} + X_{14} Q_{4d} Q_{d1} + Y_{43} Q_{3c} Q_{c4} \right) \tag{5.86}$$

$$W_{mass} = m_2 Q_{a2} Q_{2b} + m_3 Q_{b3} Q_{3c} + m_4 Q_{c4} Q_{4d} + m_1 Q_{d1} Q_{1a} \tag{5.87}$$

Taking the Seiberg dual of node 2 gives.

$$W_{flavordual} = \lambda' \left(S^1_{3b} Q_{b3} + R^1_{a1} Q_{1a} + X_{14} Q_{4d} Q_{d1} + Y_{43} Q_{3c} Q_{c4} \right) \tag{5.88}$$

$$W_{massdual} = m_2 \underline{X_{ab}} + m_3 Q_{b3} Q_{3c} + m_4 Q_{c4} Q_{4d} + m_1 Q_{d1} Q_{1a} \tag{5.89}$$

$$\begin{aligned} W_{mesons} &= h \left(\underline{X_{ab} \tilde{Q}_{b2} \tilde{Q}_{2a}} \right. \\ &+ R^1_{a1} \tilde{X}_{12} \tilde{Q}_{2a} + R^2_{a1} \tilde{Y}_{12} \tilde{Q}_{2a} \\ &+ S^1_{3b} \tilde{Q}_{b2} \tilde{X}_{23} + S^2_{3b} \tilde{Q}_{b2} \tilde{Y}_{23} + S^3_{3b} \tilde{Q}_{b2} \tilde{Z}_{23} \\ &+ M^1_{31} \tilde{X}_{12} \tilde{X}_{23} + M^2_{31} \tilde{X}_{12} \tilde{Y}_{23} + M^3_{31} \tilde{X}_{12} \tilde{Z}_{23} \\ &+ \left. M^4_{31} \tilde{Y}_{12} \tilde{X}_{23} + M^5_{31} \tilde{Y}_{12} \tilde{Y}_{23} + M^6_{31} \tilde{Y}_{12} \tilde{Z}_{23} \right) \end{aligned} \tag{5.90}$$

where we have not included the original superpotential. Now, the crucial point is that the underlined terms will appear for any quiver gauge theory once we have placed the D7–branes in the stated configuration. Indeed, we saw in appendix 5.9 that we can always place D7–branes so as to give flavors to all bifundamentals of a superpotential term. This configuration will give cubic 73-33-37 couplings to each bifundamental in the term, and gauge invariant mass terms to all the flavors. So with this configuration, there will always be in the original quiver (before dualizing), one flavor field in the fundamental and one in the anti-fundamental of the node we wish to dualize (e.g Q_{a2} ,Q_{2b} in Figure 5.18). Also, these fields will always have a cuadratic coupling in W_{mass} (e.g $m_2 Q_{a2} Q_{2b}$). After dualization, the mass term becomes a linear meson term (e.g X_{ab}) and this meson gets a cubic coupling to the dualized fields in W_{mesons} (e.g $X_{ab} \tilde{Q}_{b2} \tilde{Q}_{2a}$). It is also obvious that this meson does not appear in any other terms. SUSY is broken when taking the F-term with respect to this meson, which gives

$$\tilde{Q}_{b2} \tilde{Q}_{2a} = \mu^2 \mathbf{1}_{N_f} \tag{5.91}$$

where $h\mu^2 = -m_2$. This induces SUSY breaking for $N_f > N_c$, where N_f is the rank of the flavor group[15] and N_c is the rank of the dualized gauge group (e.g node 2)[16].

[15]Recall that the mass terms break the flavor groups to a diagonal subgroup.

[16]The condition $N_f > N_c$ must be verified case per case, but can be assumed for now

The most symmetric assignation of vevs is[17]

$$\tilde{Q}_{b2} \,=\, \begin{pmatrix} \mu \mathbf{1}_{N_c} \\ 0 \end{pmatrix} \quad ; \; \tilde{Q}_{2a} \,=\, (\mu \mathbf{1}_{N_c} \,;\, 0) \tag{5.92}$$

with all other vevs set to zero. This solves all other F-term equations. Parametrizing the perturbations around this minimum, we get

$$\tilde{Q}_{b2} \,=\, \begin{pmatrix} \mu + \phi_1 \\ \phi_2 \end{pmatrix} \quad ; \; \tilde{Q}_{2a} \,=\, (\mu + \phi_3 \,;\, \phi_4) \quad ; \; X_{ab} = \begin{pmatrix} X_{00} & X_{01} \\ X_{10} & X_{11} \end{pmatrix} \tag{5.93}$$

and the underlined term gives

$$\begin{aligned} h X_{ab} \tilde{Q}_{b2} \tilde{Q}_{2a} - h\mu^2 X_{ab} \;&=\; h X_{11}\, \phi_2\, \phi_4 - h\mu^2 X_{11} + h\mu\, \phi_2\, X_{01} + h\mu\, \phi_4\, X_{10} \\ &+\; h\mu\, \phi_1\, X_{00} + h\mu\, \phi_3\, X_{00} + h\, \phi_1\, \phi_3 X_{00} + h\, \phi_2\, \phi_3 X_{01} \\ &+\; h\, \phi_1\, \phi_4 X_{10} \end{aligned} \tag{5.94}$$

It is important to note that all the fields in (5.93) will have cuadratic couplings only in the underlined term (5.94). Thus, one can safely study this term, and the conclusions are independent of the other terms in the superpotential. Diagonalizing (5.94) gives

$$\begin{aligned} h X_{ab} \tilde{Q}_{b2} \tilde{Q}_{2a} - h\mu^2 X_{ab} \;&=\; h X_{11}\, \phi_2\, \phi_4 - h\mu^2 X_{11} + h\mu\, \phi_2\, X_{01} + h\mu\, \phi_4\, X_{10} \\ &+\; \sqrt{2} h\mu\, \phi_+\, X_{00} + \frac{h}{2}\, \phi_+^2\, X_{00} - \frac{h}{2}\, \phi_-^2\, X_{00} \\ &+\; \frac{h}{\sqrt{2}}\, (\xi_+ - \xi_-)\, \phi_2 X_{01} + \frac{h}{\sqrt{2}}\, (\xi_+ + \xi_-)\, \phi_4 X_{10} \end{aligned} \tag{5.95}$$

where

$$\xi_+ = \frac{1}{\sqrt{2}}\, (\phi_1 + \phi_3) \quad ; \quad \xi_- = \frac{1}{\sqrt{2}}\, (\phi_1 - \phi_3) \tag{5.96}$$

This term is similar to the generalized asymmetric case studied in appendix 5.8.2 with

$$X_{11} \to X \,;\, \phi_4 \to \phi_1 \,;\, \phi_2 \to \phi_2 \,;\, X_{10} \to \phi_3 \,;\, X_{01} \to \phi_4 \tag{5.97}$$

So here X_{11} is the linear term that breaks SUSY, and ϕ_2, ϕ_4 are the SUSY breaking fields. In (5.95), the only massless fields at tree-level are X_{11} and ξ_-. Comparing to the ISS case in Section 5.2.1 shows that $\mathrm{Im}\, \xi_-$ is a Goldstone boson and X_{11}, $\mathrm{Re}\, \xi_-$ get mass at tree-level. As for ϕ_2 and ϕ_4, setting $\rho_+ = \frac{1}{\sqrt{2}}(\phi_2 + \phi_4)$ and $\rho_- = \frac{1}{\sqrt{2}}(\phi_2 - \phi_4)$ gives us $\mathrm{Re}(\rho_+)$ and $\mathrm{Im}\,(\rho_-)$ massless and the rest massive. Following the discussion in Section 5.2.1, $\mathrm{Re}(\rho_+)$ and $\mathrm{Im}\,(\rho_-)$ are just the Goldstone

[17] Here we take $N_f = 2$ and $N_c = 1$ for simplicity. This does not affect our conclusions.

bosons of the broken $SU(N_f)$ symmetry[18]. We have thus shown that the dualized flavors (e.g $\tilde{Q}_{b2}$, $\tilde{Q}_{2a}$) and the meson with two flavor indices (e.g X_{ab}) get mass at tree-level or at 1-loop unless they are goldstone bosons. Now, we need to verify that this is the case for the rest of the remaining fields.

The Seiberg dual of the original quiver diagram is shown in Figure 5.20. Now, the

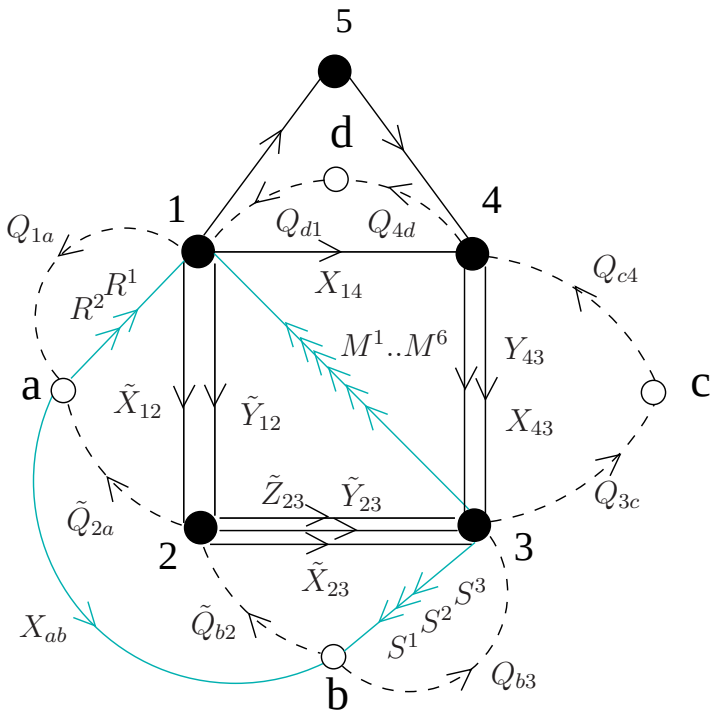

Figure 5.20: Quiver after Seiberg duality on node 2.

dualized bifundamentals come in two classes. The first are the ones that initially (before dualizing) had cubic flavor couplings, there will always be only two of those (e.g $\tilde{X}_{12}$, $\tilde{X}_{23}$). The second are those that did not initially have cubic couplings to flavors, there is an arbitrary number of those (e.g $\tilde{Y}_{12}$, $\tilde{Y}_{23}$, $\tilde{Z}_{23}$). Figure 5.21 shows the relevant part of the quiver for the first class. Recall the superpotential terms

$$W_{flavordual} = \lambda' \big(\underbrace{S^1_{3b} Q_{b3}}_{1} + \underbrace{R^1_{a1} Q_{1a}}_{2} + X_{14} Q_{4d} Q_{d1} + Y_{43} Q_{3c} Q_{c4} \big) \tag{5.98}$$

$$W_{massdual} = m_2 X_{ab} + \underbrace{m_3 Q_{b3} Q_{3c}}_{1} + m_4 Q_{c4} Q_{4d} + \underbrace{m_1 Q_{d1} Q_{1a}}_{2} \tag{5.99}$$

[18]In the case where the flavor group is $SU(2)$, these Goldstone bosons are associated to the generators t_x and t_y.

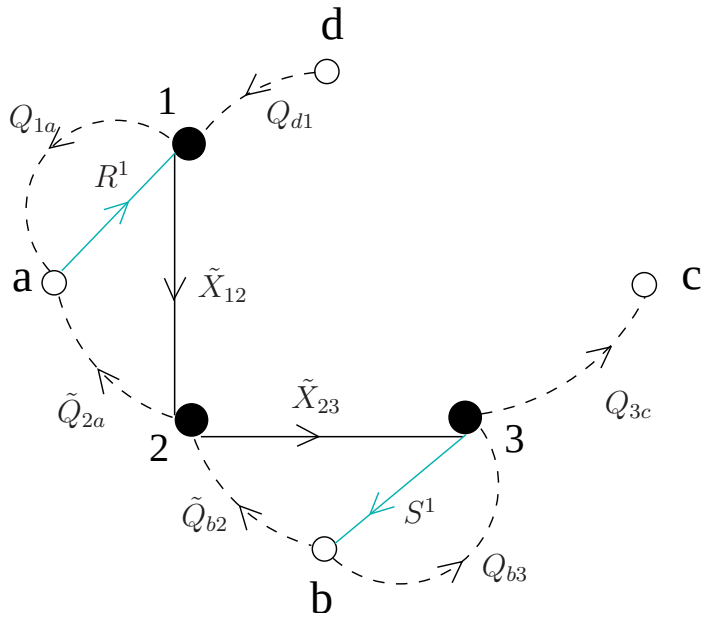

Figure 5.21: Relevant part of dual quiver for first class of bifundamentals.

$$\begin{aligned} W_{mesons} &= h\,(\, X_{ab}\tilde{Q}_{b2}\tilde{Q}_{2a} \\ &+ \underbrace{R^1_{a1}\tilde{X}_{12}\tilde{Q}_{2a}}_{2} + R^2_{a1}\tilde{Y}_{12}\tilde{Q}_{2a} \\ &+ \underbrace{S^1_{3b}\tilde{Q}_{b2}\tilde{X}_{23}}_{1} + S^2_{3b}\tilde{Q}_{b2}\tilde{Y}_{23} + S^3_{3b}\tilde{Q}_{b2}\tilde{Z}_{23} \\ &+ M^1_{31}\tilde{X}_{12}\tilde{X}_{23} + M^2_{31}\tilde{X}_{12}\tilde{Y}_{23} + M^3_{31}\tilde{X}_{12}\tilde{Z}_{23} \\ &+ M^4_{31}\tilde{Y}_{12}\tilde{X}_{23} + M^5_{31}\tilde{Y}_{12}\tilde{Y}_{23} + M^6_{31}\tilde{Y}_{12}\tilde{Z}_{23}\,) \end{aligned} \tag{5.100}$$

Now, if we want to look for tree-level masses, these can arise in $W_{flavordual}$ and $W_{massdual}$. Also, remembering our assignation of vevs in (5.92), tree-level masses can also arise in W_{mesons} from cubic couplings involving the SUSY breaking fields (e.g $\tilde{Q}_{b2}$, $\tilde{Q}_{2a}$). The first class of bifundamentals (e.g $\tilde{X}_{12}$, $\tilde{X}_{23}$) only appear in W_{mesons} coupled to their respective mesons (e.g R^1, S^1). In turn these mesons will appear in cuadratic terms in $W_{flavordual}$ coupled to flavors (e.g. $S^1_{3b}Q_{b3}$ and $R^1_{a1}Q_{1a}$), and these flavors each appear in one term in W_{mass} (recall that mass terms are gauge invariant). Thus there are two sets of three terms which are coupled at tree-level and which always couple in the same way. These terms are underlined and numbered 1 and 2 in the above equations. Looking at term 1

$$\lambda'\, S^1_{3b}Q_{b3} + m_3 Q_{b3}Q_{3c} + h\, S^1_{3b}\tilde{Q}_{b2}\tilde{X}_{23} = \lambda'\,(S_1\ S_2)\begin{pmatrix} B_1 \\ B_2 \end{pmatrix} + m_1(C_1\ C_2)\begin{pmatrix} B_1 \\ B_2 \end{pmatrix}$$

$$
\begin{aligned}
&+ \quad h\,(S_1\ S_2)\begin{pmatrix}\mu+\phi_1\\ \phi_2\end{pmatrix}\tilde{X}_{23}\\
&= \quad \lambda'(S_1B_1+S_2B_2)+m_1(B_1C_1+B_2C_2)\\
&+ \quad h\mu\,S_1\,\tilde{X}_{23}\ +\ h\,S_1\,\phi_1\,\tilde{X}_{23}\ +\ h\,S_2\,\phi_2\,\tilde{X}_{23}
\end{aligned}
\tag{5.101}
$$

where S_i, B_i, C_i and $\tilde{X}_{23}$ are the perturbations around the minimum[19]. Diagonalising, we get that all terms except one get tree-level masses. This massless field has a cubic coupling to $\phi_2\,\tilde{X}_{23}$ and gets mass at 1-loop since ϕ_2 is a SUSY breaking field[20].

Figure 5.22 shows the relevant part of the quiver for the second class of bifundamentals (i.e those that are dualized but do not have cubic flavor couplings).

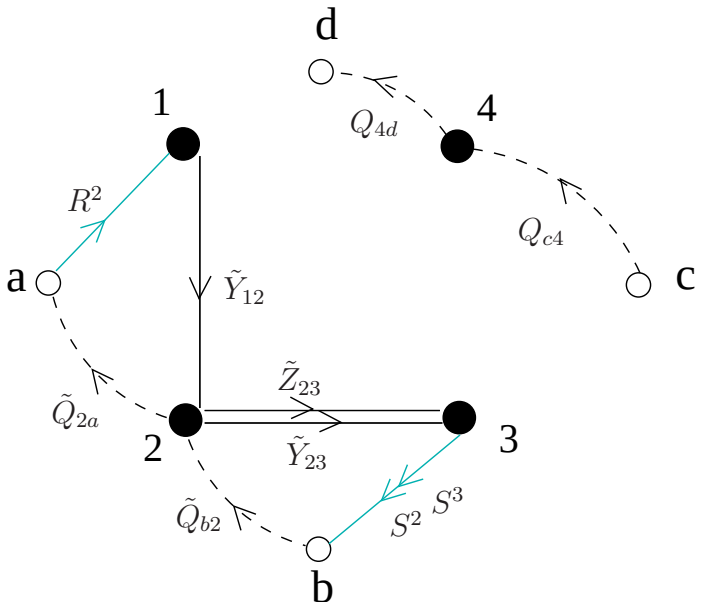

Figure 5.22: Relevant part of dual quiver for second class of bifundamentals.

These fields and their mesons only appear in one term, so will always couple in the same way. Taking as an example

$$
\begin{aligned}
h\,R_{a1}^2\tilde{Y}_{12}\tilde{Q}_{2a} &= \begin{pmatrix}R_1\\ R_2\end{pmatrix}\tilde{Y}_{12}\,(\mu+\phi_3\,;\,\phi_4)\\
&= \mu R_1\,\tilde{Y}_{12}\ +\ R_1\,\phi_3\,\tilde{Y}_{12}+R_2\,\phi_4\,\tilde{Y}_{12}
\end{aligned}
\tag{5.102}
$$

[19]Recall that all fields except those in (5.92) have vevs zero. Also, as before we take $N_f=2$ and $N_c=1$)

[20]Assuming all couplings are real and $m_1\neq 0$. The couplings can be set to real by a redefinition of fields.

This shows that R_1 and $\tilde{Y}_{12}$ get tree-level masses and R_2 gets a mass at 1-loop since it couples to the SUSY breaking field ϕ_4. The only remaining fields are the flavors which do not transform in a gauge group adjacent to the dualized node[21] (e.g Q_{c4}, Q_{4d}). And these get a gauge invariant mass and hence are massive at tree-level since they only appear cuadratically in this term.

So, as stated, all fields except those that appear in the original superpotential (i.e mesons with gauge indices and bifundamentals which are not dualized) get masses either at tree-level or at one-loop. So we only need to check the dualized original superpotential to see if we have a metastable vacua.

[21] Recall that we gave cubic flavor couplings to all bifundamentals of a term in the superpotential. This term corresponds to a loop in the quiver. What we mean by adjacent is that it is not directly connected via this loop to the dualized gauge group.

le

Chapter 6

Gauge Mediated Supersymmetry Breaking with Branes at Singularities

In Chapter 3 we saw how fractional branes placed at toric singularities can lead to dynamical supersymmetry breaking in the infrared. However, when one takes into account the closed string modes, this leads to a runaway and supersymmtery is recovered at infinity. This behavior was resolved in [24] where, working on the ideas introduced in [25], they were able to generate metastable vacua in the infrared by adding massive flavors. These arise from D7-branes passing through the singularity. In Chapter 5 we summarised these ideas and generalised them to arbitrary toric singularities. Namely, we showed how one can easily determine the existence of metastable vacua for fractional DSB branes coupled to D7-branes. In Chapter 4, we showed how one can determine the gauge theory for D3-branes at arbitrary toric singularities using the dimer diagram representation. We saw how this representation encodes the web diagram characterising the singularity via its structure of zig-zag paths. We also saw how one can obtain two daughter singularities from the partial resolution (blow-up of an S^2) of a mother singularity. This resolution corresponds to a higgsing of the mother gauge theory by turning on Fayet-Iliopoulos terms. We were also able to determine in a precise manner the assignation of vevs necessary to generate the two daughter gauge theories. In terms of the branes, this process corresponds to D3 and fractional branes placed at a mother singularity which, after turning on FI terms, separate into branes placed at the two daughter singularities as shown in Figure 6.1. The distance separating the branes is given on the geometry

side by the size of the S^2, and on the gauge theory side by the FI terms.

Each of these results is useful in and within itself, however it is possible to combine them in a configuration which is both flexible and useful for model building. As stated in the introduction to this work, our principal objective is using String Theory to obtain the Standard Model in the infrared. Now, although models of D-branes at singularities exist which closely resemble the MSSM [26], no mechanism exists to break these models to a realistic non-supersymmetric configuration. Indeed, breaking supersymmetry is not trivial since tree-level couplings of the MSSM to a SUSY breaking sector would necessarily lead to lower masses for the squarks, not observed experimentally [27]. An elegant mechanism to resolve this issue is that of gauge-mediated supersymmetry breaking (GMSB). In this model, the supersymmetry breaking sector contains supermultiplets which get non-degenerate masses for their component fields (e.g the real and imaginary parts of the scalar in a chiral multiplet). Although these fields do not couple at tree-level to the MSSM sector, they are charged with respect to its gauge groups. The MSSM fields thus get non-degenerate masses and break SUSY at one or two loops through interactions involving the gauge bosons. In [28], the authors succeeded in the construction of string compactifications with semi-realistic visible sectors and a sector of DSB branes. These were the first serious attempts to implement GMSB in string theory.

In this chapter we continue along those lines, using the results of the previous chapters to improve it in several ways. We propose a fairly general framework to discuss models of GMSB in String Theory. The construction is based on the use of local (namely non-compact) configurations, with two sectors of D-branes describing the visible and supersymmetry breaking sector, decoupled at the massless level, but coupled via a messenger sector whose mass scale is controlled by the distance between the D-brane sectors, which is much smaller than the string scale. In fact, it is this latter fact that motivates considering *local* configurations, since the physics of the mediation is naturally insensitive to the global structure of the compactification [1]. We propose explicit realizations of this construction, which is nevertheless quite flexible and allows for many generalizations.

Some of the nice features of our proposal and explicit models are:

• Being local, they manifestly show the UV insensitivity of the construction.

[1] Of course, in the regime of distance much larger than the string scale, the system corresponds to a model of gravity mediation, but the latter would be sensitive to the global structure of the compactification, hence rendering the local model less useful.

• As opposed to previous proposals, the computation of the spectrum and interactions of the messenger sector can be explicitly described.

• The construction is simple and flexible enough to allow for many generalizations.

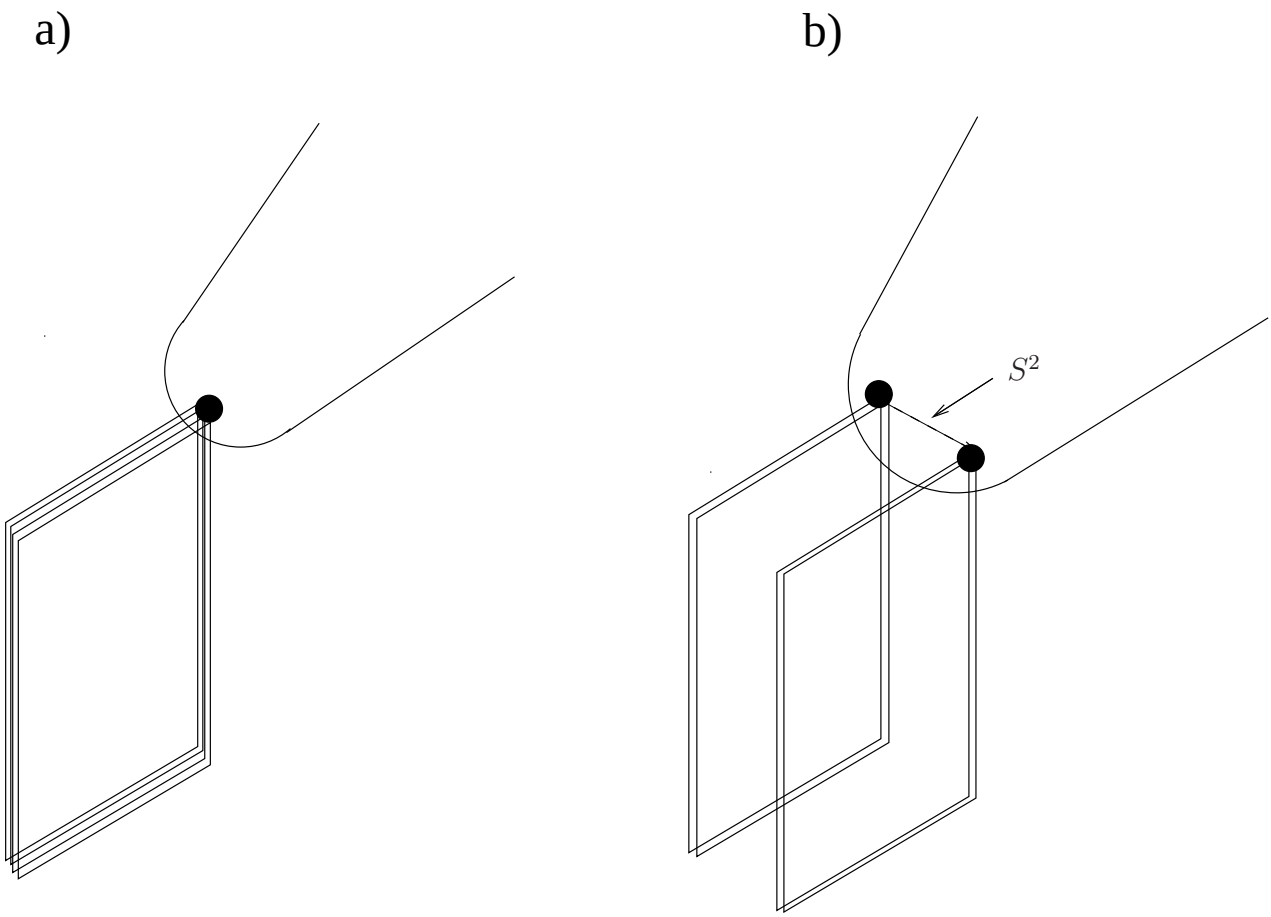

Figure 6.1: (a) D–branes at mother singularity (b) D–branes at daughter singularities, separated by an S^2.

6.1 Background material

6.1.1 D-branes at singularities and dimer diagrams

In chapter 4, we showed how gauge theories of D3–branes at toric singularities are completely encoded by dimer diagrams. These correspond to a bi-partite tiling of the torus, where faces correspond to gauge groups, edges to bifundamentals and nodes to superpotential terms.

One example, corresponding to D3-branes at the $\mathbb{C}^3/\mathbb{Z}_3$ singularity (also known as the complex cone over dP_0, hence denoted dP_0 singularity), is shown in Figure 6.2a. The gauge theory corresponding to the dimer diagram in Figure 6.2a is described in Figure 6.2b in terms of its quiver diagram, where nodes correspond to gauge factors, arrows correspond to chiral multiplets, and the superpotential needs to be specified explicitly. In this case we have

$$\begin{aligned} W &= \mathrm{Tr}\,(\,X_{12}Y_{23}Z_{31} - X_{12}Z_{23}Y_{31} + X_{23}Y_{31}Z_{12} - X_{23}Z_{31}Y_{12} + \\ &+ X_{31}Y_{12}Z_{23} - X_{31}Z_{12}Y_{23}\,) \simeq \epsilon_{ijk}\,\mathrm{Tr}\,(\,X_{12}^{(i)}X_{23}^{(j)}X_{31}^{(k)}\,) \end{aligned} \tag{6.1}$$

with obvious notation (in the last expression we have written $X^{(i)}$, $i = 1, 2, 3$ for X, Y, Z, respectively). Traces in superpotential terms will be implicit in what follows.

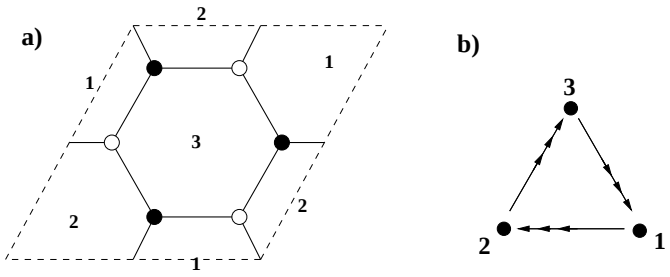

Figure 6.2: (a) The dimer diagram (as a tiling of the $\mathbf{T^2}$ upon identifying sides of the parallelogram) and (b) the quiver diagram of the gauge theory on D3-branes at the $\mathbb{C}^3/\mathbb{Z}_3$ singularity.

For future use, we show another example of a dimer diagram in Figure 6.3a, corresponding to D3-branes at a singularity given by the complex cone over dP_1. The corresponding gauge theory (denoted dP_1 theory) is described by the quiver diagram shown in Figure 6.3b, with the superpotential given by

$$\begin{aligned} W &= X_{12}Y_{24}X_{41} - Y_{12}X_{24}X_{41} + X_{31}Y_{12}X_{23} - \\ &- Y_{31}X_{12}X_{23} + Z_{12}X_{24}X_{43}Y_{31} - Z_{12}Y_{24}X_{43}X_{31} \\ &\simeq \epsilon_{ij}X_{12}^iX_{24}^jX_{41} + \epsilon_{ij}X_{31}^iX_{12}^jX_{23} + \epsilon_{ij}Z_{12}X_{24}^iX_{43}X_{31}^j \end{aligned} \tag{6.2}$$

where fields X^i, $i = 1, 2$ denote X, Y.

Recall that dimer diagrams encode the toric geometry through their structure of zig-zag paths. A zig-zag path is a path made of dimer edges, such that it turns maximally to the left at e.g. black vertices and maximally to the right at white vertices. Each zig-zag path defines a closed loop on $\mathbf{T^2}$, and carries a non-trivial

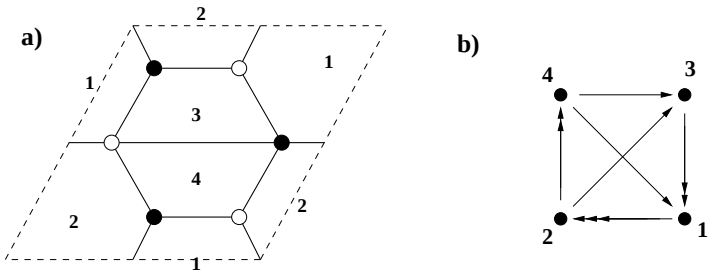

Figure 6.3: The dimer diagram (a) and quiver diagram (b) of the gauge theory on D3-branes at a singularity given by a complex cone over dP_1.

(p, q) homology charge. Each zig-zag path corresponds to an external leg in the web diagram, with the (p, q) label of the leg given by the (p, q) charge of the path. It is easy to recover the web diagrams of different singularities from the zig-zag paths of the dimer diagram, as one can check in our examples[2]. The structure of zig-zag paths for the dP_0 and dP_1 dimer diagrams are shown in Figures 6.4b and 6.5b.

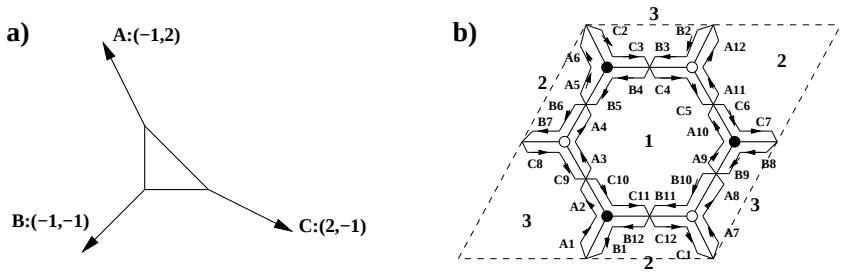

Figure 6.4: (a) Web diagram for the dP_0 singularity. For clarity we show the geometry for a non-zero size of the internal pieces. (b) Dimer diagram and zig-zag paths for the dP_0 theory. The (p, q) homology class of the path is related to the (p, q) label of an external leg in the web diagram of the geometry.

Also recall, as explained in Chapter 4, that D3–branes at toric singularities in Type IIB are mirror, to D6-branes intersecting on a Riemann surface Σ with punctures. This Riemann surface can be regarded as a thickening of the web diagram of the toric singularity, where punctures in Σ correspond to external legs in the web diagram. Now, the tiling of this Riemann surface can be obtained by untwisting the zig-zag paths of the dimer diagram. All the information of the dimer diagram is also encoded in this Riemann surface, where the gauge groups correspond to non-trivial 1-cycles

[2]Recall that for a given singularity, the web diagram is defined up to an overall $SL(2, \mathbb{Z})$ transformation on the (p, q) labels.

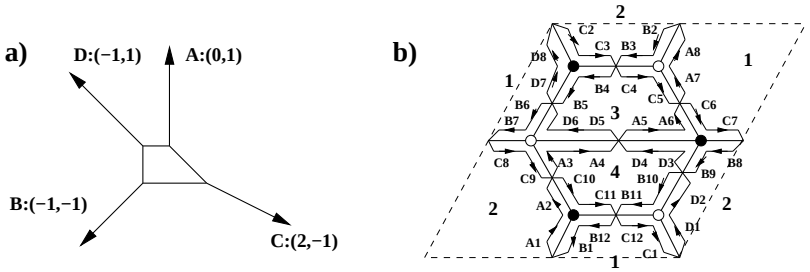

Figure 6.5: (a) Web diagram for the dP_1 singularity. For clarity we show the geometry for a non-zero size of the internal pieces. (b) Dimer diagram and zig-zag paths for the dP_1 theory. The (p, q) homology class of the path is related to the (p, q) label of an external leg in the web diagram of the geometry.

wrapped by the D6–branes, bifundamentals correspond to intersections between these cycles and superpotential terms correspond to disks in Σ bounded by pieces of different 1-cycles (D6-branes).

Adding D7-branes

Now we can also introduce D7-branes passing through a system of D3-branes at a singularity. Namely, one introduces D7-branes wrapped on holomorphic 4-cycles of the singular CY. From the viewpoint of the 4d gauge theory, this implies the introduction of a set of flavors for the different D3-brane gauge factors (from the open strings between the D3- and D7-branes) and interactions (e.g. from 73-33-37 interactions). The gauge group on the D7-branes behaves as a global symmetry from the viewpoint of the 4d gauge theory in this non-compact setup.

As we mentioned in Chapter 5, D7–branes also have an interpretation in terms of the Σ Riemann surface. They represent non-compact 1-cycles on Σ, stretching between two punctures (see Figure 6.6. The intersections of the D7-brane 1-cycle with the 1-cycle corresponding to the D3-branes gives rise to chiral multiplets in bifundamentals of the D3- and D7-brane symmetry groups, thus providing the D3-D7 spectrum. Finally, disks in Σ bounded by one D7-brane 1-cycle and two D3-brane 1-cycles lead to a cubic superpotential term of the form 73-33-37.

This more detailed description underlies the recipe which we will state directly in terms of the dimer diagram.

As described in [24], for each 33 bifundamental in the D3-brane sector, there exists

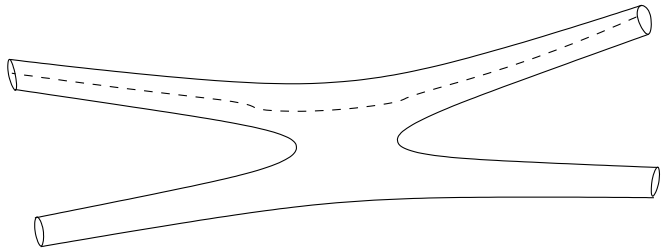

Figure 6.6: Schematic representation of D7–branes on the mirror Riemann surface. In this case the Riemann surface is that of a conifold singularity and the D7–branes represent non-compact 1-cycles extending from one puncture to another. They are shown as dashed lines.

one kind of D7-brane leading to 37, 73 chiral multiplets coupling to the 33 state. Hence, a simple representation of a D7-brane in the dimer diagram is as a segment stretching across an edge, joining the mid-points of adjacent faces. One such segment stretching across an edge associated with an $(\Box_1, \overline{\Box}_2)$ bifundamental, gives rise to chiral multiplets in the $(\Box_2; \overline{N_{D7}})$ and $(N_{D7}; \overline{\Box}_1)$, where N_{D7}, $\overline{N_{D7}}$ represent the D7-brane global symmetries. Heuristically, the D7-brane segment touches the faces at its endpoints, leading to the D7-D3 and D3-D7 sectors according to orientation. There is a superpotential coupling 33-37-73 involving these states. The representation as a segment facilitates an easy identification of the gauge theory matter content and interactions corresponding to a system of D3- and D7-branes at singularities. In Figure 6.7 we show one particular example of this kind of diagram, which we denote extended dimer diagram. Notice that there are other possible D7-brane choices, namely one for each 33 bifundamental, and that for different 33 bifundamentals with the same gauge quantum numbers, the corresponding D7-branes lead to the same 37, 73 spectrum, but different 33-37-73 interactions.

An important point is that there are non-trivial consistency conditions on configurations of D3- and D7-branes at singularities. Concretely, the total charge of the D-brane system under RR fields living at the singular points should vanish. Equivalently, the 4d gauge theory should be free of non-abelian anomalies [3]. In all our forthcoming examples we enforce this property.

[3] As discussed in chapter 1, the $U(1)$ mixed anomalies are canceled by a Green-Schwarz mechanism, and do not require additional constraints. Also, all anomalous $U(1)$s (plus some non-anomalous ones in certain cases) have $B \wedge F$ couplings, which gives them a mass of order the string scale. The only linear combination of $U(1)$s that generically remains massless is the 'diagonal' combination $\sum_a \frac{1}{N_a} Q_a$, where Q_a is the $U(1)$ generator of the a^{th} gauge factor $U(N_a)$.

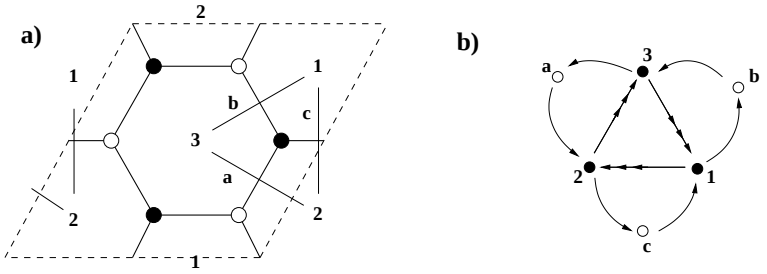

Figure 6.7: (a) Extended dimer diagram of the dP_0 theory with some examples of D7-branes represented as segments across the edges. (b) Quiver diagram including D7-branes (represented as white nodes). There are 33-37-73 couplings involving the 33 bifundamental across which the corresponding D7-brane stretches.

One can use these tools to construct interesting gauge theories. As a particular application to phenomenological model building, it is easy to construct configurations leading to MSSM like spectra [26]. In Figure 6.8a we show an extended dimer diagram for a system of D3- and D7-branes at a $\mathbb{C}^3/\mathbb{Z}_3$ singularity studied in [26]. As can be easily read out from the picture, it leads to a $U(3)\times U(2)\times U(1)$ gauge group and 3 families of quarks and leptons (plus additional fields, with vector-like quantum numbers under the Standard Model gauge group). The only massless $U(1)$ linear combination (in a convenient normalization) is $Q_Y = -\frac{1}{2}(\frac{1}{3}Q_3 + \frac{1}{2}Q_2 + Q_1)$. This is crucial, since it precisely reproduces the correct hypercharges of the matter fields. In Figure 6.8b we show the quiver diagram for this gauge theory [4], with arrows labeled by the corresponding (Minimal Supersymmetric) Standard Model field. Notice that, in contrast with the MSSM, the model contains a triplicated sector of Higgs fields, and also that there are three copies of fields, vector-like under the D3-brane gauge interactions, with quantum numbers of D_R quarks (and conjugates $\overline{D_R}$). See [26] for further details. Later in this chapter, we will use this configuration as our (toy) model for the visible sector in a truly realistic string compactification.

[4] As discussed before, several possible D7-branes can lead to the same D3-D7 spectrum (but different interactions). Our dimer diagram is just one of the possible ones leading to the same chiral spectrum.

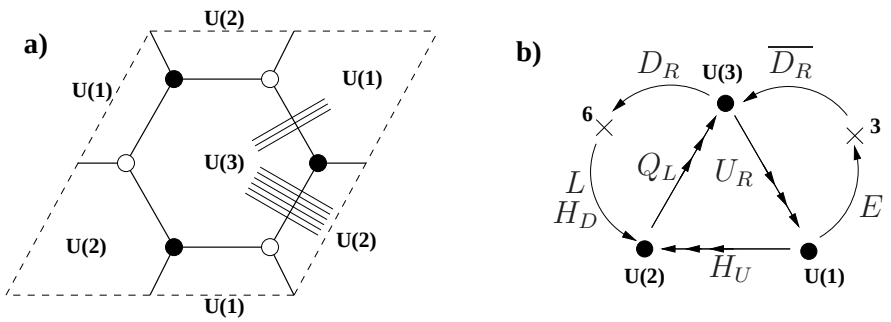

Figure 6.8: Dimer diagram (a) and quiver diagram (b) for a configuration of D3/D7-branes realizing a gauge theory close to the MSSM.

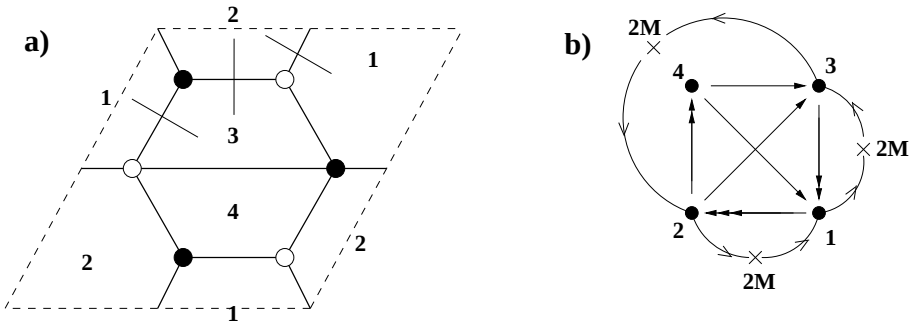

Figure 6.9: (a) Dimer diagram for a configuration of D3- and D7-branes in the dP_1 singularity leading to a gauge theory with meta-stable supersymmetry breaking vacua. (b) Extended quiver diagram for the theory.

6.1.2 DSB from D-branes at singularities

In Chapter 3, we saw how placing fractional branes on a dP_1 singularity generates dynamical supersymmtery breaking in the infrared. However, when closed string modes are taken into account, the FI terms become dynamical and we get a runaway potential with supersymmetry restored at infinity. As explained in Chapter 5, the authors of [24] showed that adding D7–branes to the above configuration generates supersymmetry-breaking local minima, which are metastable and long-lived. On the gauge theory side, this modification corresponds to adding massive flavors, with mass much smaller than the dynamical scale of the theory. The extended dimer diagram corresponding to this configuration is shown in Figure 6.9.

An alternative possibility to obtain stable non-supersymmetric minima from DSB branes, mentioned in [28] is the following. As mentioned above, the runaway behav-

ior can be regarded as a non-trivial potential for a certain Kahler modulus of the singularity. In global compactifications, it is possible that there are other sources of potential for these moduli, which could presumably stabilize its runaway (for instance non-perturbative contributions arising from euclidean D3-brane instantons). This is however difficult to verify in concrete models including realistic sectors. Moreover, the properties of such local minima (including its very existence) would be strongly sensitive to the details of the global compactification. This goes against our strategy to attempt the construction of a visible plus DSB sector with no UV sensitivity.

In other words, one can rephrase the above by saying that in our specific local models, which are UV insensitive by construction, there are no other sources of potential for the Kahler moduli involved in the runaway. Hence, the above proposal to modify the gauge theory by adding slightly massive flavors is a UV independent way to generate supersymmetry breaking minima in these gauge theories, and a natural one to be implemented in local models.

6.1.3 Local CY models with several singularities

Geometrical construction from partial resolution

As we saw in the previous chapters as well as in the appendix on toric geometry, given a toric singularity, it is possible to obtain two less singular points by the method of partial resolution. This corresponds to the blow-up of an S^2 and is illustrated in the web and toric diagrams of Figure 6.10 for the case of a partial resolution of the double conifold to two conifold singularities[5].

Notice that this process can be easily inverted. If one is interested in constructing a local CY with two isolated singularities of specified type, one simply needs to consider combining their web diagrams into a larger one by joining one external leg of each diagram into one finite size segment [6]. This will be useful in the construction of geometries in Section 6.2.

Finally recall that the partial resolution, when regarded in terms of the mirror

[5]The original and final singularities are simpler to recognize if one keeps track of the collapsed finite segments, by showing them with a small size. Recall however that the singularities are obtained when such finite pieces have zero size.

[6]Notice that in doing so, we have the freedom to perform an $SL(2,\mathbb{Z})$ transformation on the web diagrams to facilitate the gluing.

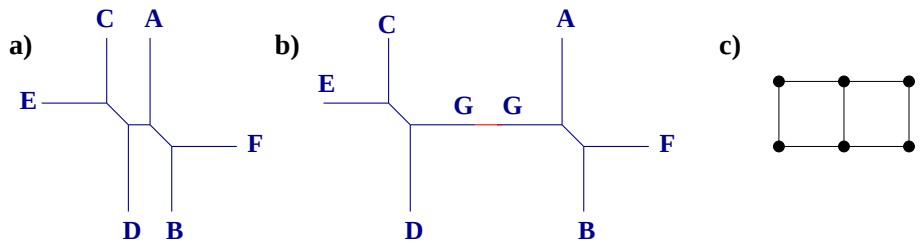

Figure 6.10: (a) The web diagram for the double conifold singularity $xy = s^2w^2$. (b) The partial resolution to a geometry with two conifold singularities. (c) Description in terms of the toric diagram.

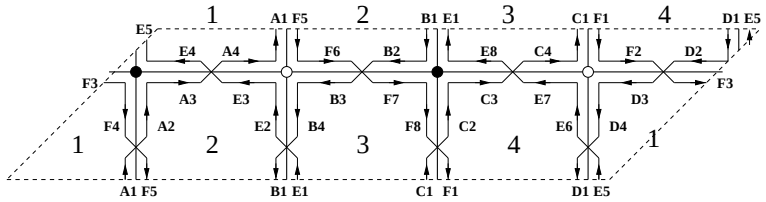

Figure 6.11: Zig-zag paths for the dimer diagram of the double conifold. The path names agree with the names of the legs in the web diagram in Figure 6.10a, and the numbers label the different gauge factors.

Riemann surface Σ, simply corresponds to elongating a tube. By pinching this tube (or elongating it infinitely) one obtains two daughter Riemann surfaces that describe the mirror of the two daughter singularities.

Effect on D-branes

As explained in Chapter 4, the above mechanism is easily implemented on the gauge theory side using dimer diagrams. Since zig-zag paths correspond to external legs of the web diagram, the gauge theory of the daughter singularities is that obtained after keeping only the zig-zag paths corresponding to the external legs of the daughter web diagrams. To these one should add a new zig-zag path corresponding to the external leg of the daughter web diagram that arises from the finite size segment in the initial web diagram. The example of the double conifold studied in Chapter 4 is illustrated in Figures 6.11 and 6.12.

As discussed in Chapter 4, the specific pattern of edges that survives in the different

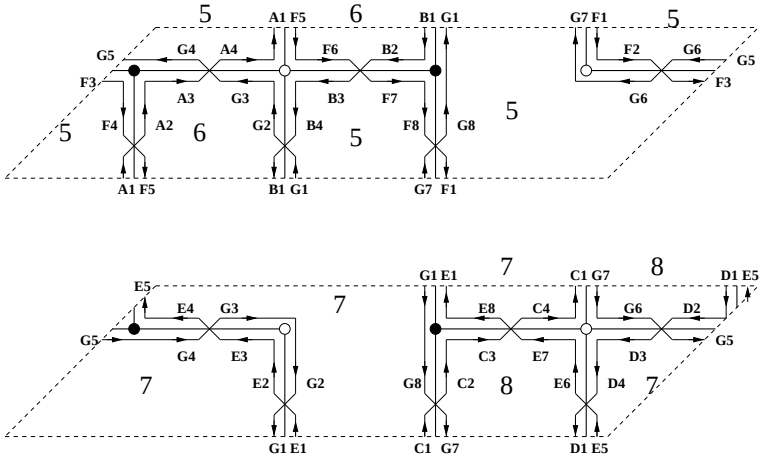

Figure 6.12: Zig-zag paths corresponding to the two daughter theories, in the splitting of the double conifold singularity to two conifold singularities, with the corresponding dimers shown as thick lines. The numbers label the different gauge groups.

daughter dimer diagrams determines the specific vevs acquired by the bifundamental multiplets in the Higgsing of the initial gauge theory. Specifically, let us denote edges of type 1 those disappearing in the second daughter diagram, of type 2 those disappearing in the first, and of type 3 those present in both (namely, those through which the path G passes). Denoting the corresponding bifundamental vevs by Φ_1, Φ_2, Φ_3 the pattern of vevs for those fields in the partial resolution Higgs mechanism is

$$\Phi_3 = \begin{pmatrix} 0 & 0 \\ 0 & 0 \end{pmatrix} \quad ; \quad \Phi_2 = \begin{pmatrix} v\,\mathbf{1}_{N_1} & 0 \\ 0 & 0 \end{pmatrix} \quad ; \quad \Phi_1 = \begin{pmatrix} 0 & 0 \\ 0 & v\,\mathbf{1}_{N_2} \end{pmatrix} \tag{6.3}$$

where N_1, N_2 denote the number of D3-branes at the first and second daughter singularity. These vevs are flat with respect to the F-terms and non-abelian D-terms. Their deviations from $U(1)$ D-flatness is compensated by the FI terms controlled by the closed string modes carrying out the geometric blow-up (Kahler modulus).

The Higgs mechanism interpretation allows one to obtain the spectrum of massive states in the partially resolved geometry (namely the massive open strings stretching between D3-branes at different singularities) by starting with the initial gauge theory and computing the spectrum of multiplets becoming massive in the Higgs mechanism. The computation reduces to some dimer diagram gymnastics, and is described in Appendix 6.5. The result can be summarized as follows:

• **1** For each edge which disappears in the i^{th} daughter dimer diagram, there is a

massive vector multiplet in the adjoint of the $U(N_i)$ gauge factor corresponding to that location (i.e. that arising from the diagonal of the gauge factors of the two faces the edge used to separate in the initial theory).

• **2** For each face in the original dimer diagram, we obtain two massive vector multiplets in the bifundamental $(N_1, \overline{N_2})$ and its conjugate, of the gauge factors at the corresponding location.

• **3** For each edge present in both daughter dimer diagrams, there is one $(N_1, \overline{N_2})$ chiral multiplet in the corresponding bifundamental representation (i.e. charged under faces separated by the edge) becoming massive. The dimer diagram ensures that globally, these chiral multiplets pair up consistently to form massive scalar multiplets.

• **4** Finally, if the daughter dimer diagrams contain bi-valent nodes (nodes with two edges) the corresponding edges each describe a massive scalar multiplet in the bifundamental of the two faces they separate.

Let us illustrate this with an example. For instance, the partial resolution of the double conifold to two conifolds is given by the following spectrum:

Vector multiplets in the adjoint: There are two edges of type 1, both giving rise to massive vector multiplets in the adjoint of the gauge factor 7 (see Figure 6.12). Similarly, the two edges of type 2 give massive vector multiplets in the adjoint of 5.

Vectors in the bifundamental We obtain massive vectors in the representations

$$(5, \overline{7}) + (6, \overline{7}) + (5, \overline{7}) + (5, \overline{8}) + \text{c.c.} \tag{6.4}$$

Scalar multiplets One finds the following spectrum of massive scalar multiplets:

$$2\,(5, \overline{7}) + (6, \overline{7}) + (5, \overline{8}) \tag{6.5}$$

Other examples are worked out similarly. A more complicated resolution will be described in section 6.2.1.

Including D7-branes

The effect of partial resolutions on D7-branes was not described in [4], but the discussion can be carried out using the description in Section 6.1.1.

Recall the representation of D7-branes as segments across an edge in the dimer diagram (leading to 37, 73 states coupling to the corresponding 33 bi-fundamental

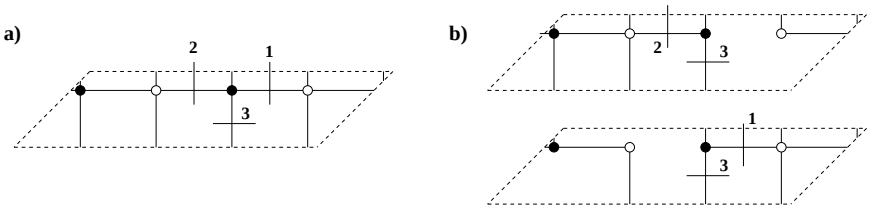

Figure 6.13: The fate of different D7-branes in a partial resolution. D7-branes associated to edges of type 1 resp. 2 become D7-branes absent in the first resp. second dimer diagram, hence passing through the second resp. first daughter singularity. For type 3 edges, the D7-branes remains in both daughter dimer diagrams, hence passes through both daughter singularities.

in the D3-brane gauge theory). Let us consider the possible D7-branes in the parent dimer diagram, and consider their fate in a partial resolution. This is essentially determined by the behavior of the edge in this process:

- A D7-brane across an edge which survives only in the first daughter dimer diagram, survives as a D7-brane passing through the first daughter singularity. It corresponds to the D7-branes of the daughter singularity naturally associated to the corresponding edge in the daughter dimer (namely leading to 73, 73 states coupling to the 33 bifundamental of the corresponding gauge sector in the daughter theory).

- Similarly for D7-branes across edges surviving only in the second daughter dimer diagram.

- Finally, a D7-brane across an edge that survives in both daughter dimer diagrams corresponds to a D7-brane passing through both daughter singularities.

In Figure 6.13 we provide examples of these possibilities in the partial resolution of the double conifold to two conifolds.

ZZZZZ MAYBE PUT PICTURE HERE The rules are easily justified by considering the picture of D7-branes as 1-cycles in the mirror Riemann surfaces, stretching between two punctures. Recall also that a D7-brane is naturally associated to a dimer diagram edge (in the sense that the corresponding 33, 37, 73 states couple) over which the two zig-zag paths associated to the punctures overlap. From this it follows that D7-branes stretching between two punctures remaining in e.g. the first daughter Riemann surface, descend to D7-branes of the first daughter singularity. They are naturally associated to edges which survive only on the first daughter dimer diagram (since the two zig-zag paths correspond to punctures surviving in

the first daughter Riemann surface). Similarly for D7-branes represented by 1-cycles stretching between punctures remaining in the second Riemann surface. The last possibility is a D7-brane represented by a 1-cycle stretching between punctures ending up in different daughter Riemann surfaces. Since it passes through the elongated tube in the partial resolution, it leads to two D7-branes in the two daughter theories.

The above description nicely fits with the field theory description in terms of Higgsing. A D7-brane leads to D3-D7 states with couplings 37-73-33 with the 33 bi-fundamental associated to the edge across which the D7-brane segment stretches. If the edge disappears from e.g. the first daughter dimer diagram, the corresponding 33 entries get a vev and give masses to the open string states stretching between the D7's and the first stack of D3-branes. On the other hand, open string states stretching between the D7's and the second stack of D3-branes remain massless, hence the D7-branes passes through the second daughter singularity, and can be represented as a segment in the second daughter dimer diagram (across the same edge). Similarly for edges disappearing in the second dimer diagram. Finally, for edges appearing in both daughter dimer diagrams, the 33 bi-fundamentals get no vev, so all D3-D7 open string states remain massless, showing that the D7-brane passes through both daughter singularities. From this discussion it is clear that the rule to obtain the massive set of multiplets from D3-D7 open string states is:

• **5** For each D7-brane passing through an edge of type 1 (resp. type 2) there is a massive scalar multiplet in the fundamental representation of the $U(N_2)$ (resp $U(N_1)$) gauge factor corresponding to the resulting recombined face. For N_{D7} across such an edge the massive multiplets transform as $(N_{D3}, \overline{N}_{D7})$.

6.2 Basic strategy and some examples

Using the previous results, we shall construct systems of D-branes at a local CY with two singular points, leading to two chiral gauge theories describing the visible and supersymmetry breaking sectors. The system reproduces a model of gauge mediated supersymmetry breaking in the regime where the distance between the D-brane stacks is smaller than the string scale.

6.2.1 A simple example

Let us consider one simple example of the above strategy. We would like to consider a non-compact Calabi-Yau with two singularities, with their local structures being that of a complex cone over dP_0, and a complex cone over dP_1 respectively. We would like to locate D3-branes at each of these singularities, so as to obtain two gauge sectors, which are decoupled at the level of massless states (although massive open strings stretched between the two stacks provide a massive messenger sector).

The simplest toric geometry realizing this is described by the web diagram in Figure 6.14a. As usual, and for clarity, we have shown the geometry with all 2- and 4-cycles of finite size. The geometry of interest, with the two singularities is better represented by Figure 6.14b, more specifically when the two small faces in the web diagram are collapsed to zero size. The two singularities are described by the sets of legs A, C, G and G, E, B, D. The finite leg G with the dashed piece describes the 2-cycle which controls the distance between the two singularities, and thus the mass scale of the messenger sector.

Regarding Figure 6.14b as preceding Figure 6.14a illustrates a simple algorithm to construct local Calabi-Yau geometries containing several singularities. One simply considers the web diagrams for the different daughter singularities, and glues them together by combining external legs of the daughter web diagrams into finite size legs (which is always possible by using the $SL(2,\mathbb{Z})$ freedom in defining each of the daughter web diagrams) [7].

D3-branes at the dP_0 singularity can provide a toy model of the MSSM. For the time being, we can consider e.g. 3 D3-branes (without fractional branes) at the dP_0 singularity, so that the gauge theory content is

$$\begin{aligned} \text{Vector}: &\qquad U(3)_{1'} \times U(3)_{2'} \times U(3)_{3'} \\ \text{Chiral}: &\quad 3\,[\,(3,\overline{3},1) + (1,3,\overline{3}) + (\overline{3},1,3)\,] \end{aligned} \tag{6.6}$$

and there is a superpotential coupling (6.1). In fact, this is one example of the so-called trinification models extending the MSSM.

Similarly, D-branes at the dP_1 singularity can provide a toy model of a sector with dynamical supersymmetry breaking. Specifically, we consider introducing M fractional D-branes at the dP_1 singularity, so that the gauge theory is precisely that

[7] In doing this, some additional external legs may cross, implying that they are actually internal legs in the complete diagram, see Section 6.3 for some such examples.

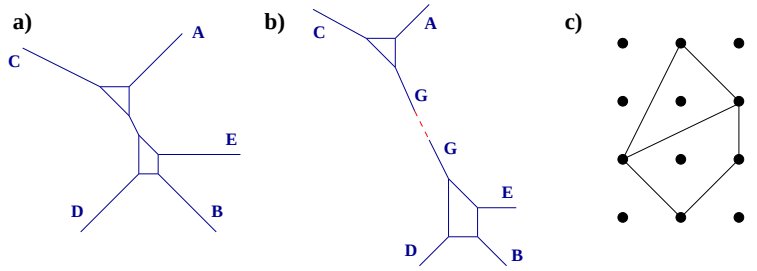

Figure 6.14: (a) Web diagram for a local CY with dP_0 and dP_1 singularities, for generic sizes of all 2- and 4-cycles. (b) The two singularities are obtained when the cycles corresponding to the two finite faces shrink to zero size, while the leg G remains finite and controls the distance between the singularities. (c) Toric diagram for the geometry, with the partial resolution leading to the two separated singularities.

studied in Section 6.1.2, namely

$$\begin{aligned} &\text{Vector}: && U(3M)\times U(2M)\times U(M) \\ &\text{Chiral}: && (3M,\overline{2M},1)\,+\,3(1,2M,\overline{M})\,+\,2(\overline{M},1,M) \end{aligned} \tag{6.7}$$

Recall (see Chapter 3) there is a superpotential coupling $X_{23}X_{31}Y_{12}-X_{23}Y_{31}X_{12}$, and that the $U(1)$'s are actually massive due to their couplings to closed string modes.

Modulo the runaway issue in the dP_1 theory (to be fixed via the stabilization of Kahler moduli, or by the addition of massive flavors as in the next section), this is a simple configuration realizing gauge mediated supersymmetry breaking in a local setup. In particular, it is a very tractable example of a theory similar to those introduced in [28]. Moreover, it has the advantage that new ingredients can be easily added to improve its properties, so that new variants are easily implemented. For instance it is straightforward to introduce D7-branes to turn the runaway dP_1 sector into the flavored dP_1 theory with a local supersymmetry breaking minimum discussed in Section 6.1.2 (see Section 6.2.2).

A more fundamental advantage is that it is possible to describe explicitly the physics of this theory when the scale of mediation is small compared with the string scale. Namely, when the distance between the two singularities (and hence of the two D-brane stacks) is shorter than the string length. Since this distance is controlled by a Kähler parameter, classical geometry is not a good approximation. The real dynamics is captured by including the messenger sector, which is far lighter than the cutoff scale (string scale), in the effective theory. Namely, by considering the

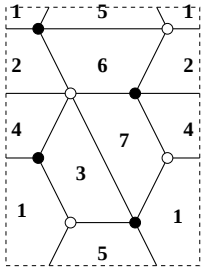

Figure 6.15: The dimer diagram for the $X^{3,1}$ theory.

complete field theory obtained when the two singularities coalesce, with the two singularities arising from a small partial resolution. Equivalently, with the gauge symmetry slightly broken by Higgs expectation values (induced by the FI terms from the closed string vevs blowing up the singularity). Moreover, as described in Section 6.1.3, one can keep track of the multiplets becoming massive in the Higgs mechanism to obtain an explicit description of the massive messenger sector. So this is one of the few frameworks where such a spectrum is actually computable.

As should be clear, we thus need to consider the geometry whose web diagram is shown in 6.14a, in the limit where all finite pieces collapse to zero size, and there is a single singularity, and study the gauge theory on D3-branes (and fractional branes) at such a singularity. For a general toric singularity, one can use general techniques to obtain such field theories. Happily, this task has already been carried out in our case. The geometry of interest is a particular example $X^{3,1}$ in the infinite family of geometries $X^{p,q}$ introduced in [29]. The dimer diagrams for the gauge theory on D3-branes at these geometries have been determined in [15], and for the $X^{3,1}$ it is shown in Figure 6.15.

The partial resolution of the $X^{3,1}$ singularity to a geometry with dP_0 and dP_1 singularities is a Higgs mechanism which can be studied as in Section 6.1.3 (or Chapter 4). Namely the splitting of the web diagram into two daughter web diagrams, as in Figure 6.14b, leads to two sets of paths (A, C, G, and B, D, E, G) which define the daughter dimer diagrams of the D3-branes at the two daughter singularities. The paths and the resulting daughter diagrams are shown in Figure 6.16a, b. In fact, after integrating out matter with mass couplings in the superpotential (due to bi-valent nodes), one can show they correspond to the dimer diagrams of D3-branes at the dP_0 and dP_1 singularities, respectively. This is shown in Figure 6.17 for the dP_0 case and in Figure 6.18 for the dP_1 case.

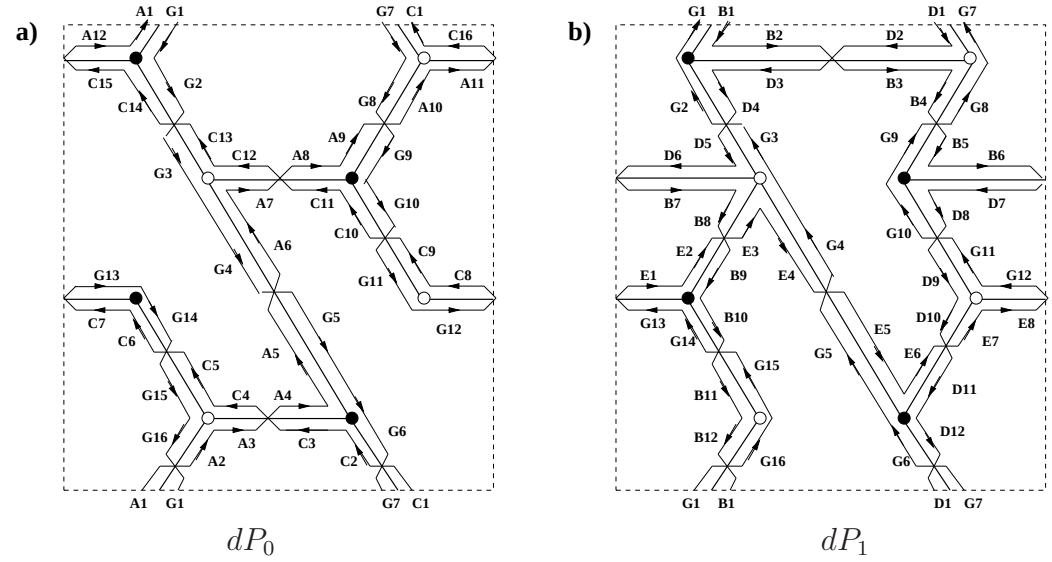

Figure 6.16: Daughter dimer diagrams obtained in the partial resolution of $X^{3,1}$ to a geometry with dP_0 and dP_1 singularities. The dimer diagrams indeed describe the gauge theories of D3-branes at these two singularities.

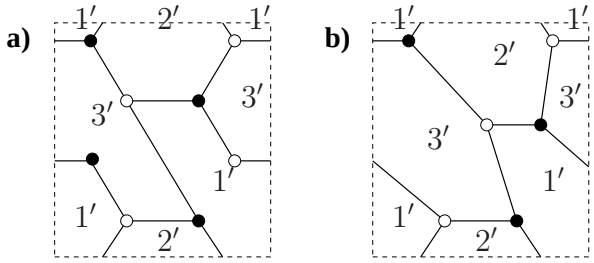

Figure 6.17: (a) The dimer diagram in Figure 6.16a. (b) Upon integrating out matter massive due to bi-valent nodes one obtains a dimer diagram corresponding to the dP_0 theory.

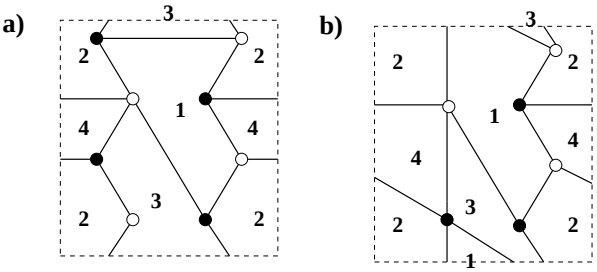

Figure 6.18: (a) The dimer diagram in Figure 6.16b. (b) Upon integrating out matter massive due to bi-valent nodes one obtains a dimer diagram corresponding to the dP_1 theory.

Given this general framework, we can be more specific about the choice of D3-brane structure we are considering. We consider the particular case

$$\begin{aligned} N_1 = 3+2M \quad , \quad N_2 = 3+2M \quad , \quad N_3 = 3+3M \quad , \quad N_4 = 3 \\ N_5 = 3+3M \quad , \quad N_6 = 3+M \quad , \quad N_7 = 3+M \quad , \end{aligned} \tag{6.8}$$

Namely 3 regular D3-branes and one fractional D-brane. The dimer diagram for the original $X^{3,1}$ theory is shown in Figure 6.19a, and the dimer diagrams for the two stacks of branes after partial resolution are shown in Figure 6.19b. Notice that the total rank on each region of the original dimer diagram is equal to the sum of the ranks in the corresponding regions in the daughter dimer diagrams. This is the condition for consistent partial resolution in the presence of fractional branes determined in Chapter 4. Following the rank assignment in Figure 6.19b through the process in Figure 6.18, it is easy to see that the fractional brane descends to a fractional brane of the daughter dP_1 singularity. Namely, using the notation in Figures 6.2 and 6.3, the rank assignments in each daughter gauge theory are

$$\begin{aligned} dP_0 \quad &: \quad N_1' = N_2' = N_3' = 3 \\ dP_1 \quad &: \quad N_1 = M \, , \, N_2 = 2M \, , \, N_3 = 3M \end{aligned} \tag{6.9}$$

So we easily identify the two gauge theory sectors described at the beginning of this section.

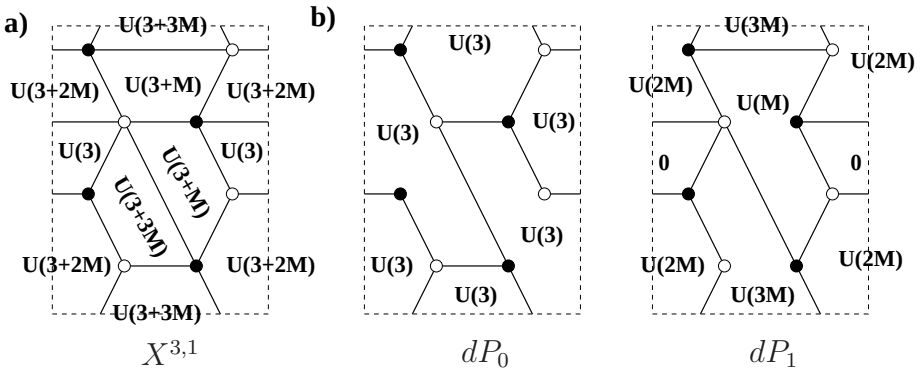

Figure 6.19: Rank assignment for the gauge theories (a) when the two singularities are collapsed into an $X^{3,1}$ singular point, (b) for the two gauge sectors corresponding to D3-branes at the isolated dP_0 and dP_1 singularities obtained after partial resolution.

As discussed in Section 6.1.3, the dimer diagram allows to easily read off the bi-fundamental vevs leading to this Higgsing, and to obtain the massive spectrum of mediators. We will use the notation of Figures 6.17 and 6.19 for the gauge groups in

dP_0 and dP_1 respectively, and we denote fundamental representations for the group $1'$ by $1'$ and fundamentals of $U(2M)$ by $2M$ (similarly for antifundamentals).

Vector multiplets in the adjoint: There are 7 massive vector multiplets in adjoint representations, coming from the 7 edges of type 2 (associated to the fields X_{56}, X_{24}, X_{43}, X_{71}) or type 1 (associated to X_{21}, X_{76} and X_{56}). They lead to massive vector multiplets in the representation

$$\mathrm{Ad}_{1'} + \mathrm{Ad}_{2'} + 2\,\mathrm{Ad}_{3'} + \mathrm{Ad}_{M} + \mathrm{Ad}_{2M} + \mathrm{Ad}_{3M} \tag{6.10}$$

Vectors in bifundamentals: There is one such massive vector multiplet for each face in the original gauge group. They transform in the representation

$$\begin{aligned}&(1', \overline{2M}) + (3', \overline{2M}) + (3', \overline{3M}) + \\ &(2', \overline{3M}) + (2', \overline{M}) + (1', \overline{M}) + \text{c.c.}\end{aligned} \tag{6.11}$$

Note that face 4 of the $X^{3,1}$ dimer does not contribute, as the corresponding gauge factor in the dP_1 dimer has rank 0 with our choice of fractional brane.

Scalar multiplets Using the rules described in Section 6.1.3, one finds the following spectrum of scalar multiplets:

$$(3', \overline{2M}) + 2\,(1', \overline{3M}) + 2\,(2', \overline{2M}) + 2\,(3', \overline{M}) \tag{6.12}$$

It would be interesting to compute the effects of supersymmetry breaking in models of this kind. This remains an open question.

6.2.2 A more complete construction

As already mentioned, one additional advantage of the present setup is its flexibility. For instance, maintaining the same geometry, it is extremely simple to describe variants of the theory in the previous section, by changing the D-brane configuration. We illustrate this by building a version with a more realistic visible sector, and an improved supersymmetry breaking sector (in that it is independent of the stabilization of Kahler moduli needed to prevent the runaway of the dP_1 theory in the previous section).

This can be done by adding D7-branes in $X^{3,1}$. Figure 6.20a shows the D7-branes present in the original $X^{3,1}$ singularity as well as the rank assignment arising from fractional branes. We have not shown the N regular D3-branes present in $X^{3,1}$ and

which only survive in the dP_1 sub-dimer. As stated in Section 6.1.3, D7-branes crossing edges of type 1(2) only survive in sub-dimer 1(2), whereas D7-branes crossing edges of type 3 appear in both sub-dimers. Thus, after resolution we obtain the dimers in Figure 6.20b which correspond to the quivers shown in Figures 6.8 and 6.9 with the rank of the flavor gauge groups in dP_1 equal to 3. Also, the condition for the supersymmetry breaking sector dP_1 to contain supersymmetry breaking local minima which are metastable and long-lived imposes $M = 2$ in Figure 6.20.

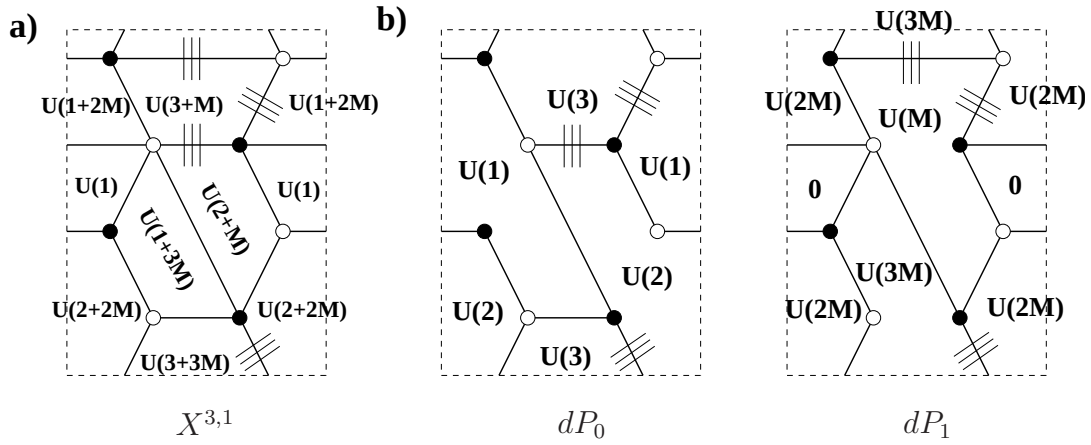

Figure 6.20: Gauge theories with D7-branes at (a) $X^{3,1}$, (b) dP_0 and dP_1 singularities obtained after partial resolution.

6.3 Some additional possibilities

In this section we describe some generalizations and other model building possibilities, which, although they involve more complicated geometries, lead to interesting or novel features.

6.3.1 Flavor universal supersymmetry breaking for $\mathbb{C}^3/\mathbb{Z}_3$

The $X^{3,1}$ (or $dP_0 + dP_1$) model studied in sections 6.2.1 and 6.2.2, has an important drawback from the viewpoint of the phenomenology of supersymmetry breaking. Namely, the complete geometry treats the three families in an asymmetric way, eventually resulting in a lack of universality in the soft terms, in particular the squark masses, in conflict with known constraints in flavor physics.

The root of the problem is the following. The different families on D3-brane models

at singularities are associated to the three complex directions of the transverse space. Hence in the $\mathbb{C}^3/\mathbb{Z}_3$ singularity the three families are treated symmetrically [8]. This symmetry appears in the web diagram as a cyclic rotation of the diagram (this is manifest when the diagrams are shown in a slightly tilted way, see coming pictures), implemented by the order-3 $SL(2,\mathbb{Z})$ action

$$\begin{pmatrix} -1 & -1 \\ 1 & 0 \end{pmatrix} \tag{6.13}$$

acting on the (p,q) labels. The symmetry of the configuration is however not preserved by the complete $X^{3,1}$ geometry, as is manifest in the web diagram (Figure 6.14). Upon partial resolution, one recovers the $\mathbb{C}^3/\mathbb{Z}_3$ singularity, and the symmetry of the different families at the level of the massless spectrum and its interactions, but not in the interactions of the different families with the massive messenger sector.

Understanding of this problem leads to a natural solution. One should enforce the symmetry between complex planes in the complete geometry. Namely, the complete web diagram should be invariant under the action of (6.13). This is easily achieved by construction: the $X^{3,1}$ geometry can be regarded as obtained by adding a dP_1 web diagram to the dP_0 web diagram, along a specific external leg of the latter. The choice of this special leg breaks the symmetry between the complex planes. Therefore, in order to preserve the symmetry, the same operation must be carried out in all external legs of the dP_0 web diagram. Namely we end up with a geometry obtained by adding three dP_1 web diagrams along the three legs of the dP_0 diagram.

In Figure 6.21 we show the web diagram and toric diagram of a possible resulting geometry [9]. We have shown the diagrams slightly tilted in order to make the $\mathbb{Z}_3$ symmetry manifest. Despite the complicated appearance of the diagrams, they are in principle tractable, since the complete geometry corresponds to an orbifold of the complex cone over dP_3, for which the dimer diagram and gauge theory data are easily computable. The result is however not particularly illuminating, and we skip its discussion.

Nevertheless, the idea is that upon partial resolution, which can be systematically analyzed, we obtain a dP_0 gauge theory, describing a visible sector, coupled in a

[8] In models with D7-branes, they have to be introduced in a way that maintains this, but it can be easily arranged, see [26].

[9] When the dP_1 web diagrams are added to the dP_0 one, some of the external legs of the former cross. This simply means that they are actually internal legs of the complete web diagram. The final external legs stem from junctions of the crossing legs. Figure 6.21 illustrates one possible choice of such junctions, leading to a relatively simple geometry.

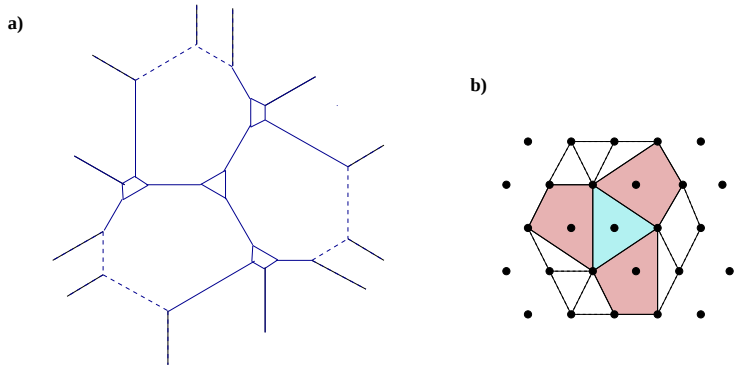

Figure 6.21: The web diagram (a) and toric diagram (b) for a singularity admitting a partial resolution with one dP_0 singularity (in blue) and three (symmetrically distributed) dP_1 singularities (in red).

flavor symmetric way to three dP_1 supersymmetry breaking sectors. Choosing the dynamical scale of the latter gauge sectors equal (in line with the symmetry we try to preserve), the soft terms induced in the dP_0 sector arise symmetrically for the three families [10].

6.3.2 Complex deformation of toric singularities

In this chapter we have described the construction of configurations of D-branes at different singularities in a local CY geometry, obtained by partial resolution. This has the advantage of allowing for a simple computation of the messenger sector. On the other hand, it requires an additional discussion of the stabilization of distance between singularities (via some mechanism of Kahler moduli stabilization, whose description is not completely clear in the local model).

We would like to briefly mention an alternative proposal, based on CY geometries where the structure of singularities arises after complex deformation. As in the previous situation, the construction of a geometry containing e.g. two isolated singularities of the desired kind can be systematically carried out, by combining the corresponding web diagrams. Specifically, a toric singularity admits a complex deformation to a geometry with two daughter singularities if the external legs of the web diagram of the parent singularity can be separated in two subsets, corresponding

[10] Of course it is an interesting question to determine the extent to which this symmetry constraints other properties of the model, like its Yukawa couplings. We leave this kind of analysis as an open question.

to the external legs of the web diagrams of the daughter singularities (see appendix on toric geometry).

The complex deformation setup has the advantage that the modulus controlling the distance between the singularities is a complex structure modulus, which can be stabilized using 3-form fluxes. One may interpret this as a source of UV sensitivity. However, the complex structure deformation can be entirely described in terms of the gauge theory of the initial singularity, as the confining gauge dynamics of a set of fractional D-branes (the so-called deformation branes described in Chapter 3). Efficient tools to carry out this gauge theory analysis, and hence determine the effect of complex deformation on the D-brane sectors, have been introduced in [4]. From the viewpoint of the gauge theory, the distance between the final D-brane stacks is related to the strong dynamics scale of the deformation fractional branes, clearly showing that it is not a modulus of the configuration (more precisely, it still has a dependence on the string coupling, which is nevertheless not a local modulus, hence its stabilized value depends on the global structure). In fact, it is this gauge theory description, rather than the geometric one, which is reliable in the regime of interest where the distance between the singularities is smaller than the string scale.

Hence one can in principle describe the complete dynamics in terms of the gauge theory associated to D-branes at the singularity obtained by shrinking all cycles in the geometry. This is similar to what happened in the partial resolution setup. However, the splitting of this initial singularity into several is a strong coupling effect triggered by confinement of the deformation fractional branes. The low-energy dynamics after this confinement can be determined reliably, and leads to two decoupled sectors corresponding to D3-branes at the two daughter singularities. On the other hand, the messenger sector corresponds to the massive states of the confining theory (with mass determined by the strong dynamics scale, or the complex deformation parameter in geometric terms) and cannot be reliably computed.

Since this setup lacks the computability of the partial resolution setup, we skip its detailed discussion, and simply mention one example of a singularity admitting a complex deformation to a geometry with a dP_0 and a dP_1 singularity. The relevant web diagram and toric diagrams are shown in Figure 6.22. The model building application of such configurations are very similar to those described in the partial resolution setup. The relevant gauge theory analysis to obtain the final two decoupled gauge theory sectors from the gauge theory of D3-branes at the parent singularity are provided in [4].

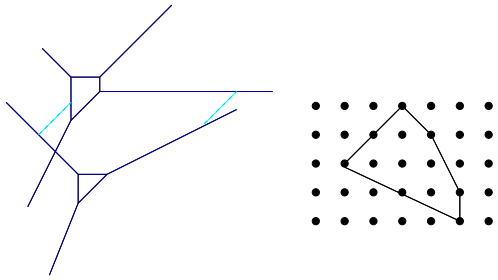

Figure 6.22: Web diagram and toric diagram of a singularity admitting a complex deformation to a geometry with a dP_0 and a dP_1 singularities. For clarity we have shown the web diagram explicitly split in two sub-webs, namely after the complex deformation. The finite size 3-cycle is shown as a dashed grey segment.

6.4 Conclusion

In this chapter we have exploited the results of chapters 3, 4 and 5 to construct models of gauge-mediated supersymmetry breaking in String Theory. Indeed, by placing D3, D7 and fractional branes at two separated toric singularities, we have obtained a model with a metastable supersymmetry breaking sector coupled to an MSSM-like sector via gauge mediation. We have also been able to determine the exact spectrum of the massive states which act as messengers of supersymmetry breaking. The construction is simple and flexible and allows for many generalizations. We have not computed the detailed parameters of the low-energy theory such as the Yukawa couplings and exact masses of all the fields after GMSB since the results would be very model dependent.

It would however be interesting to develop tools to study the effects of supersymmetry breaking both on the visible sector, and on the geometry itself. In this latter respect, it would be interesting to determine the effects of supersymmetry breaking on the Kahler moduli which control the distance between the brane stacks (and which we have assumed to be stabilized at a high scale).

6.5 Appendix: Massive sector in partial resolutions

In this appendix we provide the derivation of the spectrum of states becoming massive in the partial resolution of a singularity into two. The derivation is based on the description in [4].

In a partial resolution, the dimer diagram leads to two daughter dimer diagrams. Denote F, E, V and F_i, E_i, V_i, $i = 1, 2$ the number of faces, edges and vertices in the initial and daughter diagrams. Recall they satisfy the Euler formulas $F-E+V = 0$, $F_i-E_i+V_i = 0$ (since the dimer is a tiling of T^2). Also, each daughter dimer diagram has the same vertices as the initial one, hence $V_i = V$. Finally, we denote N_i the number of D3-branes at the i^{th} daughter singularity, and $N = N_1 + N_2$ the initial number.

The number of gauge bosons becoming massive in the Higgs mechanism associated to the partial resolution (namely $U(N)^F \to U(N_1)^{F_1} \times U(N_2)^{F_2}$) is

$$n_V \;=\; F(N_1+N_2)^2-F_1(N_1)^2-F_2(N_2)^2 = (F-F_1)N_1^2+(F-F_2)N_2^2+2FN_1N_2 \quad (6.14)$$

Also, the number of chiral multiplets which become massive is

$$n_{ch} \;=\; E(N_1+N_2)^2 - E_1(N_1)^2 - E_2(N_2)^2 = (E-E_1)N_1^2 + (E-E_2)N_2^2 + 2EN_1N_2 \quad (6.15)$$

Of these latter, n_V of them are eaten by the massless vector multiplets to lead to massive vector multiplets. Using the Euler formulas and $V_i = V$ we have

$$(F-F_i)-(E-E_i) = F-E-(F_1-E_1) = 0 \;\to\; F-F_i = E-E_i \quad (6.16)$$

Hence $(E-E_i)N_i^2$ chiral multiplets are eaten by the $(F-F_i)N_i^2$ vector multiplets, and similarly $2FN_1N_2$ chiral multiplets out of the $2EN_1N_2$ are eaten by the corresponding vector multiplets. The remaining chiral multiplets, which are $2(E-F)N_1N_2 = 2VN_1N_2$ in number, pair up into massive scalar multiplets via superpotential terms as we show below.

Now, let us try to specify how all the multiplets become massive. Consider first the $(F-F_1)N_1^2$ disappeared vector multiplets. The disappearance is due to the fact that some faces in the initial diagram recombine in the first daughter diagram. They do so because there are $(E-E_1)$ edges which have disappeared, due to the vev of the $N_1 \times N_1$ block in the corresponding bifundamental. This shows that

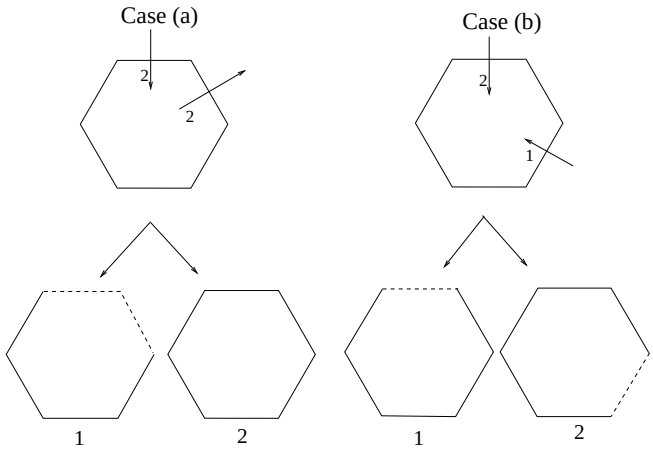

Figure 6.23: Two possible configuration of edges for a face.

the $(F - F_1)N_1^2$ vector multiplets eat up the $(E - E_1)N_1^2$ chiral multiplets, leading to $F - F_1 = E - E_1$ massive vector multiplets in the adjoint of the $U(N_1)$ gauge symmetry of the corresponding recombined face. Similarly for the $(F-F_2)N_2^2$ vector and chiral multiplets. This is rule number **1** in Section 6.1.3.

In order to understand the additional $2FN_1N_2$ disappeared vector multiplets, it is useful to have a more precise picture of how the edges of a face in the initial diagram can behave. Notice that for a given face in the original dimer diagram, it is impossible that all edges are of type 3 (present in both sub-dimers). If all edges in a face would be of type 3, and given the fact that at each node there can only be two edges of type 3 (this will be proven later), then that face would correspond to a cycle on the Riemann surface wrapping the new puncture G coming from the resolution. However, since this cycle corresponds to a face in the dimer, its (p,q) charge would be zero, which is impossible. Thus every face has to have at least two edges which are not of type 3, so either two edges of the face are of type 1, i.e. disappear from sub-dimer 2, (or two are of type 2) or one edge is of type 1 and another of type 2 (see Figure 6.23). We denote these two cases (a) and (b)

The $2FN_1N_2$ disappeared vector multiplets arise from open strings stretching between subdimers 1 and 2, at the same face location in both. They become massive by eating up chiral multiplets associated to open strings stretching between both sub-dimers, across disappeared edges. In case (a), the coupling occurs as shown in Figure 6.24.

The vector multiplets (shown as wavy arrows) A_{12} and B_{21} couple to the chiral

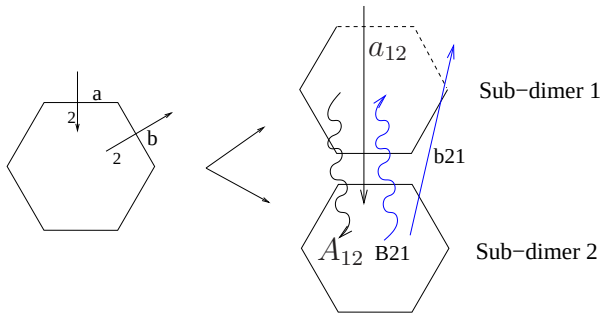

Figure 6.24: Coupling between chiral and vector multiplets for the case when a face has two edges of the same type.

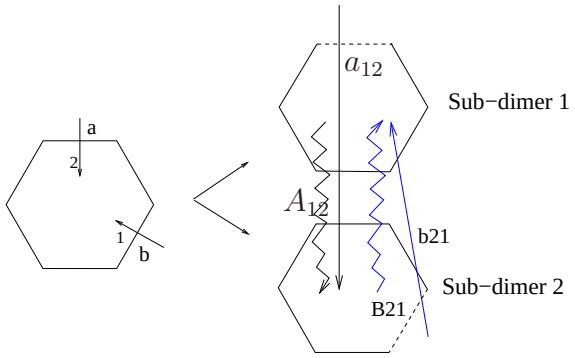

Figure 6.25: Coupling between chiral and vector multiplets for the case when a face has one edge of each type.

multiplets a_{12} and b_{21} respectively (which stretch across edges a and b respectively). In case (b), the coupling occurs as shown in Figure 6.25. The vector multiplets A_{12} and B_{21} couple to a_{12} and b_{21} respectively. a_{12} and b_{21} stretch across edges a and b respectively. This can be easily generalised to a face with an arbitrary assignation of edges. The above discussion shows that for each face in the original dimer diagram, we obtain two massive vector multiplets in the bifundamental $(N_1, \overline{N_2})$ and its conjugate, of the gauge factors at the corresponding location. This is rule number **2** in Section 6.1.3

Let us now consider the remaining $2(E-F)N_1N_2 = 2VN_1N_2$ chiral multiplets. As we show, they become massive due to the V superpotential terms. These chiral multiplets arise from open strings stretching between the two dimer diagrams (with both orientations), across edges of type 3. The fact that each superpotential term leads to a mass for a chiral multiplet in the $(N_1, \overline{N_2})$ and $(\overline{N_1}, N_2)$ (of the faces separated by the corresponding edge) follows from the fact that each node has necessarily two edges of type 3. Namely, all fields in the superpotential term, except

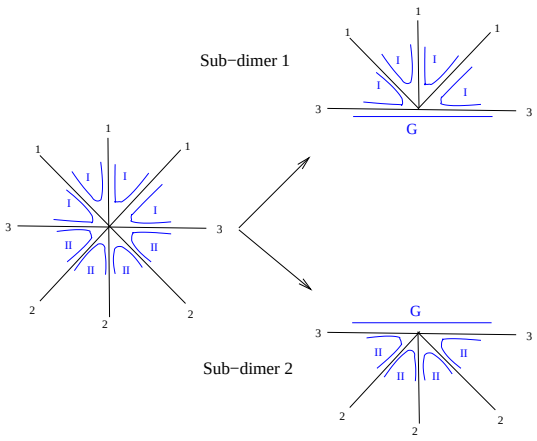

Figure 6.26: Resolution for the case when only two edges at a given node are of type 3. G represents the new puncture which arises in the resolution

the two chiral multiplets, acquire vevs, leading to a mass term for the latter. Hence one recovers rule number **3** in Section 6.1.3.

The property that each node necessarily has two edges of type 3 can be shown as follows. In a partial resolution, the zig-zag paths of the original dimer diagram are split in two sets I and II. That is, the daughter dimer diagram 1 is obtained by removing the zig-zag paths II and adding the zig-zag path G which corresponds to the new puncture. Similarly for dimer diagram 2, with the zigzag G being the same but with opposite orientation. Now, at each node, two edges of type 1 and 2 have to be separated by at least one edge of type 3 [11]. A little thought shows that if there are more than two edges of type 3 at any given node, the zig-zags G in both subdimers cannot be the same. This is illustrated in Figures 6.26 and 6.27. In the first Figure one sees that when only two edges of type 3 are present at a given node, then they separate the graph into two regions of type 1 and 2 respectively. Now, in the daughter dimer diagram 1 (resp. 2) all edges of type 2 (resp. 1) are absent. Hence the zigzag G of the new puncture passes through the boundary of region 1 (resp. 2), consistently leading to the same G with opposite orientation in the two diagrams. The situation for a node with more than two edges of type 3 is shown in Figure 6.27. Since it clearly leads to paths G which are not the same in the two dimer diagrams, we conclude that such node structure is not possible.

One small subtlety is that for a given edge of type 3, there are actually two chiral

[11] This is obvious if one recalls that and edge of type 1 is crossed by two zig-zag paths of type I and an edge of type 2 is crossed by two zig-zag paths of type II.

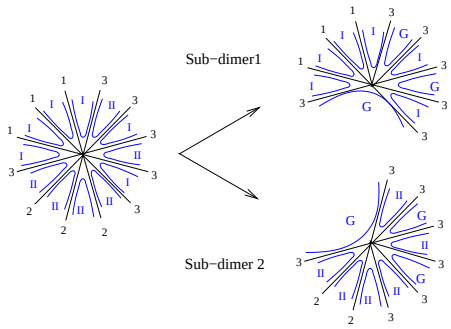

Figure 6.27: Resolution for the case when more than two edges at a given node are of type 3. G represents the new puncture which arises in the resolution.

multiplets becoming massive. These correspond to open strings stretching across this edge and going from the first daughter dimer diagram to the second and vice-versa. Each superpotential term pairs only one of these chiral multiplets (coupling it to only one of the chiral multiplets in the other adjacent type 3 node). And for a given edge of type 3, both modes acquire mass thanks to the two superpotential terms at the nodes of the edge.

Chapter 7

Conclusion

In Chapter 3 we saw how fractional branes placed at toric singularities can lead to dynamical supersymmetry breaking in the infrared. On the gauge theory side, supersymmetry is broken in the infrared due to non-perturbative effects whereas on the geometric side, fractional branes at geometries which do not admit a deformation (blow-up of an S^3) generically lead to DSB. However, when one takes into account coupling to closed string modes, this leads to a runaway behavior and supersymmetry is recovered at infinity. This behavior was resolved in [24] where, working on the ideas introduced in [25], they were able to generate metastable vacua in the infrared by adding massive flavors. The metastable vacuum is separated from the runaway direction by a large potential barrier and can thus be made parametrically long-lived. The massive flavors arise from D7-branes passing through the singularity. In Chapter 5 we summarized these ideas and saw how one can apply them to arbitrary toric singularities. Namely, we showed how one can easily determine the existence of metastable vacua for fractional DSB branes coupled to D7-branes.

In Chapter 4, we showed how one can determine the gauge theory for D3-branes at arbitrary toric singularities using the dimer diagram representation. We saw how this representation encodes the web diagram characterizing the singularity via its structure of zig-zag paths. We also saw how one can obtain two daughter singularities from the partial resolution (blow-up of an S^2) of a mother singularity. This resolution corresponds to a higgsing of the mother gauge theory by turning on Fayet-Iliopoulos terms. We were also able to determine in a precise manner the assignation of vevs necessary to generate the two daughter gauge theories. In terms of the branes, this process corresponds to D3 and fractional branes placed at a mother

singularity which, after turning on FI terms, separate into branes placed at the two daughter singularities. The distance separating the branes is given on the geometry side by the size of the S^2, and on the gauge theory side by the FI terms. In Chapter 6 we used the above results to implement a specific model of gauge mediation. By placing D3, D7 and fractional branes on a mother toric singularity, we showed how this singularity can be resolved and leads to two sets of D–branes located at daughter singularities. By placing the first set at a $\mathbb{C}^3/\mathbb{Z}_3$ singularity and the second set at a dP_1 singularity, we were able to generate a model which had a visible sector with a 3-family MSSM-like theory and a hidden sector with a metastable supersymmetry breaking minimum. When the separation distance between the branes is less than the string length, supersymmetry is transmitted via gauge mediation (it is transmitted via gravity mediation for separations greater then the string length)[28]. We also showed how the model can be extended to contain universal flavor couplings, crucial in the suppression of flavor changing neutral currents [27].

The examples studied in Chapter 6 represent an interesting framework for model building and hopefully open new avenues for incorporating SUSY breaking into string theory. However, although a few models were presented exhibiting supersymmetry breaking via gauge mediation, no rigorous analysis has been performed since that would be very model-dependent. The object of this work being more to develop a framework for model building rather than the analysis of particular models. So it remains an open question to determine the characteristics of these models, such as Yukawa couplings, particle spectra, and scale of SUSY breaking.

Although this work led to many interesting developments, several open questions remain. Klebanov, Witten [32] extended the AdS/CFT correspondence by showing that D3–branes on a conical singularity are dual to Type IIB on $AdS_5 \times X_5$, where X_5 is the base of the conical singularity. In [20, 13], the authors extended this result by showing that fractional branes at toric singularities which lead to confining gauge theories in the infrared, correspond on the supergravity side to warped geometries where the singularity at the origin is deformed (blow-up of an S^3). These results were used in [2] to generate supergravity throat solutions admitting different warp factors, and leading to an MSSM-like theory in the infrared. Although the AdS/CFT correspondence is clear for fractional branes related to deformations of the toric singularity, the same cannot be said of DSB fractional branes. Indeed, the supergravity dual does not correspond in the infrared to a deformation of the sin-

gularity preserving the Calabi-Yau condition. This was illustrated in [3], where we showed that the infrared resolution of the naked singularity repels a D3-brane probe away from the origin. So, it would be interesting to determine the supergravity dual of fractional branes leading to dynamical supersymmetry breaking in the infrared.

In Chapter 4, we saw how partial resolution (blow-up of an S^2) of a singularity can be encoded in the dimer diagram. This also has an interpretation in terms of the mirror Riemann surface, where the two singularities are stretched away from each other and recombine to give two isolated singularities (see Figure 4.16). In [4], we also showed how complex deformation (blow-up of an S^3) can be implemented in the dimer diagram. However the interpretation of this in terms of the Type IIA mirror Riemann surface is not clear and remains an open question.

Also, although only briefly mentioned, most models of metastable vacua studied in Chapter 5 contain free fields present in the quiver but not in the superpotential (see [24, 6] for details). These do not affect the SUSY breaking minimum since they run orthogonal to the runaway direction. However, although it is assumed that some will get mass at 2-loops, others correspond to axions of a broken $U(1)$ symmetry. The lifting of these moduli still remains an open question.

The analysis of Chapter 5, where we showed that all pseudo-moduli are lifted at 1-loop, was done solely by analysing the effective gauge theory. It would be interesting to provide a stringy interpretation of these results. A positive step in this direction was provided in [37, 36, 38] where the authors construct a configuration of NS-, D4- and D6–branes in Type IIA leading to metastable supersymmetry breaking vacua. These are however not dual to the Type IIB configurations we studied in Chapter 5.

Also, as stated in the introduction, we have focused in this work on branes at singularities since one can gather information such as gauge groups and matter content all from the local geometry. Our results are thus insensitive to the ultraviolet. Although this is an advantage if we wish to obtain the Standard Model as a low-energy effective theory, it offers us no clue as to how this theory couples to gravity. Thus this theory is not ultraviolet complete. Also, embedding the toric singularities into a compact Calabi-Yau manifold is not a trivial task. There is no systematic way

of constructing Calabi-Yau manifolds containing specific toric singularities. A positive step in this direction was achieved in [39], where the authors showed how it is possible to embed a dP_8 Calabi-Yau singularity into a compact Calabi-Yau manifold.

Finally, in this work we have focused mainly on implementing supersymmetry breaking mechanisms using D–branes at singularities. Numerous issues remain to be solved in String Theory, such as finding an exact replica of the Standard Model at low-energies, stabilizing all moduli, solving the cosmological constant problem and determining the Landscape of possible vacua. We hope that the humble results we have presented here aid in achieving the lofty goals set by String Theory.

Appendix A

Phases of SUSY gauge theories and Seiberg duality

A.1 Introduction

In [34] Seiberg and Intriligator analyse the phases of supersymmetric gauge theories. We summarize their work stating the useful results.

The moduli space of a supersymmetric gauge theory is given by solving the D–term and F–term equations and by quotienting by the gauge group to obtain the space of gauge inequivalent vacua. If the superpotential is zero, one only need solve the D–term equation

$$\sum_f \phi_f^\dagger T_f^a \phi_f = 0 \tag{A.1}$$

Now, solving the D–term equations then quotienting by the gauge group is equivalent to quotienting by the complexified gauge group (e.g D–terms $= 0$ and $(\phi_1, \ldots, \phi_f) \simeq (e^{i\alpha q_1}\phi_1, \ldots, e^{i\alpha q_f}\phi_f)$ is equivalent to $(\phi_1, \ldots, \phi_f) \simeq (\lambda^{q_1}\phi_1, \ldots, \lambda^{q_f}\phi_f)$ with $\lambda \in (\mathbb{C} - \{0\})$. It is a mathematical result that the space of chiral superfields modulo the complexified gauge group can be parametrized by the gauge invariant polynomials [34].

For example, consider SUSY QCD with $SU(N_c)$ gauge group and N_f quark flavors Q_i (chiral superfields) in the fundamental representation and $\tilde{Q}_{\tilde{i}}$ in the anti-fundamental representation with $i, \tilde{i} = 1, \ldots, N_f$. Now assuming no superpotential, the classical moduli space is given by solving the D–term equations which in this case are

$$Tr\left[Q^\dagger T_a^{\text{fund}} Q + \tilde{Q}^\dagger T_a^{\text{anti-fund}} \tilde{Q}\right] = 0 \tag{A.2}$$

but for $SU(N)$, $T_a^{\text{anti-fund}} = -(T_a^{\text{fund}})^*$ and $Tr\ T_a = 0$, so we get

$$Tr\left[T_a(QQ^\dagger - \tilde{Q}\tilde{Q}^\dagger)\right] = 0 \tag{A.3}$$

where Q is an $N_c \times N_f$ matrix. Diagonalizing Q and $\tilde{Q}$ one gets for $N_f < N_c$ the moduli space given by

$$Q = \tilde{Q} = \begin{pmatrix} a_1 & & \\ & \ddots & \\ & & a_{N_f} \\ & & \end{pmatrix} \tag{A.4}$$

and for $N_f \geq N_c$

$$Q = \begin{pmatrix} a_1 & & \\ & \ddots & \\ & & a_{N_c} \end{pmatrix} \quad \tilde{Q} = \begin{pmatrix} \tilde{a}_1 & & \\ & \ddots & \\ & & \tilde{a}_{N_c} \end{pmatrix} \tag{A.5}$$

with $|a_i|^2 - |\tilde{a}_i|^2 =$ indep of i.

Now for $N_f < N_c$, the gauge invariant description of the classical moduli space is given by vevs for the "mesons" $M_{i\tilde{j}} = Q_i^c \tilde{Q}_{\tilde{j}}^c$ where $i, \tilde{j}$ are flavor indices and a sum in the color indices c is implied.
For $N_f \geq N_c$ it is also possible to form "baryons"

$$B^{i_1 \cdots i_{N_f - N_c}} = \epsilon^{i_1 \cdots i_{N_f - N_c} \cdots i_{N_f}} \epsilon^{a_1 \cdots a_{N_c}} Q^{a_1}_{i_{N_f - N_c + 1}} Q^{a_2}_{i_{N_f - N_c + 2}} \cdots Q^{a_{N_c}}_{i_{N_f}} \tag{A.6}$$

and "anti-baryons"

$$\tilde{B}^{i_1 \cdots i_{N_f - N_c}} = \epsilon^{i_1 \cdots i_{N_f - N_c} \cdots i_{N_f}} \epsilon^{a_1 \cdots a_{N_c}} \tilde{Q}^{a_1}_{i_{N_f - N_c + 1}} \tilde{Q}^{a_2}_{i_{N_f - N_c + 2}} \cdots \tilde{Q}^{a_{N_c}}_{i_{N_f}} \tag{A.7}$$

Thus, with A.5 we get for $N_f \geq N_c$

$$M = \begin{pmatrix} a_1\tilde{a}_1 & & \\ & \ddots & \\ & & a_{N_c}\tilde{a}_{N_c} \\ & & \end{pmatrix} \tag{A.8}$$

and

$$B^{1, \cdots, N_f - N_c} = a_1 a_2 \cdots a_{N_c} \tag{A.9}$$

$$\tilde{B}^{1, \cdots, N_f - N_c} = \tilde{a}_1 \tilde{a}_2 \cdots \tilde{a}_{N_c} \tag{A.10}$$

Therefore the rank of M is at most N_c, if it is less, then $B = 0$ or $\tilde{B} = 0$. If the rank of M is equal to N_c then B and $\tilde{B}$ have rank one. The results of Seiberg and Intriligator [34] lead to the following conclusions when analysing the different regimes of SUSY QCD (i.e different rank of flavor N_f and color N_c).

A.2 SUSY QCD for $N_f < N_c$

Now, as is known, the superpotential of a supersymmetric theory is not renormalized perturbatively. Since this theory is confining one can ask whether it acquires non-perturbative corrections in the infrared (IR). The global symmetries of SUSY QCD are $SU(N_f)_L \times SU(N_f)_R \times U(1)_A \times U(1)_B \times U(1)_R$ with the quarks transforming as

$$Q \qquad (N_f, 1, 1, 1, \tfrac{N_f - N_c}{N_f}) \tag{A.11}$$

$$\tilde{Q} \qquad (1, \bar{N}_f, 1, -1, \tfrac{N_f - N_c}{N_f}) \tag{A.12}$$

and $U(1)_A$ anomalous in the quantum theory. Now, the only term compatible with these symmetries is

$$W_{eff} = (N_c - N_f) \left(\frac{\Lambda^{3N_c - N_f}}{det_{i,\tilde{j}}\ Q_i^c \tilde{Q}_{\tilde{j}}^c} \right) \tag{A.13}$$

where Λ is the dynamically generated scale of the theory and the determinant runs over the flavor indices. W_{eff} is generated by instantons for $N_f = N_c - 1$ and for $N_f < N_c - 1$, it is associated with gaugino condensation (i.e $\lambda^\alpha \lambda_\alpha$ in the vector multiplet acquires a vev).

This superpotential leads to a scalar potential (recall $V = \left| \frac{\partial W}{\partial \phi} \right|^2$) which goes to zero as $det\, Q\tilde{Q} \to \infty$. We therefore went from a classical theory with an infinite set of vacua (parametrized by the mesons) to a quantum theory which in the infrared has no vacuum.

A.3 SUSY QCD for $N_f = N_c$

For this theory, assuming no classical superpotential, the classical moduli space is given by the meson and (anti)baryon vevs . When $N_f = N_c$ they are not independent and obey the relation

$$det\, M \ - \ B\tilde{B} \ = \ 0 \tag{A.14}$$

which follows from the Bose statistics of Q and $\tilde{Q}$. However, in the IR the moduli space gets instanton corrections thus changing the constraint to

$$det\, M \;-\; B\tilde{B} \;=\; \Lambda^{2N_c} \tag{A.15}$$

This constraint can be directly implemented by adding a term $W = A(\, detM - B\tilde{B} - \Lambda^{2N_c})$ to the superpotential, where A is a Lagrange multiplier. It is not dynamical and is thus replaced by its equations of motion giving the constraint A.15.
Because the origin $M = B = \tilde{B} = 0$ is not part of the moduli space the vevs necessarily break the anomaly free chiral symmetry. For example, setting $M_{i\tilde{j}} = \delta_{i\tilde{j}}$ and $B = \tilde{B} = 0$ gives

$$SU(N_f)_L \times SU(N_f)_R \times U(1)_B \times U(1)_R \to SU(N_f)_V \times U(1)_B \times U(1)_R \tag{A.16}$$

A.4 SUSY QCD for $N_f \geq 3N_c$

The theory is not asymptotically free, so the coupling constant becomes smaller in the IR and the superpotential does not acquire any perturbative corrections.

A.5 SUSY QCD for $\frac{3}{2}N_c < N_f < 3N_c$

The theory is asymptotically free, i.e the coupling constant increases in the IR. The β–function of SUSY QCD is given by

$$\beta(g) = -\frac{g^3}{16\pi^2}\frac{3N_c - N_f + N_f\gamma(g^2)}{1 - N_c\frac{g^2}{8\pi^2}} \tag{A.17}$$

with

$$\gamma(g^2) = -\frac{g^2}{8\pi^2}\frac{N_c^2 - 1}{N_c} + \Theta(g^4) \tag{A.18}$$

In this range, the theory has an IR fixed point (i.e zero of the β–function) so the coupling constant does not go to infinity in the IR but to a fixed value where the theory becomes scale invariant. In this limit the theory becomes a superconformal field theory and one can use the superconformal algebra to derive that

$$D(Q\tilde{Q}) = \frac{3}{2}R(Q\tilde{Q}) = 3\frac{N_f - N_c}{N_f} \tag{A.19}$$

and

$$D(B) = D(\tilde{B}) = 3\frac{N_c(N_f - N_c)}{2N_f} \tag{A.20}$$

where D is the conformal dimension and R is the R–charge. Now, an important result is that the physics of the interacting fixed point obtained in the range $\frac{3}{2}N_c < N_f < 3N_c$ has an equivalent 'magnetic' description [33]. It is based on the gauge group $SU(N_f - N_c)$ with N_f flavors of quarks q_i and $\tilde{q_{\tilde{i}}}$ and a gauge invariant field $M_{i\tilde{j}}$ with a superpotential

$$W = \frac{1}{\mu} M_{i\tilde{j}} q_i \tilde{q_{\tilde{j}}} \tag{A.21}$$

This is referred to as the magnetic theory, with the original one referred to as the electric theory. Since this theory is also in the range $\frac{3}{2}\tilde{N_c} < \tilde{N_f} < 3\tilde{N_c}$ where $\tilde{N_c} = N_f - N_c$ and $\tilde{N_f} = N_f$, this theory also flows to an IR fixed point. The remarkable thing is that this theory flows to exactly the same fixed point. Thus although these two theories are different in the ultra-violet (UV), they flow to the same theory in the IR. This duality is generally referred to as Seiberg Duality. In the electric description $M_{i\tilde{j}} = Q_i Q_{\tilde{j}}$ has dimension two at the UV fixed point since the theory is asymptotically free and acquires anomalous dimension given by equation A.19 in the IR. In the magnetic description $M_{i\tilde{j}}$ is an elementary field of dimension one in the UV and flows to the same operator with dimension A.19 in the IR.

The magnetic theory has a scale $\tilde{\Lambda}$ which is related to the scale Λ of the electric theory by

$$\Lambda^{3N_c - N_f} \tilde{\Lambda}^{3(N_f - N_c) - N_f} = (-1)^{N_f - N_c} \mu^{N_f} \tag{A.22}$$

Now, for it to be a duality, the dual of the magnetic theory should give the electric one. This is shown to be the case. Also, an interesting and useful property derived from equation A.22 is that when the electric theory is strongly coupled, the magnetic one is weakly coupled and vice–versa. The global symmetries of the magnetic theory are the same as the electric one and the charges of its matter fields are the following with respect to $SU(N_f)_L \times SU(N_f)_R \times U(1)_B \times U(1)_R$

$$q \qquad (\overline{N}_f, 1, \frac{N_c}{N_f - N_c}, \frac{N_c}{N_f}) \tag{A.23}$$

$$\tilde{q} \qquad (1, N_f, -\frac{N_c}{N_f - N_c}, \frac{N_c}{N_f}) \tag{A.24}$$

and $M_{i\tilde{j}}$ has the charges of $Q_i \tilde{Q}_{\tilde{j}}$.

A.6 SUSY QCD for $N_c + 2 \leq N_f \leq \frac{3}{2}N_c$

In this case, the electric theory also has a dual magnetic description as above. However, whereas the electric theory is UV free, the magnetic one is IR free. The UV free electric theory flows at long distance to the IR free magnetic theory [35].

A.7 SUSY QCD for $N_f = N_c + 1$

This theory also admits a magnetic description as above, but without magnetic gauge fields. The classical moduli space is described by mesons M, baryons B^i and anti-baryons $\tilde{B}^{\tilde{i}}$. There is a constraint given by

$$detM \left(\frac{1}{M}\right)^{i\tilde{j}} - B^i \tilde{B}^{\tilde{j}} = 0 \tag{A.25}$$

$$M_{i\tilde{j}} B^i = M_{i\tilde{j}} \tilde{B}^{\tilde{j}} = 0 \tag{A.26}$$

The moduli space is not modified perturbatively. So the quantum moduli space is the same as the classical one and the constraint can be implemented in the superpotential via a term $W_{eff} = \frac{1}{\Lambda^{2N_c-1}}(M_{i\tilde{j}} B^i \tilde{B}^{\tilde{j}} - detM)$.

A.8 Quiver Diagrams

Generically, the SUSY gauge theories living on D3–branes at singularities can be represented by so–called quiver diagrams [12]. In these diagrams an arrow represents a bifundamental chiral superfield and a node represents a gauge group with the associated vector multiplet. For example, the gauge theory for D3–branes on an SPP singularity (see section on toric geometry) is represented by the quiver diagram in figure A.1. We thus have three gauge groups $U(N_1) \times U(N_2) \times U(N_3)$ with three

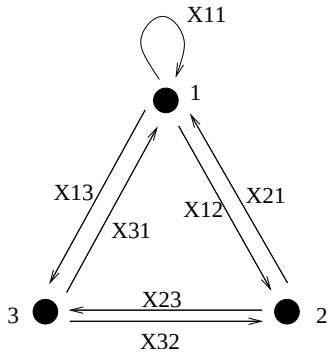

Figure A.1: Quiver diagram of the SPP

associated vector multiplets. We also have seven chiral superfields transforming as

$$\begin{array}{cccc} & U(N_1) & U(N_2) & U(N_3) \\ X_{12} & \square & \overline{\square} & \\ X_{21} & \overline{\square} & \square & \\ X_{23} & & \square & \overline{\square} \\ X_{32} & & \overline{\square} & \square \\ X_{13} & \square & & \overline{\square} \\ X_{31} & \overline{\square} & & \square \\ X_{11} & Adj & & \end{array} \tag{A.27}$$

Cancellation of anomalies imposes that at each node (gauge group), the number of flavors of chiral multiplets in the fundamental representation be equal to the number of flavors in the anti–fundamental representation. Seiberg duality acts on the quiver diagram in the following way. If a node is strongly coupled, the other can be neglected and acts as a global symmetry (quenched approximation). Thus each arrow with an end on the dualized node is inverted giving the dual q and $\tilde{q}$ and one adds the mesons $M_{i\tilde{j}}$ which correspond to the gauge invariants. Also, after adding the superpotential $W = Mq\tilde{q}$, one eliminates all the massive fields. For example, when dualizing node 2, one gets the quiver diagram shown in figure A.2.

Where $M_{11} = X_{12}X_{21}$, $M_{13} = X_{12}X_{23}$, $M_{31} = X_{32}X_{21}$, $M_{22} = X_{23}X_{32}$. Now the original superpotential is

$$W = Tr[X_{21}X_{12}X_{23}X_{32} - X_{32}X_{23}X_{31}X_{13} + X_{13}X_{31}X_{11} - X_{12}X_{21}X_{11}] \tag{A.28}$$

In terms of the new variables, this becomes

$$W = Tr[M_{13}M_{31} - M_{33}X_{31}X_{13} + X_{13}X_{31}X_{11} - M_{11}X_{11}] \tag{A.29}$$

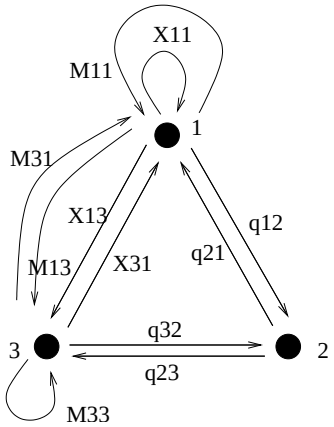

Figure A.2: Quiver diagram of the SPP after dualizing node 2

and one adds a new term which arises from Seiberg duality (e.g A.21) so that the full potential becomes[1]

$$\begin{aligned} W = \quad & Tr\,[M_{13}M_{31} - M_{33}X_{31}X_{13} + X_{13}X_{31}X_{11} - M_{11}X_{11} \\ & - M_{13}q_{32}q_{21} - M_{31}q_{12}q_{23} + M_{33}q_{32}q_{23} + M_{11}q_{12}q_{21}] \end{aligned} \tag{A.30}$$

Since M_{11}, X_{11}, M_{13} and M_{31} become massive, they are replaced by their equations of motion ($\frac{\partial W}{\partial \phi} = 0$) so that the resulting superpotential is

$$W = Tr[-M_{33}X_{31}X_{13} + X_{13}X_{31}q_{12}q_{21} - q_{32}q_{21}q_{12}q_{23} + M_{33}q_{32}q_{23}] \tag{A.31}$$

with the quiver diagram given by figure A.3. We thus retrieve the original theory,

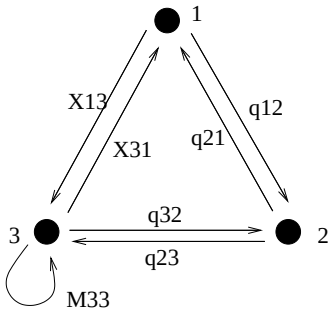

Figure A.3: Quiver diagram of the SPP after dualizing node 2 and integrating out the massive fields

with the same charges and superpotential.

[1]Generically the terms are added such that each field appears with opposite signs, this is the toric condition.

Appendix B

Toric Geometry

In this appendix we shall give a descriptive and intuitive picture of toric geometry, the mathematically rigorous one being quite involved. The results are based on [40, 41, 42, 43, 13, 10, 19, 44].

Calabi–Yau 3–folds (i.e six dimensional manifolds) are considered toric if they can be expressed as a fibration of circles ($U(1)$'s) over a base $\mathbb{R}^3$. The simplest example is $\mathbb{C}^3$, where the base $\mathbb{R}^3$ consists of the three radii and the fiber $U(1)^3$ consists of the three phases. Toric geometries often arise when one studies D3–branes at singularities. In this case, the moduli space of the gauge theory on the D3–branes describes the geometry of the transverse six–dimensional Calabi-Yau space. The moduli space is obtained by solving the F–term and D–term equations of the supersymmetric gauge theory. Generically, the transverse geometry is toric if the gauge theory is abelian and has a superpotential such that each bifundamental appears exactly twice and with opposite signs in the terms.

The general toric construction is as follows. Assume a SUSY gauge theory with $U(1)^k$ gauge group and Φ_i $i = 1, \ldots, n$ chiral mulitplets. Assume zero superpotential so that there are no F–term equations. One thus obtains k D–term equations

$$\sum_i Q_i^a \left|\Phi_i\right|^2 = r^a \tag{B.1}$$

$a = 1, \ldots, k$ and r^a are the Fayet–Ilipoulos terms. The moduli space is obtained by quotienting the solution by the gauge group.

$$(\Phi_1, \ldots, \Phi_n) \sim (e^{i\alpha Q_1^a}\Phi_1, \ldots, e^{i\alpha Q_n^a}\Phi_n) \tag{B.2}$$

As an aside, an interesting result is that the moduli space given by solving the D–term equations and quotienting by the gauge symmetries is equal to quotienting the

fields by the complexified gauge symmetry after having removed specific points.

$$\frac{\text{Fields with D–terms} = 0}{\text{Gauge symmetry}} \quad = \quad \frac{\text{Fields - } \mathrm{F}_\Delta}{\text{Complexified gauge symmetry}} \tag{B.3}$$

where F_Δ are the points to be removed and the complexified gauge symmetry acts as

$$(\Phi_1, \ldots, \Phi_n) \sim (\lambda^{Q_1^a}\Phi_1, \ldots, \lambda^{Q_n^a}\Phi_n) \tag{B.4}$$

with $\lambda \in \mathbb{C}^* = \mathbb{C} - \{0\}$.

Now, the moduli space is completely given by the charge matrix Q_i^a. This moduli space is also parametrized by the gauge invariant monomials

$$P_j = \Phi_1^{k_1^j}\Phi_2^{k_2^j}\cdots\Phi_n^{k_n^j} \quad \text{with} \quad j = 1, \ldots, n-k \tag{B.5}$$

which are invariant under all the $U(1)$'s. Now under $U(1)_a$, $\Phi_i \to e^{i\alpha Q_i^a}\Phi_i$ so $P_j \to e^{i\alpha\sum_i k_i^j Q_i^a}P_j$. Thus for the monomials to be invariant under all the $U(1)$ gauge symmetries we want

$$\sum_i k_i^j Q_i^a = 0 \quad \forall a \tag{B.6}$$

Thus k is the kernel of Q and one thus obtains j vectors k^j in an n–dimensional space which completely characterizes the moduli space (transverse geometry). Now given an invariant monomial P_j specified by the n–dimensional vectors k^j, the monomial given by $ak^j + bk^l$, $a, b \in \mathbb{Z}$ is also an invariant. Thus the k^j's span a vector space and one only need specify the basis . Since the k^j's take integer values, the vector space is a lattice with basis vectors k^j. Now if the moduli space is Calabi–Yau, the k^j's lie in a hyperplane. Examples will clarify these concepts.

The conifold is given by the moduli space of a gauge theory with four chiral multiplets and with one $U(1)$ gauge group with charges

$$\begin{array}{cccccc} & \Phi_1 & \Phi_2 & \Phi_3 & \Phi_4 \\ Q & 1 & 1 & -1 & -1 \end{array} \tag{B.7}$$

The invariant monomials are thus $P_1 = \Phi_1\Phi_3$, $P_2 = \Phi_1\Phi_4$, $P_3 = \Phi_2\Phi_3$, $P_4 = \Phi_2\Phi_4$. But P_4 is not independent since $P_1P_4 = P_2P_3$. So we have three independent monomials. The k^j vectors are

$$k^1 = (1, 0, 1, 0) \tag{B.8}$$

$$k^2 = (1, 0, 0, 1) \tag{B.9}$$

$$k^3 = (0, 1, 1, 0) \tag{B.10}$$

and the vectors describing the toric diagram are given by taking the transpose vectors, thus obtaining four three dimensional vectors v_i.

$$\begin{pmatrix} 1 \\ 1 \\ 0 \end{pmatrix} \begin{pmatrix} 0 \\ 0 \\ 1 \end{pmatrix} \begin{pmatrix} 1 \\ 0 \\ 1 \end{pmatrix} \begin{pmatrix} 0 \\ 1 \\ 0 \end{pmatrix} \tag{B.11}$$

Equivalently, these vectors v_i (edges of the fan) can be obtained by solving

$$\sum_{i=1}^{n} Q_i^a v_i = 0 \quad \forall\ a \tag{B.12}$$

where n is the number of chiral superfields and $a = 1, \ldots, s$ is the number of $U(1)$ gauge groups. Looking at these vectors (figure B.1) one can easily see that they

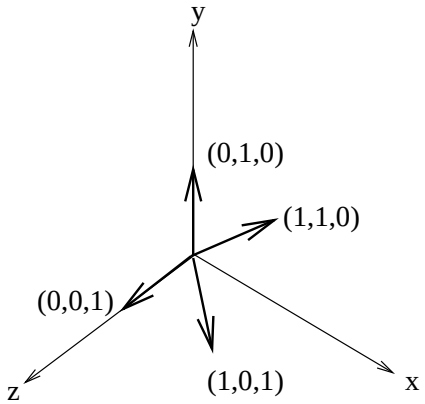

Figure B.1: Edges of the fan for the conifold

all lie in a two dimensional plane. The toric diagram is given by the tips of the vectors in the hyperplane as shown by figure B.2. Thus, any toric geometry can be

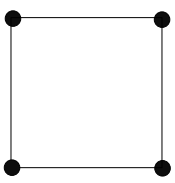

Figure B.2: Toric diagram of the conifold

expressed as points in a two dimensional integer lattice .

Now, a toric diagram has singularities if its diagram is not composed of minimal triangles (i.e triangles of area 1/2, assuming that the distance between two adjacent

points is 1). For example, the conifold above contains a singularity; it is removed by blowing up a 2–sphere leading to the resolved conifold seen in figure B.3. This is done by giving a FI–term to the D–term equation.

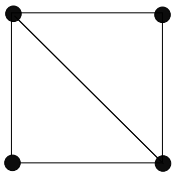

Figure B.3: Toric diagram of the resolved conifold

For example, the toric diagram for the Suspended Pinch Point SPP ($xy = zw^2$) is shown in figure B.4. It can be resolved in two different ways as shown in figure B.5.

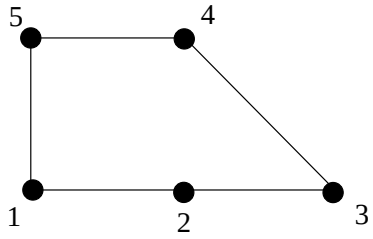

Figure B.4: Toric diagram of the SPP

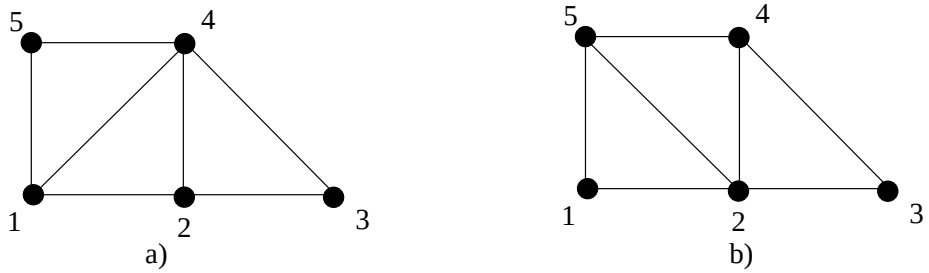

Figure B.5: Toric diagram of the SPP after having removed all singularities

When one does a $\mathbb{Z}_n$ quotient of a geometry, this is equivalent to a refinement of the lattice by index n. For example, performing a $\mathbb{Z}_2$ quotient of the conifold leads to two possible toric diagrams (depending on the action of the $\mathbb{Z}_2$) as shown in figure B.6.

Performing a $\mathbb{Z}_3$ quotient of the SPP leads to two possible toric diagrams as shown in figure B.7.

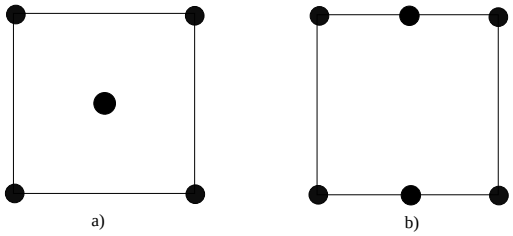

Figure B.6: Toric diagram of the conifold/$\mathbb{Z}_2$

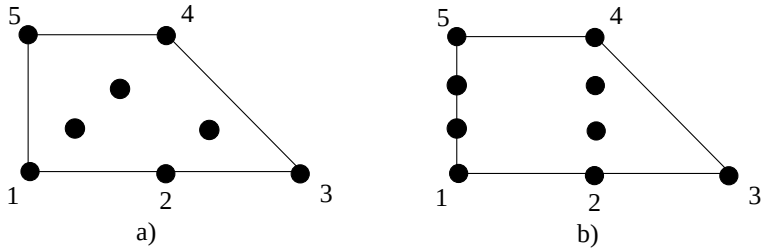

Figure B.7: Toric diagram of the SPP/$\mathbb{Z}_3$

Now, one can retrieve the following information from the toric diagram :

- The number of (homologically inequivalent) 4–cycles is equal to the number of interior points (e.g one for the conifold over $\mathbb{Z}_2$).
- The sum of (homologically inequivalent) 0–cycles, 2–cycles and 4–cycles is equal to the number of triangles in the toric diagram.
- The number of points inside a line (not on the edges) gives the number of singular lines in a geometry.

As an example, the SPP (figure B.4) has one point which is not an edge (point 2), so it has a line singularity parametrized by arbitrary z in $xy = zw^2$. And since the SPP is connected it has one 0–cycle. Since it has no internal points it has zero 4–cycles. Therefore it has two (homologically inequivalent) 2–cycles.

The toric diagram description only lets one visualize the possible deformations of a geometry which consist in blowing up collapsed 2–cycles and 4–cycles. An alternative description is the web diagram, which is easily obtained from the toric diagram by passing a perpendicular line through each edge of a toric diagram. This is more easily shown using examples.

For the conifold one obtains the web diagram shown in figure B.8. For the resolved

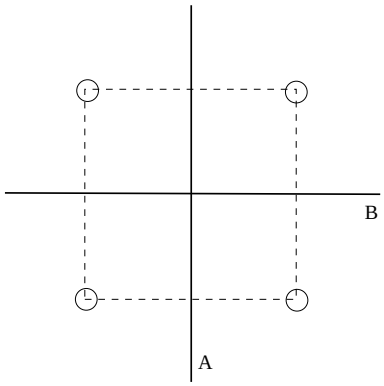

Figure B.8: Web diagram of the conifold

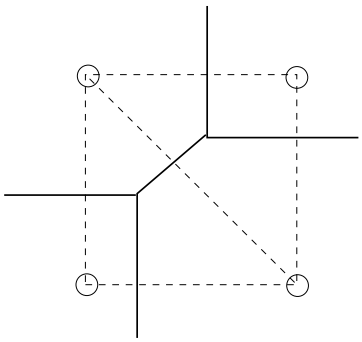

Figure B.9: Web diagram of the resolved conifold

conifold one obtains the web diagram shown in figure B.9. For the SPP one obtains the web diagram shown in figure B.10. For the resolved SPP one obtains the web

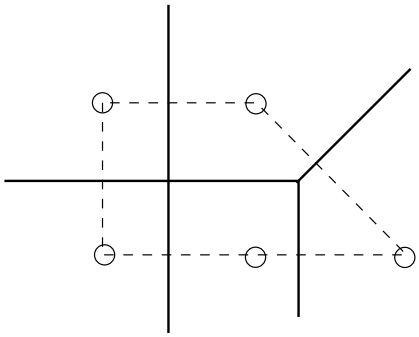

Figure B.10: Web diagram of the SPP

diagram shown in figure B.11.

Now, the web diagram can be seen as a fibration of a T^3 (three $U(1)$'s) over a base $\mathbb{R}^3$. The planar diagram represents the subspace $\mathbb{R}^2$ where one of the three $U(1)$'s

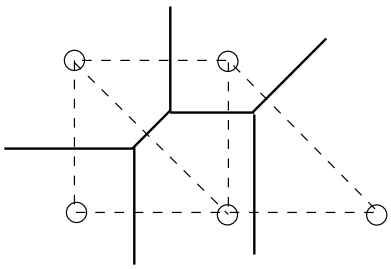

Figure B.11: Web diagram of the SPP after having removed all singularities

has degenerated (gone to zero size). The lines in the planar diagram represent the points where one of the two $U(1)$'s degenerates, with the angle specifying which cycle degenerates (e.g a horizontal line specifies that the (1,0) cycle degenerates and a diagonal line specifies that a linear combination of the two cycles degenerates). The intersection of two or more lines is where both $U(1)$'s degenerate. For example, for the conifold shown in figure B.8, one of the $U(1)$'s degenerates on line A and the orthogonal one degenerates on line B and both degenerate at the intersection.

Now given a web diagram, we can give an orientation to each edge and label it by its slope (charges) as shown in figure B.12. The Calabi–Yau condition of vanishing

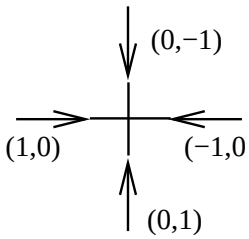

Figure B.12: Web diagram of the conifold with edges labelled by the corresponding charges

first Chern class imposes that at each vertex the sum of charges going in equals the sum of charges going out. Another example is the SPP as shown in figure B.13. Both examples show cancellation of charge at each vertex. Now to see if there are 2 or 4–cycles which can be blown up, one looks for the possibility of adding internal legs at a vertex consistent with cancellation of charges. For example, the conifold in figure B.12 above can be deformed to the resolved conifold shown in figure B.14. One can see that the internal line is a S^2 since it is the fibration of a $U(1)$ over a finite segment and the $U(1)$ degenerates over the edges, as illustrated in figure B.15. Now, the resolved conifold is smooth since at no vertex can one add internal lines consistent with cancellation of charges. This is also illustrated by the fact that if

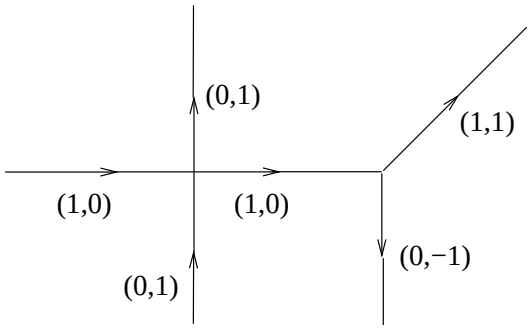

Figure B.13: Web diagram of the SPP with edges labelled by the corresponding charges

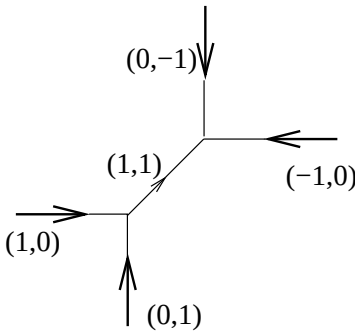

Figure B.14: Web diagram of the resolved conifold

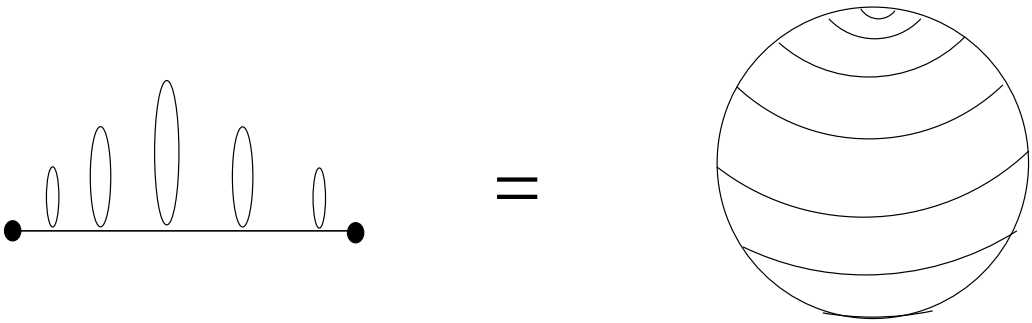

Figure B.15: The two–sphere S^2 can see as the fibration of a $U(1)$ over a finite segment degenerating at the edges

one looks at one of the vertices shown in figure B.16, its dual is shown in figure B.17. This is a minimal triangle and thus corresponds to $\mathbb{C}^3$ (the same is true of the other vertex). If one can add internal legs such as to form a closed surface then that internal surface corresponds to a 4–cycle since it is the fibration of two $U(1)$'s over a two dimensional compact plane.

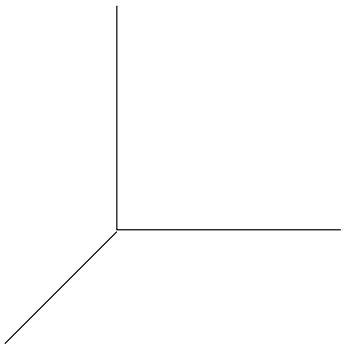

Figure B.16: Vertex of the resolved conifold

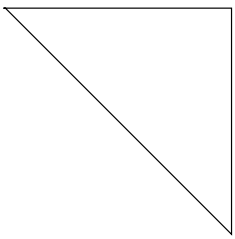

Figure B.17: Dual toric diagram

Now the advantage of the web diagram description is that it permits one to not only visualize the possible 2 and 4–cycle blow–ups but also the 3–cycle blow–ups. These are given by choosing a subset of the external legs such that the sum of their charges cancels. The external legs are then moved in the three dimensional direction thus generating a blow–up. This will be illustrated with examples.
The conifold admits the deformation which corresponds to the deformed conifold.

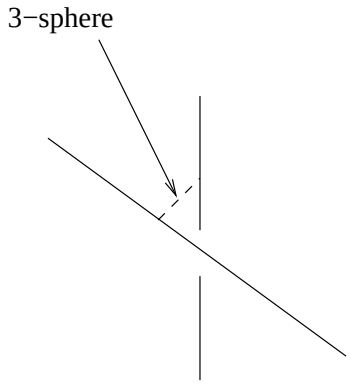

Figure B.18: Deformation of the conifold corresponding to blowing up a 3–sphere

This diagram is in three dimensions, thus the third $U(1)$ is no longer degenerate, the dotted line can be seen to be S^3 since it corresponds to a segment with a $U(1)^2$

fibration where each one degenerates at one end and this is known to correspond to an S^3. For example, the SPP admits the deformation which also corresponds to the

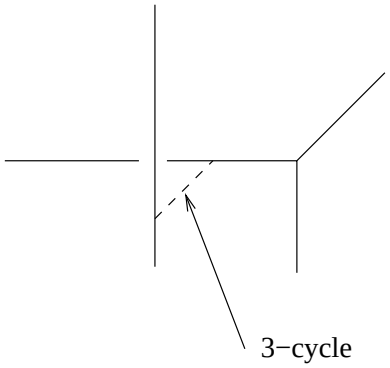

Figure B.19: Deformation of the SPP corresponding to blowing up a 3–cycle

blow–up of a 3–cycle.

Now, just by looking at the web and toric diagrams one can extract the following information on the gauge theory of D3–branes transverse to the geometry:

- The number of triangles in the toric diagram is equal to the number of gauge groups of the gauge theory living on the D3-branes.
- Looking at the web diagram, the number of bifundamental fields of the gauge theory is found using the formula

$$n_{fields} = \sum_{i>j} \left| det \begin{pmatrix} p_i & q_i \\ p_j & q_j \end{pmatrix} \right| \tag{B.13}$$

  where p_i, q_i are the charges of the external leg i

As an example, the SPP toric diagram (figure B.4) has three triangles, thus the gauge theory of D3–branes on an SPP singularity has three gauge groups. And from the SPP web diagram shown in figure B.13, the number of bifundamental fields is seven, which agrees with its web diagram.

Thus, by looking at toric and web diagrams one is able to extract vast amounts of information on the geometry, its possible deformations and the gauge theory living on the D3–branes. Also, since the toric geometries correspond to the moduli space of the gauge theory living on the D3–branes, the possible deformations correspond to different branches in the moduli space (i.e different higgsings). One can thus construct new geometries by starting with a geometry which is very singular, finding

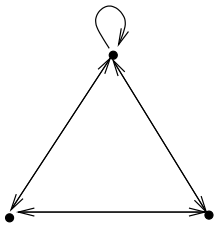

Figure B.20: The quiver diagram of the D3–brane gauge theory placed on an SPP singularity

the associated gauge theory and choosing appropriate vevs to lead to another gauge theory. The moduli space of the residual gauge theory after higgsing corresponds to the geometry after deformation. This is what was done by Feng, Hanany and He [19] to obtain the so-called del Pezzo surfaces starting from the gauge theory living on $\mathbb{C}^3/\mathbb{Z}_3 \times \mathbb{Z}_3$, as seen in figure B.21.

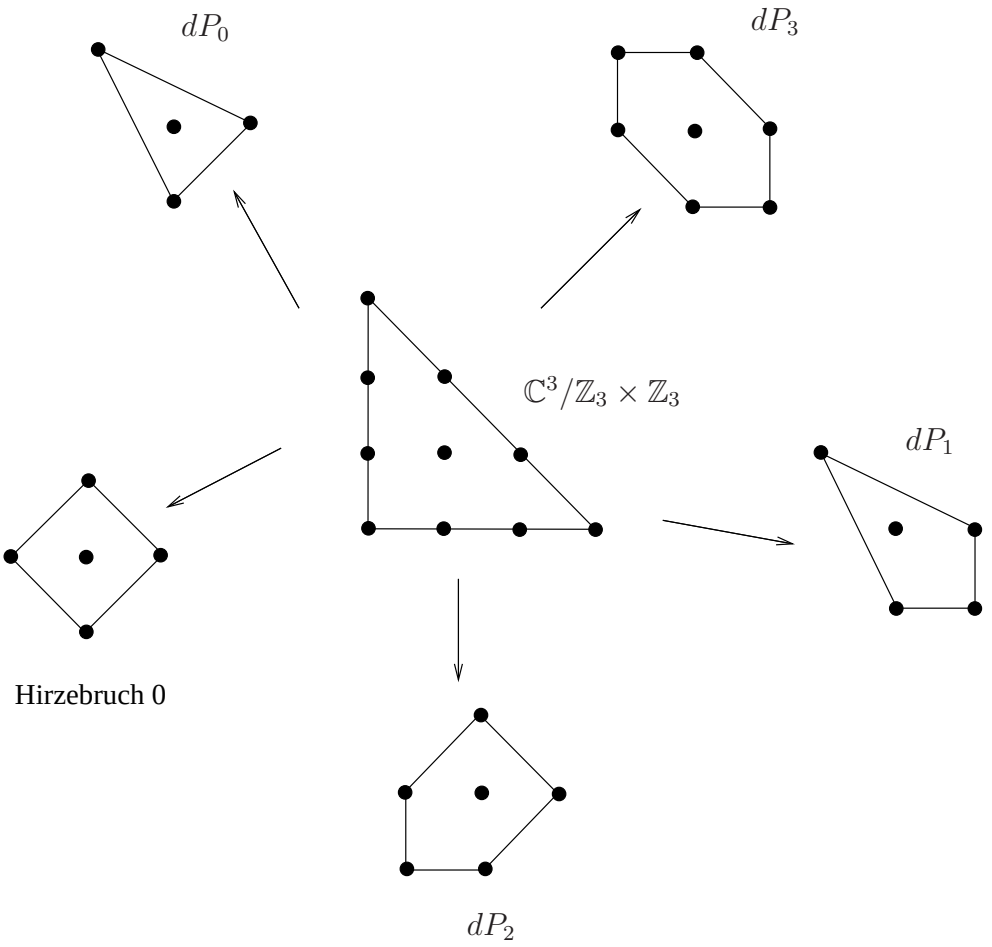

Figure B.21: The possible geometries obtained by higgsing the $\mathbb{C}^3/\mathbb{Z}_3 \times \mathbb{Z}_3$

Bibliography

[1] S. Weinberg, "The quantum theory of fields. Vol. 2: Modern applications," *Cambridge, UK: Univ. Pr. (1996) 489 p*

[2] J. F. G. Cascales, F. Saad and A. M. Uranga, "Holographic dual of the standard model on the throat," JHEP **0511**, 047 (2005) [arXiv:hep-th/0503079].

[3] S. Franco, A. Hanany, F. Saad and A. M. Uranga, "Fractional branes and dynamical supersymmetry breaking," JHEP **0601**, 011 (2006) [arXiv:hep-th/0505040].

[4] I. Garcia-Etxebarria, F. Saad and A. M. Uranga, "Quiver gauge theories at resolved and deformed singularities using dimers," JHEP **0606** (2006) 055 [arXiv:hep-th/0603108].

[5] I. Garcia-Etxebarria, F. Saad and A. M. Uranga, "Local models of gauge mediated supersymmetry breaking in string theory," JHEP **0608** (2006) 069 [arXiv:hep-th/0605166].

[6] F. Saad, I. Garcia-Etxebarria and A. M. Uranga, "SUSY Breaking Metastable vacua in quiver gauge theories," Work in Progress.

[7] A. Uranga, Lecture notes on String Theory, available at http://gesalerico.ft.uam.es/paginaspersonales/angeluranga/index.html

[8] D. R. Morrison and M. R. Plesser, "Non-spherical horizons. I," Adv. Theor. Math. Phys. **3** (1999) 1 [arXiv:hep-th/9810201].

[9] M. R. Douglas, B. R. Greene and D. R. Morrison, "Orbifold resolution by D-branes," Nucl. Phys. B **506** (1997) 84 [arXiv:hep-th/9704151].

[10] J. Park, R. Rabadan and A. M. Uranga, "Orientifolding the conifold," Nucl. Phys. B **570** (2000) 38 [arXiv:hep-th/9907086].

[11] A. M. Uranga, "Brane configurations for branes at conifolds," JHEP **9901**, 022 (1999) [arXiv:hep-th/9811004].

[12] M. R. Douglas and G. W. Moore, "D-branes, Quivers, and ALE Instantons," arXiv:hep-th/9603167.

[13] S. Franco, A. Hanany and A. M. Uranga, "Multi-flux warped throats and cascading gauge theories," JHEP **0509** (2005) 028 [arXiv:hep-th/0502113].

[14] A. Hanany and K. D. Kennaway, "Dimer models and toric diagrams," arXiv:hep-th/0503149.

[15] S. Franco, A. Hanany, K. D. Kennaway, D. Vegh and B. Wecht, "Brane dimers and quiver gauge theories," arXiv:hep-th/0504110.

[16] B. Feng, Y. H. He, K. D. Kennaway and C. Vafa, "Dimer models from mirror symmetry and quivering amoebae," arXiv:hep-th/0511287.

[17] S. Franco and D. Vegh, "Moduli spaces of gauge theories from dimer models: Proof of the correspondence," arXiv:hep-th/0601063.

[18] A. Hanany and D. Vegh, "Quivers, tilings, branes and rhombi," arXiv:hep-th/0511063.

[19] B. Feng, A. Hanany and Y. H. He, "D-brane gauge theories from toric singularities and toric duality," Nucl. Phys. B **595** (2001) 165 [arXiv:hep-th/0003085].

[20] I. R. Klebanov and M. J. Strassler, "Supergravity and a confining gauge theory: Duality cascades and chiSB-resolution of naked singularities," JHEP **0008** (2000) 052 [arXiv:hep-th/0007191].

[21] I. R. Klebanov and A. A. Tseytlin, "Gravity duals of supersymmetric SU(N) x SU(N+M) gauge theories," Nucl. Phys. B **578** (2000) 123 [arXiv:hep-th/0002159].

[22] I. Affleck, M. Dine and N. Seiberg, "Dynamical Supersymmetry Breaking In Supersymmetric QCD," Nucl. Phys. B **241** (1984) 493.

[23] Y. Shadmi and Y. Shirman, "Dynamical supersymmetry breaking," Rev. Mod. Phys. **72**, 25 (2000) [arXiv:hep-th/9907225].

[24] S. Franco and A. M. .. Uranga, "Dynamical SUSY breaking at meta-stable minima from D-branes at obstructed geometries," JHEP **0606** (2006) 031 [arXiv:hep-th/0604136].

[25] K. Intriligator, N. Seiberg and D. Shih, "Dynamical SUSY breaking in meta-stable vacua," JHEP **0604** (2006) 021 [arXiv:hep-th/0602239].

[26] G. Aldazabal, L. E. Ibanez, F. Quevedo and A. M. Uranga, "D-branes at singularities: A bottom-up approach to the string embedding of the standard model," JHEP **0008** (2000) 002 [arXiv:hep-th/0005067].

[27] G. F. Giudice and R. Rattazzi, "Theories with gauge-mediated supersymmetry breaking," Phys. Rept. **322** (1999) 419 [arXiv:hep-ph/9801271].

[28] D. E. Diaconescu, B. Florea, S. Kachru and P. Svrcek, "Gauge - mediated supersymmetry breaking in string compactifications," JHEP **0602** (2006) 020 [arXiv:hep-th/0512170].

[29] A. Hanany, P. Kazakopoulos and B. Wecht, "A new infinite class of quiver gauge theories," JHEP **0508** (2005) 054 [arXiv:hep-th/0503177].

[30] S. R. Coleman and E. Weinberg, "Radiative Corrections As The Origin Of Spontaneous Symmetry Breaking," Phys. Rev. D **7** (1973) 1888.

[31] A. Brini and D. Forcella, "Comments on the non-conformal gauge theories dual to Y(p,q) manifolds," JHEP **0606** (2006) 050 [arXiv:hep-th/0603245].

[32] I. R. Klebanov and E. Witten, "Superconformal field theory on threebranes at a Calabi-Yau singularity," Nucl. Phys. B **536** (1998) 199 [arXiv:hep-th/9807080].

[33] N. Seiberg, "Electric - magnetic duality in supersymmetric nonAbelian gauge theories," Nucl. Phys. B **435**, 129 (1995) [arXiv:hep-th/9411149].

[34] K. A. Intriligator and N. Seiberg, "Lectures on supersymmetric gauge theories and electric-magnetic duality," Nucl. Phys. Proc. Suppl. **45BC** (1996) 1 [arXiv:hep-th/9509066].

[35] K. Intriligator and N. Seiberg, "Lectures on supersymmetry breaking," arXiv:hep-ph/0702069.

[36] S. Franco, I. Garcia-Etxebarria and A. M. Uranga, "Non-supersymmetric meta-stable vacua from brane configurations," JHEP **0701** (2007) 085 [arXiv:hep-th/0607218].

[37] H. Ooguri and Y. Ookouchi, "Meta-stable supersymmetry breaking vacua on intersecting branes," Phys. Lett. B **641** (2006) 323 [arXiv:hep-th/0607183].

[38] I. Bena, E. Gorbatov, S. Hellerman, N. Seiberg and D. Shih, "A note on (meta)stable brane configurations in MQCD," JHEP **0611** (2006) 088 [arXiv:hep-th/0608157].

[39] M. Buican, D. Malyshev, D. R. Morrison, M. Wijnholt and H. Verlinde, "D-branes at singularities, compactification, and hypercharge," JHEP **0701** (2007) 107 [arXiv:hep-th/0610007].

[40] M. Aganagic and C. Vafa, "G(2) manifolds, mirror symmetry and geometric engineering," arXiv:hep-th/0110171.

[41] O. Aharony and A. Hanany, "Branes, superpotentials and superconformal fixed points," Nucl. Phys. B **504**, 239 (1997) [arXiv:hep-th/9704170].

[42] O. Aharony, A. Hanany and B. Kol, "Webs of (p,q) 5-branes, five dimensional field theories and grid diagrams," JHEP **9801**, 002 (1998) [arXiv:hep-th/9710116].

[43] N. C. Leung and C. Vafa, "Branes and toric geometry," Adv. Theor. Math. Phys. **2**, 91 (1998) [arXiv:hep-th/9711013].

[44] M. Marino, "Chern-Simons theory and topological strings," Rev. Mod. Phys. **77**, 675 (2005) [arXiv:hep-th/0406005].

[45] B. Feng, S. Franco, A. Hanany and Y. H. He, "Unhiggsing the del Pezzo," JHEP **0308** (2003) 058 [arXiv:hep-th/0209228].

[46] B. Feng, S. Franco, A. Hanany and Y. H. He, "Symmetries of toric duality," JHEP **0212**, 076 (2002) [arXiv:hep-th/0205144].

[47] F. Cachazo, B. Fiol, K. A. Intriligator, S. Katz and C. Vafa, "A geometric unification of dualities," Nucl. Phys. B **628**, 3 (2002) [arXiv:hep-th/0110028].

[48] B. Feng, A. Hanany and Y. H. He, "Phase structure of D-brane gauge theories and toric duality," JHEP **0108**, 040 (2001) [arXiv:hep-th/0104259].

[49] A. Hanany and A. Iqbal, "Quiver theories from D6-branes via mirror symmetry," JHEP **0204**, 009 (2002) [arXiv:hep-th/0108137].

[50] L. E. Ibanez, R. Rabadan and A. M. Uranga, "Anomalous U(1)'s in type I and type IIB D = 4, N = 1 string vacua," Nucl. Phys. B **542** (1999) 112 [arXiv:hep-th/9808139].

[51] D. Berenstein, C. P. Herzog, P. Ouyang and S. Pinansky, "Supersymmetry breaking from a Calabi-Yau singularity," JHEP **0509** (2005) 084 [arXiv:hep-th/0505029].

[52] M. Bertolini, F. Bigazzi and A. L. Cotrone, "Supersymmetry breaking at the end of a cascade of Seiberg dualities," Phys. Rev. D **72**, 061902 (2005) [arXiv:hep-th/0505055].

[53] C. P. Herzog, Q. J. Ejaz and I. R. Klebanov, "Cascading RG flows from new Sasaki-Einstein manifolds," JHEP **0502** (2005) 009 [arXiv:hep-th/0412193].

[54] J. P. Gauntlett, D. Martelli, J. Sparks and D. Waldram, "Sasaki-Einstein metrics on S(2) x S(3)," Adv. Theor. Math. Phys. **8**, 711 (2004) [arXiv:hep-th/0403002].

[55] J. P. Gauntlett, D. Martelli, J. F. Sparks and D. Waldram, "A new infinite class of Sasaki-Einstein manifolds," Adv. Theor. Math. Phys. **8**, 987 (2006) [arXiv:hep-th/0403038].

[56] J. P. Gauntlett, D. Martelli, J. Sparks and D. Waldram, "Supersymmetric AdS backgrounds in string and M-theory," arXiv:hep-th/0411194.

[57] D. Martelli and J. Sparks, "Toric geometry, Sasaki-Einstein manifolds and a new infinite class of AdS/CFT duals," Commun. Math. Phys. **262**, 51 (2006) [arXiv:hep-th/0411238].

[58] S. Benvenuti, A. Hanany and P. Kazakopoulos, "The toric phases of the Y(p,q) quivers," JHEP **0507**, 021 (2005) [arXiv:hep-th/0412279].

[59] S. Benvenuti, S. Franco, A. Hanany, D. Martelli and J. Sparks, "An infinite family of superconformal quiver gauge theories with Sasaki-Einstein duals," JHEP **0506**, 064 (2005) [arXiv:hep-th/0411264].